

DEPARTMENT OF GEOSCIENCES – EARTH SCIENCES
UNIVERSITY OF FRIBOURG (SWITZERLAND)

TECTONICS OF THE WESTERN SWISS MOLASSE BASIN DURING CENOZOIC TIMES

THESIS

**presented to the Faculty of Science at the University of Fribourg (Switzerland) in
consideration for the award of the academic grade of Doctor rerum naturalium**

By

Tobias Ibele

from Ravensburg, Germany

Thesis No: 1714

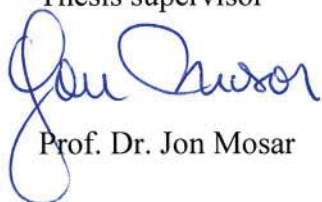
Multiprint SA, Fribourg, 2011

Accepted by the Faculty of Science of the University of Fribourg (Switzerland) upon the recommendation of

| | | |
|----------------------------|------------------------|-------------------|
| Prof. Dr. Jon Mosar | University of Fribourg | Thesis supervisor |
| Prof. Dr. Neil Mancktelow | ETH Zürich | Expert |
| Prof. Dr. Klaus Reicherter | RWTH Aachen | Expert |
| Prof. Dr. Bernard Grobéty | University of Fribourg | Jury president |

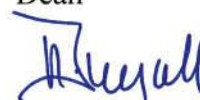
Fribourg, 21. Juni 2011

Thesis supervisor

A handwritten signature in blue ink, appearing to read 'Jon Mosar', with a large loop at the end.

Prof. Dr. Jon Mosar

Dean

A handwritten signature in blue ink, appearing to read 'R. Ingold', with a stylized, cursive script.

Prof. Dr. Rolf Ingold

TABLE OF CONTENTS

| | |
|------------------------|---|
| ABSTRACT | 1 |
| ZUSAMMENFASSUNG | 3 |
| ACKNOWLEDGEMENTS | 5 |

1 - INTRODUCTION

| | |
|--|----|
| 1.1 SCOPE OF THE STUDY | 7 |
| 1.2 GEOGRAPHIC LOCATION AND SETTING..... | 7 |
| 1.3 GEOLOGY OF THE SWISS MOLASSE BASIN | 9 |
| 1.4 TECTONIC EVOLUTION OF THE WESTERN SWISS MOLASSE BASIN | 11 |
| 1.4.1 Inception and evolution of the Northern Alpine Foreland Basin | 11 |
| 1.4.2 Influence of the Upper Rhine Graben Rift | 11 |
| 1.4.3 The folding of the Jura Mountains | 13 |
| 1.4.3.1 <i>In-situ folding model</i> | 13 |
| 1.4.3.2 <i>Fernschub hypothesis</i> | 14 |
| 1.4.4 Consequences of the folding of the Jura Mountains for the Molasse Basin | 15 |
| 1.4.5 Strike-slip faulting in the Jura Mountains | 16 |
| 1.4.6 Deformation of the western Swiss Molasse Basin | 16 |
| 1.4.7 The Subalpine Molasse | 16 |
| 1.4.8 The Jura Mountains-Molasse Basin- Alps connection | 17 |
| 1.5 THE TOP OF BASEMENT STRUCTURE IN THE WESTERN MOLASSE BASIN | 17 |
| 1.6 PALEOSTRESS AND RECENT STRESS IN THE WESTERN MOLASSE BASIN | 18 |
| 1.7 SEISMOTECTONICS OF THE NORTHERN FORELAND OF THE CENTRAL ALPS | 20 |

2 - DEFORMATION BANDS IN THE SANDSTONES OF THE WESTERN SWISS MOLASSE BASIN: MICRO-MECHANICS AND BRITTLE DEFORMATION

| | |
|----------------|----|
| ABSTRACT | 23 |
|----------------|----|

| | |
|--|----|
| 2.1 INTRODUCTION | 24 |
| 2.2 BACKGROUND | 25 |
| 2.2.1 Geologic setting | 25 |
| 2.2.2 Brittle deformation bands in sandstone | 27 |
| 2.2.3 Riedel shear model and SC-fabrics | 28 |
| 2.3 FIELD DATA | 30 |
| 2.3.1 Host rock of deformation bands | 30 |
| 2.3.2 Outcrop conditions in the western Swiss Molasse Basin | 31 |
| 2.3.3 Macroscopic occurrence of deformation bands in the Molasse sandstone | 32 |
| 2.3.4 Field data and its interpretation | 33 |
| 2.4 MICROSCOPE ANALYSIS | 38 |
| 2.4.1 Optical microscopy | 38 |
| 2.4.1.1 <i>Deformation bands and micro- fault gouges</i> | 38 |
| 2.4.1.2 <i>SC-structures in the micro-fault gouge</i> | 42 |
| 2.4.2 Scanning electron microscopy | 44 |
| 2.4.2.1 <i>Backscatter electron micrographs</i> | 44 |
| 2.4.3 Chemical composition | 47 |
| 2.5 DISCUSSION | 48 |
| 2.5.1 Evolution of deformation bands | 48 |
| 2.5.2 Conceptual model for the evolution of micro-fault gouge | 49 |
| 2.5.3 Riedel shears versus SC-fabric | 50 |
| 2.5.4 Implications for fluid flow | 51 |
| 2.5.5 Significance of the macroscopic geometry of DBs in the Molasse sandstone | 52 |
| 2.5.6 Seismic versus aseismic nature of the DBs | 53 |
| 2.6 CONCLUSION | 53 |

3 - THE ORIGIN OF PLYGORSKITE IN FAULT GOUGES OF THE WESTERN SWISS MOLASSE

| | |
|------------------------------|----|
| ABSTRACT | 55 |
| 3.1 INTRODUCTION | 55 |
| 3.2 ANALYTICAL METHODS | 56 |

| | | |
|-------|--|----|
| 3.3 | THERMODYNAMIC MODELLING | 58 |
| 3.4 | PALYGORSKITE | 59 |
| 3.4.1 | Crystal chemistry of palygorskite | 59 |
| 3.4.2 | Thermodynamic data for palygorskite | 59 |
| 3.5 | RESULTS AND DISCUSSION | 60 |
| 3.5.1 | Host rock compositions | 60 |
| 3.5.2 | Fault gouge and deformation band compositions | 60 |
| 3.5.3 | Palygorskite formation | 61 |
| 3.6 | DISCUSSION AND CONCLUSION | 63 |

4 - STRIKE-SLIP DEFORMATION IN THE WESTERN SWISS PLATEAU MOLASSE

| | | |
|---------|---|-----|
| | ABSTRACT | 67 |
| 4.1 | INTRODUCTION | 68 |
| 4.2 | GEOLOGIC SETTING | 68 |
| 4.2.1 | Geology of the study area | 70 |
| 4.3 | METHODS | 71 |
| 4.3.1 | Mapping | 71 |
| 4.3.2 | Paleostress analysis | 71 |
| 4.4 | BRITTLE TECTONIC STRUCTURES | 73 |
| 4.4.1 | Planar tectonic structures | 73 |
| 4.4.1.1 | <i>Brittle deformation bands in sandstone</i> | 73 |
| 4.4.1.2 | <i>Slickensides</i> | 74 |
| 4.4.1.3 | <i>Unspecified fractures</i> | 75 |
| 4.4.1.4 | <i>Orientation patterns of planar meso-scale brittle structures</i> | 75 |
| 4.4.2 | Non-planar structures | 76 |
| 4.4.2.1 | <i>Pitted conglomerate pebbles</i> | 76 |
| 4.5 | FAULT ZONES | 77 |
| 4.5.1 | Palygorskite type fault zones and dense fracture type fault zones | 78 |
| 4.5.2 | Clayey cataclasite type fault zones | 80 |
| 4.5.3 | Open fracture type fault zones | 80 |
| 4.6 | ORIENTATION OF MESO-SCALE STRUCTURES AND DERIVED PALEOSTRESSES | 80 |
| 4.6.1 | Brittle deformation bands | 80 |
| 4.6.2 | Slickensides | 86 |
| 4.6.3 | Unspecified fractures | 90 |
| 4.6.4 | Solution pits in conglomerate pebbles | 91 |
| 4.6.5 | Slickensides in the Subalpine Molasse | 94 |
| 4.7 | DEFORMATION CHARACTERISTICS | 96 |
| 4.8 | OUTCROP CONDITIONS AND DISTRIBUTION OF DEFORMATION | 98 |
| 4.9 | THE FAULT ZONE NETWORK | 98 |
| 4.10 | THE TRANSITION ZONE BETWEEN PLATEAU MOLASSE AND SUBALPINE MOLASSE | 100 |
| 4.11 | TIMING OF DEFORMATION | 103 |
| 4.12 | CONCLUSION | 104 |

5 - STRUCTURAL GEOLOGY AND TECTONIC EVOLUTION OF THE WESTERN SWISS MOLASSE BASIN

| | | |
|---------|---|-----|
| | ABSTRACT | 107 |
| 5.1 | INTRODUCTION..... | 108 |
| 5.2 | GEOLOGIC SETTING..... | 108 |
| 5.3 | SURFACE DATA..... | 111 |
| 5.3.1 | Deformation structures | 112 |
| 5.3.2 | Implications of structure type for deformation conditions | 112 |
| 5.3.3 | Orientation of planar structures, their kinematics and derived paleostress | 114 |
| 5.3.4 | Implications for fault zone extent in the Tertiary Molasse | 116 |
| 5.3.5 | Interpretation of superordinate shear zones | 118 |
| 5.3.6 | Fault zones recorded in the Tertiary Molasse only | 118 |
| 5.3.6.1 | <i>The Subalpine Molasse thrust front</i> | 119 |
| 5.4 | DEEP STRUCTURE | 120 |
| 5.4.1 | Structures in the basement | 120 |
| 5.4.2 | Structures in the Mesozoic units | 120 |
| 5.5 | INTERPRETATION OF DEFORMATION ZONES IN THE MESOZOIC AND TERTIARY COVER | 120 |
| 5.5.1 | The Fribourg zone – a complex polyphase structure | 121 |
| 5.5.2 | The La Lance fault – a right-lateral strike-slip fault system | 124 |
| 5.5.3 | The Courtion structure – an inversion and anticlinal structure | 124 |
| 5.5.4 | The Broye structure – a reactivated graben structure | 124 |
| 5.6 | KINEMATIC MODEL | 128 |
| 5.6.1 | Kinematic decoupling | 129 |
| 5.6.2 | Kinematic interactions of the cover structures | 130 |
| 5.6.2.1 | <i>Kinematics in adjacent areas</i> | 131 |
| 5.7 | DISTRIBUTION OF ACTIVE SEISMIC FAULTING IN THE STUDY AREA | 131 |
| 5.7.1 | Implications of fault network characteristics for possible earthquake magnitude | 132 |
| 5.8 | TECTONIC EVOLUTION | 134 |
| 5.9 | CONCLUSION | 138 |

| | |
|------------------|-----|
| REFERENCES | 139 |
| APPENDICES | 149 |

| | | |
|--------------|--|-----|
| Appendix 1.1 | list of instrumentally recorded earthquakes | 150 |
| Appendix 2.1 | List of thin section samples | 152 |

| | | |
|------------------------|---|-----|
| Appendix 4.1 | Overprinting relationships | 153 |
| Appendix 4.2 | Lower hemisphere plots of slickenside populations from the Plateau Molasse and derived paleostress axes (P-T axes method and Right Dihedra Method) | 154 |
| Appendix 4.3 | Lower hemisphere plots of slickenside populations from the Subalpine Molasse and derived paleostress axes (P-T axes method and Right Dihedra Method) | 163 |
| CURRICULUM VITAE | | 165 |

ABSTRACT

The western Swiss Molasse Basin is a flexural foreland basin that presently is in a wedge-top position above a décollement formed in Triassic evaporites near the base of the underlying Mesozoic units. In front of the western Swiss Molasse Basin, the décollement tectonics led to folding and thrusting of the Jura Mountains. The latter are widely accepted to represent the thin-skinned foreland fold-and-thrust belt of the central Alps. In contrast to the Jura Mountains, the western Swiss Molasse Basin lacks larger tectonic structures. Folds are very low in amplitude and strike-slip faults are known only locally. It nevertheless can be considered as part of the foreland fold-and-thrust belt, since it sits on top of the same detachment and since the boundary to the Jura Mountains is an erosional contact only. The boundary to the Alpine orogenic wedge s.s. is marked by the basal thrust of the Subalpine Molasse, representing a shallower and more internal detachment at the base of the Tertiary units.

This study investigates the deformation of the western Swiss Molasse Basin in the larger Canton Fribourg area. Based on structural field work, it shows that in addition to low amplitude folding, the western Swiss Molasse is affected by strike-slip deformation in a general NW-SE compressional stress field. The mapped structures are fractures, slickensides, brittle deformation bands and faults as well as pressure solution pits on surfaces of conglomerate pebbles. The deformation is examined in terms of mechanics, geochemistry and its impact on regional tectonics.

Deformation in the sandstones initiates with the formation of brittle deformation bands. The operating mechanism is grain crushing, porosity reduction and interlocking of grain fragments along planar zones. The interlocking leads to strain hardening, so that ongoing deformation forms new subparallel bands. Microscopic investigation of the brittle deformation bands from the Molasse show that fault gouges

develop in the bands following the initial grain crushing. In these micro-fault gouges, regular foliation structures develop in alternation with chaotic structures, implying a cyclic change in deformation mode from instantaneous fracturing to continuous shear, i.e. from seismic to aseismic faulting on the micro-scale. The foliations are composed of fibrous palygorskite, a Mg-rich clay mineral that forms in the course of deformation. In contrast to grain interlocking, the appearance of palygorskite causes strain softening and hence strain accumulation in the fault gouges of the bands.

X-ray diffraction analyses of fault gouges and host rock samples as well as electron dispersive spectroscopy of micro-fault gouges from brittle deformation bands revealed that palygorskite is common in fault zones on every scale, but absent in the host rock. Equilibrium calculations carried out with the host rock mineralogy and a variety of formation waters from the region revealed palygorskite to be stable, while chlorite (present in the host rock) is unstable in that configuration and at surface temperatures. This implies a chlorite-consuming reaction for palygorskite formation triggered by deformation, i.e. by contact of the ground material with the fluid phase.

The populations of slickensides and brittle deformation bands mapped at different localities are arranged in pairs with synthetic and antithetic orientation and are interpreted as different shears of a Riedel system. The fractures can be subdivided into mode I cracks parallel to σ_1 and sheared fractures parallel to the slickenside populations. The mapped faults comprise cataclastic fault cores and damage zones with dense networks of fractures, slickensides and brittle deformation bands oriented in Riedel-type geometries. The mapped faults rarely exceed one kilometre in length, but individual faults may compose larger fault zones in which shear is distributed. The orientation of the mapped structures is subvertical,

and kinematics are left-lateral strike-slip in the case of N-S orientation and right-lateral strike-slip in the case of WNW-ESE to NW-SE orientation. The calculated paleostress is NW-SE compression and uniform throughout the study area. Overprinting relationships show no system, which underlines that deformation is the response to only one stress regime.

The availability of new interpretation of seismic surveys reveals the structures in the deeper levels of the study area, especially fault zones located in the Mesozoic units. While the Tertiary Molasse at the surface shows N-S striking and WNW-ESE striking faults, the Mesozoic units show considerably fewer WNW-ESE striking faults. In addition, the Mesozoic units also show NE-SW striking faults not present in the Tertiary Molasse at the surface. In cross-section, the faults in the Mesozoic units mostly show half-grabens, although offset is partly reverse. Taking into account the regional tilt of the strata towards southeast, N-S striking faults can mostly be interpreted as left-lateral strike-slip faults and WNW-ESE striking faults as right-lateral strike-slip faults. All faults within the Mesozoic level root with listric terminations in the Triassic evaporites. The NE-SW and N-S striking faults are interpreted as former normal faults formed by E-W and NW-SE extension, respectively, that became inverted by NW-SE compression.

The deformation zones derived from surface mapping and the structures revealed by the seismic interpretations are combined in a 3-D kinematic model of the study area. In this model, deformation is characterised by a kinematic decoupling of the Mesozoic and Tertiary levels along Triassic evaporites. In the internal parts a second decoupling is developed at the base of the Tertiary Molasse. It corresponds to the basal thrust of the Subalpine Molasse extending underneath the Plateau Molasse, with a blind end located about 10 km northwest of the most frontal imbricate of the Subalpine Molasse. Interaction of strike-slip faulting in the Plateau Molasse and thrusting at the front of the Subalpine Molasse indicate that deformation in both tectonic units is contemporaneous.

The timing of deformation is poorly constrained by the data. NW-SE compression probably starts with the formation of the Jura Mountains-Molasse Basin foreland fold-and-thrust belt in the upper Miocene. It postdates the Oligocene-Miocene deposition of the Molasse as well as the E-W and NW-SE extension recorded in the Mesozoic units, which most likely took place in the Paleogene. The current seismicity of the region reveals that strike-slip faulting according to NW-SE compression, starting in the Neogene, is still active and partly related to the proposed deformation zones.

ZUSAMMENFASSUNG

Der Schweizer Faltenjura gilt allgemein als der Vorland-Falten- und Überschiebungsgürtel der Zentralalpen. Faltung und Überschiebung sind auf das Deckgebirge oberhalb eines in triassischen Evaporiten lokalisierten Abscherhorizonts beschränkt. Das im Sinne der alpinen Orogenese weiter intern gelegene westschweizer Molassebecken und seine mesozoische Unterlage sind zeitgleich entlang desselben Abscherhorizonts passiv um den Verkürzungsbetrag der Jurafaltung nach Nordwesten transportiert worden. Im Gegensatz zum Faltenjura zeigt die Westschweizer Molasse aber nur unauffällige tektonische Strukturen. Die Falten sind sehr flach ausgebildet und Blattverschiebungen nur von wenigen Orten im Grenzbereich zum Faltenjura bekannt. Das zeitgleiche Abscheren entlang desselben Abscherhorizonts und die Tatsache, dass die nur erosiv ausgebildeten Grenze zum Faltenjura zeigen, dass das Westschweizer Molassebecken gemeinsam mit dem Faltenjura zum Vorland-Falten- und Überschiebungsgürtel dazu gezählt werden muss. Die Grenze zum alpinen Orogenkeil im engeren Sinn ist die basale Überschiebung der Subalpinen Molasse, die ihrerseits einen Abscherhorizont an der Basis des Tertiärs und somit in einem höheren Stockwerk darstellt.

Diese Arbeit beschäftigt sich mit der Deformation der Westschweizer Molasse in der Gegend des Kantons Freiburg. Basierend auf strukturgeologischen Felddaten zeigt sie, dass die Molasse des Arbeitsgebiets über die schwache Faltung hinaus auch durch weit verbreitete Blattverschiebungsstrukturen gekennzeichnet ist. Im Feld wurden Brüche, Harnische, spröde Deformationsbänder, Störungen und Lösungsgruben in Konglomeratgeröllen als tektonische Strukturen aufgenommen. Die kartierte Deformation wird unter mechanischen, geochemischen und regionaltektonischen Gesichtspunkten analysiert.

Spröde Deformationsbänder sind charakteristische Strukturen beginnender Deformation in porösen Sandsteinen. Dabei bilden sich planare Zonen (Bän-

der), entlang derer Scherung durch Kornzertrümmerung und Reduktion des Porenraums aufgenommen wird. Durch das Verkeilen der Kornfragmente kommt es zu Verformungshärtung dieser Zonen, so dass fort-dauernde Deformation zur Bildung neuer subparallel-er Deformationsbänder führt. Die mikroskopische Untersuchung der spröden Deformationsbänder aus der Molasse zeigte jedoch, dass die einzelnen Bänder nach ihrer Entstehung durchaus weitere Verformung aufnehmen können. Die mikroskopischen Störungsbrekzien sind sowohl durch regelmäßige Strukturen einer Foliation als auch durch chaotische, aus Katak-lase hervorgegangene Strukturen gekennzeichnet. Damit weisen sie auf einen zyklischen Wechsel des Deformationsstils zwischen ruckartigem Versagen und kriechender Verformung hin, wobei ersteres möglicherweise seismischen Ereignissen, letzteres interseismischen Phasen einer andauernden Deformation zugeschrieben werden können. Die in den mikroskopischen Störungsbrekzien beobachteten Foliationen bestehen aus faserigem Palygorskit, einem Mg-reichen Tonmineral, das während oder unmittelbar nach der Deformation neu gebildet wird. Im Gegensatz zur Verkeilung der Kornfragmente führt die Bildung von Palygorskit in der Störungsbrekzie zu Verformungserweichung und daher zur fort-dauernden Scherung eines spröden Deformationsbandes.

Röntgendiffraktionsanalysen von Störungsmaterial und Umgebungsgestein sowie energiedispersive Spektroskopie der mikroskopischen Störungsbrekzien ergaben, dass Palygorskit in Störungen aller Größenordnungen, nicht aber im Umgebungsgestein vorkommt. Berechnungen des chemischen Gleichgewichts anhand der Mineralogie des Umgebungsgesteins und verschiedenen Formationswässern der Region zeigten, dass Palygorskit im Gegensatz zu dem im Umgebungsgestein vorhandenen Chlorit die stabile Phase ist. Daraus lässt sich eine Chlorit-konsumierende Reaktion ableiten, die an die Deformation gebunden ist.

Die in den Aufschlüssen gemessenen Harnische und spröden Deformationsbänder sind in synthetischen und antithetischen Störungsflächen orientiert und werden als Einzelstörungen eines Riedelsystems interpretiert. Die Brüche können zu einem Teil als initiale Dehnungsbrüche (Klüfte) parallel zu σ_1 , als Scherbrüche ohne Lineation interpretiert werden. Die grösseren kartierten Störungen zeigen einen regellos orientierten kataklastischen Kern und ein dichtes Netzwerk von Brüchen, Harnischen und spröden Deformationsbändern in den Randzonen. Die einzelnen Störungen sind wahrscheinlich selten länger als ein Kilometer, bilden aber weiter ausgedehnte Störungszonen innerhalb derer die Gesamtverformung auf mehrere kleinere, fiederartig oder konjugiert angeordnete Störungen verteilt ist. Die Orientierung der kartierten Strukturen ist durchgängig subvertikal. Dabei sind N-S bis NNE-SSW streichende Störungen sinistral und WNW-ESE bis NW-SE streichende Störungen dextral ausgebildet. Der aus den Strukturen und ihrer Kinematik bestimmte Paläostress zeigt eine im ganzen Arbeitsgebiet einheitliche NW-SE bis NNW-SSE gerichtete Kompression und entsprechende NE-SW bis ENE-WSW gerichtete Dehnung. Da Überprägungskriterien keine Systematik aufweisen, ist die Deformation als einphasig anzusehen.

Die Verfügbarkeit einheitlicher Neuinterpretationen aller seismischen Linien (durch verschiedene Autoren und Koautoren) ergibt ein differenziertes Bild der Störungen im Untergrund, vor allem innerhalb der mesozoischen Einheiten. Im Gegensatz zu den an der Oberfläche vorherrschenden Störungen mit N-S und WNW-ESE Streichen finden sich im Mesozoikum vor allem Störungen mit N-S und NE-SW Streichen, und nur untergeordnet solche mit WNW-ESE Streichen. Im Profilschnitt weisen die Störungen vorwiegend Halbgrabengeometrien auf, doch ist ihr relativer Versatz zum Teil aufschiebend. Im Hinblick auf das südostwärts gerichtete regionale Einfallen der

Schichten können einige der N-S streichenden Störungen auch als sinistrale, die WNW-ESE streichenden Störungen als dextrale Blattverschiebungen interpretiert werden. All diese Störungen wurzeln mit listrischen Verflachungen in den triassischen Evaporiten. Die N-S und NE-SW streichenden Störungen werden als ältere, durch E-W und NW-SE gerichtete Dehnung entstandene Abschiebungen interpretiert, die während der späteren NW-SE gerichteten Kompression invertiert beziehungsweise reaktiviert wurden. Bereits die ältere Dehnung ist entlang der triassischen Evaporite von den tieferen Stockwerken entkoppelt.

Die Deformationszonen aus der Oberflächenkartierung und die Störungen aus den Interpretationen seismischer Linien werden in einem dreidimensionalen kinematischen Modell des Arbeitsgebiets zusammengefasst. Nach diesem Modell verteilt sich die Deformation in der Horizontalen auf mehrere konkrete Blattverschiebungs- und Einengungszonen. In der Vertikalen ist sie geprägt durch die kinematische Entkoppelung des tertiären und mesozoischen Deckgebirges vom Grundgebirge entlang des triassischen Evaporithorizonts, sowie durch eine Teilentkopplung zwischen den vorstrukturierten mesozoischen Einheiten und der nicht vorstrukturierten tertiären Molasse. Die Teilentkopplung zwischen mesozoischen Einheiten und der tertiären Molasse ist im internen Teil des Arbeitsgebiets vollständig ausgebildet und durch die basale Abscherung der Subalpinen Molasse bedingt.

Die NW-SE gerichtete Kompression findet nach der Molassesedimentation statt und setzt mit der Bildung des Vorland-Falten- und Überschiebungsgürtels im oberen Miozän ein. Entsprechend der Herdmechanismen rezenter Erdbeben dauert sie bis heute an. Die E-W und NW-SE gerichtete Dehnung der mesozoischen Einheiten ist wahrscheinlich paläogenen Alters.

ACKNOWLEDGEMENTS

I gratefully acknowledge the Etablissement Cantonal d'Assurance des Bâtiments (ECAB), Fribourg for financing this work, and especially their former director Dr.h.c. Pierre Ecoffey whose interest in the regional geology made this support possible. I sincerely thank PD Dr. Jon Mosar for offering me the opportunity to work together with him on this project.

I am grateful to the following persons for their help and stimulating discussions on scientific questions: Prof. Dr. Jürgen von Raumer for help with the microscopy and mineralogy, Prof. Dr. Bernard Grobéty for help with the mineralogy, Dr. Anna Sommaruga for help with the seismic interpretation and Dr. Herfried Madritsch for joint field trips.

I would like to thank Dr. Ildiko Katona-Serneels for the XRD analyses, Christoph Neururer for the EDS analyses, Naomi Vouillamoz and Martinus Abednego for their help with the database, and Lisa Nommensen for her help with the English language.

Last but not least I want to thank my wife Lisa Nommensen for her patience and encouragement, and my little son Rasmus for the many enjoyable hours we spent together before and after work.

1 - INTRODUCTION

1.1 SCOPE OF THE STUDY

A series of small and medium-sized earthquakes was recorded in recent years near the city of Fribourg, situated in the densely populated foreland of the Swiss Alps. The localisation of these earthquakes reveals a N-S alignment and points to the existence of an active tectonic structure. The question arose whether earthquakes in the region could be potentially larger and cause substantial damage to infrastructure and population. It turned out that little is known about subsurface deformation in the region. In collaboration with different partners from the industry a research program was founded at the University of Fribourg with the aim to investigate the tectonic evolution and neotectonic activity of the western Swiss Molasse Basin. The work presented here is part of this study.

The objective of this work is to improve the knowledge of the tectonic evolution by detailed investigation of the deformation in the field. It is the first systematic structural mapping approach that was applied to a region in the Molasse Basin of Switzerland (Canton Fribourg area). The mapped structures were analysed with microscopic and geochemical methods in order to characterise deformation conditions. The stress field was calculated from the collected orientation and kinematic data, and a deformation history established. The surface structures are compared with structures from the subsurface Mesozoic and basement levels. A 3-D model of the fault network was established and the nature of kinematic coupling of the different depth levels discussed. The results of these investigations will help to find possible active structures and to characterise their size, mechanics and potential rupture magnitude.

The manuscript is organized in five parts. The first part (chapter 1) is an introduction to the state of knowledge of the northern Alpine foreland of Switzerland in terms of structural geology, tectonic evolution, deep

structure, paleostress- and recent state of stress and its seismotectonics. The second part (chapter 2) describes tectonic microstructures of the Molasse sandstone, their mechanical characteristics and inferences for deformation conditions. The third part (chapter 3) reports the occurrence of palygorskite as a newly-formed clay mineral in fault gouges in the region. The fourth part (chapter 4) summarises the mapped surface structures and presents the calculated paleostress field as well as the surface network of deformation. In the fifth part (chapter 5) the surface structures are compared to subsurface structures and a kinematic model for the region is proposed.

1.2 GEOGRAPHIC LOCATION AND SETTING

The Molasse Basin represents the northern Alpine foreland basin. It extends from Vienna in the east to Savoy south of Geneva in the West, following the northern rim of the Alpine chain for about 700 km. Its total width changes along-strike, as well as its tectonic position. While the width of the basin reaches 130 km in the eastern part, it decreases to about 50 km in central Switzerland and 30 km in western Switzerland. It completely wedges out south of Geneva between the Jura Mountains and the Subalpine chains of the French Alps (figures 1.1, 1.3). In central and western Switzerland, the Molasse Basin is tectonically linked to the Jura Mountains fold-and-thrust-belt that developed to its north with remnants of Molasse sediments preserved in its synclines. East of central Switzerland (i.e. east of the eastern Jura Mountains termination) the Molasse Basin rests on the more or less undeformed European foreland of the Alps.

The western Swiss Molasse Basin covers the area of the western part of the “Mittelland“ between the cities of Bern and Geneva, the foothills of the geographic Alps and the southeastern edge of the Jura Mountains. It is generally known as the Plateau

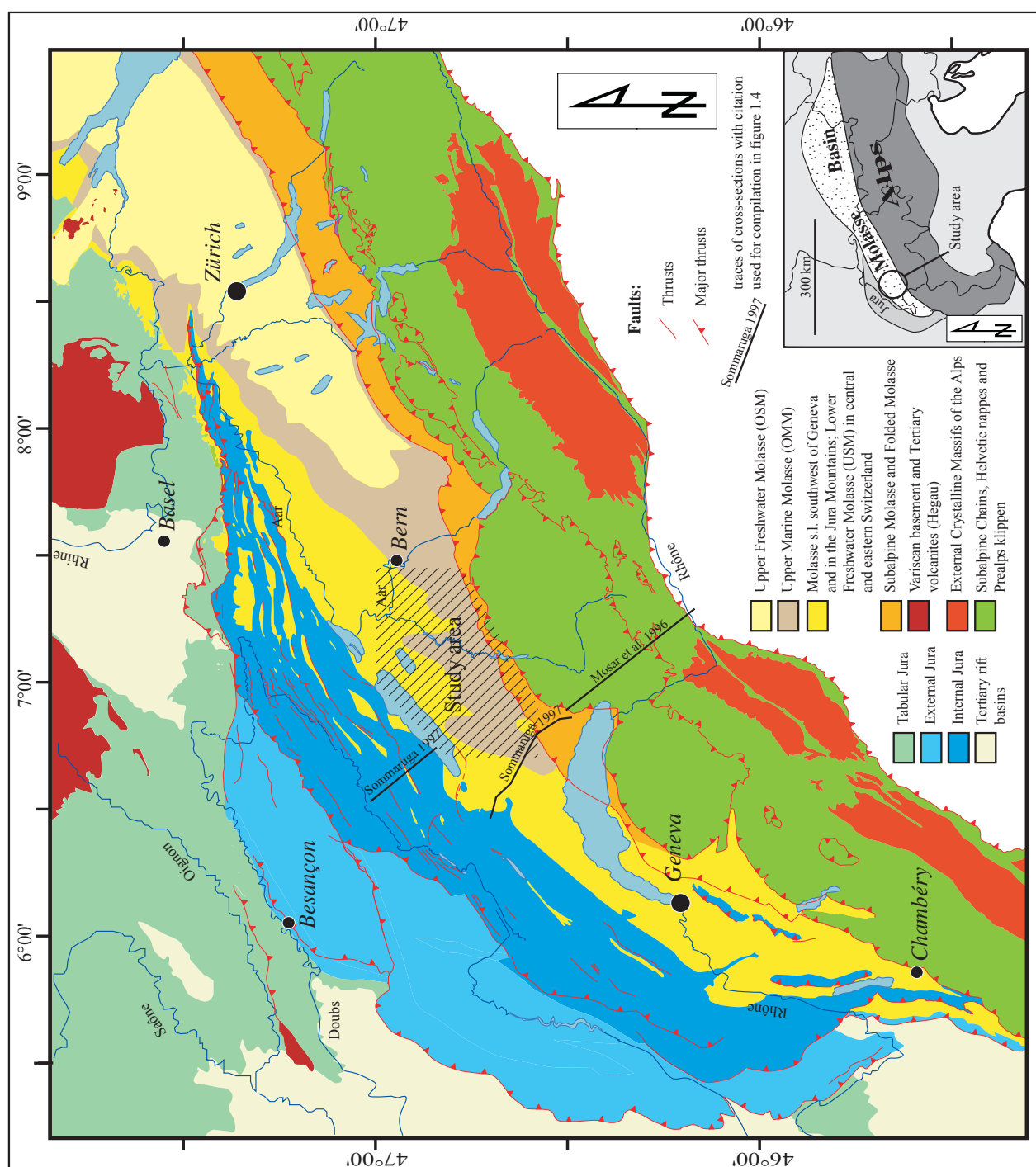


Figure 1.1: Geologic-tectonic overview of the Swiss Molasse Basin and adjoining areas with location of the study area.

Molasse as opposed to the Subalpine Molasse, which consists of a series of closely imbricated thrust slices running along the northern edge of the geographic Alps (figures 1.1, 1.3).

Between the folds and thrusts of the Subalpine

Molasse and the Jura Mountains, the sequences of the Plateau Molasse are relatively un-deformed. Gentle anticlines and synclines, as well as some strike-slip faults, characterise the geologic landscape. Multiple Pleistocene glaciations formed the landscape and left a widespread cover of glacial deposits.

1.3 GEOLOGY OF THE SWISS MOLASSE BASIN

The northern Alpine Molasse Basin is a typical peripheral foreland basin, formed by flexing of the European crust under the load of the Alpine thrust wedge (Karner & Watts 1983, Pfiffner 1986, Allen et al. 1991). It initiated in early Tertiary times when the Alpine orogenic wedge started to incorporate the European passive margin (Pfiffner 1986, Kempf & Pfiff-

ner 2004). Subsequent convergence of the Adriatic and European domains until Pliocene times led to a further northward and northwestward migration of the deformation front and with it of the peripheral foreland Molasse Basin. Because of this basin migration, foreland deposits became incorporated into the Alpine nappe pile, while younger deposits progressively on-lapped onto the Mesozoic of the European crust with an increasing time discordance (Homewood et al. 1986, Pfiffner 1986, figure 1.2).

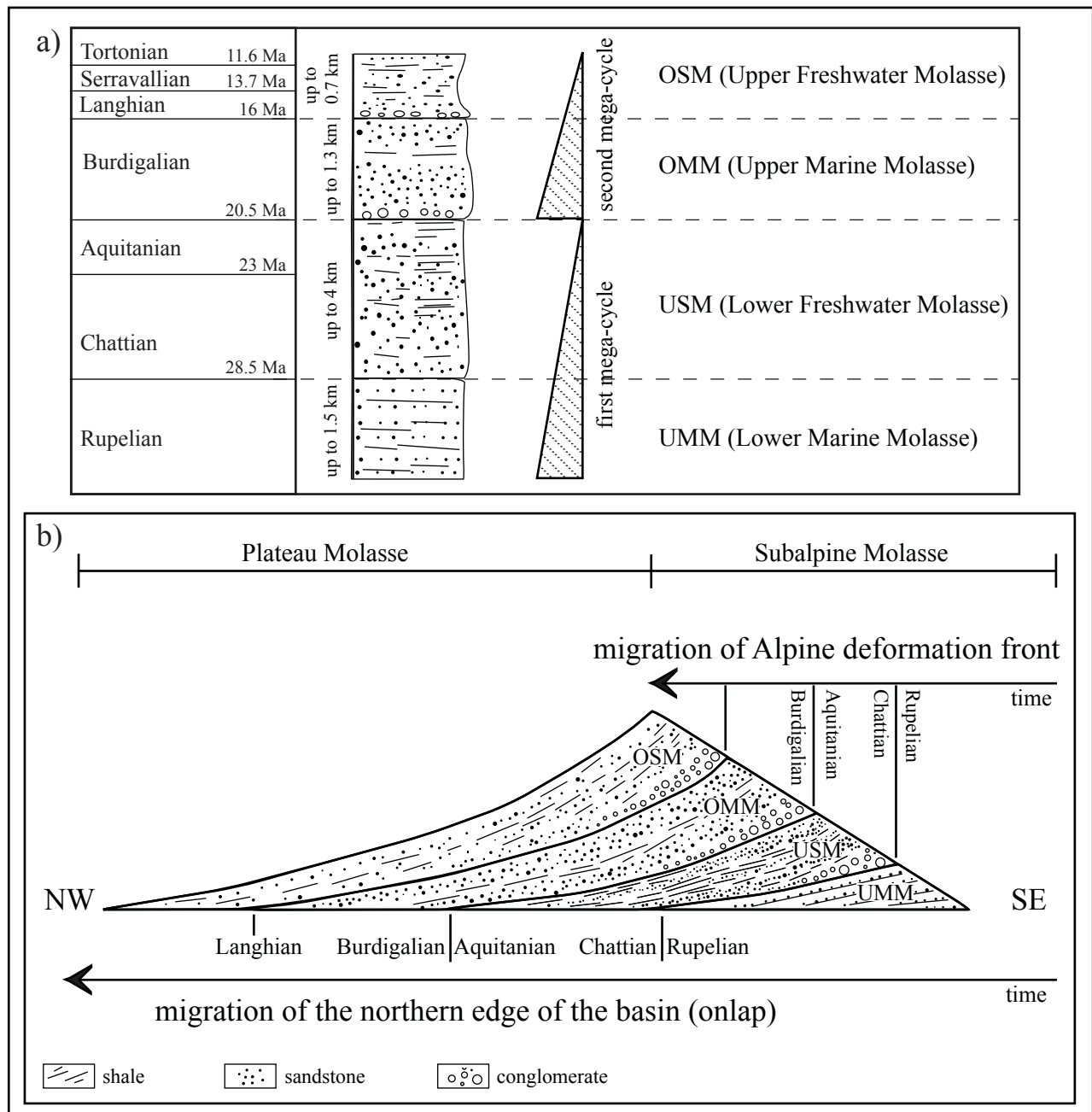


Figure 1.2: a) Simplified stratigraphic column of the Molasse units. b) Sketch to illustrate sedimentation in the geodynamic context of the migrating northern alpine foreland basin prior to formation of the Jura Mountains. The sedimentary prism of the Molasse lithologies is given after restoring any erosion and tectonics. Thicknesses in the stratigraphic column after Matter et al. (1980).

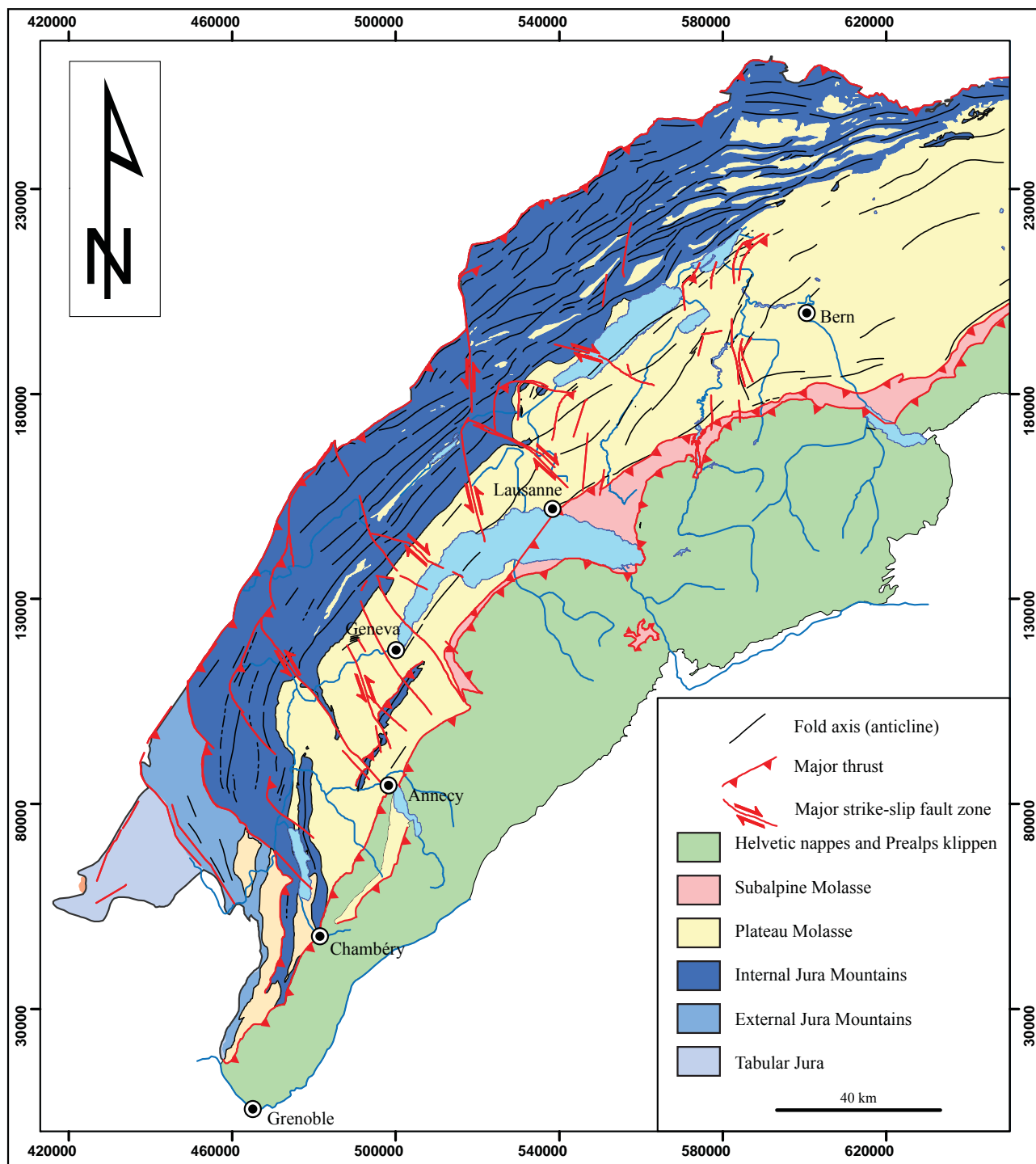


Figure 1.3: Tectonic overview of the western Swiss Molasse Basin.

During foreland basin evolution, an early underfilled Flysch-type stage can be distinguished from a later overfilled Molasse type stage with the transition occurring in the lower Oligocene when deposition switched from deep marine (North Helvetic Flysch) to shallow marine (Lower Marine Molasse) (Allen et al. 1991, Sinclair 1997). During the upper Oligocene and lower Miocene, sedimentation remains clastic and oc-

curs in two shallowing-up megacycles (Lower Marine Molasse to Lower Freshwater Molasse, Upper Marine Molasse to Upper Freshwater Molasse) (Trümpy 1980, Homewood et al. 1986, figure 1.2). The sedimentary detritus was shed from the rising Alps in the south and the rocks are dominated by proximal conglomerates and distal sands and shales (Heim 1919).

Sedimentation ceased in the uppermost Miocene. This event marked the onset of considerable erosion in central and western Switzerland. The estimated amount of erosion ranges between 1 km (Monnier 1982) and 4 km (Kälin et al. 1992), based on vitrinite reflectance (Schegg & Leu 1998), porosity studies (Kälin et al. 1992), illite crystallinity (Monnier 1982) and apatite fission track cooling ages (Schegg & Leu 1998, Cederbom et al. 2004, Mazurek et al. 2006). Today the Lower Freshwater Molasse and the Upper Marine Molasse are the main near-surface units in the western Swiss Molasse Basin, while outcrop of the Upper Freshwater Molasse is still widespread further east (figure 1.1). Due to their contemporaneity, erosion was considered to have been initiated by the formation of the Jura Mountains foreland fold-and-thrust belt north of the western Molasse Basin (Kuhlemann & Kempf 2002). The uplift that resulted from the passive transport of the Molasse in the rear of the Jura Mountains is, however, not sufficient to account for the overall amount of erosion (Pfiffner et al. 1997), and additional causes are likely. One such cause could be enhanced exhumation of the whole Alpine wedge forced by a change in climate toward higher precipitation and hence higher denudation rates (Cederbom et al. 2004). Alternatively, a switch from an eastward-oriented drainage system to a drainage system oriented towards the Atlantic could have caused a drop in base level followed by a rapid increase in erosion in the western Alpine foreland (Schlunegger & Mosar 2010).

1.4 TECTONIC EVOLUTION OF THE WESTERN SWISS MOLASSE BASIN

Different opinions exist with regard to the tectonic evolution of the western Swiss Molasse Basin and the adjacent Jura Mountains. The early Tertiary development as a peripheral foreland basin of the Alpine orogeny is widely accepted. However, the mechanics of the later deformation events in the region and their effect on the western Swiss Molasse Basin are still debated. A series of tectonic processes may have influenced the western Swiss Molasse Basin. These include the Eocene-Oligocene rifting of the Rhine-Bresse graben system, the late Miocene folding and thrusting of the Jura Mountains, and possible ongoing shortening of the Alps until recent times, and the related exhumation/uplift of the External Crystalline Massifs. Inherited structures of the former European passive margin such as Permo-Carboniferous grabens, as well as the distributions of Triassic evaporates, may play an important role in the localisation of deformation

during these events.

1.4.1 Inception and evolution of the Northern Alpine Foreland Basin

Peripheral foreland basins in general are asymmetric basins that form in front of an advancing orogenic wedge by the flexing of continental lithosphere under the load of this wedge (Dickinson 1974, Beaumont 1981, Jordan 1981). In contrast to the subduction of dense oceanic lithosphere, the less dense continental lithosphere is flexed and successively incorporated into the orogenic wedge. The northern Alpine foreland basin was formed during flexing of the European lower plate in early Tertiary times when the final collision of Adria and Europe occurred (Kempf & Pfiffner 2004).

The most important process during the subsequent early Tertiary evolution of the basin is the transition from an underfilled flysch-type basin to the overfilled Molasse Basin. While the former is a deep and narrow trough, the latter forms a broad and shallow basin (Allen et al. 1991, Sinclair 1997). This different geometry reflects the flexural properties of the basin's substratum (Beaumont 1981), i.e. the European lithosphere. Rheologic models of continental lithosphere show that the amplitude of the flexed crust may depend on convergence velocity as well as on the thickness of the crust (Beaumont 1981). In the case of velocity dependence, the transition from the Flysch to the Molasse Basin is caused by a decrease in convergence rate and an increase in isostatic rebound of the Alps. The latter would increase their elevation and intensify their erosion, leading to overfill of the basin (Sinclair & Allan 1992). Alternatively, if the amplitude of flexure is dependent on the thickness of the flexed crust, the switch from the Flysch-type to the Molasse-type basin would occur at the same time as the migrating foreland basin reaches the transition from the thin oceanic lithosphere to the continental lithosphere of the passive margin, and hence coincide with the onset of continental collision with the European plate (Allan et al. 1991). In case of the northern Alpine foreland basin one or both of these causes are applicable.

1.4.2 Influence of the Upper Rhine Graben Rift

The Upper Rhine Graben (URG) is a 300 km long, NNE-SSW striking graben structure that forms the central and most prominent part of the European

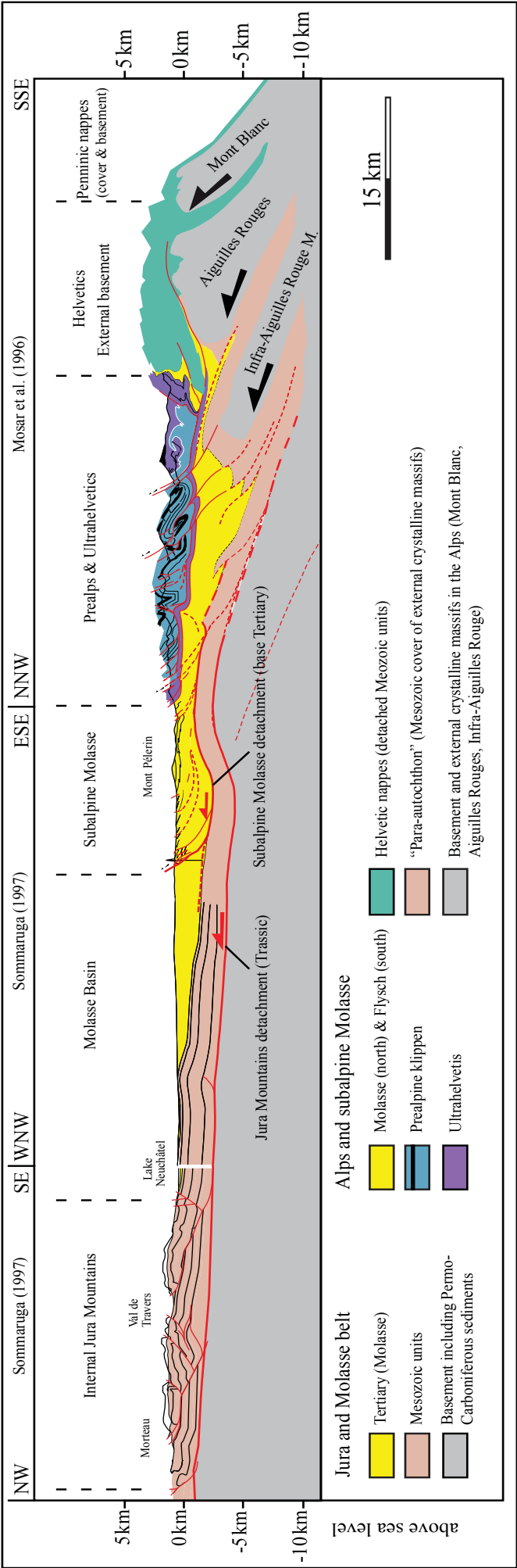


Figure 1.4: Compiled cross-section of the external (Helvetic) Alps, the Molasse Basin and the Jura Mountains. See figures 1.1 and 1.3 for the trace of the cross-section. Mesozoic units of the European passive margin are subdivided according to facies differences in: Jura Mountains (with sub-units), the cover of the external crystalline massifs and the detached Helvetic nappes. The position of these boundaries is artificial as they are largely unknown underneath the Molasse Basin and likely gradual in nature. Note the different position of the two most external detachments at the base of the Subalpine Molasse and underneath the Jura Mountains. Modified after Sommaruga (1997) and Mosar et al. (1996). See figure 1.1 for the traces of cross-sections used for compilation.

Cenozoic rift system (ECRS, Illies 1977, Ziegler 1992, Dèzes et al. 2004). In its southern parts, the URG spatially interact with the northern front of the Jura Mountains. Within the ECRS, the URG is connected towards west-southwest with the Bresse Graben via the Rhine-Bresse Transfer Zone (RBTZ) (Illies 1977, Ziegler 1992).

The URG initiated in the Eocene and mainly developed during the Oligocene (Schumacher, 2002), showing vertical offset of several kilometres in the southern part. The Miocene to recent tectonic history of the URG is generally dominated by the reactivation of border faults according to NW-SE compression, resulting in oblique left-lateral movement with a normal component (Schumacher 2002, Plenefisch & Bonjer 1997).

The concept of the existence of Upper Rhine Graben-related, NNE-SSW trending basement faults extending southwards into the Molasse Basin has been proposed repeatedly (e.g. Revertera, 1927, Plancherel 1979, Rybach et al. 1980, Kastrup et al. 2007). Such southwards extended fault zones would influence the tectonic and neotectonic evolution of the western Molasse Basin into which they project. This hypothesis has resurfaced recently in the frame of studies on seismicity in Switzerland (Kastrup 2002, Kastrup et al. 2007) and became highly topical as a key parameter in earthquake magnitude assessment (ENSI 2010).

Paleogeographic studies of sedimentary facies (Berger et al. 2005a, 2005b, Sissingh 1998) revealed Eocene rift-related conglomeratic fans at the southern boundary of the recent URG, suggesting rising topography and hence the southern end of the rift-valley. From their sedimentological studies of Mesozoic rocks in the northern Jura Mountains, Allenbach & Wetzel (2006) concluded that the URG-RBTZ-Bresse Graben geometry is an inherited Paleozoic structure, reactivated at several times during Earth history and responsible for the formation of the recent framework. Ziegler (1992) related the spatial distribution of the structures of the ECRS to the distribution of Permo-Carboniferous troughs. In fact the RBTZ was shown to be a multiply reactivated zone of such late Paleozoic graben structures (Madritsch et al. 2009). This geologic evidence indicates that the URG rifting was

linked to the Bresse graben via the RBTZ rather than continuing southwards.

1.4.3 The folding of the Jura Mountains

The folding of the Jura Mountains and the associated jump of the Alpine orogenic front from south of the western Swiss Molasse Basin to north of the Jura Mountains began in the uppermost Miocene (Burkhard & Sommaruga 1998, Naef 1985, Laubscher 1987). Concerning the mechanics of the Jura folding and thrusting, two conflicting hypotheses have been proposed: a model of autochthonous in-situ folding and the Fernschub hypothesis (distant-push hypothesis, figure 1.5). In addition a model in which folding of the cover units is controlled by strike-slip faulting in the basement has been proposed (Pavoni 1961). Currently the Fernshub hypothesis is the most widely accepted one.

1.4.3.1 In-situ folding model

The in-situ folding model assumes that deformation – folding and faulting - was caused by faulting in the basement (Aubert 1959). Other authors have linked these basement faults to inversion of pre-existing older normal faults in the basement (Ziegler 1982, Pfiffner et al. 1997). Gorin & Signer (1993) did not find evidence for a detachment in their seismic interpretations of the Vaud and Geneva area. Instead they pointed out many geometric similarities of young and inherited structures to confirm their in-situ folding model. The inversion of small Permo-Carboniferous grabens is thought to push up the smooth anticlinal structures of the central and western Swiss Molasse Basin. Similar graben structures of greater extent were inverted, leading to the formation of deep-seated detachments in the basement underneath the Jura Mountains and to the deformation of the cover units including some local salt flows (Pfiffner et al. 1997). Oligocene synsedimentary normal faults were recorded in the central Molasse Basin by seismic surveys and interpreted as reaching down into the basement. Such normal faults had been the most widely used argument against the Fernschub hypothesis (Pfiffner et al. 1997). Since they would offset the Triassic evaporite

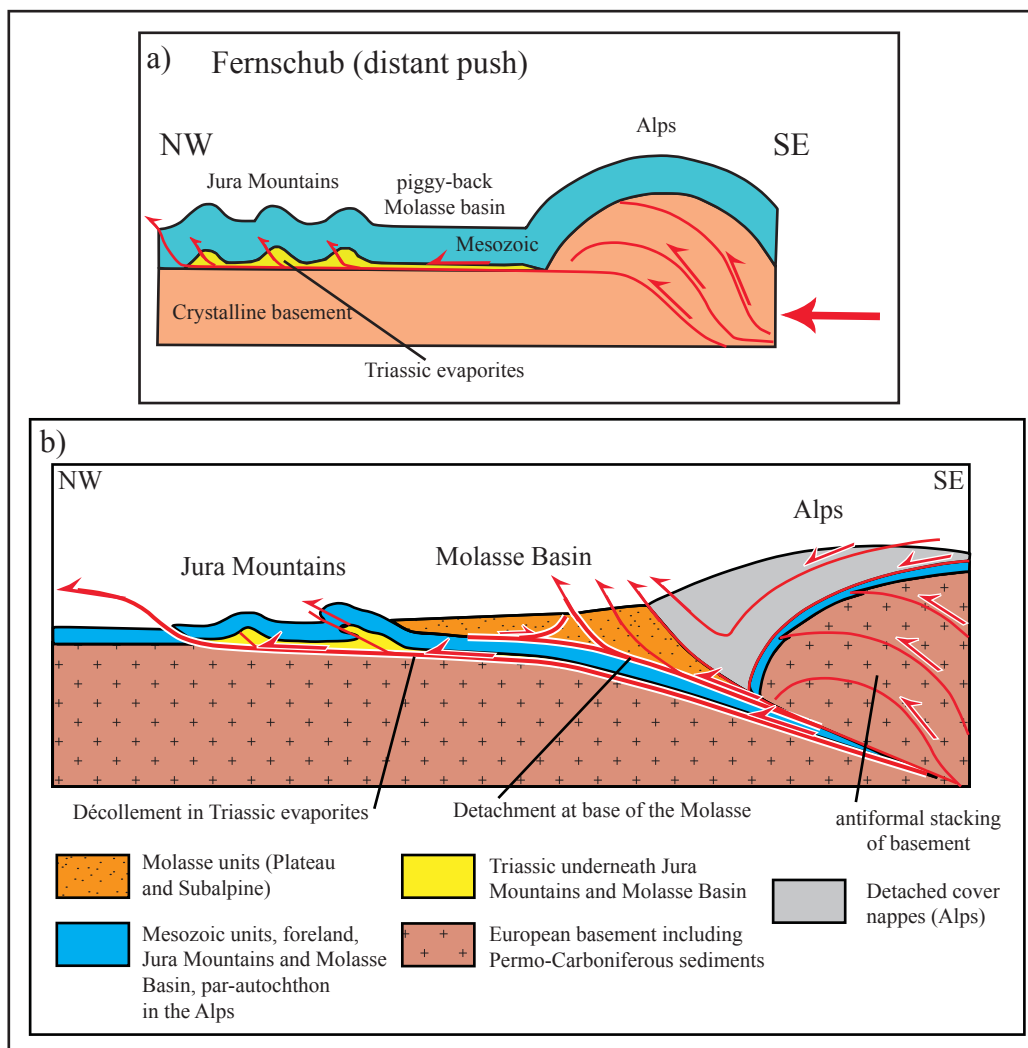


Figure 1.5: Sketches to illustrate a) the principle of the Fernschub hypothesis and b) of foreland deformation in the Swiss Alps. The deformation of the Jura fold-and-thrust belt took place over a décollement horizon in Triassic evaporites and originates due to a distant push of the Alps. Cover shortening in the Jura Mountains corresponds to basement shortening by antiformal stacking in the Alps. A second detachment is developed at the base of the Molasse units representing the basal thrust of the Subalpine Molasse.

horizon, they would not allow for a large detachment to develop as proposed by the Fernschub hypothesis.

1.4.3.2 *Fernschub hypothesis*

The Fernschub (distant-push) hypothesis (figure 1.5) was first proposed by Buxtorf (1916) from field and subsurface evidence and further developed by Laubscher (1961). The sedimentary cover sequences of the Molasse Basin and the future Jura Mountains became detached along Triassic evaporites and were pushed towards north and northwest. The result was the passive transport of the Molasse Basin and thin-skinned folding and thrusting of the Jura Mountains. The regional coexistence of Triassic evaporites and the Jura Mountains fold-and-thrust belt strongly sup-

ports the Fernschub hypothesis (Boigk & Schöneich 1974, Sommaruga 1997, figure 1.6). In addition, microstructural investigations of the evaporites in the hinterland of the Jura Mountains indicate high-strain deformation, evidence for large-scale decoupling in this horizon (Jordan 1992, 1994). Further support for the Fernschub explanation comes from considerations of balanced cross-sections showing that considerable displacement, implying décollement, is indeed required (Burkhard 1990, Boyer & Elliott 1982). Based on the interpretation of seismic data, Sommaruga (1997) argues that the thickness variations of the Triassic evaporites under the western Swiss Molasse Basin and the Jura Mountains are much higher than the differences in elevation of the top of the basement reflector. Therefore elevation differences of the sub-Triassic do not necessarily work as a barrier to large-

scale decoupling.

Based on these findings the Fernschub hypothesis is considered as the most reliable in this work

1.4.4 Consequences of the folding of the Jura Mountains for the Molasse Basin

The Fernschub hypothesis consequently includes passive transport of the Plateau Molasse along a distance that corresponds to the shortening in the Jura fold and thrust belt. As the latter decreases from the central Jura Mountains along-strike towards NE, the Plateau Molasse had to undergo differential amounts of transport, indicating clockwise rotation (Burkhard 1990). On scale of the Swiss Molasse Basin paleomagnetic data indeed show such clockwise

rotation (Kempf et al. 1998). Shortening estimations of the Jura Mountains and the Subalpine Molasse based on several restored cross-sections along-strike reveal strain partitioning between both fold-and-thrust belts (Burkhard 1990). The results show that shortening in the Subalpine Molasse increases from southwest towards northeast, while it decreases by the corresponding amount in the Jura Mountains. Burkhard (1990) concluded that shortening of both deformation belts occurred contemporaneously and that the intermediary Molasse Basin underwent right-lateral shear. Formation of the Jura Mountains fold-and-thrust-belt by northwestward compression alone was considered by Hindle & Burkhard (1999). They attributed the arc shape of the belt to strong strike-slip components in the limbs. In this view, no rotational deformation in the Plateau Molasse indenter is needed. In order to accommodate lower magnitudes of displacement in the limbs of the arc, Affolter & Gratier (2004) proposed a

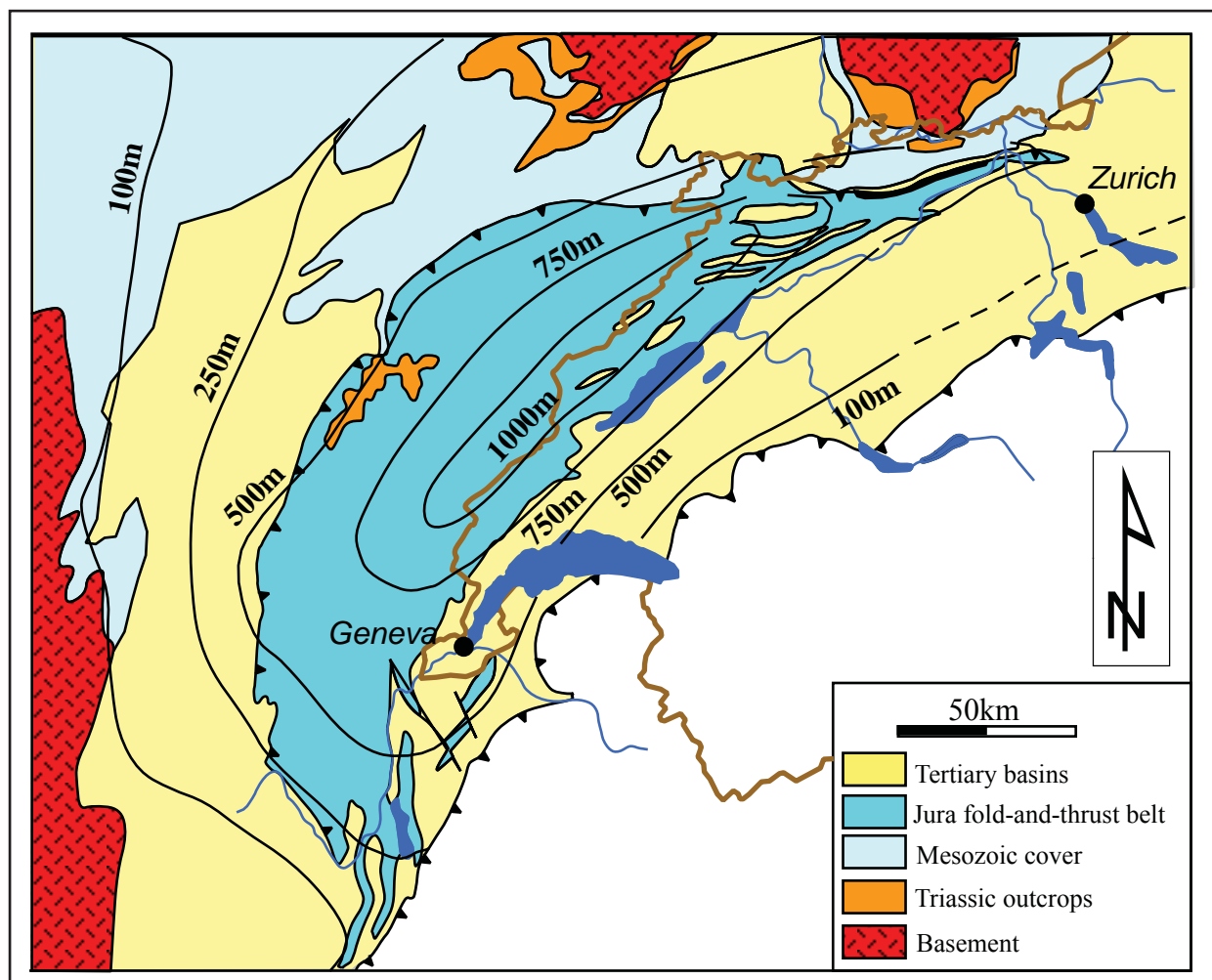


Figure 1.6: Isopachs (thickness in meters) of the Triassic layers (without Buntsandstein) in the Jura Mountains and adjoining areas. The sketch map shows the spatial coexistence of the Jura fold-and-thrust belt and its Molasse hinterland with a thick Triassic series including the evaporites. (After Sommaruga (1997) and references therein).

relative clockwise rotation of the northeastern hinterland and a relative counter-clockwise rotation of the southwestern one.

1.4.5 Strike-slip faulting in the Jura Mountains

Syn- to post-folding strike-slip faults are prominent structures in the central and southwestern Jura Mountains, crosscutting the fold belt (Heim 1915, Aubert 1959, Sommaruga 1997). They appear along-strike of the chain, forming conjugate networks of individual fault zones several kilometres in length that also transect the transition regions between Jura Mountains and Plateau Molasse (Jordi 1951, 1990, Gorin et al. 2003). They increase in size toward the southwest.

South of Geneva, the Vuache fault zone transects the entire internal Jura Mountains and the sub-basins of the narrow Molasse. It is described as a NW-SE-striking tectonic element, repeatedly active since the Mesozoic. The fault zone shows a top-to-the-SW reverse movement in the early Miocene, and a left-lateral strike-slip movement from the upper Miocene onwards (Blondel et al. 1988). Recent seismicity demonstrates ongoing tectonic activity along the Vuache fault zone (Sambeth & Pavoni 1988, Thouvenot et al. 1998, Courboux et al. 1999). The focal planes of earthquakes change gradually from a left-lateral strike-slip to a thrusting mechanism as the fault zone bends into the frontal thrust system of the internal Jura Mountains (Sambeth & Pavoni, 1988). Similarly, the thrust between internal and external Jura was interpreted in its southern parts as a lateral ramp with left-lateral movement, induced by the basement-involving Culoz fault (Philippe 1995). The same author considers this southern limb of the Jura arc to be a complex transfer zone between the Jura Mountains and the Subalpine Chain, marking the southern rim of the Triassic evaporites and hence the limit of thin-skinned décollement tectonics.

1.4.6 Deformation of the western Swiss Molasse Basin

The formation of the Jura Mountains by décollement tectonics brought the western Molasse Basin into its wedge-top position behind the orogenic front (Willett & Schlunegger 2010). This tectonic position changes towards the East. In eastern Switzerland, Germany and Austria the Molasse Basin re-

mains in its foreland basin position s.s. with no Alpine deformation front located north of the Subalpine Molasse. South of Geneva, ramp anticlines in the underlying Mesozoic units, such as the Salève anticline or the Gros Foug anticline, divide the Molasse Basin into sub-basins (Gorin & Signer 1993). These sub-basins narrow southwards to synclines in the region of the Jura Mountains - Subalpine Chains transition. In the same region synsedimentary growth of anticlines during the deposition of the Upper Marine Molasse was documented (Beck et al. 1998), indicating shortening to be active prior to décollement tectonics, which are generally thought to post-date the sedimentation of the Upper Freshwater Molasse.

The western Swiss Plateau Molasse represents an area of little shortening between the folds and thrusts of the Jura Mountains and the Subalpine Molasse (figures 1.1, 1.3, 1.4). Its internal structure is dominated by low amplitude folds and some strike-slip faults. The folds trend SW-NE, parallel to the basin axis, except in the region between Fribourg and Bern where the orientation of fold axes bend from SW-NE to N-S (Kopp 1946). This bending has been termed the Fribourg zone (“Querzone von Freiburg”) by Schuppli (1950). In the following it will, however, be termed the Fribourg structure in a more general sense, in order to not confuse it with a zone of faults in the Mesozoic units situated in the eastern part of the Fribourg structure for which the term Fribourg zone was recently widely used (Mosar et al. 2011).

The regional structural configuration at the southwestern termination of the Molasse Basin and in the transition area between Molasse Basin and Jura Mountains, as described by various authors, indicates a closely related tectonic evolution. It seems reasonable to assign both mega-units to one tectonic unit, representing the foreland fold-and-thrust belt of the central Alps.

1.4.7 The Subalpine Molasse

The Subalpine Molasse represents a fold-and-thrust belt of deformed Molasse units running parallel to the Alps at the southern edge of the undeformed Molasse (figures 1.1, 1.3, 1.4). It changes along-strike from a narrow band of imbricates in the southwest to a broad fold belt in the east and vanishes towards the eastern reaches of the Molasse Basin.

The youngest stratigraphically dated thrust of the Subalpine Molasse is associated with the Hornbühl

Melange located near Luzern, and was active until mid- to late Miocene times (Homewood et al. 1986). Shallowly inclined thrusts of Subalpine Molasse as well as Helvetic nappes and Prealpine nappes further south, both cutting steeper imbricates of the Subalpine Molasse, are known from several localities (Trümpy 1980) and imply young, out-of-sequence thrusting. Recent studies of apatite fission track cooling ages reveal movement along thrusts in the Subalpine Molasse of central Switzerland after 5 Ma (von Hagke et al. 2010). Subsidence-uplift estimations based on clay mineralogy of borehole sections underneath the Subalpine Molasse basal thrust indicate that considerable erosion has taken place prior to thrusting (Monnier 1982). If thrusting of the Subalpine Molasse post-dates erosion of the Plateau Molasse, it has to post-date deposition of the Upper Freshwater Molasse plus the time span of erosion. It would then probably be attributed to the uppermost Miocene or Pliocene.

East of central Switzerland, the thrust front of the Subalpine Molasse forms the actual Alpine deformation front and is characterised by triangular structures with a basal blind thrust and subsurface stacking (Berge & Vial 2005, Müller et al. 1988, Vollmayr & Wendt 1987). Such structures are also reported locally for the western Molasse Basin (Vollmayr & Wendt 1987), where the thrust front represents the border between the Alpine nappes and their foreland fold-and-thrust belt formed by the Jura Mountains and the western Molasse Basin.

Whereas the detachment of the foreland fold-and-thrust belt runs along the Triassic evaporates near the base of the Mesozoic units and above the basement, it is located at the base of the Tertiary Molasse above the Mesozoic units in the case of the Subalpine Molasse (figures 1.4, 1.5).

1.4.8 The Jura Mountains-Molasse Basin-Alps connection

The different models for the Jura Mountains deformation also require different models for the Jura Mountains - Molasse Basin - Alps connection. Especially the Fernschub hypothesis needs to explain the causes of the distant push. In contrast to the in-situ folding model, it further requires a location where basement shortening, equivalent to the shortening of the Mesozoic units in the Jura Mountains, has taken place. In an early interpretation, Laubscher (1961) proposed gravitational gliding of the cover sequence from the rising Alps as a possible mechanism. Up-

lift of the external crystalline massifs, either isostatic (Neugebauer et al. 1980) or by thickening due to distributed internal flow mechanisms (Marquer 1990), was considered as the possible cause for gravitational gliding of the foreland sequences. However, Burkhard (1990) argues that there are not enough extensional features to be found in front of the Aar Massif to explain the Jura folding by gravitational gliding. Boyer & Elliott (1982) established the idea of the basal detachment being rooted somewhere under the Alps. This model accommodates basement shortening by antiformal stacking and associated uplift of the external crystalline massifs. Burkhard (1990) quantified shortening of the Jura Mountains and the Subalpine Molasse and related these thin-skinned foreland deformations to antiformal stacking of the external crystalline massifs according to the model of Boyer & Elliott (1982). He argues that the detachment has to be rooted underneath the frontal parts of the crystalline massifs as there is no potential provenance behind them to restore Jura Mountains and Molasse Basin to. Furthermore, in case of the Aar Massif, exhumation and associated back folding and steepening of the Helvetic nappes was still active at the time of folding of the Jura Mountains (Burkhard 1990). At the current state of research, the model of Boyer & Elliott (1982) seems to best explain strain partitioning between Alps, Molasse Basin and Jura Mountains.

1.5 THE TOP OF BASEMENT STRUCTURE IN THE WESTERN MOLASSE BASIN

The deep structure of the western Swiss Molasse Basin has been investigated by local borehole drilling, seismic surveys and by recording of potential magnetic field data. The top of basement topography is of special interest as a detailed knowledge of this could help discriminate between pre-Mesozoic and Mesozoic-to-present fault patterns, to recognize the distribution of Permo-Carboniferous grabens, and to better understand the links between inherited structures and post-Triassic tectonics.

Recent studies have confirmed that the top of basement in the western Swiss Molasse Basin is in general a smooth, SE-dipping surface (isopach maps in Valasek & Mueller 1997), as expected from the flexural basin model. It dips with an average angle of 1° - 3° (Sommaruga 1997, 1999). The top of the magnetic basement also corresponds to the overall geometry of a SW-NE-striking and SE-dipping surface (Klingelé & Mueller 1987). Detailed analyses show a number of deviations from this overall smooth SW-NE trend.

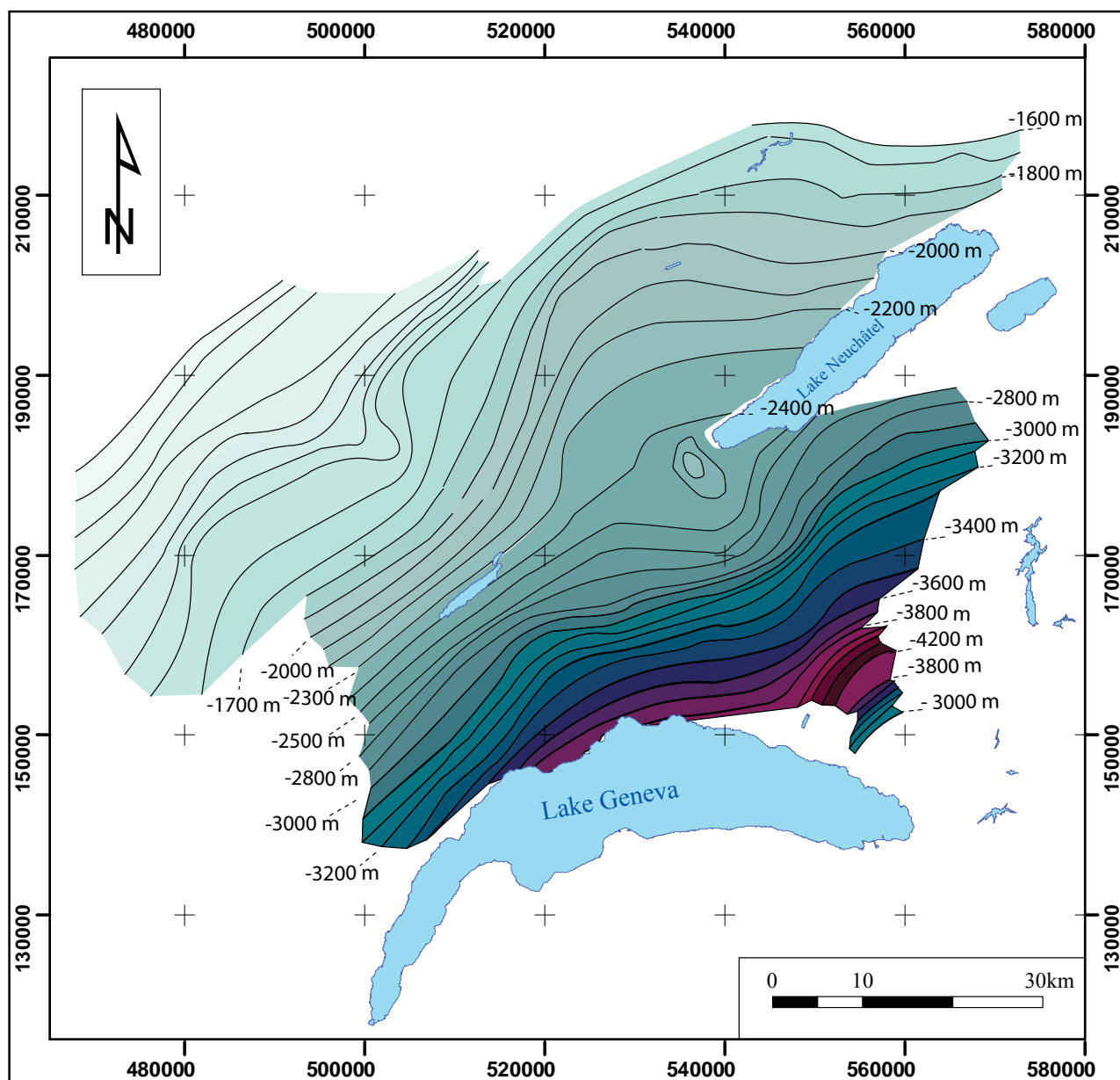


Figure 1.7: Map showing the depth of top of basement in the central Jura Mountains and western Swiss Molasse Basin. Isolines give depth in meters with reference to sea level. Modified after Sommaruga (1997).

The E-W strike of the basement in the Neuchâtel area (figure 1.7) is not in accord with the SW-NE strike of the overlying folds of the Jura Mountains and is an argument against the involvement of the basement in the cover deformation (Sommaruga 1997). In addition, the isoline map presented in Sommaruga (1997, modified in figure 1.7) shows a basement high in the Treykovagnes area, as well as an ascending top-to-basement south of the front of the Subalpine Molasse. The latter may also correspond to inversion of a Permo-Carboniferous trough (Gorin et al. 1993 Mosar et al. 1996). Late Paleozoic clastic sediments occur in the Alps (e.g. Trümpy 1980, Pfiffner 1993) and in

the subsurface of northwestern Switzerland (Diepold 1985, Matter 1987). They are also present beneath the Molasse Basin, but their precise extent remains disputed.

1.6 PALEOSTRESS AND RECENT STRESS IN THE WESTERN MOLASSE BASIN

Based on the orientations of fault planes and slickensides, the paleostress field for the central European platform (Bergerat 1987) and, in more detail, for the Jura Mountains (Homberg et al. 2002), shows

NW-SE compression during Miocene, with a local deviation in the Jura Mountains. Here compression axes change toward N-S in the eastern limb and E-W in the southwestern limb of the arc-shaped mountain belt. A similar stress field was also proposed by Laubscher (1972) based on the major trend of fold axes and faults (figure 1.8), as well as by Schrader (1988a, 1988b), who investigated solution pits in pebbles in conglomerates of the Molasse sediments (figure 1.8). The latter study is the only paleostress analysis in the Molasse Basin itself and it was restricted to conglomeratic ho-

rizons. For the Jura Mountains, paleostress was further estimated from stylolites (Plessmann 1972) and from calcite twins (Tschanz 1990) (figure 1.8). The established overall directions are also NW-SE in the central Jura (Tschanz 1990), and fan-shaped on the scale of the whole Jura belt (Plessmann 1972). Both authors additionally distinguished between a NW-SE direction in the highly deformed parts of fold belts and a N-S direction in intermediate plateau-like areas. Tschanz (1990) proposed that this N-S direction represents an older stress field preserved in the less deformed ar-

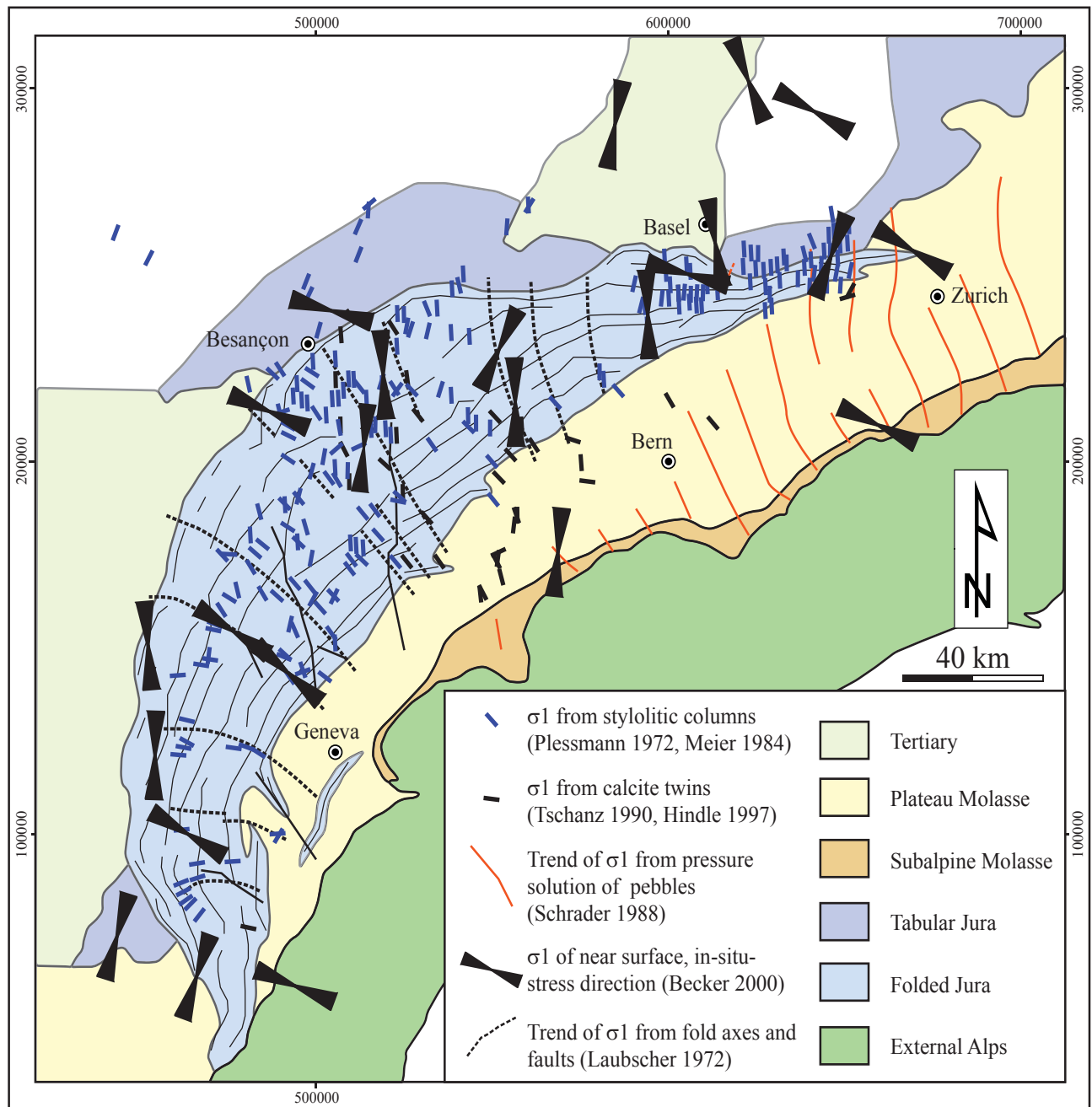


Figure 1.8: Paleostress in the Jura Mountains and the western Swiss Molasse Basin as revealed by different methods (after Becker 2000).

eas.

The recent stressfield has been investigated by in-situ stress measurements (figure 1.8), interpretation of focal mechanisms of earthquakes and by horizontal movements derived from GPS surveys.

Based on several in-situ stress measurements, the compiled world stress map (Zoback 1992) specifies an overall NW-SE direction of maximum horizontal stress in central and western Europe. In the northern foreland of the Alps, a deviation is recorded toward a maximum compression direction perpendicular to the strike of the Alps (Reinecker et al. 2010). However, since the Alpine chain curves, this is NNW-SSE to NW-SE in Switzerland as well. Detailed in-situ stress measurements for the Jura Mountains and parts of its Molasse hinterland show that the recent near-surface stress field deviates from both paleostress and from recent stress directions perpendicular to the Alps (Becker 2000, figure 1.8). While the latter fan around NW-SE compression, the detailed recent stress field can be subdivided into provinces of different stress directions (figure 1.8). The author assumed that thin-skinned deformation ceased and a new tectonic regime was established including both cover and basement. On the contrary, in-situ stress measurements in deep boreholes show NNE-SSW-directed stress above and NW-SE-directed stress below the Triassic detachment horizon, indicating the decoupling of near-surface stress from the stress field in the basement (Becker 1987).

The maximum horizontal stress derived from focal mechanisms of earthquakes (Kastrup et al. 2004) in the Alpine foreland of Switzerland is located within the NW-SE quadrant but rotating therein counter-clockwise from east to southwest. The fault plane mechanisms are dominantly strike-slip with an increasing component of thrust faults towards the southwestern termination of the Molasse Basin (Kastrup et al. 2004). The contemporaneous rotation of the maximum horizontal compressive stress into a nearly E-W orientation is in accordance with the E-W convergence in the adjacent Subalpine Chains of the French Alps, recorded by long-term GPS measurements (Jouanne et al., 1998).

1.7 SEISMOTECTONICS OF THE NORTHERN FORELAND OF THE CENTRAL ALPS

The European plate is internally structured by Paleozoic and Tertiary fracture zones including the

boundaries of ancient micro-plates in the Alps (Frisch 1979, Schmid et al. 2004). In the present plate tectonic configuration, the northern Alpine foreland is, however, situated in an intraplate setting. Both historically and instrumentally recorded earthquakes are characteristic for such a setting. Very low magnitude earthquakes are relatively frequent, up to magnitude 5 (local magnitude) earthquakes are rare but do occur, and both are mostly bound to known tectonic fracture zones (Appendix 1.1). According to paleoseismic records it is probable that earthquakes larger than magnitude 5 (local magnitude) reoccur at time intervals exceeding the historical record (Schnellmann et al. 2002, 2006, Strasser et al 2006).

In Switzerland, earthquake activity is generally considered to be characterised by shallow earthquakes in the Alps and by deep ones in the Alpine foreland (Pavoni 1977, Kastrup et al. 2004). It is, however, important to note that in the foreland shallow earthquakes do also occur, i.e. the defining characteristic is the absence of deep ones in the Alps.

The focal mechanisms of the recorded earthquakes in the Alpine foreland of Switzerland indicate predominantly strike-slip movement and minor normal faulting (Kastrup et al. 2004, Appendix 1.1). Reverse faulting is rare and restricted to a few events only located in the basement of the frontal parts of the Jura Mountains (Pavoni & Peterschmitt 1974, Bear et al. 2005).

The Alpine foreland of Switzerland was subdivided by Pavoni (1977) into three parts according to seismicity, a western (south and west of Bern-Solothurn-Basel), a central and an eastern part. In the western part of this subdivision, some of the earthquakes could be related to strike-slip fault zones located in the Jura Mountains.

Ongoing recording by a continuously improving network of seismic stations has refined Pavoni's picture. In the western Swiss Molasse Basin and the adjacent Jura Mountains, several additional small to medium earthquakes were recorded (figure 1.9). They are often shallow and tend to occur in specific clusters and lineaments, some of which are related to known tectonic structures. Some important examples of these earthquakes are:

- 1) The earthquake of Jeurre in the southwestern Jura Mountains. It is located in the sedimentary cover and shows a strike-slip mechanism according to NW-SE compression. The local magnitude was 4.4 (Pavoni

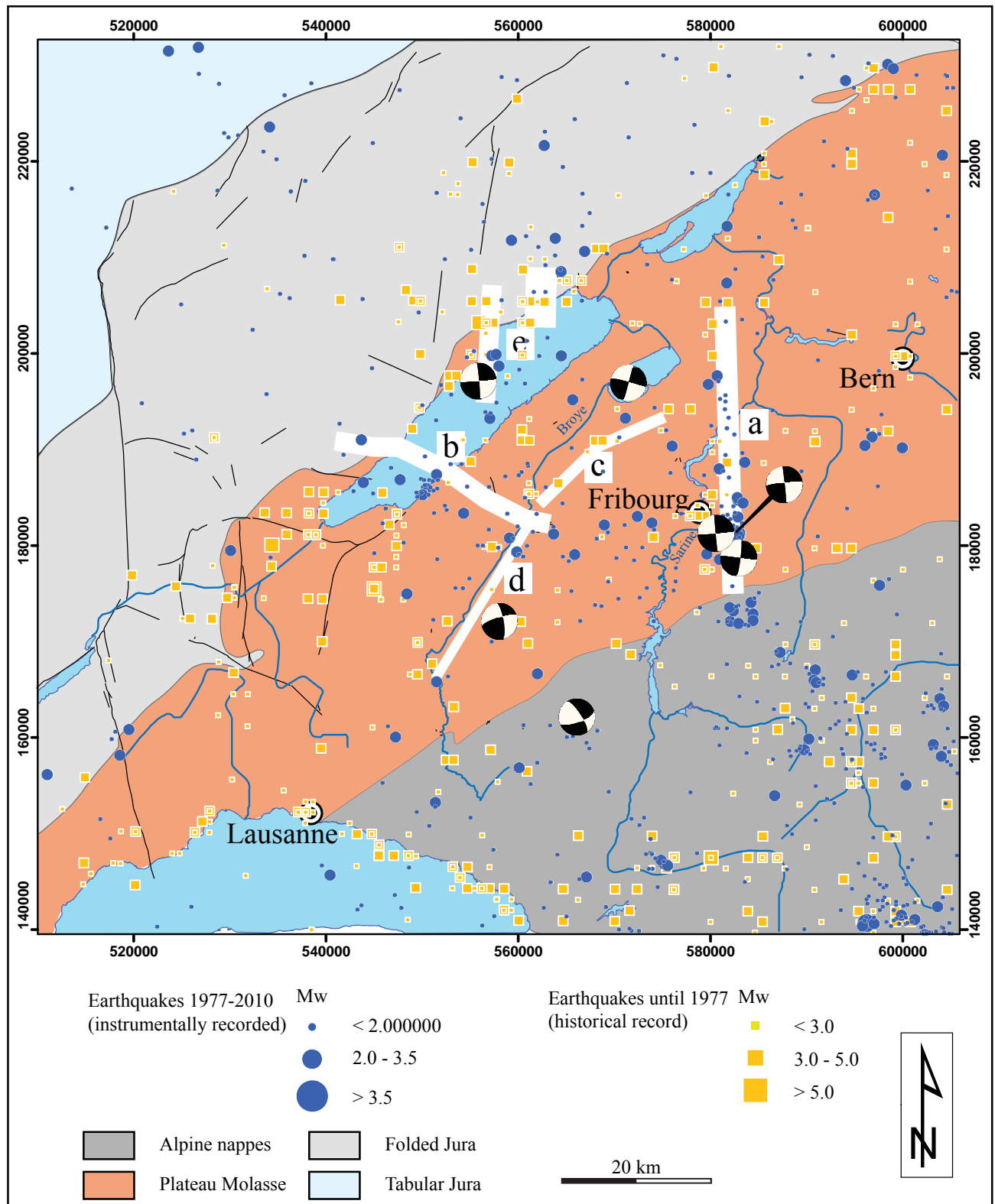


Figure 1.9: Tectonic map of the western Swiss Molasse Basin and the central Jura Mountains with epicentres of instrumentally and historically recorded earthquakes (SED 2010). A tendency of earthquakes to cluster along certain lineaments can be discussed (white bands). Such clusters occur along the N-S striking Fribourg structure (a), the La Lance fault zone (b), the Courtion structure (c), the Broye structure (d) and near Neuchâtel. Focal mechanisms are given for some larger earthquakes.

& Peterschmitt 1974).

2) The earthquakes that cluster in the region of Neuchâtel. These are not more than 2 km deep and show strike-slip mechanisms with a NW-SE compression direction. Local magnitudes are up to 3.2 (Deichmann et al. 2004, Bear et al. 2007).

3) The earthquakes in the area of Fribourg. These show a conspicuous N-S alignment and are usually situated in the Mesozoic units. The focal mechanisms are predominantly strike-slip related to NW-SE compression. Local magnitudes are up to 4.3 (Deichmann et al. 2000, Kastrup et al. 2007, Deichmann et al. 2010).

4) The earthquakes occurring along the Vuache fault

zone. They are located in the Mesozoic units and focal mechanisms are strike-slip related to WNW-ESE compression. Magnitudes are up to 5.3 (Sambeth & Pavoni 1988, Thouvenot et al. 1998, Courboux et al. 1999).

In the western Swiss Molasse Basin, seismicity resembles that of the Jura Mountains with strike-slip mechanisms related to NW-SE compression (figure 1.9). Strike-slip fault zones like in the Jura Mountains are less known in the western Swiss Molasse Basin but the tendency of focal mechanisms to align (figure 1.9) implies that they do exist and tend to locate recent tectonic activity.

2 - DEFORMATION BANDS IN THE SANDSTONES OF THE WESTERN SWISS MOLASSE BASIN: MICROMECHANICS AND BRITTLE DEFORMATION

Ibele, T., Mosar, J.

submitted to Journal of Structural Geology

ABSTRACT

Brittle deformation in porous sandstone produces brittle deformation bands (DBs), which are zones of reduced porosity typically a few mm in width that result from reduction of grain size by fracturing. The denser packing of angular subgrains leads to strain hardening, and ongoing deformation creates new DBs subparallel to the initial ones. Increasing strain is accommodated by several anastomosing DBs forming deformation band shear zones (DBSZs) and finally by a discrete slip plane.

Structural mapping revealed DBs to be common structures in the sandstones of the western Swiss Molasse Basin. The investigation of their micro-fault gouges by optical and electron microscopy shows that they initiate from grain crushing, similar to DBs described in the literature, but that subsequent deformation is different. A considerable amount of the investigated micro-fault gouges from both DBs and DBSZs show strain accumulation either before or without a discrete slip plane being formed. These fault gouges feature foliations with SCC' fabrics, providing a microscopic shear sense indicator. The foliations are made of palygorskite fibres, a Mg-rich clay mineral, which forms in the course of deformation. Equilibrium calculations showed that palygorskite is stable with the host rock mineralogy and the formation waters at surface temperature, while chlorite, pre-existing in the host rock, is unstable in this configuration. The mineral reaction is triggered by grain grinding, i.e. the contact of ground material with the fluid phase, and compatible with brittle, near-surface deformation. The appearance of palygorskite is thought to cause strain softening and hence (re-)concentration of strain in existing DBs.

The observed micro-fault gouges are composed of regular structures forming the foliation network, as well as chaotic structures found in the area between the foliations. The fault gouges therefore most likely develop in two alternating modes, one of ongoing shear (foliations) and the other of instantaneous failure (chaotic structures), which implies periods of aseismic and seismic faulting.

The mapped DBs occur as conjugate sets and complete Riedel-type geometries. They run subparallel to mapped slickenside populations but tend to be more steeply inclined with respect to σ_1 . DBSZs frequently narrow to zones of concentrated shear with an orientation slightly rotated towards σ_1 . These zones of constriction probably represent the transition from deformation banding to slip along discrete faults. Micro-fault gouges of DBs and DBSZs often directly develop into macroscopic-scale gouges.

The tectonic regime in the western Swiss Molasse basin reveals strike-slip faulting due to NW-SE compression. The DBs mapped in this area represent the stage of fault initiation in the Molasse sandstones. The orientation and kinematics of the mapped DBs correlate well with those elaborated from slickensides in the study area. They developed in a strike slip regime under NW-SE compression that started in the upper Miocene and has persisted until recent times.

2.1 INTRODUCTION

The Molasse Basin of western Switzerland occupies a piggy-back position behind the foreland fold-and-thrust belt of the Jura Mountains. In contrast to the strong deformation of the internal Alps and the external Jura Mountains, the Molasse Basin lacks obvious deformation as outcrop conditions are poor and inclination is generally sub-horizontal. In our study we investigated the tectonics of the western Swiss Molasse Basin and found deformation bands to be both common structures in the field and to be of great importance for the understanding the tectonic history.

Deformation in porous sandstone has been described as a grain breaking and reorganisation processes rather than involving whole rock fracturing (Mandl et al. 1977). These processes deform and reduce pore space, taking place along mm-wide planar zones called brittle deformation bands (DB; Aydin 1978, Aydin & Johnson 1978, Antonellini et al. 1994, Davis et al. 1999, Fossen et al. 2007). The DBs strain-harden as the grain fragments interlock, resulting in the formation of new sub-parallel bands. With increasing strain, bundles of anastomosing bands are formed, each band accounting for a few mm of the total offset. These deformation band shear zones (DBSZ) may eventually develop a discrete slip plane which accommodates larger slip rates (Aydin & Johnson 1978; figure 2.1). During the last decades, DBs were also described in un-lithified or poorly lithified porous media (Rawling & Goodwin 2003, Cashman & Cashman 2000) and reproduced in the laboratory by rock fracturing experiments (Mair et al. 2000, Main et al. 2001). Different varieties such as bands with clay smearing in clay-rich sandstones or slipped deformation bands with higher offset were found (Rotevatn et al. 2008). The micro-structure of natural brittle DBs was investigated and classified (Antonellini et al. 1994; table 2.1), the ex-

isting work summarised and the classification refined (Fossen et al. 2007; table 2.1).

Brittle DBs have been reported for normal, thrust and strike-slip environments and were linked to rupture events on nearby seismic faults (Cashman & Cashman 2000). They are the first structures to form in intact rock, usually in the tip regions and in the damage zones of larger faults (Shipton & Cowie 2001). During evolution from DB to fault zone, the bands commonly form shears belonging to a Riedel system (Davis et al. 1999, Ahlgren 2001, Katz & Weinberger 2005).

The macroscopic orientations of the DBs in this study resemble conjugate sets of Riedel shears that subsequently evolve to superordinate Riedel shear zones. Their microscopic investigation revealed that micro-fault gouges derived from grain crushing show structures hitherto described for macroscopic fault gouges and cataclasites. These structures include foliations (Chester et al. 1985, Chester & Logan 1987) arranged in SCC'-geometries (Lin 2001) and shape-preferred orientations of relict grains from the host rock (Cladouhos 1999a). The foliation geometry is similar to mylonitic SCC'-fabrics and provides a shear sense indicator. In contrast to classical DBs, the bands in this study evolve and translate from micro-fault gouges directly to macroscopic gouges with accumulating strain. The foliations observed in the micro-fault gouges are formed by a new mineral phase identified as palygorskite. The new growth of this Mg-rich hydrous clay mineral has important implications for the deformation conditions and fluid flow.

In this article we describe the macroscopic geometries and regional pattern of the DBs in the study area as well as the fabric and characteristics of the microscopic fault gouge. We discuss the differ-

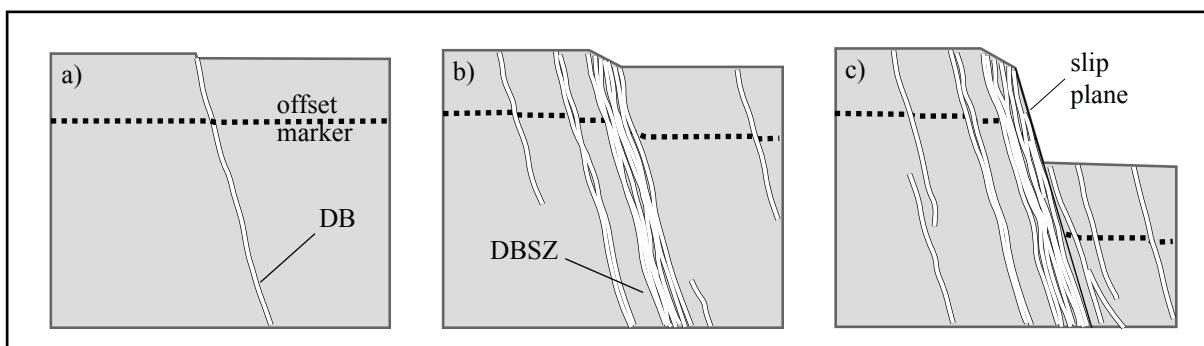


Figure 2.1: Scheme for the sequential evolution of DBs, DBSZs and a final discrete slip plane after Aydin & Johnson (1978), modified from Pollard & Fletcher (2005). a) Formation of a single DB. b) Increasing strain accounts for further sub-parallel DBs arranged in a DBSZ. c) Finally a discrete slip plane evolves, accounting for larger offset.

ences from “classical” DBs and present a conceptual model for fault gouge evolution. Macroscopic and microscopic study of the DBs provides important insights into the regional tectonics, especially concerning the modes of initial and continuing deformation. The results obtained are used to discuss the question of the seismic vs. aseismic nature of deformation in the western Swiss Molasse Basin.

2.2 BACKGROUND

2.2.1 Geologic setting

The Swiss Molasse Basin is the western part of the former peripheral foreland basin of the Alps (figure 2.2). During the orogenic evolution it progressively evolved from an underfilled Flysch basin to an overfilled Molasse Basin (Pfiffner 1986, Allan et al.

1991, Sinclair 1997).

The Molasse-type sedimentation took place in two shallowing-up megacycles in Oligocene and lower Miocene times (Trümpy 1980, Homewood et al. 1986, Berger et al. 2005). The detritus was eroded from the Alps rising in the south and deposited as proximal conglomeratic fans, and distal sandstones and shales (Heim 1919). Small-scale vertical and lateral facies variations between these lithologies are frequent (Matter et al. 1980). The main formations were named according to their sedimentological characteristics – lower marine Molasse (UMM), lower freshwater Molasse (USM), upper marine Molasse (OMM) and upper freshwater Molasse (OSM) (Studer 1853, Trümpy 1980).

A stratigraphic gap separates the Oligocene Molasse sediments of the study area from the under-

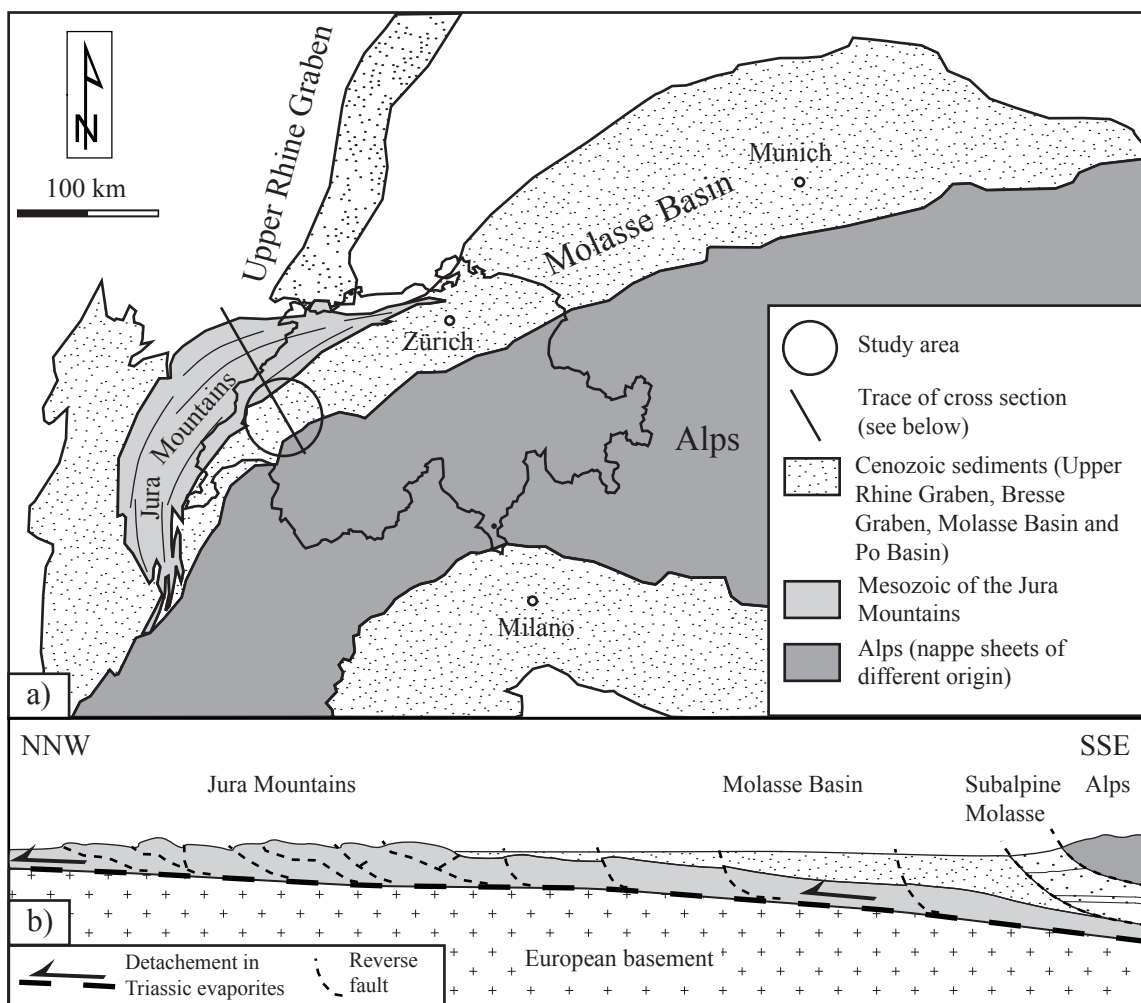


Figure 2.2: a) General map of the Molasse Basin with major tectonic units and b) schematic cross section through the study area and adjacent Jura Mountains. The location of the study area and trace of the schematic cross section are indicated in the map.

lying Mesozoic units. The latter consists of partly evaporitic Triassic and usually shaley lower Jurassic, followed by middle to upper Jurassic platform carbonates. In the southwestern parts sedimentation continued into lower Cretaceous times (Trümpy 1962, Büchi et al. 1965, Trümpy 1980, Bachmann et al. 1987). For the most part these non-metamorphic cover units directly overlay basement, though in places they rest on post-Variscan graben structures filled with Permo-Carboniferous clastic sediments (Diepold 1985, Matter 1987, Bachmann et al. 1987, Pfiffner et al. 1997).

Ongoing NW-ward migration of the Alpine orogen and its peripheral foreland basin during the Molasse sedimentation lead to progressive onlapping of younger Molasse sediments on the Mesozoic of the down-flexed European crust (Pfiffner 1986, Home-wood et al. 1986). A restored cross-section of the undeformed Molasse sediments thus exhibits a triangular shape with the oldest sediments deposited only in the southeastern part and the youngest sediments only in the northwestern part (figure. 2.3). The interplay of sedimentation and NW-ward migration of the foreland basin caused synsedimentary deformation. In eastern Switzerland and adjacent Germany, growth faults oriented parallel to the basin axis represent normal faulting on the down-flexing lithosphere (Laubscher 1978, Bachmann et al. 1987, Bachmann & Müller 1992), whereas in Savoie (F) synsedimentary folding

occurs (Beck et al. 1998). This indicates a change in the basin's along-strike geodynamic situation towards southwest.

In the southeastern parts of the basin, the older sediments were imbricated as a result of ongoing NW-ward migration of the orogen, forming the narrow band of the subalpine Molasse located along the former front of the Alps. In contrast, the less deformed Plateau exhibits only slightly folded, subhorizontal units taking up most of the area between the Alps and the Jura Mountains. Sedimentation turned to erosion in Serravallian times when a large-scale decollement developed in the Triassic evaporites underlying the Molasse Basin. This decollement triggered the formation of the Jura Mountains in front of the Molasse Basin, incorporating the latter into the northern Alpine foreland fold-and-thrust belt. The Molasse Basin was passively translated and uplifted into its present position as the thicker and less deformed rear part of the fold-and-thrust belt (Buxtorf 1916, Laubscher 1961, Burkhard 1990, Burkhard & Sommaruga 1998).

Erosion since the Serravallian accounts for up to 4 km of exhumation in the western part of the Plateau Molasse, where it has nearly completely removed the OSM (Schegg et al. 1997, Schegg & Leu 1998, Mazurek et al. 2006, Cederboom et al. 2004). The region has been found to be deformed by a network of meso-scale faults, slickensides and the DBs this study

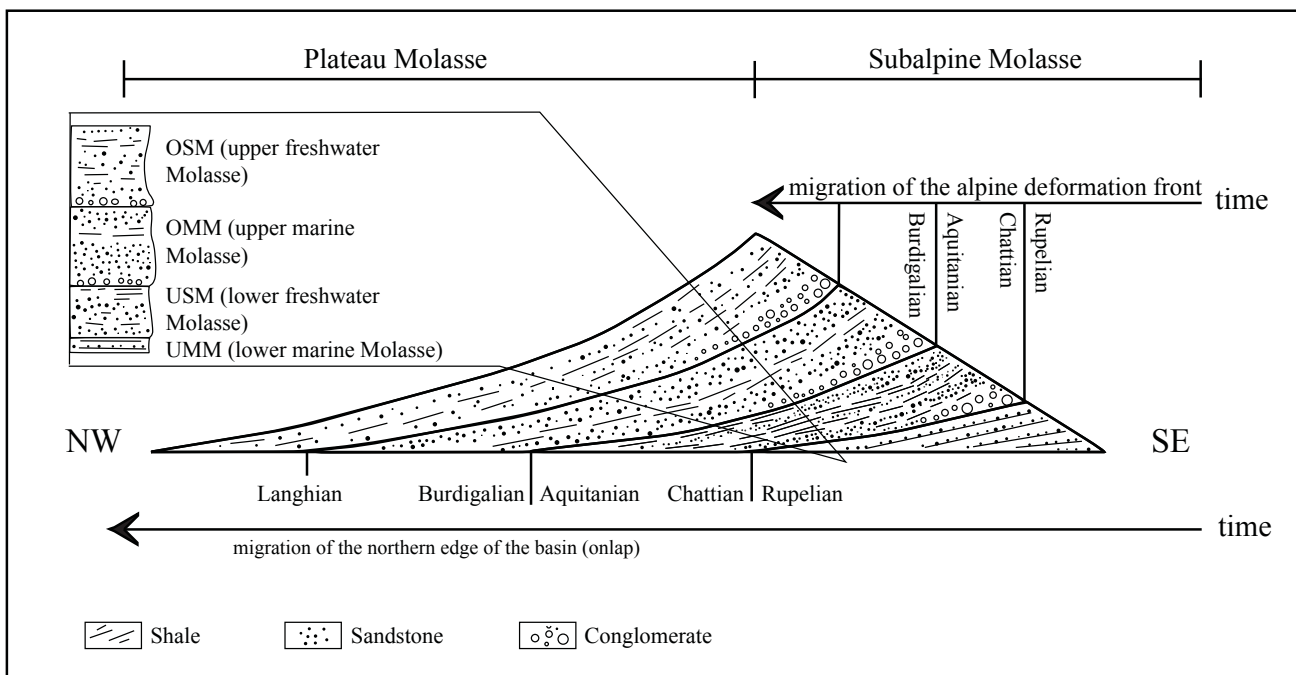


Figure 2.3: Sketch illustrating sedimentation in the geodynamic context of the migrating northern Alpine foreland basin prior to formation of the Jura Mountains. A stratigraphic column and a time frame are given, as well as the sedimentary prism of the Molasse lithologies (represented in their theoretical sequence not accounting for erosion and tectonics).

is focusing on. The established strike-slip regime was governed by the same NW-SE directed compression that is still active today, as revealed by the offset of Quaternary lake deposits along the La Lance fault (Gorin et al. 2003) as well as the focal mechanisms of regional earthquakes (Kastrup et al. 2007).

2.2.2 Brittle deformation bands in sandstone

Brittle DBs were described from field and microscopic observations by Aydin (1978) and Aydin & Johnson (1978). In this “classical” model, they form after an initial phase of pore space reduction by grain breaking, grain scale cataclasis and compaction. The bands thus formed are distinct small-scale cataclastic fault zones commonly not more than a few mm thick (Aydin 1978). Pore space reduction and interlocking of grain fragments results in strain hardening leading to the formation of a new band sub-parallel to the first one. With increasing strain, a zone of closely spaced anastomosing DBs develops, whose overall offset is the sum of all single DB offsets (Aydin & Johnson 1978). The DBSZs can measure several tens of centimetres in width and often exhibit a discrete fault plane at one edge as the next phase of deformation (Aydin & Johnson 1978, 1983). While offset across a single band amounts to a few millimetres and up to some tens of centimetres across a DBSZ, offset can be large across the slip planes (figure 2.1). In the Entrada and Navajo sandstone, where the classical studies were conducted, all slip planes are reported to have developed from a DBSZ (Aydin & Johnson 1978).

Based on the different examples of brittle DBs described from all over the world, this general model was refined to account for varying pressure conditions and host rocks. Despite the small amounts of offset, the lack of a well-defined discontinuity plane and the anastomosing structures (within DBSZs) as common characteristics, Antonellini et al. (1994) described three types of DBs according to their micro-structure. 1) Deformation bands with little or no cataclasis, 2)

deformation bands with cataclasis and 3) deformation bands with clay smearing (table 2.1). DBs with no cataclasis are proposed to form under low confining pressures. They show only few or no crushed grains and exhibit a different fabric than the host rock, featuring porosity increase, porosity decrease or grain re-orientation. The thickness of these bands is directly dependent on the grain size of the host rock. DBs with cataclasis are proposed to form under elevated confining pressures and are characterised by grain breaking and compaction due to pore space reduction. They resemble the bands described by Aydin (1978) and Aydin & Johnson (1978). DBs with clay smearing develop in sandstones with considerable clay content and display larger offsets. Reorientation of the clay platelets parallel to the band is thought to facilitate slip. Concerning the micro-mechanics of DB evolution, Antonellini et al. (1994) suggested that at high confining pressure compaction begins with the onset of strain, whereas at lower confining pressure an initial phase of dilatancy occurs (due to grain rotation), later followed by grain crushing and porosity reduction. In their field observations, the authors found DBs with no cataclasis to be widely distributed over the area, while DBs with cataclasis are located in proximity to major faults and folds. In the latter case, DBs are narrow and have more offset if the clay content and/or the porosity of the host rock is high, and broader if it is low.

Fossen et al. (2007) recently summarised different types of DBs and refined the definition of Antonellini et al. (1994). They term bands with a reorganised grain assemblage disaggregation bands, or phyllosilicate bands if the reorganisation involves phyllosilicate minerals as part of the host-sandstone detritus. Bands with grain breaking are termed cataclastic bands, while bands with dissolution and cementation are termed solution and cementation bands (table 2.1).

Single DBs and arrays of DBs were produced from porous sandstone by rock fracture experiments in the laboratory (Mair et al. 2000, Main et al. 2001), largely confirming the conceptual models developed from field observations by Aydin & Johnson (1978,

| Antonellini et al. 1994 | | Fossen et al. 2007 | |
|--|--------------------------|--|-------------------------------------|
| characteristics | name | characteristics | name |
| Reorientation of grains | Bands with no cataclasis | Reorganisation of grains | Disaggregation bands |
| Fragmentation of grains | Bands with cataclasis | Fragmentation of grains | Cataclastic bands |
| Develop in sandstones with clay content, high offset | Bands with clay smearing | Reorganisation of grains involving phyllosilicates | Phyllosilicate bands |
| | | Dissolution of grains, cementation of the matrix | Bands with solution and cementation |

Table 2.1: Classification of deformation bands by Antonellini et al. (1994) and Fossen et al. (2007).

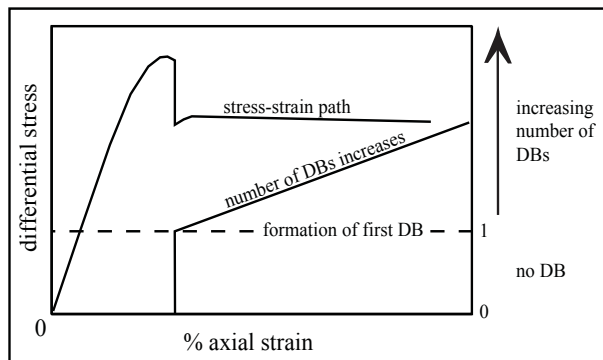


Figure 2.4: Stress-strain curve of deformation band formation in the laboratory. After Mair et al. (2000) and Main et al. (2001).

1983). Ongoing deformation after the development of the first DB was found to take place under steady conditions, as is shown by the stress-strain curves from the experiments (figure 2.4). The only macroscopic stress drop which occurs is the one when the first DB forms. This indicates the formation of the parallel bands after strain hardening of the initial band to be a continuous continuous process (Mair et al. 2000). No final discrete slip plane was achieved in the laboratory tests, probably due to limits in the experimental setup, such as limited amounts of finite strain (Main et al. 2001).

DBs were further described to develop in poorly lithified or non-lithified, near-surface porous sediments (Cashman & Cashman 2000, Rawling & Goodwin 2003). Rawling & Goodwin (2003) documented them in poorly lithified sediments near a major normal fault. Their findings suggest deformation to occur dominantly by rotation and material flow, typical for bands with no cataclasis in the sense of Antonellini et al. (1994), confirming the latter's hypothesis that these types of DBs form under low confining pressures. In contrast, Cashman & Cashman (2000) found that DBs formed "classically" by grain cracking and pore space reduction in Holocene marine terrace sands. However, these terrace sand were deformed near an active thrust fault known for its seismic activity.

DBs may have important consequences on fluid flow by reducing permeability of the porous host rock (e.g. Aydin 1978, Antonellini & Aydin 1994, Mair et al. 2000, Shipton & Cowie 2001, Fossen et al. 2007, Rotevatn et al. 2008). The low permeability of the DBs is caused by pore space reduction as a consequence of grain fracturing and chemical sealing. The latter occurs on a relatively short time scale since the ground material is highly reactive (Main et al. 2001). Rock fracture experiments reveal an initial increase

of porosity caused by dilatational grain fragmentation and thus permeability along-strike of the band (Mair et al. 2000; figure 2.5). The increased along-strike permeability may persist after the reduction of the across strike permeability (Mair et al. 2000). Enhanced permeability along the DB probably facilitates chemical sealing by keeping the fault gouge in contact with the fluid phase.

In summary DBs show a wide variety of different types that have been described and assigned to variations in physical and mineralogical properties of the host rocks. However, they all share the following most common characteristics:

- accumulation of strain by deforming pore space through grain-reorganisation or grain cracking,
- relatively low amount of offset across a band, and
- a reduction of pore space within the bands.

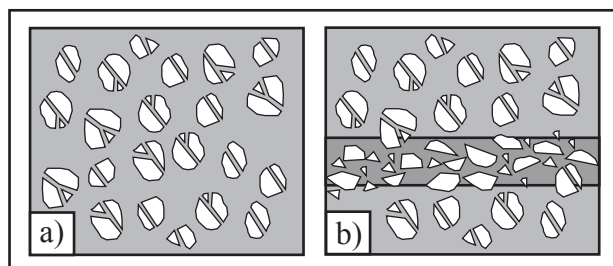


Figure 2.5: Evolution of porosity and permeability during DB formation from rock deformation experiments in the laboratory by Mair et al. (2000). a) Initial increase in porosity due to dilatational cracking of host rock grains and b) reduction of porosity and permeability in the fault gouge. The latter is characterised by emplaced fragments.

2.2.3 Riedel shear model and SC-fabrics

The Riedel shear model (figure 2.6) was developed from analogue modelling with clay (Riedel 1929, Cloos 1930, Tchalenko 1968) and described for experimentally deformed rocks (Bartelett et al. 1981), as well as natural brittle deformation zones varying in both scale and lithology (Tchalenko 1970, Davis et al. 1999, Ahlgren 2001, Katz & Weinberger 2005).

The movement of a fault zone is distributed on fault zone-internal shears with synthetic and antithetic senses of movement. The synthetic shears R and P are oriented at an ideal angle of 15° with respect to the shear zone, R at a normal angle and P at a reverse angle¹. The antithetic shears R' and X enclose ideal

¹ The orientations of elements within a super-ordinate shear zone are described with respect to that shear zone and its sense of movement as normal or reverse. The super-ordinate shear sense would result in dilatation along a element, inclined at a "normal angle" and in compression along an element, inclined at a "reverse angle"

angles of 60° with R and P, respectively. However, all angles within a Riedel system are primarily functions of the angle of internal friction (ϕ) of the fractured material, which varies according to rock type, so that angles deviate from their ideal values (Tchalenko & Ambrasey 1970). R and R' constitute a conjugate set of shears with the bisector equal to the system's σ_1 . Additional shears are Y-shears running parallel to the shear zone and T-fractures resembling tensional structures parallel to σ_1 . Given a geometric arrangement of shears that resembles a Riedel system, one needs a sense of movement for at least one of the individual shears (given for instance by the offset of another shear) to determine the sense of the superordinate shear zone. A Riedel-type geometric constellation alone remains ambiguous with respect to the sense of movement of the shear zone.

SC-foliations (figure 2.6) are typical geometries in medium-strain mylonites, and are thus structures attributed to ductile deformation (Berthé et al. 1979, Lister & Snoke 1984). However, cataclasites can have macroscopically ductile fabrics such as foliations, shear bands and SC-structures (Chester et al. 1985, Chester & Logan 1987, Lin et al. 2001). In mylonites, the S-(for "schistosity") surfaces are de-

fined by the orientation of platy phyllosilicates such as micas. They are oriented perpendicular to the local principal shortening direction and enclose an angle of about 45° with the shear plane at initial stages of deformation. The C-surfaces are sub-parallel to the shear plane and are regarded as small-scale shears offsetting the S-surfaces, which acquire a wavy form where they curve into the C-surfaces. In high-strain mylonites, S is rotated sub-parallel to the shear plane (Berthé et al. 1979), resulting in an accentuation of the C-surfaces and a penetrative mylonitic foliation parallel to the shear plane that may be further offset by C'-surfaces (also termed shear bands or extensional crenulation cleavage; White et al. 1980, Platt & Vissers 1980, figure 2.6). The C'-surfaces are oriented $20\text{--}30^\circ$ with respect to the shear plane and show offset synthetic with the shear zone (Simpson 1984). An SC-structure allows unambiguous kinematic interpretation solely on the basis of its geometry.

Since cataclasites can also show ductile type structures such as foliations (Chester et al. 1985, Chester & Logan 1987), it may be difficult to identify the planar tectonic features in their fault gouges as either Riedel shears or surfaces of an SC-fabric based only on their geometric arrangements. Especially in the

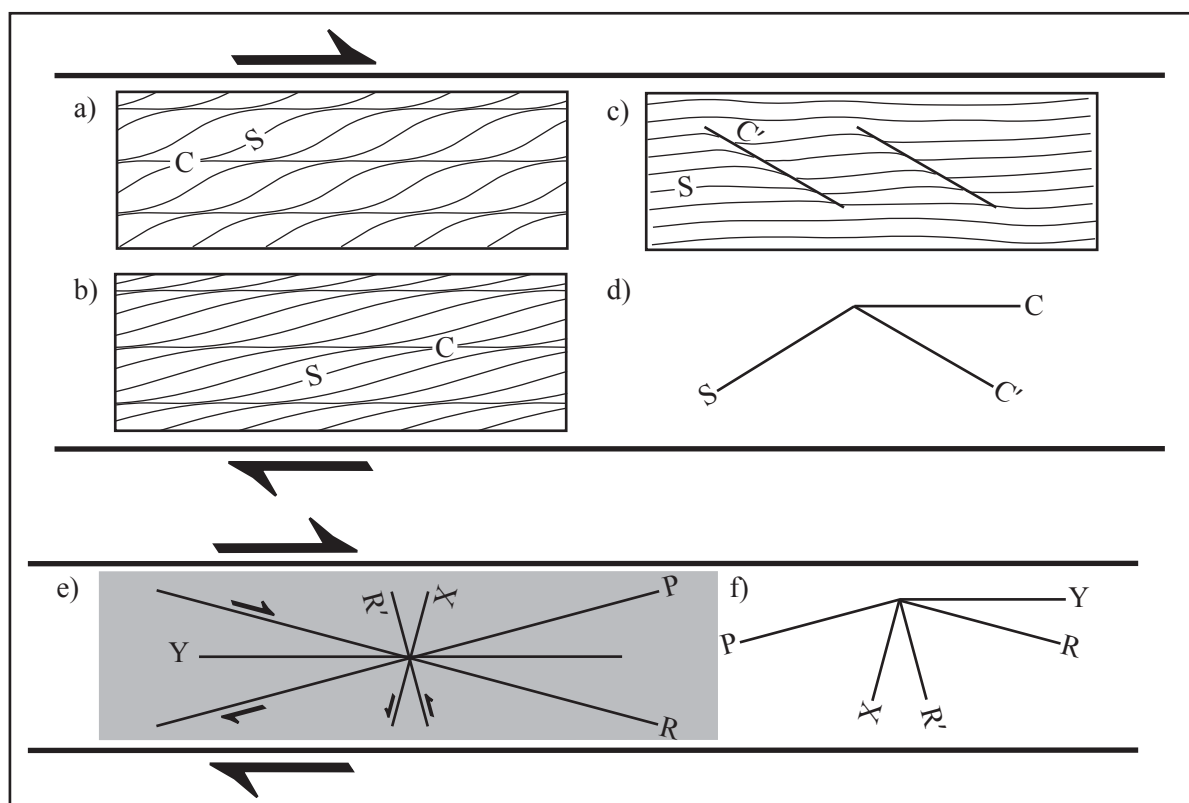


Figure 2.6: Principal geometries of an SCC'- fabric and a Riedel shear model. a) SC-mylonite, b) ongoing deformation of the SC-mylonite progressively rotates S towards C; c) combined S- and C-foliation becomes sheared by C'. e) Array of different Riedel shears in a brittle shear zone. Relative orientations for the SCC'-fabric are given in d) and for the Riedel shears in f).

| System | Structure | Orientation with respect to shear zone | Sense of movement with respect to shear zone | Deformation mode |
|---------------|-----------|--|--|------------------|
| SCC' fabric | S | 0-45°/reverse | - | pure shear |
| | C | 0° | synthetic | simple shear |
| | C' | 0-45°/normal | synthetic | simple shear |
| Riedel-system | Y | 0° | synthetic | simple shear |
| | R | 15°/normal | synthetic | simple shear |
| | P | 15°/reverse | synthetic | simple shear |
| | R' | 75°/(normal) | antithetic | simple shear |
| | X | 75°/(reverse) | antithetic | simple shear |

Table 2.2: Similarities between the structures of an SCC'-fabric and a Riedel system

case of incomplete records, this may lead to confusion and misinterpretation. Similarities and differences between the Riedel and SCC'-systems (see table 2.2) can be classified as either 1) geometric, 2) genetic or 3) kinematic in nature:

- 1) The orientations with respect to the main shear zone are quite similar for C-surfaces and Y-shears, S-surfaces and P-shears and C'-surfaces and R-shears, respectively. In an SC-fabric, there are no steep orientations with respect to the shear zone, such as the antithetic shears in the Riedel system. The two orientations usually visible in an SCC'-fabric curve into each other, while in a Riedel system one is expected to be offset by the other.
- 2) The main genetic difference is between the S-surfaces and all other surfaces of the systems – while the Riedel shears as well as C- and C'-surfaces are shear planes, the S-surfaces are foliations, i.e. minerals oriented according to the stress ellipsoid, representing its XY-plane.
- 3) Due to the genetic difference of the S surfaces, kinematics can be discussed only for C-surfaces vs. Y-shears and C'-surfaces vs. R-shears, respectively, because the relative sense of movement is similar for both pairs.

2.3 FIELD DATA

2.3.1 Host rock of deformation bands

DBs and DBSZs were found in the sandstone units of the USM and OMM in the western Swiss Molasse Basin. The sandstones are poorly lithified, mostly well-sorted and varying in clay content. They are interbedded with shales or layers with a certain amount of clay content and in fact a smooth transition between sandstone and shale exists. The sandstone may locally contain small isolated pebbles that in proximal areas may form conglomerate beds. In the field the pure

sandstones, several tens of metres thick, are found as packages of yellowish to greenish rocks with almost no internal stratification and frequent cross-bedding structures. There are varieties resistant to erosion, building huge walls in outcrop, as well as soft varieties less resistant to erosion, usually less thick and smaller in outcrop size. Sandstones with higher clay contents are typically darker, laminated, often hard and of grey-green colour in outcrop. This rock type is less resistant to erosion and therefore outcrops are inconspicuous. The shales are soft, laminated and water-saturated. They are usually grey but may be coloured (green and red) in the case of the USM. The shales are of minor importance for this study because they do not develop DBs.

The grain size of the sandstones reaches from very fine-grained (~ 0.1mm) to very coarse-grained (up to a few millimetres). Most specimens, however, classify as coarse-grained sandstone with grain diameters 0.5 - 1mm. The sands are generally well-sorted and similar-sized at thin section scale, but grain size may strongly fluctuate at outcrop scale with the occurrence of fining- or coarsening-up sequences. In some cases, single pebbles of a few centimetres in size are embedded in the sandstone.

The mineralogy of the sandstone components was quantitatively estimated from thin section analysis of 31 samples, resulting in the following average values: 40% quartz, 30% feldspar, up to 15% carbonate, 5-10% phyllosilicates (micas and chlorites) and 5-10% organic materials, with up to 15% lithic clasts in the very coarse-grained sandstones (see table 2.3). The carbonates were not distinguished further in thin section, but X-ray diffraction analysis revealed both calcite and dolomite to be abundant in the host rock. However, since calcite already occurs in the form of cement, it must not necessarily occur as a grain component as well.

The porosity of the sandstone was also roughly estimated during thin section analysis, showing val-

| Sample number | Grain diameter [mm] | classification | % Broken grains | % Porosity | % Qtz | % Fsp | % Carbonate | % Phyllosilic. | % Lithic clasts | % Organics |
|------------------|---------------------|------------------|-----------------|------------|-----------|-----------|-------------|----------------|-----------------|------------|
| 3/1 | bis 1 | coarse sand | 50 | 15 | 45 | 25 | 30 | 0 | 0 | 0 |
| 3/2 | 0.5-1 | coarse sand | 20 | - | 45 | 20 | 30 | 5 | 0 | 0 |
| 3/3 | 0.5-1 | coarse sand | 50 | 5 | 40 | 20 | 30 | 10 | 0 | 0 |
| 3/3 | 0.1 | very fine sand | 20 | 5 | 40 | 10 | 25 | 25 | 0 | 0 |
| 3/4 | 0.5 | medium sand | 15 | 5 | 35 | 20 | 40 | 5 | 0 | 0 |
| 3/4 | 0.1-0.5 | medium sand | 10 | 5 | 60 | 20 | 10 | 10 | 0 | 0 |
| 3/5 | 0.1-0.5 | medium sand | 10 | - | 40 | 20 | 20 | 20 | 0 | 0 |
| 3/6 | 0.5 | medium sand | 70 | 10 | 50 | 30 | 15 | 5 | 0 | 0 |
| 3/7 | 0.5-0.8 | coarse sand | 70 | 5 | 40 | 20 | 30 | 10 | 0 | 0 |
| 3/8 | 0.5-1 | coarse sand | 20 | 15 | 30 | 25 | 25 | 5 | 5 | 10 |
| 3/9 | 0.5-1 | coarse sand | 75 | 5 | 40 | 30 | 20 | 5 | 0 | 5 |
| 3/10 | 0.7-1 | coarse sand | 70 | 5 | 40 | 20 | 20 | 10 | 5 | 5 |
| 3/11 | 0.5-1 | coarse sand | 15 | 5 | 35 | 30 | 20 | 5 | 5 | 5 |
| 3/12 | 0.7-1 | coarse sand | 15 | 5 | 35 | 35 | 20 | 5 | 0 | 5 |
| 3/13 | 0.5-1 | coarse sand | 15 | 5 | 35 | 30 | 15 | 5 | 10 | 5 |
| 3/14 | 0.5-0.8 | coarse sand | 15 | 5 | 40 | 30 | 20 | 5 | 0 | 5 |
| 3/15 | 0.5-1 | coarse sand | 55 | 5 | 40 | 35 | 20 | 0 | 0 | 5 |
| 3/16 | 0.1-0.4 | medium sand | 5 | - | 30 | 10 | 25 | 25 | 0 | 10 |
| 3/17 | 0.5-0.8 | coarse sand | 40 | - | 40 | 30 | 15 | 5 | 0 | 10 |
| 3/18 | 0.5-1 | coarse sand | 50 | - | 50 | 35 | 5 | 5 | 0 | 5 |
| 3/19 | 1.0-3 | very coarse sand | 70 | - | 25 | 20 | 20 | 5 | 25 | 5 |
| 3/20 | 0.5-0.8 | coarse sand | 50 | - | 40 | 25 | 25 | 5 | 0 | 5 |
| 3/21 | 0.5-0.8 | coarse sand | 40 | - | 35 | 25 | 20 | 5 | 0 | 15 |
| 3/22 | 0.5-0.8 | coarse sand | 20 | - | 45 | 25 | 20 | 5 | 0 | 5 |
| 3/23 | 0.5-0.8 | coarse sand | 20 | - | 45 | 30 | 10 | 5 | 0 | 10 |
| 3/24 | 0.5-0.8 | coarse sand | 40 | - | 40 | 25 | 20 | 5 | 0 | 10 |
| 3/25 | 0.5 | medium sand | 10 | - | 45 | 30 | 10 | 5 | 0 | 10 |
| 0/0 | 0.5 | medium sand | 1 | - | 35 | 25 | 20 | 5 | 10 | 5 |
| 2/13 | 1 | coarse sand | 20 | - | 50 | 30 | 10 | 5 | 0 | 5 |
| 2/8 | 1-3 | very coarse sand | 40 | - | 40 | 30 | 10 | 0 | 15 | 5 |
| 2/9 | 0.4 | medium sand | 25 | - | 45 | 30 | 15 | 5 | 0 | 5 |
| 2/20 | 0.5 | medium sand | 20 | - | 40 | 20 | 20 | 5 | 0 | 15 |
| 2/21 | 0.5 | medium sand | 20 | - | 35 | 25 | 20 | 10 | 0 | 10 |
| 3/average | | | 31 | 7 | 41 | 25 | 21 | 6 | 11 | 7 |

Table 2.3: Petrophysical and mineralogical parameters of selected samples of Molasse sandstone as qualitatively determined by optical-microscopy. Note that all samples except for 0/0 were taken from DBs and these properties reflect the host-rock composition, not the DBs as such. Sample 0/0 is an undeformed piece of rock with no fault in its vicinity. For calculating the averages only sample series 3 (sample 3/1 – 3/25) was taken into account. In the column “% porosity”, (-) means that the respective property was not recorded for the sample. Where grain size was too small to distinguish carbonates and phyllosilicates half of the recorded sum is given for both and values noted in italics.

ues between 5 and 15%, which is relatively low compared to the rocks from “classical” DB studies.

2.3.2 Outcrop conditions in the western Swiss Molasse Basin

The outcrop conditions in the study area are poor, as Quaternary glacial and post-glacial deposits cover most of the Tertiary bedrock. Outcrops can be found only along water courses and roads or in small, inactive quarries. Along the roads and in the inactive quarries, the rocks are highly altered, which brings about some difficulties in detecting structural features. Although the rocks in creek exposure are often coated by calcareous tufa, active erosion leads to relatively

fresh outcrops. Structural mapping was carried out mostly alongside rivers and streams, resulting in a network of mapping lines with a spacing dictated by the natural occurrence of the outcrops. Although an outcrop along a river may be some hundreds of metres long, its width is normally restricted to a few metres. This means that structures such as DBs generally exceed the scale of the outcrops, i.e. their lengths are an approximation only. In addition, it is not possible to correlate DBs along-strike between neighbouring mapping lines. DBs were previously described to be some tens to hundreds of metres long (Aydin 1978), which is likely to apply to the bands of this study as well. However, they may also represent the tip regions of larger faults (Shipton & Cowie 2001), in which case they may re-emerge as a fault zone in another outcrop some kilometres away.

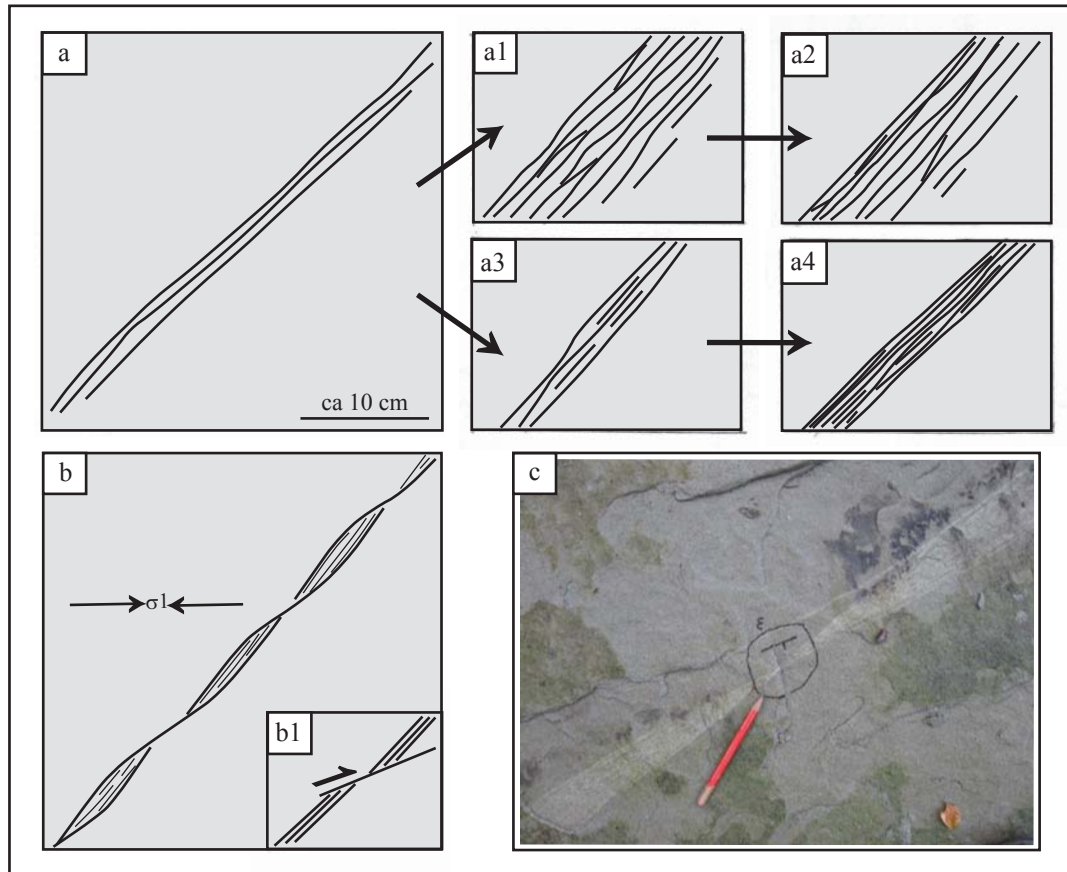


Figure 2.7: Evolution of DBSZs in the Molasse sandstone of western Switzerland. a: DBSZ consisting of a few sub-parallel DBs. Ongoing deformation either broadens the zone by the formation of new sub-parallel DBs and later a macroscopic fault gouge or slip-plane (a1 and a2), or maintains its width but densifies by developing additional DBs (a3) until a macroscopic fault gouge develops (a4). In the field, DBSZs were often found to form condensed zones (b and c) that show a slightly smaller angle with respect to the orientation of σ_1 . In b) orientation of local σ_1 is approximate (from offset criteria). Condensation and fault gouge formation in these zones probably facilitates shearing of the band in a synthetic sense (b1). Scale (see figure 2.7 a) is similar for all sub-figures.

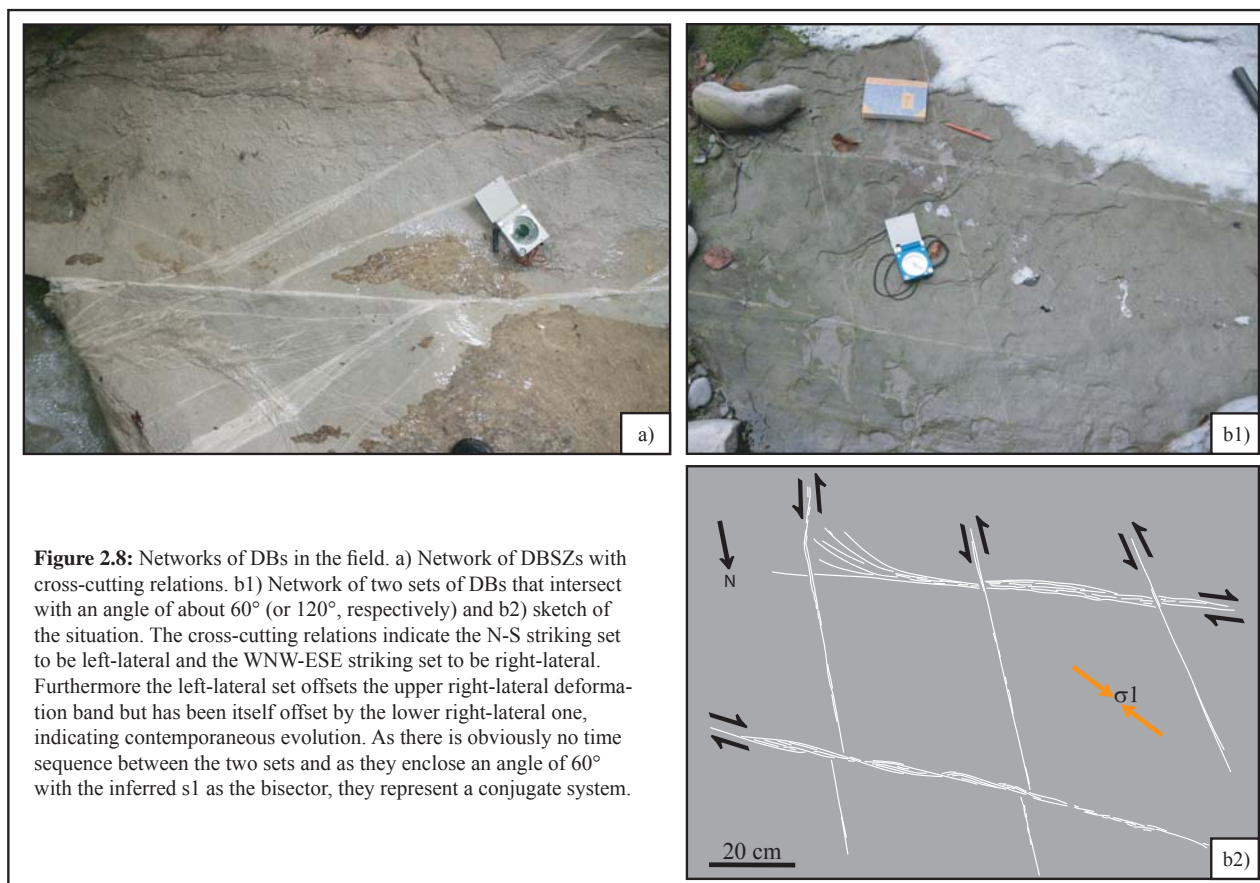
2.3.3 Macroscopic occurrence of deformation bands in the Molasse sandstone

DBs occur in the pure sandstones and in the sandstones with some clay content and can be detected in the field as light, generally straight, distinct lines on the rock surface (figure 2.8). They appear either as single bands of a few millimetres in width, or as bundles of parallel or anastomosing lines representing DBSZs. In addition there are also grey DBs darker than the host rock, and DBs containing fibrous material, the latter previously undescribed in the literature. The DBs and DBSZs occur as individual structures in the field as well as in association with, and close to, larger faults.

Where DBs hit small pebbles, the band breaks and offsets the pebbles instead of detouring around them. The DBSZs quite commonly change their width along-strike by narrowing of the individual bands, which may occur repeatedly (figure 2.7).

These zones of constriction have a slightly different orientation than the DBSZ itself. A number of individual bands may be grouped within or at the edge of a broad DBSZ, or tightly packed in zones of some millimetres to centimetres in width. Slip planes or several millimetres thick, soft fault gouges may exist in these concentrated zones. The DBSZs were observed as two types: 1) as bundles of relatively widely spaced bands with zones of host rock between them that are broader than the width of a single band, and 2) as condensed DBSZs in which single bands cannot be distinguished (figure 2.7).

A comparison to the local stress field revealed that constricted zones of DBSZs are oriented at smaller angles to the direction of maximum compression than the zone itself. A similar relationship is common for condensed zones and wide-spaced DBSZs, where the angle between the latter and σ_1 is larger by $\sim 10\text{--}20^\circ$. The slip planes that develop in the condensed parts of DBSZs show striations consisting of fibrous material, rather than being mechanically produced scratches.



2.3.4 Field data and its interpretation

The direction of strike was measured for more than 700 planes of DBs and DBSZs in the outcrops of the study area (figure 2.9a). As they do not stand out in the Molasse sandstone and only rarely develop slip planes, the DBs occur as 2D features in outcrop. Dip can therefore not be measured directly, but was estimated from the intersection with the outcrop surface. In almost all cases the dip was found to be steep to vertical, in some cases between 60° and 75°, but usually between 75° and 90°. This gives a first clue to their strike-slip nature and facilitates their statistical analysis. Due to the lack of offset markers, the sense of movement was defined for 155 DBs only.

The distribution of strike of all DBs reaches from E-W via NW-SE and N-S to NNE-SSW. Maxima occur for NNE-SSW, NNW-SSE, NW-SE and WNW-ESE (figure 2.10a). This relatively wide scatter becomes more pronounced when only the DBs with known sense of movement are taken into account, in which case an E-W, a broad NW-SE and a NNE-SSW maximum are revealed (figures 2.10b and 2.10c). In detail, the E-W as well as the western half of the NW-SE maximum correspond to right-lateral shear, while

the NNE-SSW and the northern half of the NW-SE maximum correspond to left-lateral shear. From a mechanical point of view, one would expect to find two maxima instead of three for the two senses of shear; these two maxima should enclose an angle of about 60° (or 120°, respectively) with σ_1 as the bisector (or σ_3 , respectively). It is furthermore unlikely in a simple tectonic setting to find two orientation maxima for planes of movement with opposite senses of shear in close vicinity to each other. This is, however, the case for the NW-SE striking planes.

The data was grouped into 27 sets (1 - 27 in table 2.4 and figure 2.9b) according to outcrop. The majority of these groups (18) show two sets of strike, some reveal only one set (4) and one group shows four sets. Four groups with less than five DBs were not considered. In five (no. 2, no. 12, no. 15, no. 24 and no. 27) of the 18 cases the two sets were arranged as synthetic Riedel shears, and in the other 13 cases as conjugate shears. The criteria for synthetic Riedel shears are identical sense of movement and an acute included angle of 20-40°. If the sets show opposite sense of movement and a acute included angle between 50° and 70° they were defined as conjugate sets. The orientation of σ_1 was derived as NNW-SSE in eight

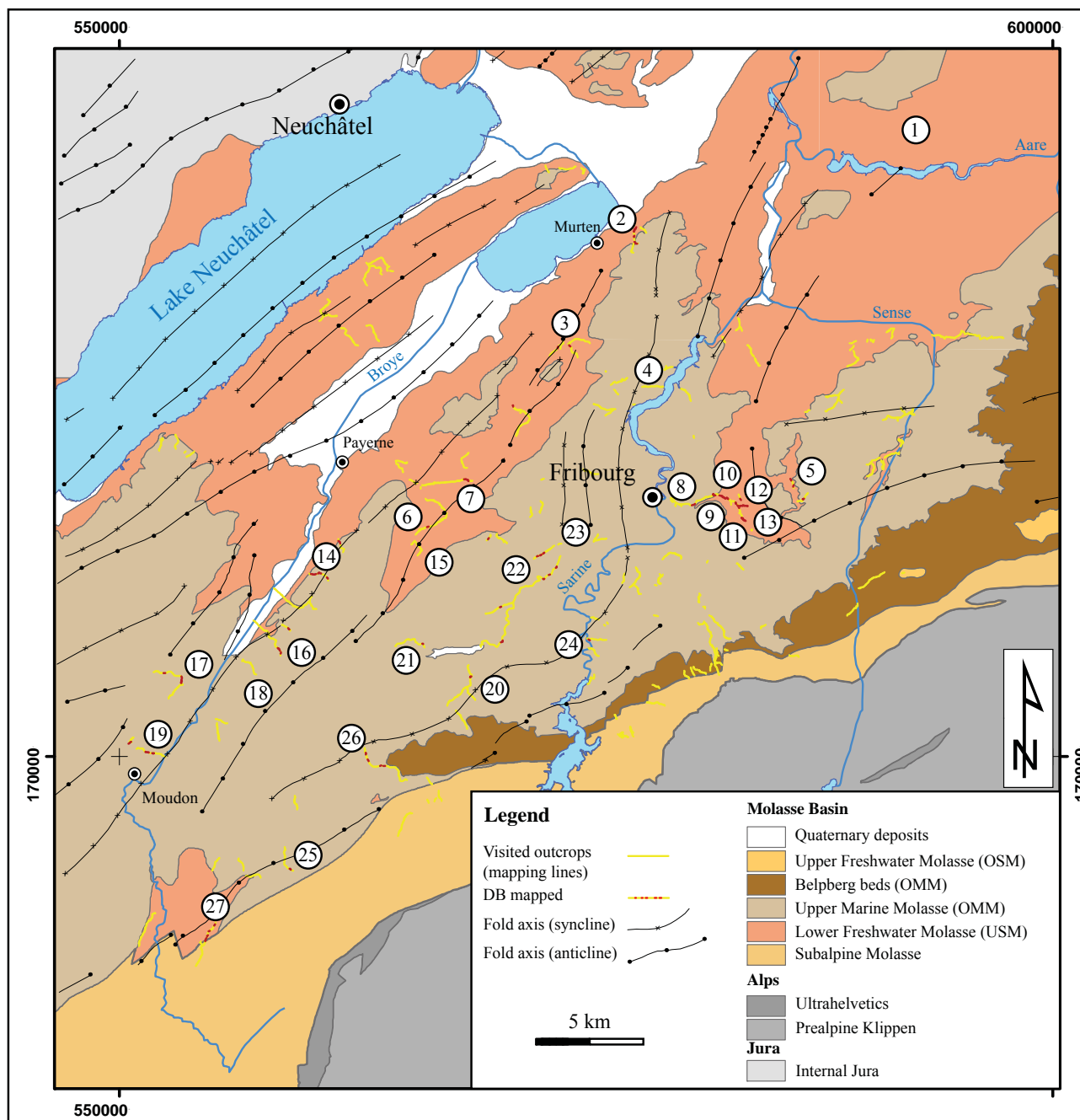
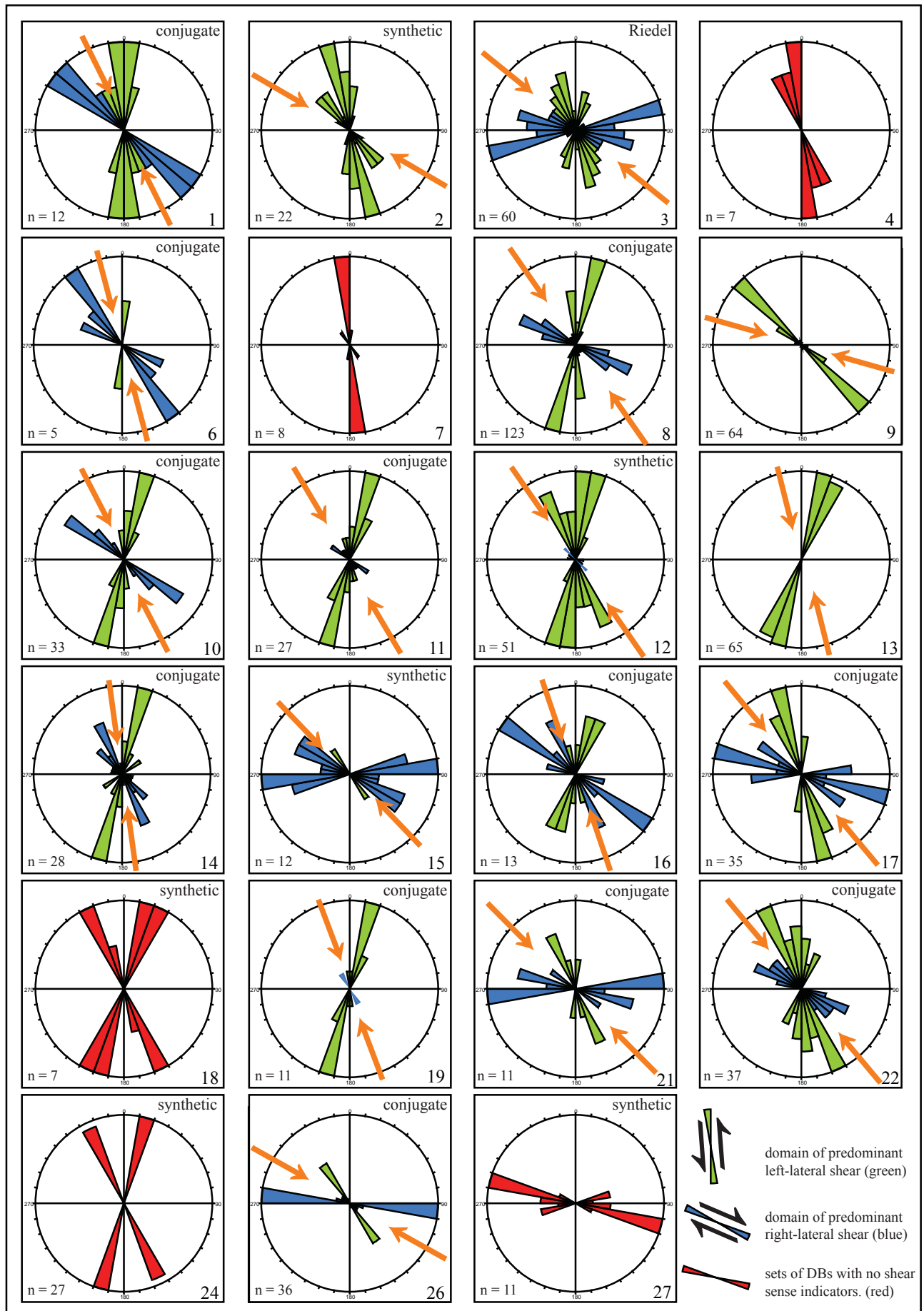


Figure 2.9a: Geological map of the study area with mapping lines and location of the DBs plotted in rose diagrams in 2.9b). Numbers 1 to 27 refer to numbers of diagrams in 2.9b) and to outcrops in Table 2.4.

of the 12 “typical” conjugate sets cases, as NW-SE in three cases and as WNW-ESE in one case. From the synthetic Riedel sets, σ_1 was estimated as WNW-ESE for no. 2 and ENE-WSW for no. 12, but could not be determined for no. 18, no. 24 and no. 27 due to the lack of shear sense indicators. The synthetic sets no. 12 and no. 15 additionally contain a very small number of conjugate shears.

60 DBs from a well-studied outcrop at a creek near the village of Wallenried demonstrate the occurrence of 4 strike maxima (figure 2.9b). These are, from most common to least common occurrence, WSW-ENE, WNW-ESE, NNW-SSE and NNE-SSW. The WSW-ENE-strike and WNW-ESE-strike correspond to right-lateral shear, while the NNW-SSE-

Figure 2.9b: Rose diagrams for sets of DBs, grouped by outcrop. Numbers refer to numbers in Table 2.4 and to locality in the map (2.9a). Arrows give the approximate direction of σ_1 inferred from the sets with given sense of movement. In case of more than one maxima of data sets, the inferred system is indicated (synthetic shears, conjugate shears or Riedel shears).



| Site | n data | Name | Orientation maximum 1 | | Orientation maximum 2 | | Orientation maximum 3 | | Orientation maximum 4 | | Orientation of inferred σ_1 |
|------|--------|-------------------------|-----------------------|-------|-----------------------|-------|---|-------|-----------------------|-------|------------------------------------|
| | | | strike | sense | strike | sense | strike | sense | strike | sense | |
| 1 | 12 | Wohlensee north | NW-SE (310°-130°) | dex | N-S (000°-180°) | - | - | - | - | - | NNW-SSE |
| 2 | 22 | Burggraben | NNW-SSE (320°-140°) | sin | NW-SE (320°-140°) | sin | - | - | - | - | NNW-SSE |
| 3 | 60 | Wallenried | WSW-ENE (255°-075°) | dex | NNW-ESE (280°-100°) | dex | NNW-SSE (340°-160°) | sin | NNW-SSW (020°-200°) | sin | NNW-ESE |
| 4 | 7 | Barbarèche | N-S (355°-175°) | - | - | - | - | - | - | - | NNW-SE |
| 5 | 4 | St. Antoni | NNE-SSW (010°-190°) | - | - | - | Less than 5 data not considered further | | | | - |
| 6 | 5 | L'Arbogne | NW-SE (320°-140°) | dex | N-S (005°-185°) | - | - | - | - | - | NNW-SSE |
| 7 | 8 | Chaudieres | N-S (355°-175°) | - | - | - | - | - | - | - | - |
| 8 | 123 | Galtera FR-567m | NNE-SSW (015°-195°) | sin | WNW-ESE (295°-115°) | dex | - | - | - | - | NNW-SSE |
| 9 | 64 | Galtera 567m-604m | NW-SE (315°-135°) | sin | - | - | - | - | - | - | - |
| 10 | 33 | Galtera 604m-Amelsmühle | NW-SE (305°-125°) | dex | NNE-SSW (015°-195°) | sin | - | - | - | - | NNW-SSE |
| 11 | 27 | Galtera Fault-632m | NNE-SSW (015°-195°) | sin | NW-SE (305°-125°) | dex | - | - | - | - | NNW-SSE |
| 12 | 51 | Galtera right tributary | NNE-SSW (010°-190°) | sin | NNW-SSE (335°-155°) | sin | NW-SE (315°-135°) | dex | - | - | NNW-SE |
| 13 | 65 | Galtera above 632m | NNE-SSW (020°-200°) | sin | - | - | - | - | - | - | NNW-SSE |
| 14 | 28 | Trey - Tomy | NNW-SSE (335°-155°) | dex | NNE-SSW (015°-195°) | sin | - | - | - | - | NNW-SSE |
| 15 | 12 | North of Corserey | W-E (265°-085°) | dex | WNW-ESE (300°-120°) | dex | NW-SE (325°-145°) | sin | - | - | NNW-SE |
| 16 | 13 | La Trémeule | NW-SE (305°-125°) | - | NNE-SSW (020°-190°) | - | - | - | - | - | NNW-SSE |
| 17 | 35 | West of Lucens | WNW-ESE (285°-105°) | dex | NNW-SSE (345°-165°) | sin | - | - | - | - | NNW-SE |
| 18 | 7 | Seigneux | NNW-SSE (335°-155°) | - | NNE-SSW (020°-200°) | - | - | - | - | - | - |
| 19 | 11 | West of Moudon | NNE-SSW (015°-195°) | sin | NNW-SSE (330°-150°) | dex | - | - | - | - | NNW-SSE |
| 20 | 1 | R. de Glebe | - | - | - | - | Less than 5 data not considered further | | | | - |
| 21 | 11 | La Glâne Chénens | W-E (265°-085°) | dex | NNW-SSE (335°-155°) | sin | - | - | - | - | NNW-SE |
| 22 | 37 | La Glâne Matran-Neyruz | NNW-SSE (340°-160°) | sin | WNW-ESE (295°-115°) | dex | - | - | - | - | NNW-SE |
| 23 | 2 | St. Apolline | NW-SE (310°-130°) | dex | - | - | Less than 5 data not considered further | | | | - |
| 24 | 27 | Vers St. Pierre | NNW-SSE (335°-155°) | - | NNE-SSW (015°-195°) | - | - | - | - | - | - |
| 25 | 2 | Le Gotto | NNE-SSW (035°-215°) | - | - | - | Less than 5 data not considered further | | | | - |
| 26 | 36 | Le Mausson | W-E (275°-095°) | dex | NW-SE (325°-145°) | sin | - | - | - | - | NNW-ESE |
| 27 | 11 | Le Maillon Oron | WNW-ESE (285°-105°) | - | WSW-ENE (255°-075°) | - | - | - | - | - | - |

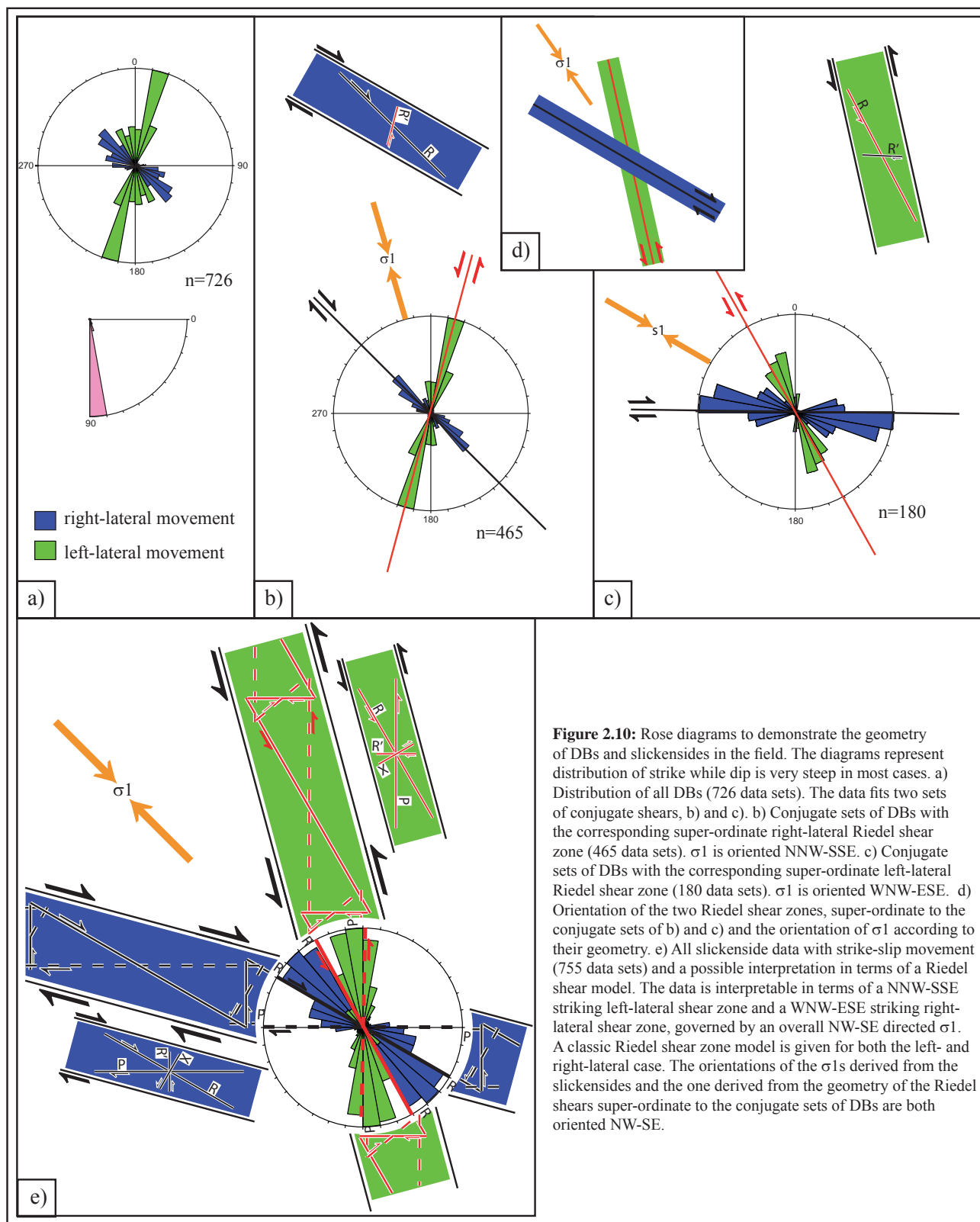


Table 2.4: Sets of deformation bands grouped by site. Numbers in the table refer to the rose diagrams in figure 2.9b and to the location in the map (figure 2.8a). Sites 5, 20, 23 and 25 (marked in grey) each have less than five data points and are not considered further. dex = right-lateral, sin = left-lateral.

strike and NNE-SSW-strike correspond to left-lateral shear. Both pairs of maxima with the same sense of movement include 30° , while an angle of 60° separates those with opposing sense of movement. This matches a complete Riedel system with the WSW-ENE-orientation representing the R-shears, the WNW-ESE-orientation the P-shears, the NNW-SSE-orientation the X-shears and the NNE-SSW-orientation the R'-shears. The outcrop may be interpreted as an E-W-striking right-lateral fault zone that developed DBs which subsequently evolved as Riedel shears. The axis of σ_1 for this system should be NW-SE.

The four outcrops with only one set show two N-S-strikes (no. 4 and no. 7), one NW-SE-strike (no. 9) and one NNE-SSW-strike (no. 13). No sense of movement could be obtained in the field for the N-S strike, whereas for the NW-SE-case left-lateral movement is given by offset relationship, and assumed from correlation with sub-parallel slickensides for the NNE-SSW-case.

The closer look at the data sub-grouped according to outcrops shows that the majority of the DBs occur in conjugate sets (figures 2.9b and 2.8). Each of these conjugate sets could be assigned to one of two groups (figures 2.10b and 2.10c): The first one containing all sets with right-lateral shears that strike NW-SE and the left lateral ones that strike NNE-SSW. This group is governed by a local σ_1 oriented NNW-SSE. The second group contains all sets with left-lateral shears that strike NW-SE and the right-lateral ones that strike E-W. This group is governed by a local σ_1 oriented WNW-ESE. The field data furthermore indicates that the DBs evolve in Riedel-type geometries, as is shown by the existence of both synthetic Riedel shear pairs as well as fully evolved Riedel systems (figures 2.8 and 2.9b). If the shears of the two conjugate systems are seen as R and R' of a Riedel system then their superordinate shear zones are right-lateral striking WNW-ESE and left-lateral striking NNW-SSE, respectively, with σ_1 oriented NW-SE (figure 2.10d). The same orientation is evident from the data of slickensides taken in the study area (article in preparation, Figure 2.10e) and reflects the main tectonic phase of the region. Some small discrepancies such as conjugate sets with a compression axis oriented NW-SE instead of NNW-SSE or WNW-ESE may be due to slight rotations of the stress field within the study area.

2.4 MICROSCOPE ANALYSIS

The micro-scale characteristics of DBs and DBSZs were analysed by optical microscopy and scanning electron microscopy (SEM). Insights into the architecture of their fault gouges were attained by optical microscopy and backscatter electron micrographs, while their chemical composition was investigated by electron dispersive spectroscopy (EDS).

2.4.1 Optical microscopy

Samples of DBs, DBSZs and slip planes evolved from DBs were studied in thin section by optical microscopy. A total of 74 thin sections were made from 47 samples taken from eight different localities within the study area. Most of the thin sections represent sub-horizontal cuts normal to the usually sub-vertical planes of deformation. In the case of slip planes, this includes orientations sub-parallel to the direction of movement. Additional thin sections in the plane normal to the plane of deformation was also performed for selected samples

2.4.1.1 Deformation bands and micro-fault gouges

Under the microscope the DBs correspond to zones of smaller grain size (figure 2.11). In the vicinity of these zones the grains of the host rock are frequently fractured, usually dissecting the whole grain. Different types of fracturing can be observed: partial cracks from one side, persistent cracks between grain contact points and completely broken grains. In some cases a preferred orientation of the cracks within the grains of the whole section can be observed, striking $\sim 30\text{--}40^\circ$ with respect to the DB and probably reflecting σ_1 .

While the grains in the host rocks are well-sorted, sorting is poor in the DBs, with grain sizes reaching from host rock size down to matrix sizes beyond the limits of the optical microscope (figure 2.12). The fractured grains in the host rock show no or only minor offset between their grain fragments, so that the outline of the original shape of the grain is still visible. The grains within the bands normally show no internal fractures. It is thought that unfractured grains are themselves fragments of larger fractured grains that have been detached from their original position during shearing. Parts of these fragments were most likely further ground to matrix size, while

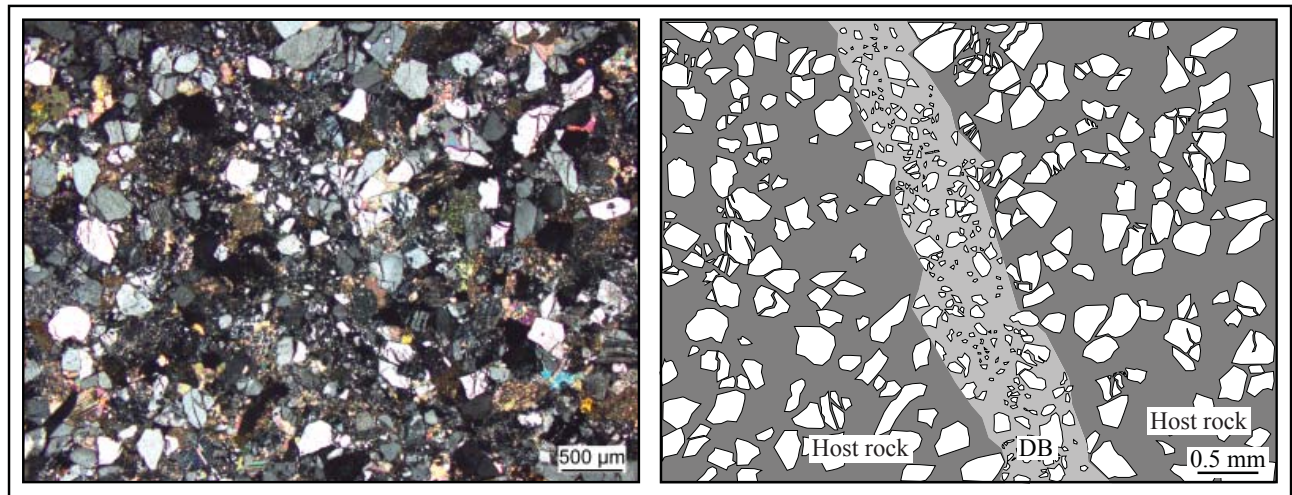


Figure 2.11: Photograph (left) and sketch (right) of a 0.5 mm DB band that evolved from grain crushing. The host rock is marked by fractured grains, implying grain crushing to be the first stage of deformation. The DB itself contains debris of different size, but always smaller than the grains of the host rock. While in several cases grain fragments in the host rock outline the shape of the original larger grain and hence no offset after cracking has taken place, the smaller grains in the band are randomly distributed and not internally fractured, indicating that rotation and/or offset and further fracturing has followed initial cracking in the band.

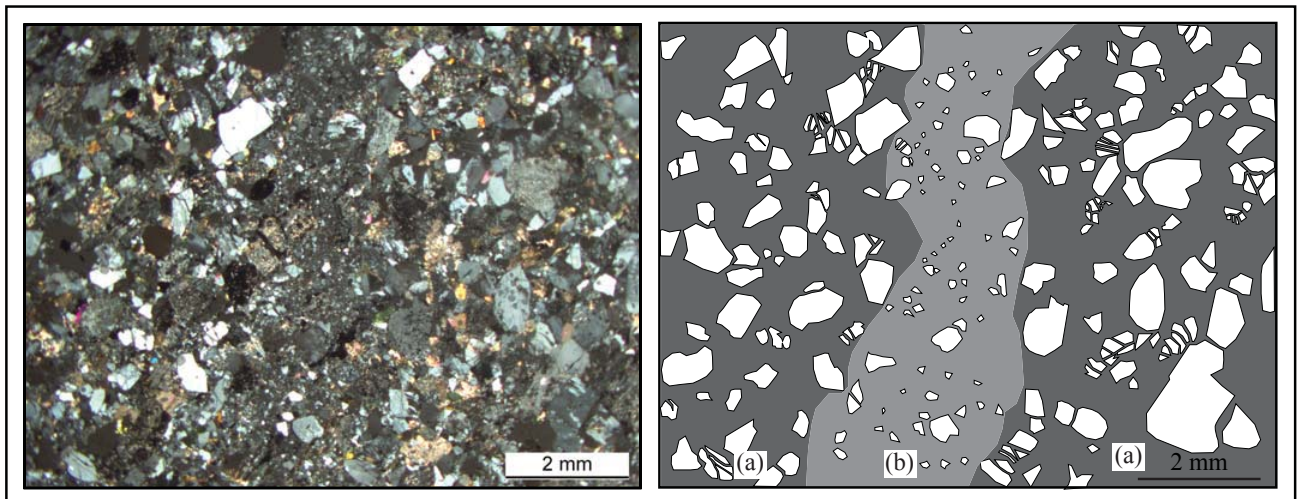


Figure 2.12: Photograph (left) and sketch (right) of a 2 mm-wide DB that evolved from grain crushing. The host rock (a) is marked by fractured grains, implying grain crushing to be the first stage of deformation. The DB itself (b) contains debris of different size, but always smaller than the grains of the host rock. The relatively large width of the band probably corresponds to the relative large grains in the host rock (a), which reach 2 mm in size. In most cases, the DBs in the sandstones of the western Swiss Molasse basin are about 0.5 to 1 mm wide and developed in host rocks with grain sizes of about 1 mm.

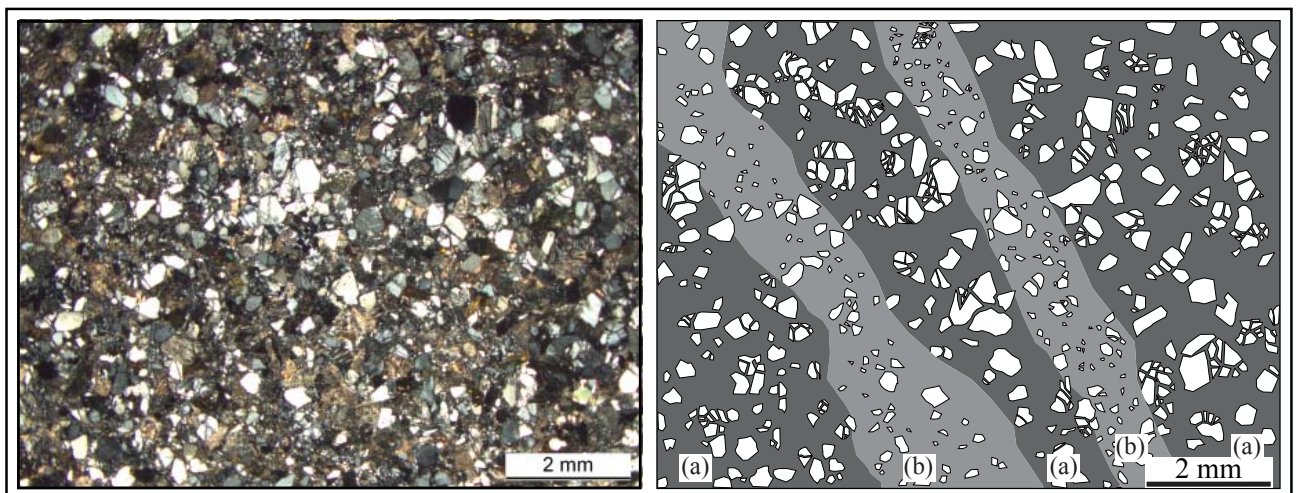


Figure 2.13: Photograph (left) and sketch (right) of a section taken from a DBSZ. The grains in the host rock (a) are strongly fractured, with the individual fragments still in place. Two sub-parallel zones (b) show smaller grain sizes, fewer internal fractures and no outline of original host grains, indicating them to be individual DBs.

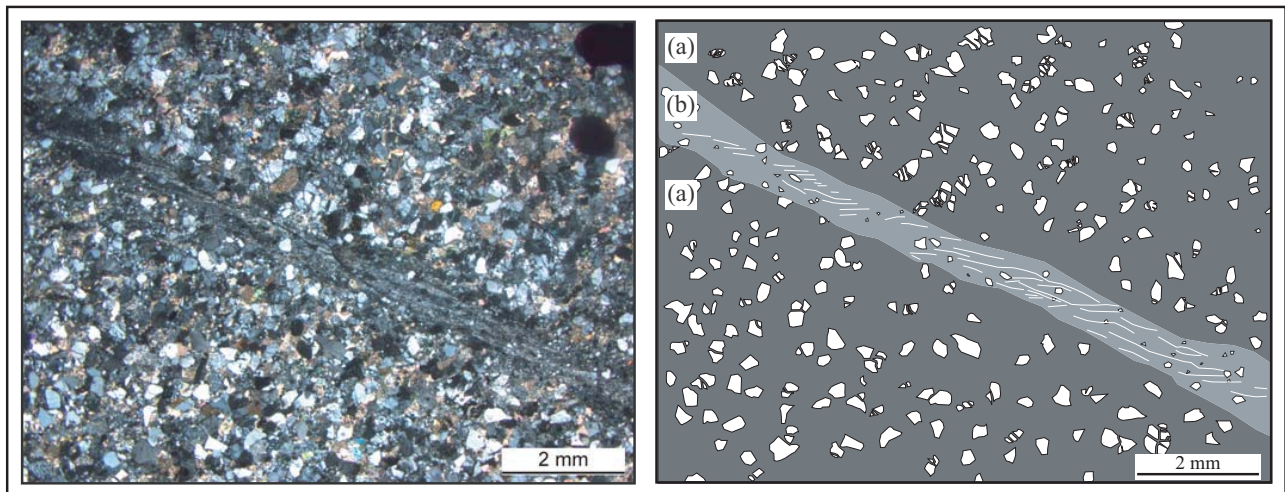


Figure 2.14: Photograph (left) and sketch (right) of a 1- 1.5 mm wide DB exhibiting a foliation. The host rock (a) is marked by fractured grains while the DB itself (b) is characterised by a fault gouge that contain debris of different size in a very fine matrix resulting from cataclasis of the grains. Furthermore a foliation of whitish filaments can be observed, representing newly-grown phyllosilicates.

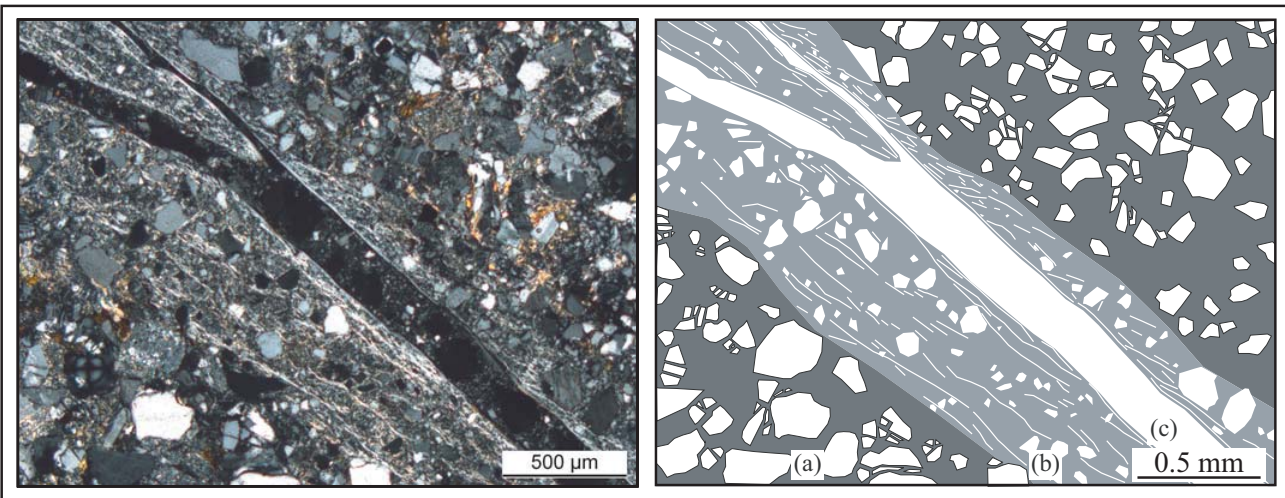


Figure 2.15: Photograph (left) and sketch (right) of a 1 mm wide DB (b) exhibiting a foliation. Some foliation filaments are steeply oriented with respect to the shear zone. An artificial crack (c) runs through the DB which appeared during preparation. (a) is the host rock.

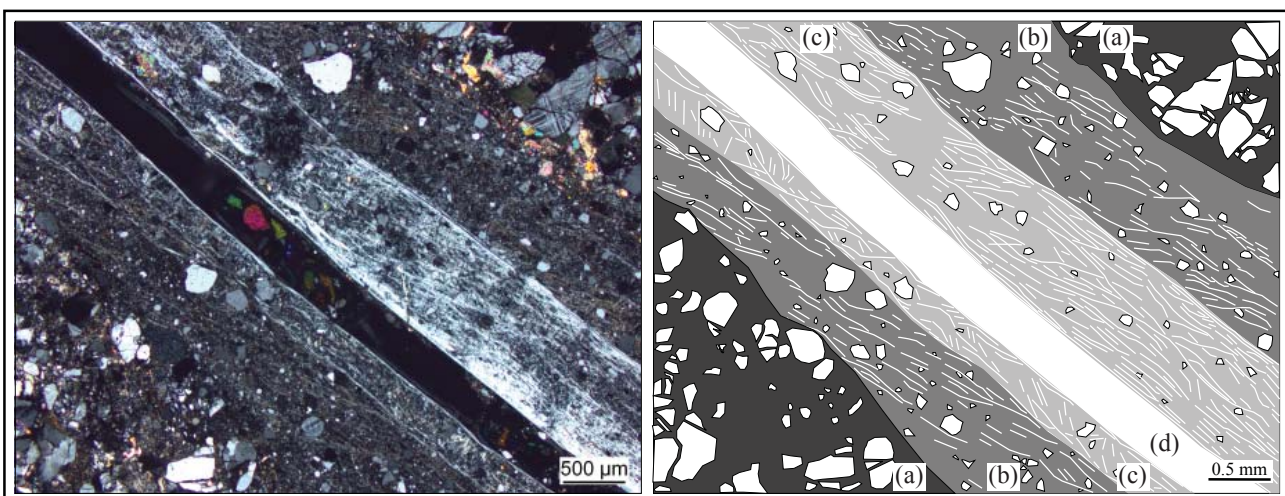


Figure 2.16: Photograph (left) and sketch (right) of a 2mm wide fault gouge with two distinct zones, an outer zone (b) and an inner zone (c). (a) is the host rock. The inner zone is more densely foliated and exhibits a higher matrix/component ratio. An artificial crack (d) runs through the DB which appeared during preparation.

a few were preserved and unfractured. As a product of fractured grains and hence cataclasis, the material of the band can be referred to as a fault gouge. In order to distinguish them from macroscopic gouges derived from whole rock cataclasis, we term them micro-fault gouges. The observed width of the micro-fault gouges ranges from 0.5 mm to a few millimetres, with width correlating to coarseness of the sandstone. Most bands in this study are around 0.5 mm wide and evolved in sandstones with an average grain size of 0.5-1 mm. If strain accumulates on a band in condensed DBSZs or in constriction zones of DBSZs (see paragraph 3.3), band width scales with the amount of strain rather than as a function of the grain size of the host rock.

Thin sections taken from DBSZs typically show an alteration of finer and coarser grain size with a generally high rate of fractured grains in the coarse portion (figure 2.13).

In several cases small filaments of similar extinction are found in the very fine-grained matrix, developing into a foliation with SC-type geometries with increasing width of the zone (figure 2.14). This foliation is visible in sections oriented normal to the plane of faulting and parallel to the slip vector, but not in sections normal to the slip vector. It shows fully evolved SC-fabrics in broad zones and near to slip surfaces and macroscopic fault gouges (figures 2.15 and 2.16), while it is absent in some narrow zones.

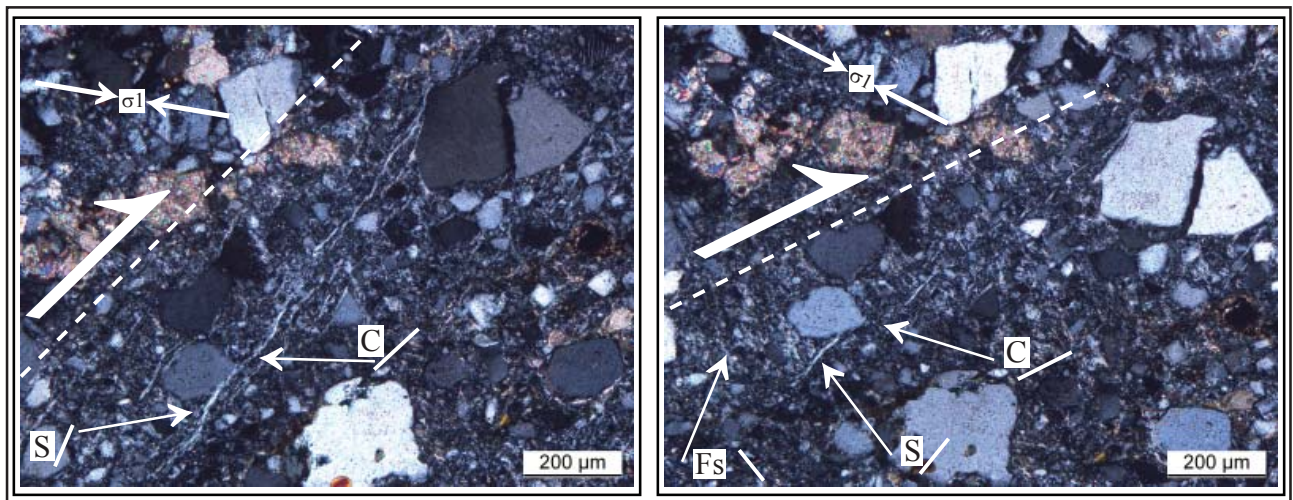


Figure 2.17: SC-structure starting to evolve in the fault gouge of a DB. Note that in the left photograph, the S-plane appears broader than the C-plane, indicating that C is a shear surface on which S has been sheared. The right photograph shows the same part of the section but rotated by 15°-20°. In the rotated position the thinner C-planes are no longer visible, S is less pronounced and an additional indistinct orientation (Fs) with a steep orientation with respect to the shear zone (i.e. the DB) appears. S, C and the strike of the band are indicated as well as direction of σ_1 and the sense of movement inferred from the SC-geometry.

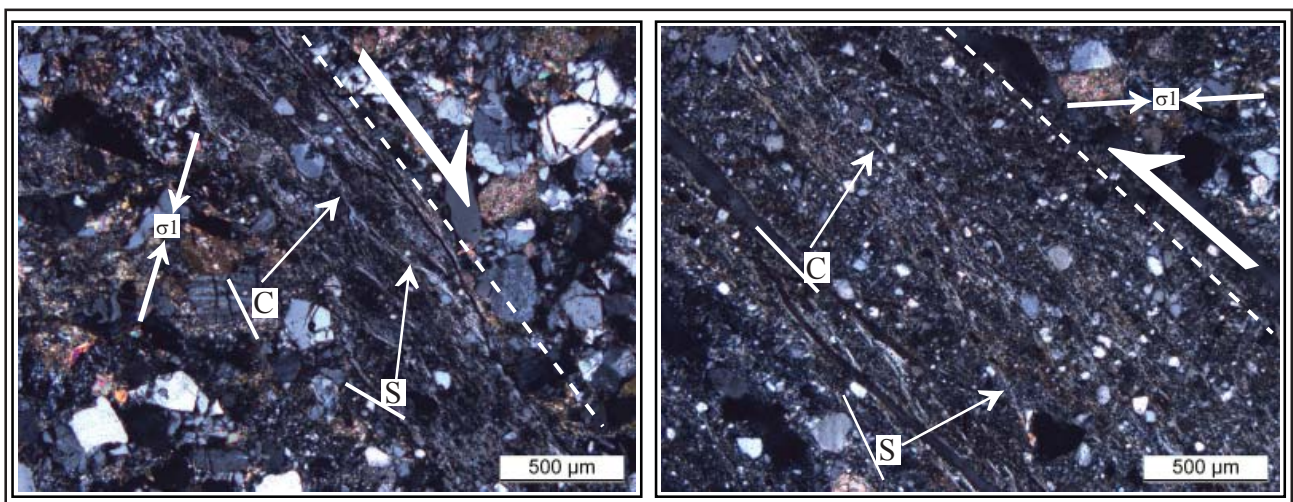


Figure 2.18: SC-structures in evolved fault gouges of DB. S, C and the strike of the band are indicated as well as the direction of σ_1 and the sense of movement inferred from the SC-geometry.

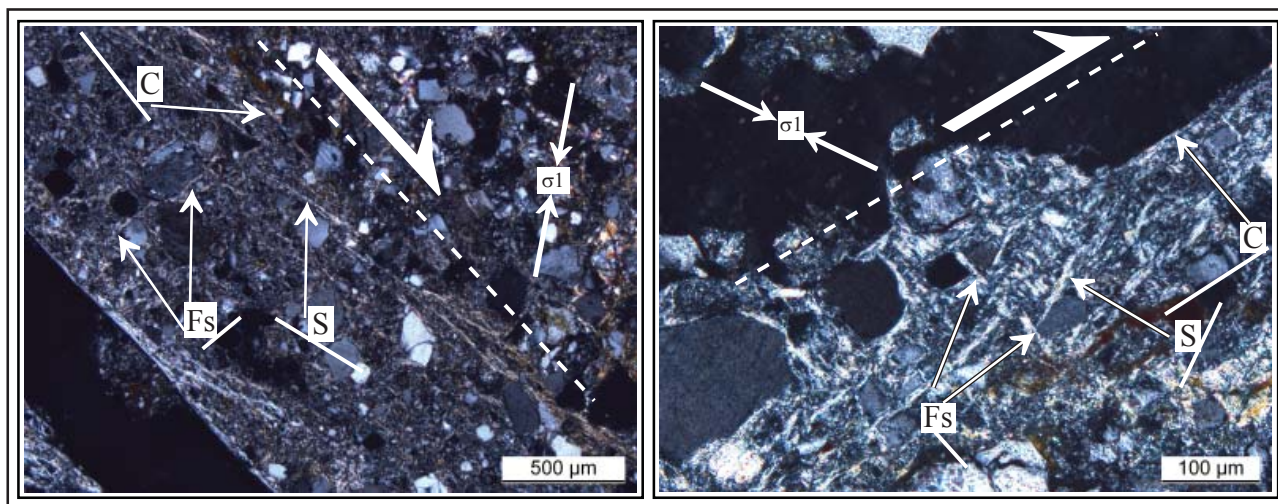


Figure 2.19: SC-structures in the evolved fault gouge of a DB. S, C and the strike of the band are indicated as well as the direction of σ_1 and the sense of movement inferred from the SC-geometry. An additional steep foliation (Fs) that evolves along the edges of residual grains is also indicated. The left photograph is taken at higher magnification than the right one, which shows that the structures occur at both scales. With polarised light, the different structures appear in slightly different positions. While the left photograph is taken in an intermediate position at which C, S and Fs can all be seen indistinctly, the right photograph was taken at a position at which Fs is clearly pronounced while S is less pronounced and C does not appear. Note the close geometric relationship between Fs and the residual grains.

A continuous evolution from one small filament in a single narrow band to a fully developed SC-type structure in a fault gouge several millimetres wide can be observed between these end-members.

In some of the broader and more developed zones, the micro-fault gouges can be subdivided into distinct sub-zones. In the case given in figure 2.16, the fault gouge itself shows clearly contrasting outer and inner parts. Both parts are characterised by a matrix with an evolved foliation and components of different size, but the inner zone displays a denser foliation and a higher matrix/component ratio.

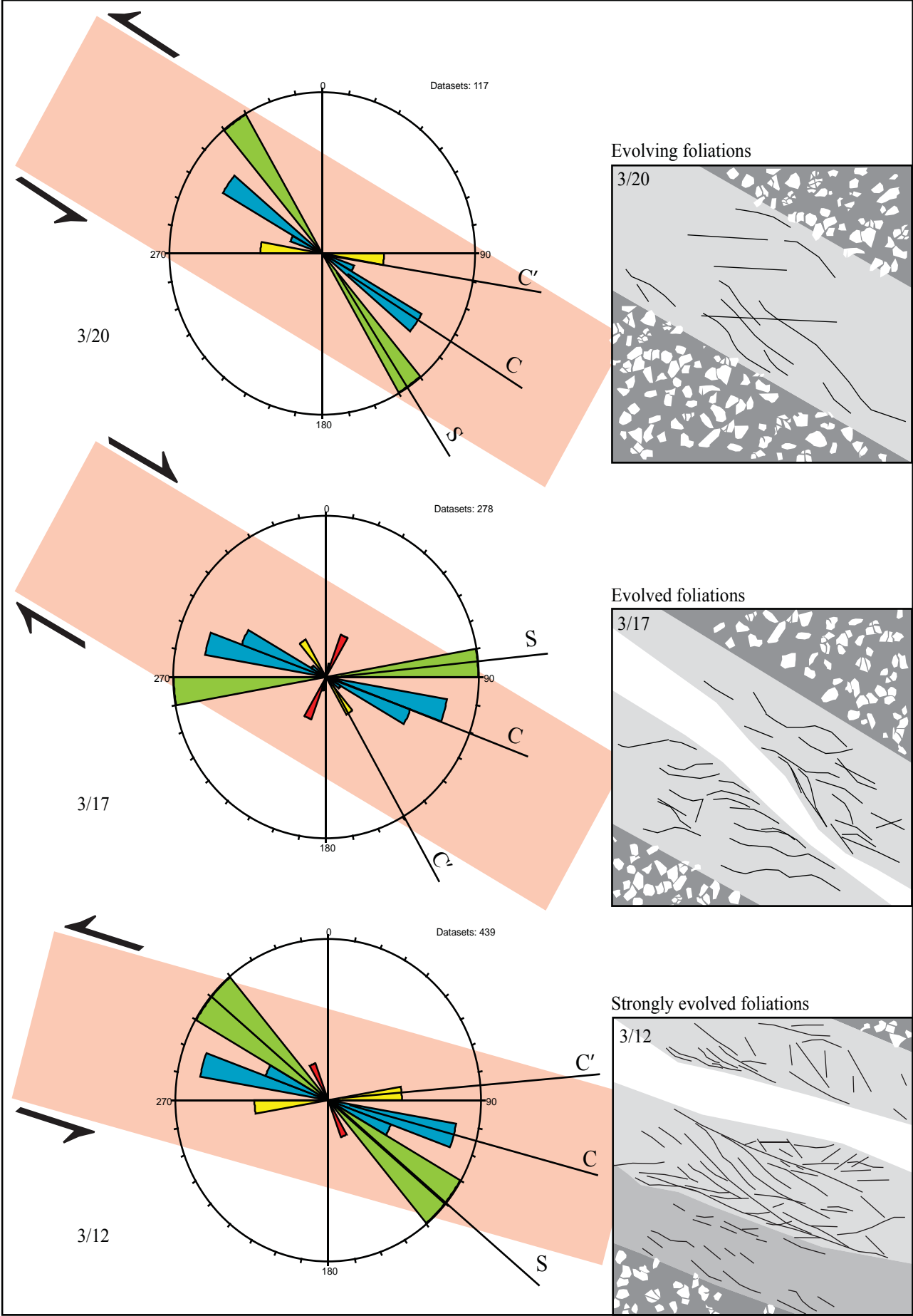
2.4.1.2 SC-structures in the micro-fault gouge

The foliation visible in the evolved zones is marked by similar extinction (i.e. similar orientation) of a newly-formed phyllosilicate. It usually occurs in two specific positions, one following the SC-structure and the other showing an indistinct preferred orientation steeply inclined with respect to the DBSZ and antithetic with respect to the SC-type geometry (figures 2.17, 2.18 and 2.19). The S-surfaces are inclined at an angle of 30° to the trend of the band, while the C-sur-

faces run sub-parallel to it. The SC-structures themselves are relatively large with respect to band width, with the length of S-segments equal to or greater than one fourth the band width, and the length of C-segments usually exceeding it. In small bands only one S-surface may exist, which exhibits multiple bending by C-surfaces. The S-surfaces are often broader in trace and less sharp at their edges than the C-surfaces, indicating that the material defining the S-surfaces is thinned out due to shearing along the C-surfaces (figure 2.17).

The foliation was mapped in detail on a selected area of three micro-fault gouges in different stages of evolution (samples no. 3/20, no. 3/17 and no. 3/12). For this purpose photographs were taken of the section in positions showing one or several clear foliations in polarized light. In a second step, the foliations were digitised and their orientation and length measured. The geometric arrangement of the orientations clearly resembles an SC-system (figure 2.20), with the S-surfaces inclined $20-40^\circ$, and the C-surfaces running sub-parallel to the shear zone. S-surfaces are slightly more frequent than C-surfaces, while C-surfaces are on average slightly longer (table 2.5). Some relatively long foliations occur at angles of $10-20^\circ$ with respect

Figure 2.20: Rose diagrams of foliations mapped in selected areas of the fault gouge of three samples (3/20, 3/17 and 3/12). The rose coloured bar indicates the strike of the whole zone; the strike of the foliations is represented in the rose diagrams as S-surfaces (green), C-surfaces (blue), C'-surfaces (yellow) and other foliations (red). The insets show simplified sketches of the foliations. The three samples represent different stages of fault gouge evolution. 3/20 is a 0.5 mm wide zone with an evolving foliation, 3/17 is a 1-1.5 mm wide zone with an evolved foliation in the matrix but with a large amount of fragments remaining in the gouge, and 3/12 is a 2 mm wide zone with a strongly evolved foliation and only few grain fragments remaining in the fault gouge. The sense of movement indicated by the rose coloured bar representing the strike of the deformation zone is derived from the SC geometry.



| Number of (image/foliation) | Number of data points | Rotation with respect to first image | Angle of foliation with respect to shear zone | Longest length [mm] | Shortest length [mm] | Average length [mm] | Interpreted type of foliation |
|-----------------------------|-----------------------|--------------------------------------|---|---------------------|----------------------|---------------------|-------------------------------|
| Thin section 3/20 | | | | | | | |
| 026/1 | 26 | 0° | 0° | 0.17 | 0.05 | 0.09 | C |
| 026/2 | 25 | 0° | 20° | 0.14 | 0.04 | 0.09 | S |
| 027/1 | 11 | 64° | 5° | 0.2 | 0.07 | 0.12 | C |
| 027/2 | 20 | 64° | 30° | 0.17 | 0.06 | 0.12 | C' |
| 030/1 | 11 | 11° | 0° | 0.11 | 0.05 | 0.08 | C |
| 030/2 | 24 | 11° | 20° | 0.13 | 0.05 | 0.08 | S |
| Thin section 3/17 | | | | | | | |
| 033/1 | 52 | 0° | 0° | 0.15 | 0.04 | 0.08 | C |
| 033/2 | 25 | 0° | 90° | 0.11 | 0.02 | 0.04 | FG |
| 033/3 | 2 | 0° | 10° | 0.09 | 0.08 | 0.08 | C' shallow |
| 034/1 | 88 | 45° | 30° | 0.12 | 0.02 | 0.06 | S, steep |
| 034/2 | 24 | 45° | 20° | 0.16 | 0.03 | 0.06 | C' |
| 035/1 | 69 | 79° | 20° | 0.13 | 0.02 | 0.06 | S |
| 035/2 | 8 | 79° | 80° | 0.09 | 0.04 | 0.05 | FG |
| 035/3 | 10 | 79° | 0° | 0.18 | 0.03 | 0.1 | C |
| Thin section 3/12 | | | | | | | |
| 002/1 | 2 | 0° | 0° | 0.29 | 0.04 | 0.13 | C |
| 002/2 | 109 | 0° | 30° | 0.35 | 0.05 | 0.14 | S |
| 002/3 | 40 | 0° | 5° | 2.66 | 2.42 | 2.54 | C |
| 003/1 | 18 | 39° | 10° | 2.22 | 0.07 | 0.44 | C, steep |
| 003/2 | 53 | 39° | 0° | 0.17 | 0.05 | 0.14 | C |
| 003/3 | 53 | 39° | 20° | 0.33 | 0.04 | 0.10 | C' |
| 004/1 | 30 | 83° | 0° | 2.0 | 0.05 | 0.29 | C |
| 004/2 | 109 | 83° | 30° | 0.25 | 0.04 | 0.11 | S |
| 004/3 | 27 | 83° | 50° | 0.48 | 0.03 | 0.11 | S, steep |

Table 2.5: (See also figure 2.20 for rose diagrams). Results derived from digitising foliations marked by similar extinction for three samples. Digitising was done on photographs taken from the same area of a thin section at positions showing a pronounced foliation. Two to three different foliation orientations could be distinguished per photograph. Note that there is always a foliation sub-parallel to the shear zone (interpreted as C), one at angles of 20° to 40° with respect to the zone (interpreted as S) and one at angles of about 20° with respect to the zone but contrary to S (interpreted as C'). The total amount of foliations is largest for the S-surfaces, followed by the C surfaces and only very few C'-surfaces. The length is shortest for S-surfaces, slightly longer for C-surfaces and even longer for C'. In section 3/17, two additional foliations with relatively short lengths appear at steep angles to the strike of the shear zone. They seem to be bound to the edges of residual grains (FG = fragment bound).

to the shear zone, but in the direction opposing the S-surfaces. They roughly correspond to the orientation of C'-surfaces, but their total number is low.

Though the three samples exhibit similar geometries, they vary in the total number of mapped foliation orientations. The two more evolved examples no. 3/17 and no. 3/12 contain additional foliations that are mapped at high angles with respect to the shear zone (figures 2.19 and 2.20, table 2.5). They belong to the above-mentioned indistinct preferred orientation. According to their orientation, they could represent antithetic X- or R'-shears of a Riedel system, but this explanation seems unlikely as there are no synthetic R- and P-shears. In sample 3/17 the steep foliations are clearly bound to residual grains of host rock embedded in the fault gouge (figure 2.19). These residual grains are often sub-rectangular in shape with edges sub-parallel and perpendicular to C-surfaces. The foliation-forming phyllosilicate minerals also seem to grow along the latter. In more developed and hence more finely ground fault gouges, the steep and indistinct foliation is still present though larger residual grains are lacking. In such cases they may either be relicts of foliations formed along large residual grains

that were destroyed during ongoing deformation, or are the sum of small and very small foliations that have been newly-formed along the edges of very small residual grains.

2.4.2 Scanning electron microscopy

SEM was used for the purpose of gaining in-depth information about the very fine-grained matrix from a number of selected samples.

2.4.2.1 Backscatter electron micrographs

Backscatter electron micrographs were taken from a selection of two samples (no. 3/3 and no. 3/13) of micro-fault gouges in different stages of evolution. They revealed the matrix of these gouges to consist of very small fragments of residual grains embedded in an extremely fine fibrous material. The fragments are either elongated or sub-quadratic but always angular in shape. The elongated fragments are parallel to the fibres and constitute a chaotic floating schlieren structure that flows around the angular fragments. The

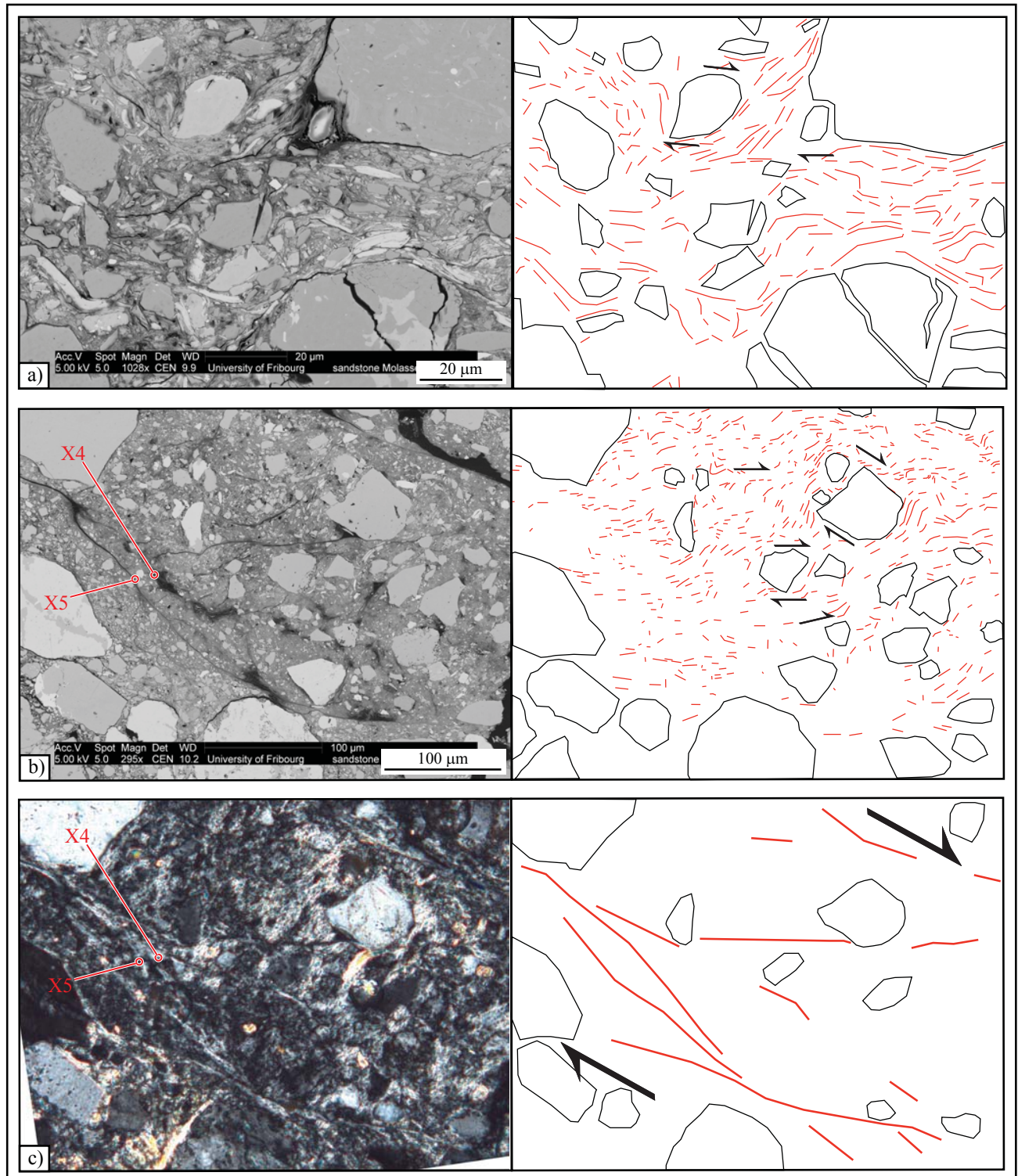


Figure 2.21: SEM micrographs at different scales (a and b) and a thin section photograph in polarised light (c) of a moderately-evolved micro fault gouge (total width of the fault gouge is up to 0.5mm). The matrix of the fault gouge consists of several small and often elongated fragments of residual grains embedded in a fibrous material, as a whole resembling a flowing structure. The preferred orientations of the fibrous material and the elongated grains were sketched (red lines) for all three images. The optical-microscope image (c) was taken from the same part of the section as (b). The foliations marked by similar extinction are sketched and correspond to zones with fewer fragments and higher content of fibrous material in the SEM micrograph (b). Within these zones, the fibrous material and the rare elongated fragments are aligned parallel to the zone. Between these zones, the flowing structure of the matrix appears chaotic but it bends into the zones. The nature of the bending as well as sigmoidal flow around fragments of residual grains (though often deviated and incomplete) contain kinematic information—mostly right-lateral in the given case. The locations of chemical analyses of the matrix given in table 2.6 are indicated by the red circles X4 and X5 in (c).

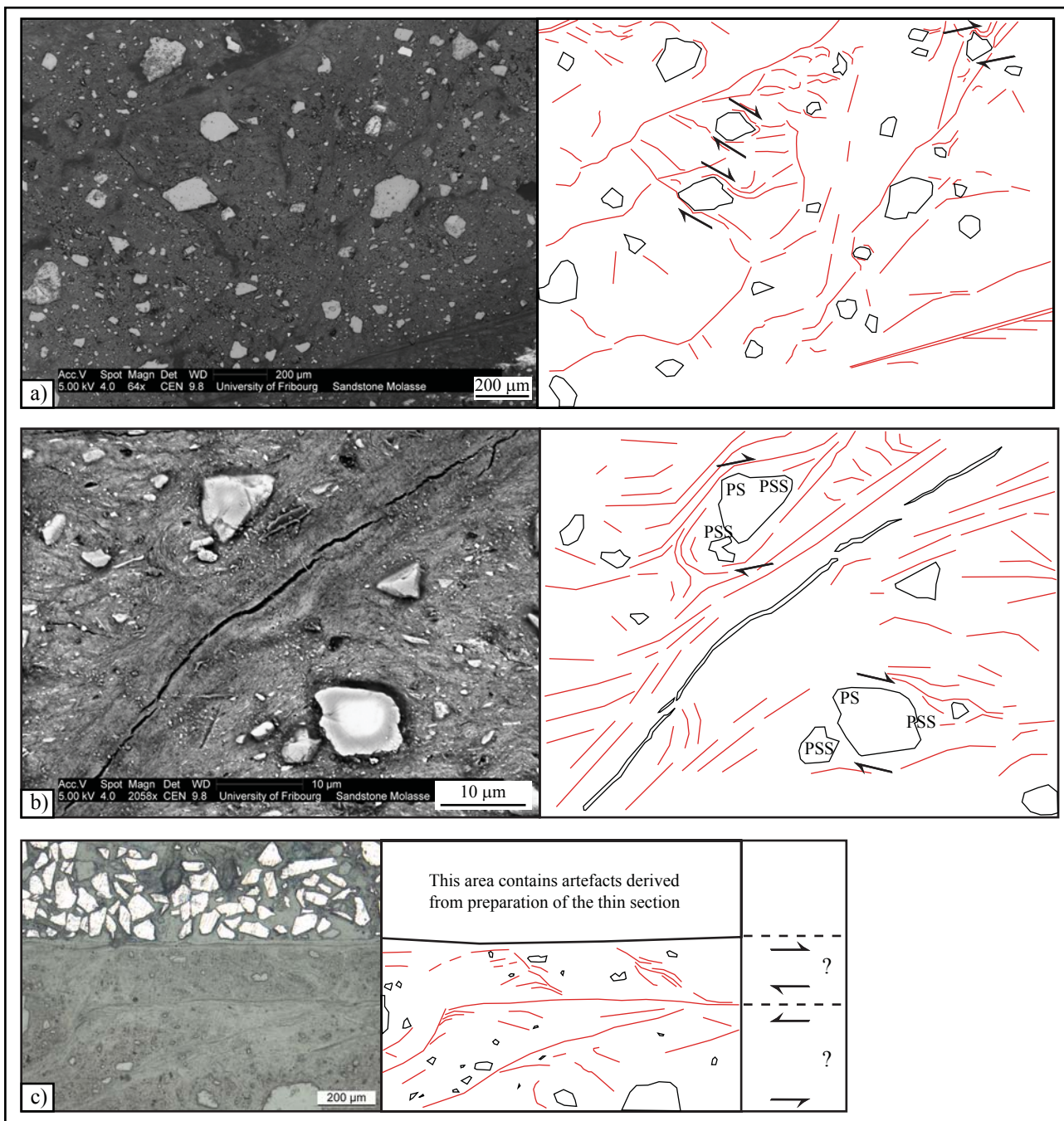


Figure 2.22: SEM micrographs at different scales (a and b) and a thin section photograph in plane light (c) of an evolved micro-fault gouge (total width of the fault gouge is up to 5mm). The preferred orientations of the fibrous material were sketched (red lines) and given for all three images. Fragments of residual grains are rare and show random orientation. The fibrous material reveal zones of chaotic flowing structures bounded by elongate zones of preferred orientation. The latter appear as foliations with similar extinction using polarized light microscopy. Their geometric arrangement as well as sigmoidal flow around fragments of residual grains (though often deviated and incomplete) contain kinematic information—mostly right-lateral in the given case. In (c) the fault gouge can be divided into two sub-zones, possibly with opposite senses of movement. PS = Pressure side and PSS = Pressure shadow side of grains with sigmoidal flow structures.

sigmoidal deviation of the flow structure around the angular fragments is caused by rotation of the latter, and may be used to derive a local sense of movement. However, these sigmoidal geometries are often incomplete or disturbed by small fragments that probably detached during rotation. In general, the fragments' pressure sides are characterised by bends around the

fragment edges, while the pressure shadow sides are marked by bends away from them (figure 2.22).

The moderately-evolved fault gouge from a 0.5 mm-wide DB in sample sample no. 3/3 (figure 2.21) shows a higher density of grain fragments than the strongly evolved fault gouge of a 5 mm-wide de-

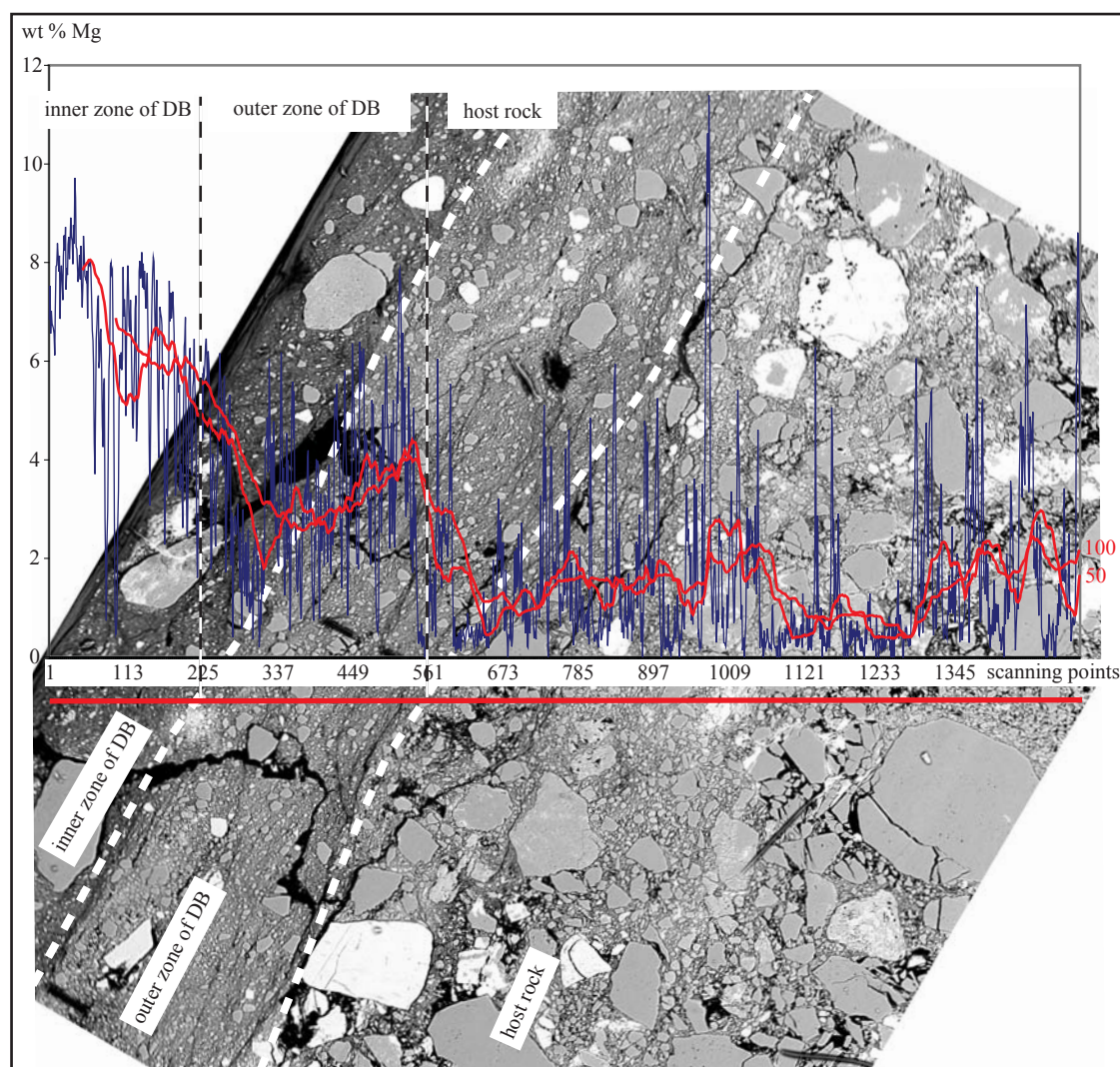


Figure 2.23: SEM micrograph of sample 3/13 with EDS line scan giving weight percent Mg. The section is about 2 mm long and runs along the red line in the image. Blue curve gives values for each of the 1583 scanning points. The red curves are regression lines with averages for every 50 and every 100 points, respectively. The dashed white lines on the image mark the borders between host rock, outer and inner zone of the DB. These borders are also indicated on the diagram. The Mg content increases stepwise from the host rock through the outer and into the inner zone of the band.

formation zone in sample sample no. 3/13, where the floating structure is almost completely composed of the fibrous material (figure 2.22). Moreover, the fewer fragments in sample no. 3/13 (figure 2.22) are all angular and about one magnitude smaller in size than in sample no. 3/3. This suggests continuing grinding of the material and transformation into fibrous phyllosilicates during ongoing deformation of the fault gouge. Sample no. 3/13 also shows a lower content of detrital mica than sample no. 3/3, which probably accounts for the lack of elongated fragments in its fault gouge.

The zones of chaotic floating schlieren structures are bounded by elongated zones of preferred orientation, which the floating structure systematically bends into. This kinematic indicator is however either local or else ambiguous, as it does not always give the

same sense of movement as the sigmoidal geometries described above. The elongated zones of preferred orientation contain few or no fragments of residual grains. They are oriented similarly and bend into each other where they meet. These zones occur where the fibrous phyllosilicate is most highly concentrated, and where the foliations marked by similar extinctions appear under the optical microscope.

2.4.3 Chemical composition

The exact mineralogy of the DB fault gouges was quantified by EDS transects, and XRD analyses of macroscopic fault gouges were carried out. For the fault gouge from sample no. 3/13 shown in figure 2.22, we were able to prepare material for the XRD

| Element | Palygorskite | Point analysis X4 | | Point analysis X5 | |
|---------|--------------|-------------------|---------------|-------------------|---------------|
| | | Weight % | Stoichiometry | Weight % | Stoichiometry |
| Mg | 1.76 | 4.71 | 1.22 | 3.36 | 0.86 |
| Al | 2 | 7.90 | 1.85 | 6.07 | 1.41 |
| Si | 8 | 35.17 | 7.91 | 37.79 | 8.42 |
| Mn | 0.08 | 0.17 | 0.02 | 0.16 | 0.02 |
| Fe | 0.05 | 1.42 | 0.16 | 1.48 | 0.17 |
| O2 | 19.4 | 50.64 | 20.00 | 51.14 | 20.00 |

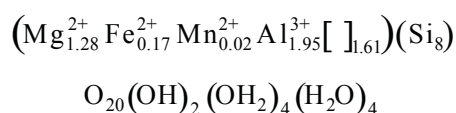
Table 2.6: Results of EDS point analyses of the very fine-grained matrix at points X4 and X5 on thin section no 3/3. See figure 2.21 for point locations. The chemical formula of palygorskite is $\text{Si}_8\text{Al}_2\text{Fe}_{0.05}\text{Mn}_{0.08}\text{Mg}_{1.76}\text{O}_{19.4}(\text{OH})_{2.6}[\text{H}_2\text{O}]$, taken from: <http://database.iem.ac.ru/mincryst>

analysis as well as provide a thin section for optical microscopy and electron microscopy. In addition to XRD analysis of fault gouge, host rock XRD was carried out for macroscopic fault zones in the study area.

All analyses clearly reveal the presence of palygorskite, but only in the fault gouge and never in the host rock. It follows that this mineral is newly-formed during deformation. In the thin section from sample no. 3/13, the micro-fault gouge is characterised by a dense array of foliations marked by similar extinction (figure 2.16) that correspond to a very fine fibrous material shown in the SEM micrographs of the same sample (see section 2.4.2.1). This material is most likely the palygorskite, and it can be found in several of the micro-fault gouges.

Element line transects provided by EDS reveal a higher amount of Mg in the fault gouge than in the host rock which, as palygorskite is an Mg-rich phyllosilicate, further validates its presence in the DB fault gouges. In the line transect from sample no. 3/13 (figure 2.23), the two sub-zones shown in figure 2.16 are reflected in the step-wise increase of the Mg-content; it is higher in the outer zone than in the host rock, but highest in the inner zone. At the same time, the inner zone shows denser foliations and a higher ratio of fibrous material to fragments of residual grains.

Point analyses of the fibrous material by semi-quantitative EDS analysis revealed the geochemistry given in table 2.6. According to these analyses, the palygorskite has the following chemical composition:



2.5 DISCUSSION

2.5.1 Evolution of deformation bands

The microscope analysis of thin sections shows that the grains of the host rock in the vicinity of a DB are frequently broken, though the individual fragments remain in place. The different types of grain breaking observed in this study are quite similar to the micro-fractures described by Aydin (1978). The fracturing of grains in the host rock, the displacement of fragments and the occurrence of finely ground matrix in the bands indicates that cataclasis of the grains is the mechanism by which the DBs are formed. They can therefore be defined as DBs in the sense of the literature (e.g. Aydin 1978, Aydin & Johnson 1978, Antonellini et al. 1994, Fossen et al. 2007), or even more precisely as DBs with cataclasis in the sense of Antonellini et al. (1994), or cataclastic DBs in the sense of Fossen et al. (2007).

Several of the DBs investigated in this study exhibit a foliation in the matrix of their fault gouge. These foliations develop from unfoliated fault gouges by narrowing of the DB and hence strain concentration, as well as with ongoing deformation and strain accumulation. They reach from single foliation filaments to densely foliated zones with fully developed SC-type geometries and micro-scale characteristics quite similar to those of macroscopic fault gouges. DBs with fully developed foliations are broader than single cataclastic bands or bands with less developed foliations. Widening of the fault gouge during its evolution is a process well-known from fault zones all over the world (Scholz 1987, Hull 1988), but is not expected for single brittle DBs, since their evolutionary models predict instantaneous strain hardening and deactivation of the band (Aydin 1978, Aydin & Johnson 1978). In the evolutionary model of Aydin and Johnson (1978), strain accumulation occurs in three sequential stages with a change in the mode of deformation from (1) pore space collapse and grain fracturing to (2) discrete faulting (figure 2, a-c). The first mode is deformation banding. It takes place as

pore space collapses and grain fracturing and is characterised by strain hardening of the material. It locally transforms the porous sandstone into non-porous media, providing the conditions for the second mode which is discrete faulting (Davis et al. 1999). The mode of deformation banding is characteristic of granular materials, whose shear resistance is determined by chains of grain contact points running sub-parallel to σ_1 (Mandl et al. 1977, Rawling & Goodwin 2003). In porous sandstone, these chains may fail by dilatational fracturing of the grains (Mandl et al. 1977, Rawling & Goodwin 2003). The smaller the resulting fragments, the smaller the pore space and the more the material behave like non-porous media that fractures by discrete faulting. Each deformational increment of the mode of deformation banding results in a new band, and offsets remain small even across bundles of DBs (Aydin & Johnson 1978). In the final stage, considerable offset accumulates across the discrete fault plane (Aydin & Johnson 1978).

For the DBs in this study the first stage is quite similar, with the width of a single band increasing with the grain size of the host rock, and strain accumulating by the formation of new sub-parallel bands. However, the second stage is different. It starts with the evolution of a micro-fault gouge of a single band, which in turn results in the development of a foliation and subsequent strain softening. In this second stage, band-width increases with strain, i.e. with increasing offset, in this way behaving like a macroscopic fault gouge. The transition between both modes of faulting can be determined only on the microscopic scale, and not by the occurrence of a discrete slip plane. It occurs in DBSZs after a considerable amount of deformation banding has taken place, but also in single DBs instead of further deformation banding, as well as in

constricted zones where the strain of several different bands concentrates.

2.5.2 Conceptual model for the evolution of micro-fault gouge

Based on the observations from the SEM micrographs of the moderately-evolved zone in sample no. 3/3, a sequence of continuous deformation can be deduced that provides a possible model for the evolution of micro-fault gouges and their foliations. We have schematically subdivided the deformation process into four steps, which are illustrated in figure 2.24.

1) In the first step, grains fracture by dilatational cracking, oriented parallel to σ_1 and about 45° in a normal sense with respect to the developing shear zone and the sense of movement. Thus grains with a preferred crystallographic orientation, such as micas, tend to form elongate fragments, whereas quartz grain fragments become sub-quadratic in shape. The latter exhibit at least one (fractured) edge oriented parallel to σ_1 .

2) Immediately after fracturing, the fragments start to rotate following the sense of shear (clockwise according to right-lateral shear in the micrograph from sample no. 3/3), thereby taking up successively steeper orientations with respect to the shear zone and the sense of movement, changing from normal to reverse.

3) Once the rotated grains have reached a position of 45° and reverse with respect to the shear zone and sense of movement they start to form elongate zones with orientations comparable to those of S-surfaces

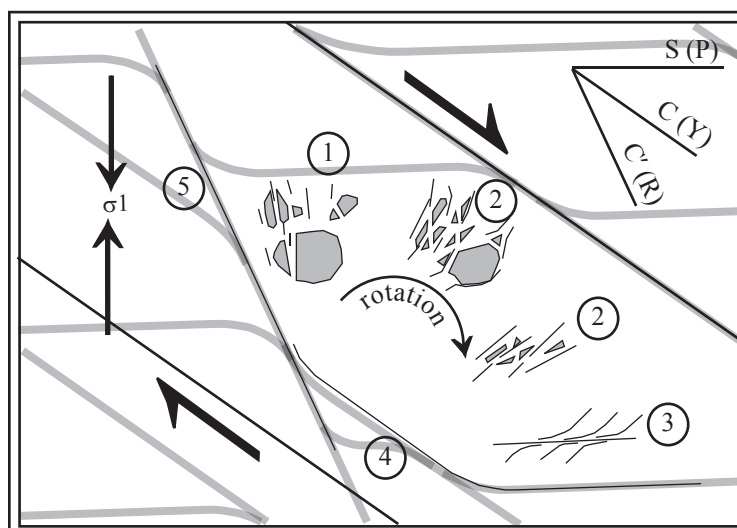


Figure 2.24: Sketch to illustrate the evolution of foliation planes in the micro-fault gouges. 1): Cracking grain fragments and formation of palygorskite fibres along the cracks; 2): Clockwise rotation (for right-lateral shear), further cracking and palygorskite formation; 3): Alignment of very fine material and palygorskite in a plane perpendicular to σ_1 (comparable in orientation to a S-type foliation), then right-lateral shear after further slight rotation (into an orientation parallel to a P-shear); 4): C-surface and 5) C'-surface, marked by the alignment of palygorskite.

or (after further slight rotation) P-shears. Asymmetric bending of material into these elongate zones from both sides indicates the existence of shear.

4) The elongate zones formed in step 3 resemble the S-type foliation visible under the optical microscope. Along-strike they bend into zones of similar appearance oriented parallel to the shear zone and comparable to C-surfaces or Y-shears. These “C-surfaces” are occasionally dragged into zones shallowly inclined and normal with respect to the shear zone and the sense of movement (C'-surfaces or R-shears).

From the beginning, this process is accompanied by the growth of palygorskite in newly formed space such as dilational cracks, as well as by further fragmentation and reshaping of the rotating grains. This leads to a progressive transformation of the fault gouge material towards palygorskite, as is illustrated by those SEM micrographs showing elongate zones with successively fewer fragments and more fibrous material. Similarly, samples no. 3/3 and no. 3/13, which differ in their degree of fault gouge evolution, also differ in their palygorskite to fragment ratio.

The space between the foliation planes is marked by chaotic orientations of both the fragments and the palygorskite fibres grown sub-parallel to them. The structural assemblage may therefore be subdivided into chaotic and regular structures, with the chaotic ones consisting of fractured and rotated grains. The regular structures are the foliations, which are those parts of the matrix with a high palygorskite to fragment ratio.

According to the conceptual model described above, the formation of the chaotic structures is a prerequisite and therefore predates the formation of the regular ones. Since failure of a force chain by dilational grain cracking alone does not lead to chaotic structures, their existence requires an additional process of formation. This additional process displaces the fragments in the fault gouge, while those in the host rock remain in place. If the fracturing occurred during catastrophic failure, the energy released would be translated into kinetic energy, displacing the fragments and resulting in an instantaneous increase of pressure on the surrounding grain fabric. Like fluid overpressure, this rapid pressure increase along the forming DB would dramatically reduce shear resistance (Boulton et al. 2009). This process of catastrophic rock failure, leading to immediate further damage by the released kinetic energy, has been termed dynamic rock fragmentation (Gardly & Kipp 1987). The

chaotic structures described in steps 1) to 4) are most likely formed by this process, accordingly termed dynamic grain fragmentation. The process of dynamic fragmentation in the fault gouges of the DBs is thus added to the process of force chain failure in the host rock. It makes the rock permeable for infiltrating fluids, which activate palygorskite formation. The regular structures then form by strain localisation in the palygorskite-rich zones, corresponding to the zones of finest grinding.

2.5.3 Riedel shears versus SC-fabric

Based on their geometry, the three orientations of planar features identified as foliations in thin section were determined as S-, C- and C'-surfaces of an SCC'-fabric. An indistinct foliation with a steep orientation relative to the shear zone also occasionally occurs in close relationship to the steep edges of grain fragments. Instead of constituting an SCC'-fabric, the three main observed foliations could also represent the geometry of an incomplete Riedel system consisting only of P- and Y-shears or, if no offset marker was present, of R- and Y-shears. However, if in the latter case S is mistaken for R, the interpreted shear sense would be the opposite. A possible way to identify R- and Y-shears of a Riedel system is the irregular spacing and an R-shear : Y-shear interval ratio of ~0.5 (Strating & Vissers 1994). In the micro-fault gouges of the DBs, neither a regular spacing nor a ratio that holds for all samples has been observed. The incompleteness of a Riedel system consisting mainly of P- and Y-shears in comparison to a fairly complete SC-fabric containing S- and C- surfaces, as well as the lack of a regular spacing between the suspected P- and Y-shears, are geometric arguments for an SCC'-fabric.

From a genetic point of view, it should be possible to distinguish between S-surfaces, which represent planes of mineral alignment, and any type of Riedel shears, which represent shear fractures. On the one hand both thin sections and SEM analysis of the DBs revealed that the foliations in the micro-fault gouges are marked by the preferred orientations of palygorskite, a mineral phase not present in the host rock and hence newly-formed during deformation. Its alignment thus suggests that the foliations are S-surfaces and sheared S-surfaces (i.e. C-surfaces). On the other hand, the SEM micrographs reveal that palygorskite is also forming between the foliations running parallel to grain fractures and in nearly every position with respect to the stress ellipsoid. Therefore the foliations

are more likely interpreted as regular zones within an otherwise chaotic matrix, whose foliated character results from shape-preferred orientation of the material (Cladouhos 1999a) rather than from newly-grown mineral phases. In the SEM micrographs, the S-surfaces of the foliations show systematic bending of the material on both sides but in opposite directions, indicating shearing to have taken place; this should strictly speaking not be the case on pure S-surfaces. However, the inferred sense of movement does correspond to that of a P-shear in a Riedel system, which from a geometric point of view closely resembles an S-surface. A foliation resulting from shape-preferred orientation of grain fragments has been termed P-foliation and can be explained by the Riedel shear model (Cladouhos 1999a and b). Although the grain fragments do rotate in the area between the foliations in the fault gouges, they are also ground further and transformed to palygorskite. At the end the foliation plane is defined nearly exclusively by the new mineral. The homogeneity thus achieved most likely facilitates shear along these surfaces.

Mylonitic SC-fabrics are indicative of moderate strain across a relatively broad zone (e.g. Simpson 1984), which contrasts with the narrow zone of a DB containing only a few parallel sets of S- and C-foliations and an obviously relatively high strain. In the brittle micro-fault gouges of the DBs, the S-type surfaces form in the same way as S-foliations, i.e. by the alignment of material and newly-formed minerals along the X-Y plane of the strain ellipsoid. Once formed, the relative homogeneity of the material along an S-surface represents a zone of weakness and the S-surfaces start to behave like the P-shears of a Riedel system and accommodate a certain amount of shear

strain. The two most prominent foliations identified in the thin section of the DBs might therefore be interpreted as an SC-foliation in terms of kinematics, but must be considered as an incomplete Riedel system with P- and Y-shears in terms of strain localisation.

2.5.4 Implications for fluid flow

The formation of palygorskite from the mineralogy of the host rock requires an excess of quartz and water; Mg is provided by chlorite and dolomite. Equilibrium calculations using the host rock mineralogy and compositions of fluids from different Molasse and Malm formations revealed palygorskite to be in equilibrium, while chlorite is in disequilibrium. This implies a chlorite-consuming and palygorskite-forming reaction that is related to deformation (Chapter 3).

The detailed study of experimentally generated DBs revealed micro-fault gouge to be chemically highly reactive due to the large total amount of fresh surfaces (Main et al. 2001). Palygorskite formation is most likely triggered by the contact of the highly reactive fault gouge with the fluid phase in the course of deformation. Laboratory experiments by Mandl et al. (1977) showed that shearing of granular material results in increased permeability parallel to the evolving shear band. Similarly, Mair et al. (2000) observed an initial pore space increase in experimentally deformed sandstone. They attributed this to dilatational cracking of the grains and proposed an increased permeability parallel to DBs due to the micro-cracks of the host rock grains in the near vicinity. This may provide the possibility for fluids to reach the fault gouge (fig-

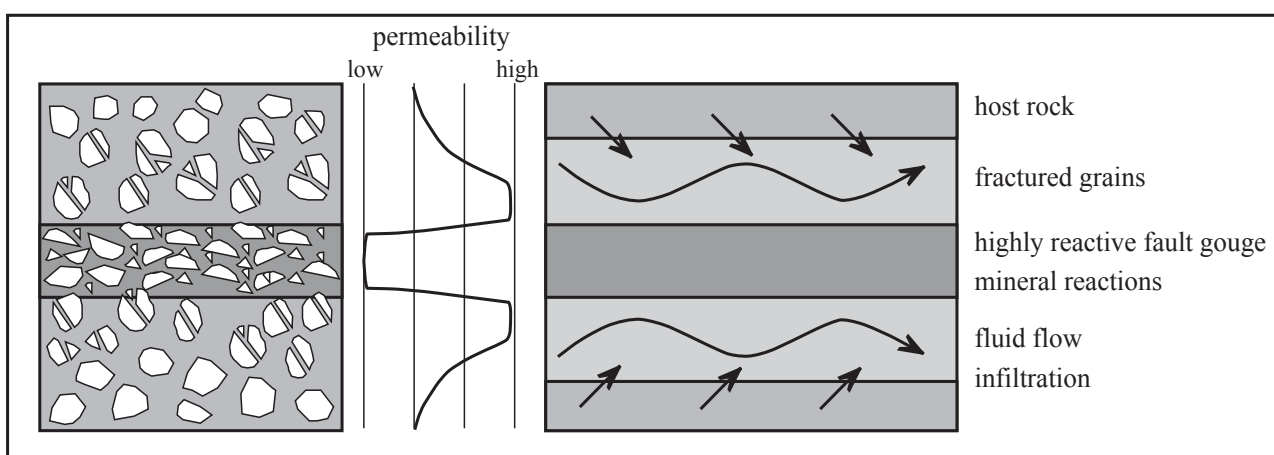


Figure 2.25: Permeability distribution around a DB as suggested from porosity evolution during DB formation in laboratory rock deformation tests (after Mair et al. (2000), see also fig. 2.5) and its implications for fluid flow and fault gouge evolution. Increased porosity by fractured grains provides a channel for fluid flow parallel to the DB. The contact of the fluid with the highly reactive fault gouge leads to mineral reactions (palygorskite formation) and further evolution of the gouge.

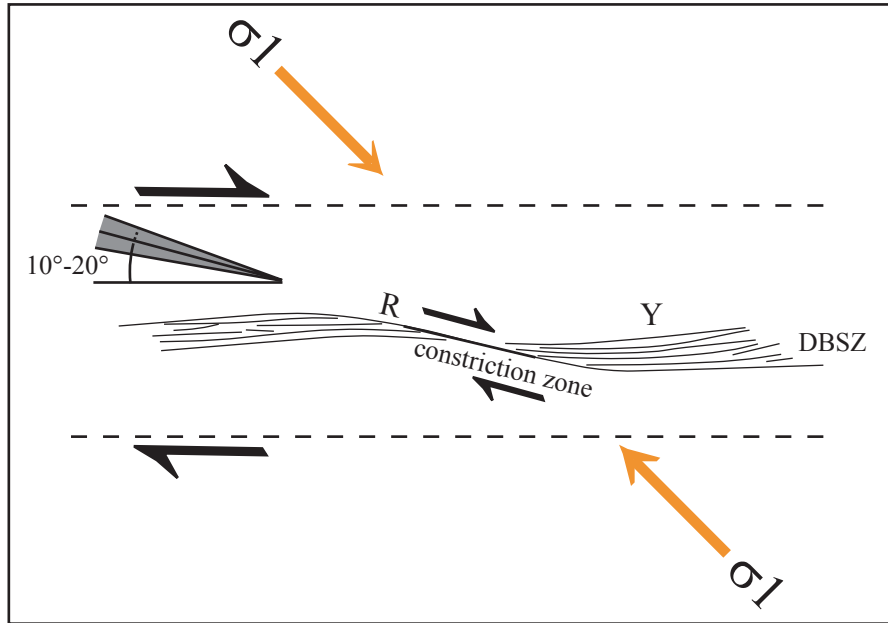


Figure 2.26: DBSZ and constriction zone, interpreted as a Y-shear (DBSZ) that becomes sheared as an R-shear (constriction zone). Observations in the field and in thin section show DBSZ and constriction zones to be orientated at angles of 10° - 20° to each other, with the DBSZ and σ_1 enclosing a larger angle than the constriction zone and σ_1 . Strain concentration is observed in the constriction zone.

ure 2.25). The onset of palygorskite formation is also a question of the amount of fluid in contact with the fault gouge. This critical amount can be reached by an increasing number of parallel channels, by the brittle shearing of a DB zone by R-shears in constriction zones of DBSZs and, if deformation occurs during seismic events, by implosion of the fault gouge and associated suction-pump effects into the micro-fault gouge. Once palygorskite formation starts, it weakens the fault gouge and the DBs gradually change from a strain-hardened to a strain-softened shear zone. This leads to the accumulation of strain in the palygorskite bands, which gradually evolve into macroscopic fault gouges.

2.5.5 Significance of the macroscopic geometry of DBs in the Molasse sandstone

The deformation of the sandstones of the western Swiss Molasse Basin is initiated by grain-scale cataclasis forming brittle DBs. From the macroscopic point of view, the DBs are mm-wide planar zones several metres in length. Ongoing deformation results in the formation of DBSZs. Strain often concentrate due to the constriction of a DBSZ with its local reorientation, or by a closer formation of individual bands. On the microscopic scale, the micro-fault gouges develop from fine-grained material to foliated gouges with palygorskite as strain accumulates. On

the macroscopic scale, ongoing deformation gradually translates dense DBSZs into macroscopic fault gouges containing palygorskite. True slickensides with mechanical scratches on their fault planes are rare, while fault planes with lineation of fibrous palygorskite are common.

The constricted zones of DBSZs are rotated towards a smaller angle with respect to σ_1 . According to the Mohr-Coulomb criterion, a small angle between a shear and σ_1 implies a high angle of internal friction of the sheared material. Therefore the formation of constricted zones of DBSZs along shears at lower angles to σ_1 than the DBSZ themselves demonstrate strain hardening of the material by deformation banding. However, as initial deformation in porous rocks occurs by deforming pore space and grain fabric (and hence with a micro-mechanism resembling cataclastic flow), its behaviour is more like a ductile material (Wong et al. 1997, Bayerlee & Brace 1968). This allows shears to develop at initial angles higher than 30° in the Mohr-Coulomb space. Field studies have reported that deformation of porous sandstone may initiate by DBs forming at high angles with respect to σ_1 , e.g. as antithetic Riedel shears (Ahlgren 2001). Deformation of granular material results in shear zone orientations not in accordance with the Mohr-Coulomb criterion, but with subsidiary shears developing in Riedel-type geometries and hence fitting the criterion (Mandl et al. 1977). The DBs in this study developed at a certain angle. Ongoing deformation forms DBSZs that represent a zone of strain-hardened

material and hence of material with a higher angle of internal friction. At a certain point, this leads to the development of “more brittle” shears that crosscut the shear zone at slightly lower angles with respect to σ_1 . The geometry of these brittle shears corresponds to R-shears of a Riedel system (figure 2.26).

Grouped by outcrop, most of the DBs mapped in the field arrange as conjugate sets that can be interpreted in terms of a Riedel system as synthetic and antithetic shears of a superordinate shear zone. The different groups can be allocated to two such superordinate shear zones, one of which strikes WNW-ESE (right-lateral) and the other NNW-SSE (left-lateral), with σ_1 oriented NW-SE. These two superordinate sets match perfectly with the orientations of the larger structures found in the study area, such as slickensides and fault zones. These larger structures occur in two conjugate Riedel systems with NW-SE compression. The close geometric relationships imply that the DBs and the larger structures have formed in the same tectonic regime. They reflect the initiation of fault zones in the Molasse sandstone, as has also been described for other regions (Shipton & Cowie 2001).

2.5.6 Seismic versus aseismic nature of the DBs

The earthquakes recorded in the study area by the seismic survey of Switzerland in the last decades reveal a low to moderate seismicity with magnitudes up to 4 (local magnitude). The focal mechanisms are predominantly strike-slip with left-lateral movement along N-S-striking fault planes and right-lateral movement along E-W-striking fault planes. The alignment of a number of these events in a zone several kilometres in length has provoked authors to postulate that moderate to large earthquakes maybe possible in the area (Kastrup et al 2007). It is therefore of interest to discuss the seismic versus aseismic nature of DB formation and evolution.

Initial deformation in the brittle regime should be seismic, although the energy released by forming a fracture is very low. The stress-strain curves for DB-SZs produced in the laboratory (Mair et al. 2000) reveal a significant stress drop only for the formation of the first band, while the subsequent bands form in a steady state. This implies deformation banding to be rather aseismic in nature.

The fabric of the evolving micro-fault gouge shows both regular semi-ductile structures as well as

chaotic arrangement of fragments. This, however, implies that the evolution of micro-fault gouge occurs in two modes that may interact with time, representing seismic slip and aseismic creep. The chaotic structures form by dynamic rock fracturing (Garday & Kipp 1987, Boulton et al. 2009), which can provide pathways for the influx of fluid in the otherwise less permeable fault gouge. The formation of palygorskite after such an event facilitates the aseismic creep by which the regular structures (e.g. the SCC'-fabrics) are formed. The amount of palygorskite increases as deformation continues i.e. creep becomes more important as the shear zone grows. These observations from the micro- and meso-scale structures indicate that earthquakes should be unlikely due to the prevalent aseismic mechanism of deformation of the Molasse sandstones. However, a larger-scale fault may be stuck at a restraining bend or within another lithology along-strike, and its rupture could be seismic. In any case, such rupture events must occur somewhere in the fault network to account for at least part of the registered earthquakes up to magnitude 4.

Porous media such as the poorly lithified Molasse sandstone is expected to be slightly weaker than non-porous rock, as stress is concentrated on grain contacts (Mandl et al. 1977, Wong et al. 1997). The possibility to form new DBs in the host rock around a restraining bend therefore most likely limits the amount of elastic strain accumulation and hence the rupture magnitude. Probably for the same reason, stick-slip behaviour was found to be absent for porous rocks (Bayerlee & Brace 1968). Another limiting factor may be fault size, since earthquakes of larger magnitudes require large rupture plane (Wells & Coppersmith 1994). However, no fault zones longer than a few kilometres were mapped in the field. Even though our mapping represents only a surface observation of the area, it does support a model of relatively frequent, low magnitude earthquakes on a network of small-scale faults. This corresponds to the recordings of the permanent seismic stations in the region during the past decades (SED 2010, annual reports of the seismic survey of Switzerland, published in the Swiss Journal of Geosciences).

2.6 CONCLUSION

The DBs mapped in the sandstone of the western Swiss Molasse Basin develop in two stages. In the first stage, they initiate as “classical” brittle DBs by grain scale cataclasis producing a micro-fault gouge. This micro-fault gouge shows poorer sorting

and reduced pore space with respect to the host rock, which causes strain-hardening. Ongoing deformation therefore promotes the formation of new bands sub-parallel to the existing ones. In the second stage, the micro-fault gouge accumulates strain and develops a foliation consisting of newly-formed palygorskite, which causes strain-softening. The strain-softened DBSZs directly translate to macroscopic fault gouges containing palygorskite.

The evolution of the micro-fault gouge occurs in two modes as revealed by the regular structure of the foliation network and the chaotic structures in the area between the foliations. We interpret the chaotic structures to be the result of instantaneous failure, and the foliations from ongoing shear facilitated by the existence of the palygorskite minerals. The regular geometry of the foliations can be interpreted as an SCC'-fabric in terms of kinematics, and thus provides a microscopic shear sense indicator. In terms of strain localisation however, the foliations must be regarded as P- and Y-shears of an incomplete Riedel system, as they represent planes of enhanced strain.

The formation of palygorskite as a new mineral phase is triggered by the grinding of the mineral grains of the host rock and the inflow of a fluid phase. The mechanism of DB formation accounts for the grinding as well as the formation of band-parallel channels of enhanced permeability.

In the field, the DBs develop in conjugate sets similar to the orientations of larger structures such as slickensides and fault zones, but with slightly larger

angles with respect to σ_1 . This is thought to reflect the lower angle of internal friction of porous media such as poorly lithified sandstone. The DBSZs frequently show zones of constriction where they narrow along a shear slightly rotated towards σ_1 . These constriction zones are interpreted as shears oriented according to an increased angle of internal friction in the strain-hardened material of a DBSZs.

The chaotic structures and the regular foliation network observed in the micro-fault gouge most likely represent seismic and aseismic deformation modes, but stress drops occur only in the range of micro-seismicity. The increasing amount of palygorskite and the number of foliations with the development of micro-fault gouges indicate that aseismic deformation becomes more important as the structure grows. Despite their seismic initiation, the DBs in the study area can therefore be interpreted as structures characteristic for aseismic deformation. However, the possibility of DB formation in the host rock also limits the accumulation of elastic strain, and therefore the possible magnitude of a rupture event along a larger fault zone.

The tectonic regime in the western Swiss Molasse Basin is strike-slip faulting with NW-SE-compression. The DBs mapped in this area represent fault initiation in the Molasse sandstones. Their micro-mechanics lead to growth of palygorskite minerals, responsible for the rather aseismic nature of subsequent shear. The DBSZs of this study imply that the possible occurrence of seismic ruptures along larger faults of the regional network is limited in magnitude.

3 - THE ORIGIN OF PALYGORSKITE IN FAULT GOUGES OF THE WESTERN SWISS MOLASSE

Ibele, T., Grobéty, B., Mosar, J.

submitted to European Journal of Mineralogy

ABSTRACT

Analyses of brittle fault gouges from the western Swiss Molasse Basin by X-Ray diffraction and electron diffraction spectroscopy revealed palygorskite - a Mg rich clay mineral - to be common in fault gouges of different scales, while absent in the host rocks. Fault gouges are also depleted in chlorite, compared to the host rock, while albite and quartz are present. Thus a chlorite-consuming reaction for palygorskite formation seems to be obvious. This reaction may have been triggered by a fluid phase that is percolating along deformation induced fractures, and that is in equilibrium with palygorskite, quartz and albite, while in disequilibrium with chlorite. Acknowledging the importance of fluid flow possibly has important consequences on the size/length of the fracture network and the associated fluid paths. Titration calculations with the host rock mineralogy and different fluids from surrounding aquifers were made in order to pinpoint such consequences. Calculations were based on composition of formation waters known from the underlying Malm limestone, in-situ waters of the Lower Freshwater and Upper Marine Molasse, taken from both shallow and deep wells. We also used sea water composition, present during the Upper Marine Molasse deposition. The results show that all tested fluids are in equilibrium with palygorskite and in disequilibrium with chlorite, i.e. no specific distinct fluid source is needed, and palygorskite formation is critically linked only to deformation and generic fluid flow. Our study reveals a new formation process for palygorskite, linked to the development of brittle fault gouges and associated fluid flow. This brittle deformation in foreland basin sediments is a quite common geologic setting. Palygorskite is therefore likely to be also present in comparable environments elsewhere.

3.1 INTRODUCTION

Brittle faulting is the major deformation mechanism in the upper crust, generating fault gouges and cataclasites with random fabrics (Sibson 1977), or, less commonly with planar fabrics and macroscopically ductile geometries (Chester & Logan 1987, Chester et al. 1985, Lin 2001). The most important element of the planar fabrics are clay minerals precipitated syn- or post-faulting. Clay formation under near-surface conditions may be triggered by the increase of reactive mineral surfaces, the release of thermal and mechanical energy, and local pressure increase during deformation (Vrolijk & van der Pluijm 1999, Main et

al 2001, Sibson 1987, 1990). Fluid flow along the fault zone is another important factor leading to clay formation. The gouge mineral assembly will be determined by the mineralogy of the faulted rock, the composition of the fluid circulating along the fault as well as by the temperature-pressure conditions during precipitation. The most common clay minerals encountered in fault gouges of acidic rocks are illite, smectite, chlorite and mixed layer phases of the latter three phases (Vrolijk & van der Puijm, 1999).

During an investigation of the tectonics of the western Swiss Molasse (figure 3.1), palygorskite, a Mg-rich clay mineral, was found in a large number

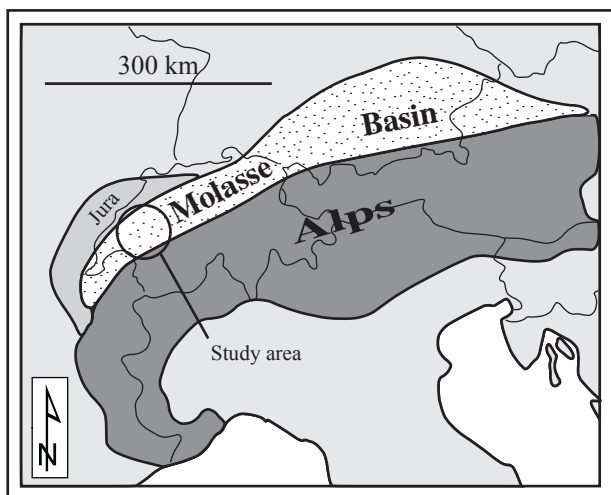


Figure 3.1: Location of the study area

of fault zones (figures 3.3 and 3.2). The Molasse units with the palygorskite-containing faults were deposited in Oligocene and Miocene times into the peripheral foreland basin of the Alps (Trümpy 1980, Pfiffner 1986, Homewood et al. 1986). They are composed of four formations, the Lower Marine- (UMM), Lower Freshwater- (USM), Upper Marine- (OMM) and Upper Freshwater Molasse (OSM), representing two shallowing up megacycles deposited under alternating fluvio-lacustrine and shallow marine conditions (Trümpy 1980, Homewood et al. 1986, Platt & Keller 1992, Berger et al. 2005). They are underlain by Mesozoic units that are detached along a Triassic evaporitic unit from the underlying basement. These Mesozoic units consist of partly evaporitic Triassic and usually shale-rich lower Jurassic, followed by middle to upper Jurassic platform carbonates. In the southwestern parts sedimentation continued into lower Cretaceous times (Trümpy 1962, Büchi et al. 1965, Trümpy 1980, Bachmann et al. 1987). The majority of these non-metamorphic cover units directly overlay basement rocks, though in places they rest on post-Variscan graben structures filled with Permo-Carboniferous clastic sediments (Diepold 1985, Matter 1987, Bachmann et al. 1987, Pfiffner et al. 1997). The samples analysed are from the USM and OMM, outcropping in the study area near Fribourg. The mostly medium-scale fault zones mapped in the western Swiss Molasse are arranged in a regional network, which is characterised by N-S striking left-lateral- and NW-SE to WNW-ESE striking right-lateral strike slip faults forming a conjugate system (s. figure 3.2). The stress related to development of this network is a NW-SE to NNW-SSE-oriented compression similar to the one responsible for folding in the Molasse and the Jura Mountains, as well as for the present-day stress field (Kastrup et al. 2004). The faults are mostly expressed by dense ar-

rays of fractures, slickensides and brittle deformation bands and often, but not always, comprise core zones with very fine fault gouges. The brittle deformation bands are a characteristic feature of initial faulting in porous sandstone (Aydin 1978, Fossen et al. 2007 for a review). Pore-space reduction and cataclasis on the grain scale along planar zones produce a micro-fault gouge instead of a discrete fault plane. In the western Swiss Molasse Basin micro-fault gouges of deformation bands reveal planar structures made of palygorskite (chapter 2)

So far palygorskite was only described from one locality in the Swiss Molasse basin, where it occurs as precipitate in fractured conglomerates (Peter & Salis 1965). Although rare, palygorskite has been found in fault gouges of volcanic rocks and carbonates (Post & Crawford 2007, Gibbs et al. 1993) and was attributed to hydrothermal fluid circulation along the faults (Gibbs et al. 1993, Garcia-Romero et al. 2006). In the Serrata de Nijar deformation zone of the Betic Cordillera (SE Spain), syn-tectonic palygorskite forms a planar fault gouge fabric found in mica-rich schists (Garcia-Romero et al. 2006). Mg-rich palygorskite requires moderate alkalinity, a high Mg and Si as well as a low Al activity (Singer 1979). It is usually encountered as an alteration product of carbonate, mafic and ultra-mafic rocks (Karpoff et al. 1989, Destigneville et al. 1998, Jones & Galan 1988, Imai & Otsuka 1984). Palygorskite may directly precipitate from pore fluids in sediments of peri-marine and coastal, as well as arid environments (Weaver & Beck 1977, Hillier 1995, Righi & Meunier 1995) and has been used as a proxy for paleo-climatic conditions (Bolle & Adatte 2001).

In this study we investigate the mineralogy and petrology of the fault gouges found in the Swiss Molasse by SEM- and X-ray diffraction analysis. Rock-water interaction modelling (titration calculation) are used to determine the palygorskite-forming reaction. The calculations are done with different fluids, which could have interacted with the host rock. The objective is to determine fluid influence and possible provenance of water during faulting.

3.2 ANALYTICAL METHODS

A total of 40 samples were taken from 8 localities in both the USM and OMM formations of the study area near the city of Fribourg (see figure 3.2). In each case deformed and leached rocks in and close to the faults, as well as unaffected host rocks farther

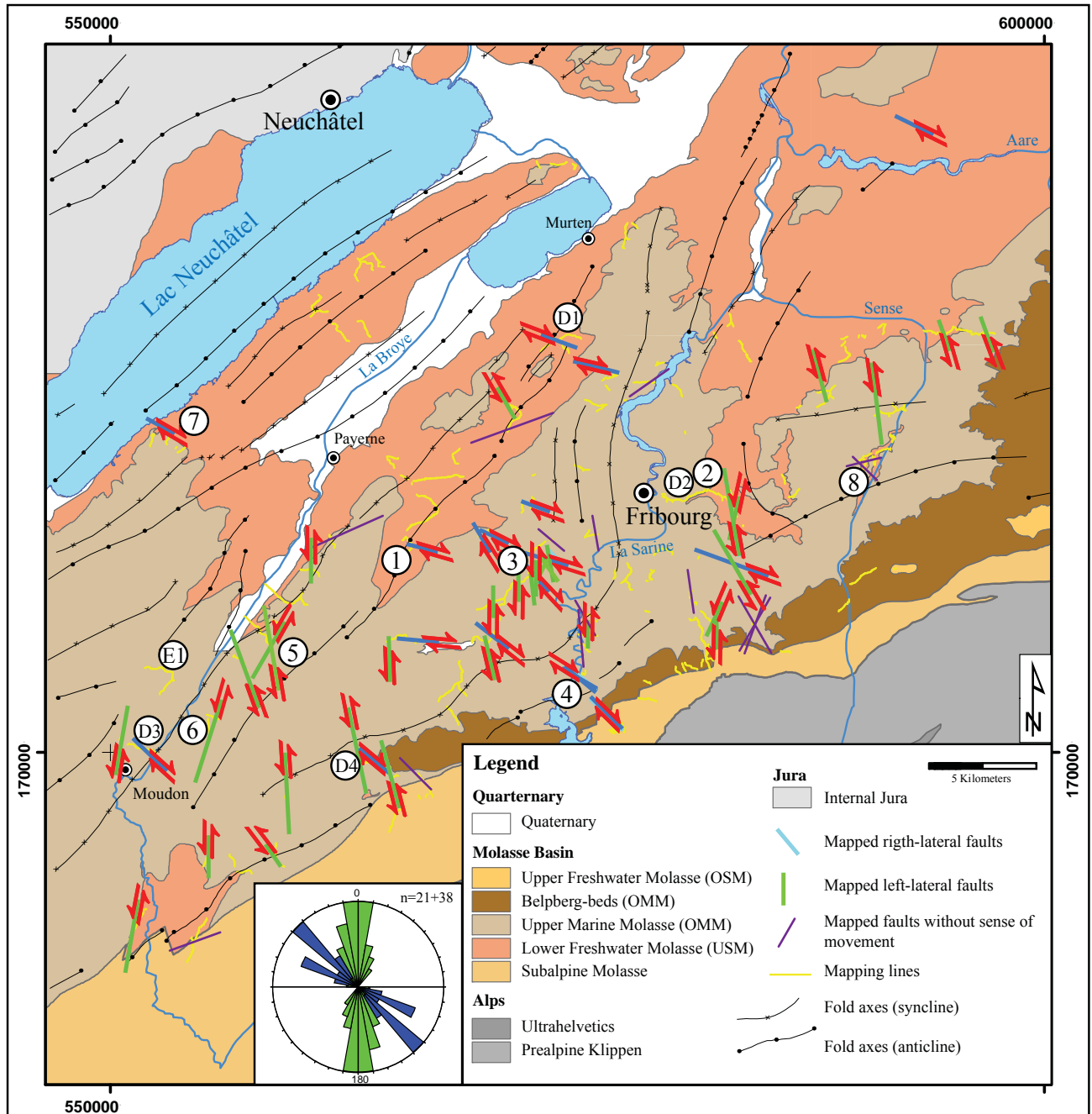


Figure 3.1: Location of the study area Figure 3.3: Study area with faults mapped in the field. NNW-SSE to NNE-SSW striking faults are sinistral and E-W to NW-SE striking faults are dextral. Faults with no recorded sense of movement are also given. Rose diagram gives strike for all right-lateral faults in blue and all left-lateral faults in green. Numbers 1 to 8 refer to location of the samples for XRD analysis given in table 3.2. E1 is location of the sample where EDS chemical point analyses were made from (see figure 3.5 and table 3.4). D1 to D4 are additional localities where palygorskite was identified in thin-sections of brittle deformation bands.

away, were sampled. Brittle deformation bands (micro fault gouges) were sampled at eight localities (s. figure 3.2). Thin sections of the samples were studied by light and scanning electron microscopy. Powdered samples were investigated by powder X-ray diffraction using a Philips PW 1710 diffractometer. Diffractograms were recorded between 3° and $65^\circ 2\theta$ in step-scan mode ($0.02^\circ/\text{step}$ and $2\text{sec}/\text{step}$). The copper X-ray tube was operated at 40 kV and 40 mA. The $\text{CuK}\beta$ radiation was filtered with a graphite monochromator.

Quantitative phase analysis by Rietveld refinement (Post & Bish, 1993) was done using the SIROQUANT software package (Taylor, 1991). The following instrumental parameters were refined: zero shift, sample displacement and peak shape parameters. The peak shape was modelled with a Pearson VII profile function. The structure parameters for the phases present in the sample were taken from the SIROQUANT data base, but only the unit cell parameters

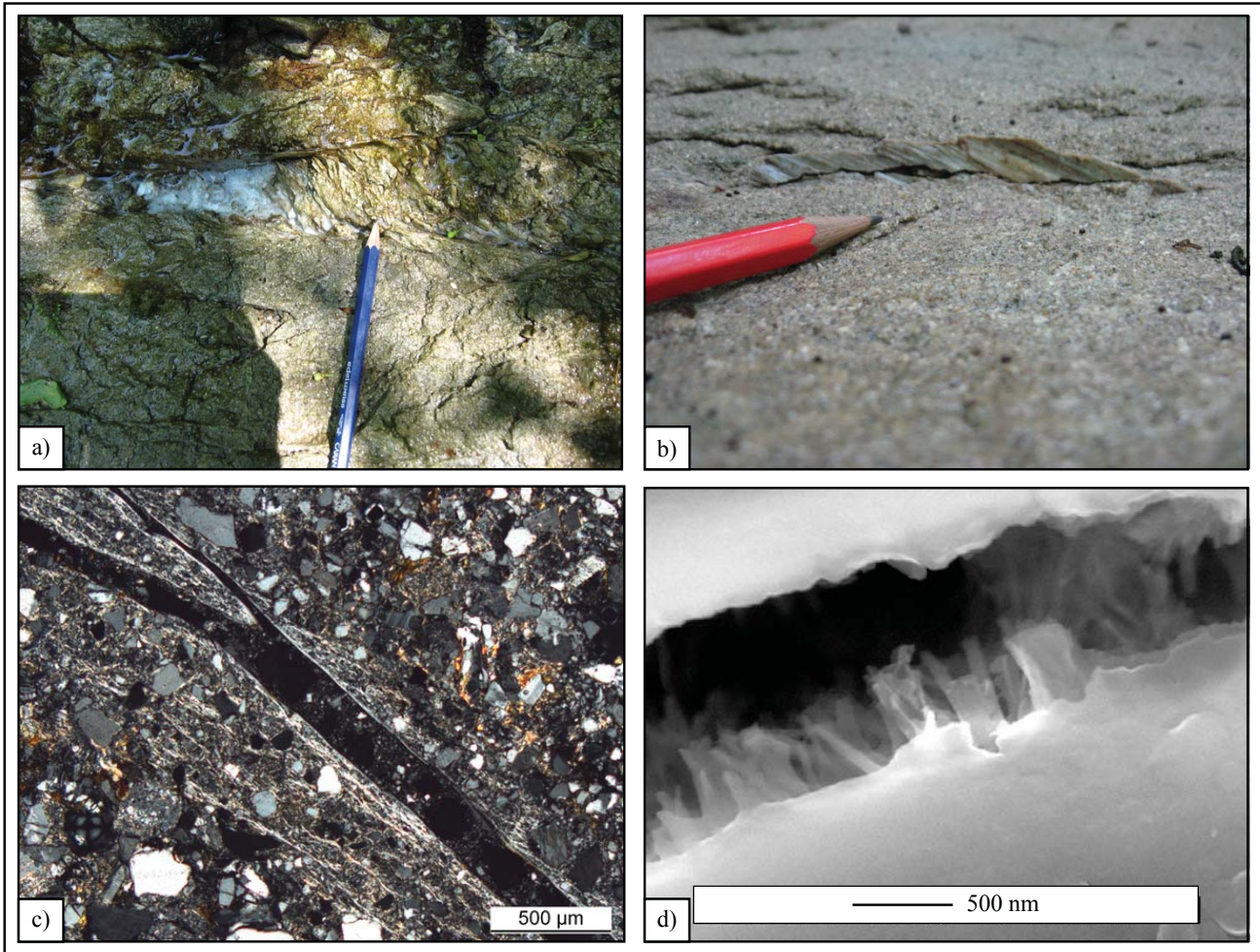


Figure 3.3: Photographs of palygorskite occurrences at different scales in fault zones of the Molasse sandstone. a) A few cm wide fault gouge of palygorskite. The alteration colour and a steep foliation are visible near the tip of the pencil while the white colour to the left represents the fresh palygorskite gouge. b) Palygorskite fibres forming lineations on a slickenside. c) Thin section (crossed polarised light) of a brittle deformation band with a foliation of whitish filaments representing palygorskite. d) SEM micrograph of palygorskite fibres in a brittle deformation band.

and the overall isotropic temperature factor were refined. The refined sample parameters are the fraction of the phases present (through the scale factor) and the preferred orientation parameter (March - Dollase function). The atomic positions and the site occupancies were kept fixed during the refinement. Iterations were performed until the refinement converged.

The composition of the minerals in the fault gauges were analyzed by scanning electron microscopy and energy dispersive spectroscopy using a FEI XL30 Sirion FEG microscope operated at 20keV and equipped with an EDAX EDS system. The EDS patterns were fitted with the Phoenix software and compositions were extracted from net intensities after correction for matrix effects (ZAF) and detector sensitivity. The elements included in line scans were Mg, Al and Si.

3.3 THERMODYNAMIC MODELLING

Thermodynamic calculations have been made with the “Geochemist Workbench (GWB)” software using the ACT2 routine for the calculation of activity diagrams and the REACT routine for reaction modelling. The calculated thermodynamic parameters for palygorskite (see below) were added to the database provided by the geochemical modelling group of the Lawrence Livermore National Laboratories (Delany & Lundeen, 1989). The activity coefficients are calculated according to an extended form of the Debye-Hückel equation. Activity diagram calculations and reaction modelling were done in the eight-component-system $\text{K}_2\text{O}-\text{Na}_2\text{O}-\text{MgO}-\text{CaO}-\text{Al}_2\text{O}_3-\text{SiO}_2-\text{CO}_2-\text{H}_2\text{O}$. The activities of K_2O , Na_2O , CaO , Al_2O_3 and CO_2 were set by the phases present in both the fault gouge and the host rock i.e. K-feldspar, albite and calcite. Reaction modelling has been performed with the “titration” and “flush” options of the REACT program. With the “ti-

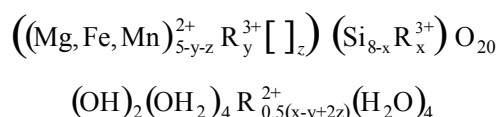
tration” option set, the water-rock interaction is simulated as repeated addition of a small aliquot of reactant (= host rock) to the solution. After each addition, the program recalculates the system’s equilibrium state by precipitating the secondary minerals reaching saturation. With the “flush” option a certain quantity of fluid is added as reactant, which displaces existing fluid. After equilibration the process is repeated. The fluids tested were standard ocean water and 4 different Molasse aquifers (s. below and table 3.4). The rock composition used for modelling was taken from the Rietveld refinement of the sample taken at Corserey (No 1 in figure 3.2 and table 3.1, TI16s (fault gouge) and TI17 (host rock) in table 3.2). The results were compared with the observed fault gouge assemblage found at the same location. The same procedure was used by Destringeville et al. (1998) to demonstrate that palygorskite is a possible alteration product in the reaction of serpentinites with sea-water.

3.4 PALYGORSKITE

3.4.1 Crystal chemistry of palygorskite

The structure of the mineral palygorskite contains tetrahedrally coordinated silicate layers in which the orientation of the apical oxygens flips over every third tetrahedral chain (T). Where apical oxygens in neighboring layers point towards each other they sandwich octahedrally (O) coordinated cations. The channels (3.7Å x 10.6Å in size) between four TOT- strips (=I-beam) are filled with 4 water mol-

ecules per unit cell. Additional 4 H₂O molecules are bound to octahedral cations. Palygorskite is classified as a phyllosilicate due to the continuous silicate layers. The general structural formula of palygorskite is given as (Jones & Galan, 1991):



The trivalent cations in the octahedral units are compensated by vacancies ([] in the formula) The divalent cations in the last part of the stoichiometric formula are located in the channels and are also compensated by vacancies. Two polymorphs (monoclinic C2/m and orthorhombic Pbm_n) have been reported in the literature (Chisholm 1992; Giustetto et al. 2006). The difference between the two structures is the position of the tetrahedral chains in adjacent I-beams along the c-axis and, as a consequence, also the position and bonding of the water molecules in the channels. Most natural palygorskite samples are a mixture of both polymorphs.

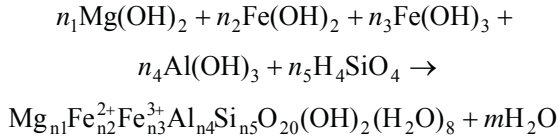
3.4.2 Thermodynamic data for palygorskite

There are no thermodynamic data available for palygorskite. Previous authors (Destringeville et al., 1998; Birsoy, 2002) used estimations of the Gibbs free energy at 25°C calculated by predictive methods

| Locality | No. in fig. 3.2 | Formation | type | Qtz | Fsp | Cal | Dol | Msc | Chl | Pal | Average of |
|-----------------|-----------------|-----------|------|-----|-----|-----|-----|-----|-----|-----|------------|
| Corserey | 1 | USM | FG | X | X | X | | | | X | 2 samples |
| | 1 | USM | HR | X | X | X | X | X | X | | |
| Galtera | 2 | USM | FG | X | X | | X | | X | X | 4 samples |
| | 2 | USM | HR | X | X | X | X | X | X | | |
| La Glâne/Matran | 3 | OMM | FG | X | X | | X | | | X | |
| La Trémeule | 5 | OMM | FG | X | X | | | | | X | 3 samples |
| | 5 | OMM | HR | X | X | X | X | X | X | | 4 samples |
| Rossens dam | 4 | OMM | FG | X | X | X | | X | | X | 5 samples |
| | 4 | OMM | HR | X | X | X | X | X | X | | 7 samples |
| Sodbach | 8 | USM | FG | X | X | X | | | | X | |
| Sodbach | 8 | USM | HR | X | X | X | X | X | | | 2 samples |
| Châtillon | 7 | USM | FG | X | X | | X | | | X | |
| Châtillon | 7 | USM | HR | X | X | X | X | X | | | |
| Lovatens | 6 | OMM | FG | X | X | | | | | X | 2 samples |
| Lovatens | 6 | OMM | HR | X | X | X | X | | | | |

Table 3.1: Mineralogy of fault gouges (FG) and host rocks (HR) for selected faults as revealed by XRD analysis. In the case of La Glâne/Matran no host rock sample was analysed, in the La Trémeule case FG analyses are from two faults and in the case of Rossens dam, the FG analyses are from 4 faults. Often more than one host rock sample (e.g. samples from both sides of and at different distances from the fault) was analysed. As there are no major differences between them, the individual host rock samples as well as the fault gouge samples from one site were summarised and the number of samples indicated in the column to the right. Note that palygorskite is only present in the fault gouges, while chlorite is always missing (except in one case). For location of the faults compare the number in the second column with the numbers on the map in figure 3.3. Qtz = quartz, Fsp = feldspar, Cal = calcite, Dol = dolomite, Msc = muscovite, Chl = chlorite, Pal = palygorskite.

(Tardy & Garrels, 1974; Nriagu, 1975). In the following calculation the method proposed by Nriagu (1975) will be used. The mineral is represented as a composite of dehydrated metal hydroxides.



The Gibbs free energy is calculated as sum of the free energies of formation of the contributing hydroxides r_i with cationic charge z_i minus the Gibbs free energy of the liberated water. An empirical correction term Q is included, which takes into account the integration of the dehydrated hydroxide modules into the final phyllosilicate structure:

$$\Delta G_f^0(\text{palygorskite}) = \sum_i n_i \Delta G_f^0(r_i) - \\ \left(\left(\sum_i n_i z_i \right) - 16 \right) \Delta G_f^0(\text{H}_2\text{O}) - Q$$

The empirical relationship for Q obtained from phyllosilicates, for which experimental data for the Gibbs free energy of formation are available, is given as:

$$Q = 0.39 m$$

with m equal the number of liberated water molecules. With palygorskite there are some uncertainties using this formula because water molecules are present as coordination species and as zeolitic water in the structure, i.e. these water molecules are not liberated but remain in the structure. In the equation above, the Gibbs free energy of the latter is set equal to that of free water. The calculated Gibbs free energy of formation of palygorskite with a composition corresponding to the EDS analyses made on gouge samples (s. below) is -11187 kJ/mol, which is close to the value obtained by Birsoy (2002) for similar compositions.

3.5 RESULTS AND DISCUSSION

3.5.1 Host rock compositions

The typical Molasse sandstones studied are medium to coarse-grained poorly lithified sandstones with a porosity ranging between 5% and 10%. The typical mineral assemblage of the sandstones determined by light microscopy and powder X-ray diffraction consist of quartz, albite, K-feldspar, calcite as well as minor amounts of white mica, smectite, dolomite, chlorite, lithic clasts and organic material (table 3.1). The phase for the white mica used in the starting model for the Rietveld refinement is muscovite, but it is likely that both muscovite and illite are present in the sample. Two of the three samples which lack muscovite/illite contain smectite/montmorillonite, which is probably an alteration product of the former (Nieto et al. 2005). The quantitative analysis (table 3.2) of the mineral assemblages by Rietveld refinement (Bish & Post, 1993) were within the range estimated from light optical observation of thin sections of the same samples.

3.5.2 Fault gouge and deformation band compositions

All 19 fault gouge samples contained quartz and albite. Palygorskite was present in 16 of the samples. It is the only mineral not present in the assemblage of the encasing rocks and hence had to precipitate during or after the gouge formation. Other minerals present in variable amounts in the gouges are muscovite/illite, dolomite and chlorite (s. table 3.1). The XRD peaks of albite, palygorskite and calcite (figure 3.4) are very broad, whereas the peaks of quartz have a much narrower full width at half maximum (FWHM). The former have, therefore, smaller coherent scattering domains, which points to small grain sizes. Quartz

| Sample | TI19 | TI22 | TI24 | TI17 | TI16S | Thin sections |
|--------------|------|------|------|------|-------|---------------|
| quartz | 47.1 | 39.4 | 41 | 48.5 | 58.6 | 40.5 |
| albite | 13.1 | 16.9 | 19.4 | 23.8 | 31.8 | 25 |
| K-feldspar | 7.3 | 7.9 | 7.7 | 3.6 | | |
| illite | 10.2 | 1.7 | 3.4 | 8.4 | | |
| chlorite | 1.3 | 5.4 | 4.3 | 6.2 | | 6.3 |
| carbonate | 21.1 | 29.3 | 28.5 | 9.6 | 0.9 | 21.7 |
| palygorskite | | | | | 8.8 | |

Table 3.2: Quantitative mineralogical composition of Molasse sandstone (samples TI17, TI19, TI22 and TI24) and fault gouge (sample TI16S) revealed by Rietveld refinement of XRD analysis and by estimation from thin sections (average of 28 thin sections). Modelling of the reaction process was carried out with TI17 as host rock. In thin section analysis, dolomite was recorded together with calcite as carbonate and muscovite together with chlorite as phyllosilicate. TI17 is the host rock sample for the fault gouge TI16S.

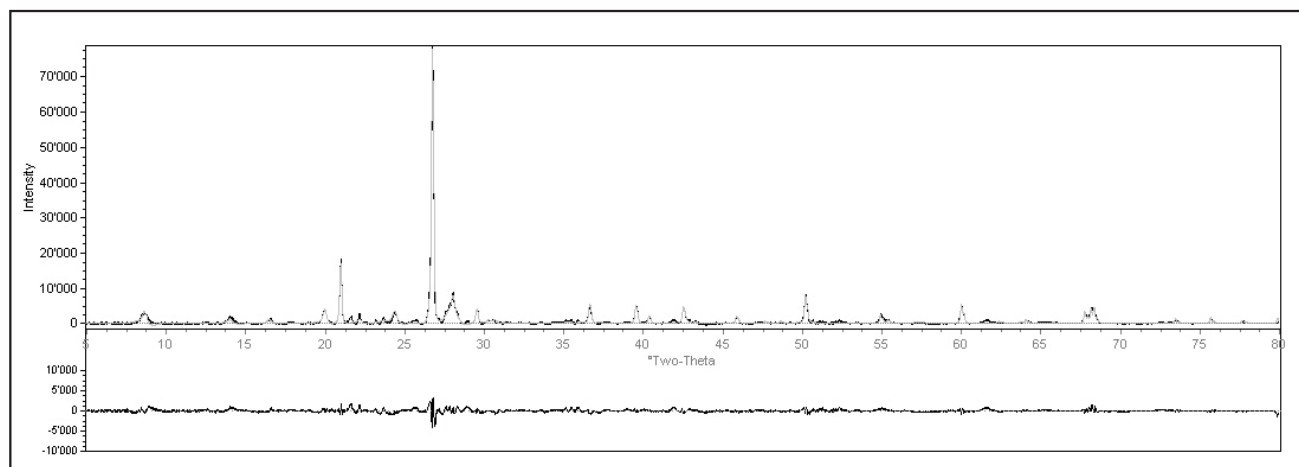
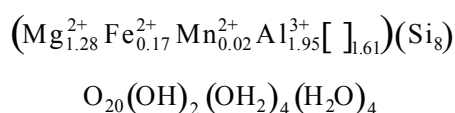


Figure 3.4: Diffraction pattern of gouge sample TI16S. The lower trace corresponds to the difference pattern. Measured (black) and calculated (grey) diffraction patterns are nearly identical.

fragments within the gouge are much larger than the ones of the other minerals, which explains the narrower FWHM. Rietveld refinements (s. figure 3.4) for the gouge diffraction patterns were only successful with the monoclinic structure for the palygorskite phase. Refinements in which both structures were included resulted in a composition with less than 1 wt % of the orthorhombic phase. The intensity for the palygorskite peaks could only be fitted by including a strong (001) preferred orientation, which corresponds to one of the monoclinic pinacoids that delimit the palygorskite fiber. Because preferred orientation, temperature factors and peak shape parameters are strongly correlated the quantitative analysis given in table 3.2 has to be taken with caution.

The brittle deformation bands are the incipient deformation structures in the Molasse sandstones. The light optical analysis of their micro fault gouges (s. figure 3.3c) revealed fine whitish filaments that resemble palygorskite found in the macro fault zones. Because the extraction of material for XRD analysis was too difficult, chemical analysis by EDS of the filaments were made on thin sections. The element maps and line scans taken from the host rock towards the micro fault gouges reveal an increase of Mg content when approaching the deformation band. Fibrous palygorskite material within the micro-fault gouge of a deformation band was analysed (figure 3.5, table 3.3) The normalization of point analyses made on fibrous palygorskite gives the following stoichiometry:



3.5.3 Palygorskite formation

The occurrence of palygorskite only in the fault gouges suggests a formation through a reaction between (hydrothermal?) fluids circulating in the faults and the encasing rock. Deformation was probably responsible for the formation of the fault network that served as fluid pathway. Cataclasis of grains and the ensuing increase of the specific surfaces of reacting minerals may also had a catalyzing effect on the palygorskite forming reactions.

Fluid sources both below and above the (paleo) sample horizon have been considered as potential reactants. These fluids have a wide range of compositions (table 3.4). Mesozoic aquifers encountered during oil and thermal water exploration drillings in the western Molasse basin change from chloridic in the Trias-, to carbonatic in the Jura- and Cretaceous- aquifers. The cations are mainly Na in the Triassic- and Ca or Ca + Mg in the Jura- and Cretaceous Formations. In the overlying Molasse units, three different groundwater types have been distinguished (figure 3.6). The limits between these aquifers are discordant with the formation boundaries. The uppermost aquifer is of earth-alkali-hydrocarbonate type followed downward by sodium- hydrocarbonate and sodium-chloride type waters (Schmassmann 1990).

Oxygen isotope data reveal that the earth-alkali-hydrocarbonate waters are Holocene in age, whereas the sodium-hydrocarbonate waters are of Pleistocene origin (Schmassmann 1990). The relative high values for the heavy oxygen isotopes as well as its high NaCl-content was interpreted to derive from marine water trapped during the deposition of the OMM in the shallow Molasse sea (Lemcke et

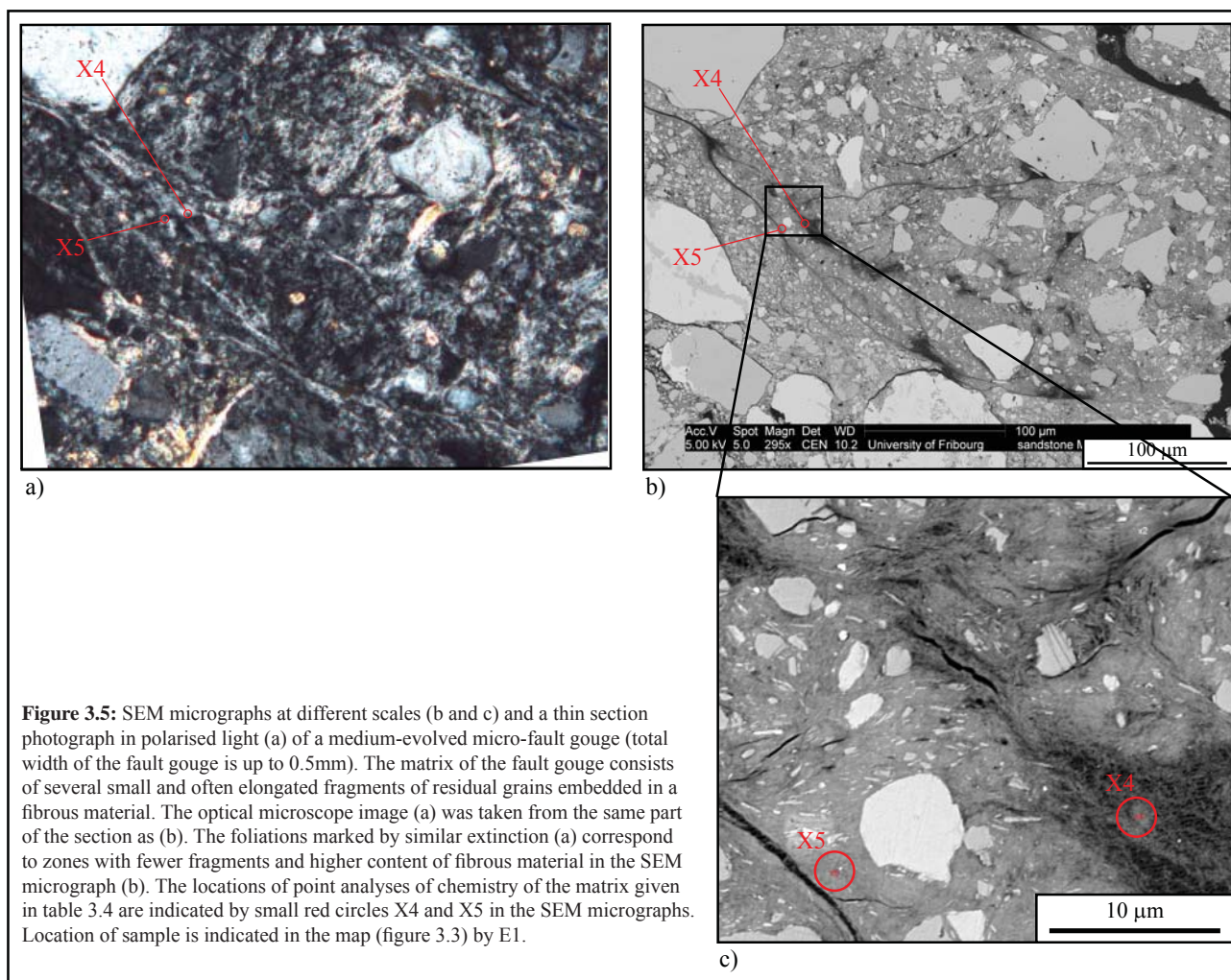


Figure 3.5: SEM micrographs at different scales (b and c) and a thin section photograph in polarised light (a) of a medium-evolved micro-fault gouge (total width of the fault gouge is up to 0.5mm). The matrix of the fault gouge consists of several small and often elongated fragments of residual grains embedded in a fibrous material. The optical microscope image (a) was taken from the same part of the section as (b). The foliations marked by similar extinction (a) correspond to zones with fewer fragments and higher content of fibrous material in the SEM micrograph (b). The locations of point analyses of chemistry of the matrix given in table 3.4 are indicated by small red circles X4 and X5 in the SEM micrographs. Location of sample is indicated in the map (figure 3.3) by E1.

| Element | Palygorskite | Point analysis X4 | | Point analysis X5 | |
|---------|--------------|-------------------|---------------|-------------------|---------------|
| | | Weight % | Stoichiometry | Weight % | Stoichiometry |
| Mg | 1.76 | 4.71 | 1.22 | 3.36 | 0.86 |
| Al | 2 | 7.90 | 1.85 | 6.07 | 1.41 |
| Si | 8 | 35.17 | 7.91 | 37.79 | 8.42 |
| Mn | 0.08 | 0.17 | 0.02 | 0.16 | 0.02 |
| Fe | 0.05 | 1.42 | 0.16 | 1.48 | 0.17 |
| O2 | 19.4 | 50.64 | 20.00 | 51.14 | 20.00 |

Table 3.3: Results of EDS point analyses of the very fine-grained matrix at points X4 and X5 on thin section no 3/3. See figure 3.5 for point locations. The chemical formula of palygorskite is $\text{Si}_8\text{Al}_2\text{Fe}_{0.05}\text{Mn}_{0.08}\text{Mg}_{1.76}\text{O}_{19.4}(\text{OH})_{2.6}[\text{H}_2\text{O}]_4$, taken from: <http://database.iem.ac.ru/mincryst>

al. 1968, Schmassmann 1990). This fossil sea water became diluted by addition of freshwater during the OSM period. This is reflected in a lower NaCl content than sea water, as well as in the fact that the top of the sodium chloride aquifer is below the upper boundary of the OMM (Lemcke et al. 1968, Schmassmann 1990). Since palygorskite is known to form in pelagic sediments and as alteration products of mafic oceanic rocks, undiluted sea water has also been considered a potential alteration fluid (Destrigneville et al. 1998).

The titration modelling of the water-rock interaction gave similar reaction products for all fluids

tested. The most important result is the disappearance of chlorite from the initial paragenesis and the appearance of palygorskite for all 5 fluids tested. This change in mineralogy is also reflected in the activity diagram $\text{Mg}^{2+}/\text{H}^+$ vs $\text{SiO}_2(\text{aq})$ in which all aquifer waters and also sea water lie in the stability field of palygorskite. The clinocllore stability field lies at lower $\text{SiO}_2(\text{aq})$, higher magnesium activity and/or higher pH (figure 3.7) In the titration runs, quartz and palygorskite are immediately saturated, whereas calcite, albite and K-feldspar start precipitating with some delay, especially for the titration with seawater. (figure 3.8a-d).

| | La Grève Malm | Schafisheim USM | Pomy USM | Matran e OMM | Sea water |
|--------------------------------------|-----------------------------|------------------|-----------------------|-----------------------------|--|
| Water type | Earth-alkali-hydrocarbonate | Sodium-chlorite | Sodium-hydrocarbonate | Earth-alkali-hydrocarbonate | Sodium chlorite |
| Temperature (°C) | 31.5 | | 12.0 | 12.2 | 25 |
| pH | 7.57 | 8.09 | 8.3 | 7.65 | given by CO ₂ (air) equilibrium |
| Eh(mv) | -122 | | | | |
| TSD(mg/l) | 337.6 | | | | |
| Na ⁺ (mg/l) | 7.5 | 3011 | 245 | 7.9 | 10760 |
| K ⁺ (mg/l) | 2.25 | 19.2 | 1.12 | 0.98 | 399 |
| Mg ²⁺ (mg/l) | 22.1 | 68.09 | 1.2 | 34.0 | 1290 |
| Ca ²⁺ (mg/l) | 39.7 | 208.4 | 2.8 | 44.0 | 411 |
| Sr ²⁺ (mg/l) | 1.8 | 0.02 | 0.29 | 2.14 | - |
| HCO ₃ ⁻ (mg/l) | 233 | 134.5 | 482 | 530 | 142 |
| Cl ⁻ (mg/l) | 2.8 | 5176 | 8.1 | 1.0 | 19350 |
| NO ₃ ⁻ (mg/l) | 0.1 | 0.124 | 0.8 | 1.0 | - |
| F ⁻ (mg/l) | 1.1 | 14.63 | 1.32 | 0.05 | - |
| SO ₄ ²⁻ (mg/l) | 12.5 | 4.47 | 133 | 9.0 | 2710 |
| SiO ₂ (aq) (mg/l) | 16.3 | 0.006 | 7.6 | 21.0 | 0.002 |
| source | Muralt et al. 1997 | Schmassmann 1990 | Thierrin 1990 | Thierrin 1990 | Harvie et al. 1980 |

Table 3.4: Composition of formation waters in the Swiss Molasse and the underlying Malm aquifer, as well as sea water composition.

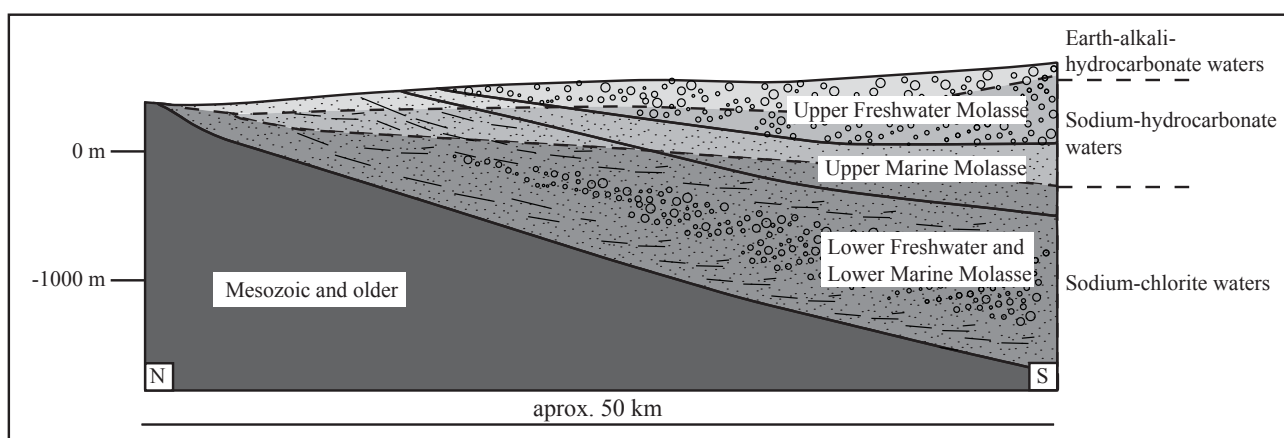
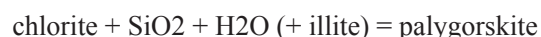


Figure 3.6: Schematic illustration of the Molasse formations and the depth distribution of the three main types of formation waters. Simplified after Schmassmann (1990).

With reaction progress, the relative proportions of the different phases become constant, except for the interaction with sea water (s. figure 3.8d). Not only the sequence of the phases, quartz > albite > palygorskite > calcite ~ K-feldspar but also their absolute quantities match remarkably well with the observed phase assemblage. Flushing the rock with the same fluids (reverse titration, rock/water ratio decreases with reaction progress) confirm the result observed during the titration: the initial proportion of the precipitated minerals corresponds to the final proportions in the titration (figure 3.9). With increasing reaction progress albite and calcite become unstable and disappear from the initial paragenesis (equivalent to the delayed precipitation during titration), whereas the amounts of the other phases remain constant. The amount of palygorskite formed depends strongly on

the chlorite and to a lesser extent on the illite content of the host rock. Reducing the initial chlorite concentration of the host rock by half lowers the final palygorskite concentration after titration by the same amount (figure 3.8). The general net palygorskite forming reaction can, therefore, be written as:



3.6 DISCUSSION AND CONCLUSION

The mineralogical and geochemical properties of the micro-fault gouges of brittle deformation bands and the fault gouges of macroscopic fault zones in the Molasse sandstone of western Switzerland were analysed. The mineralogy of the fault gouges of the

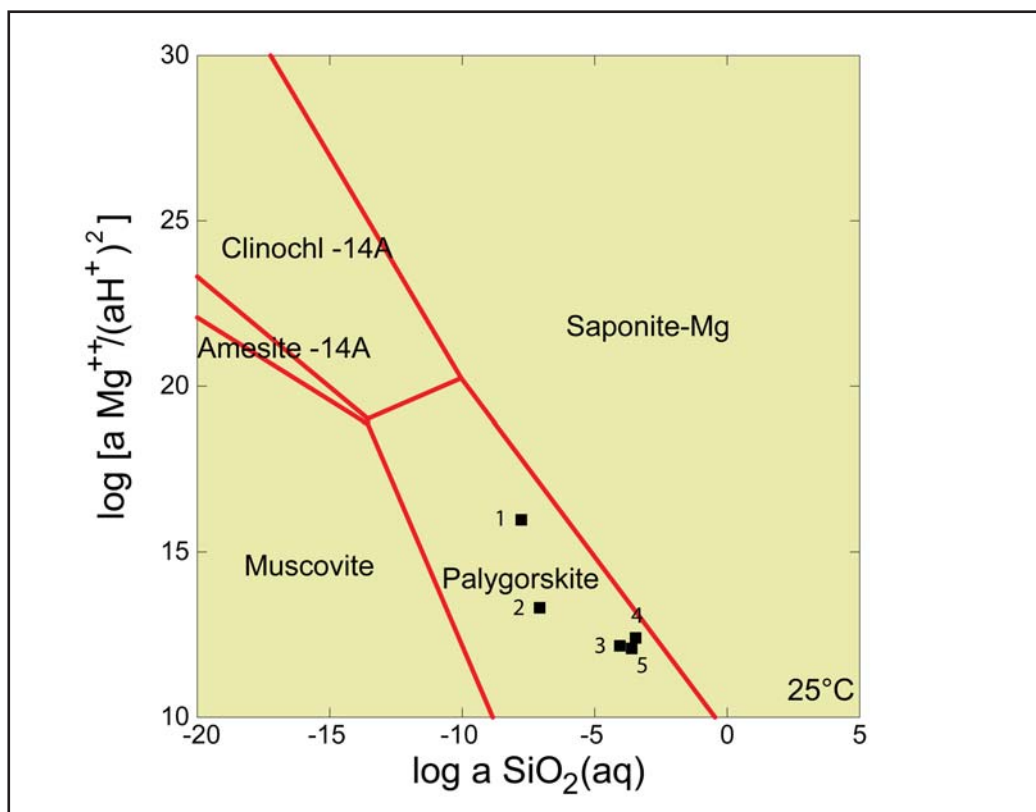
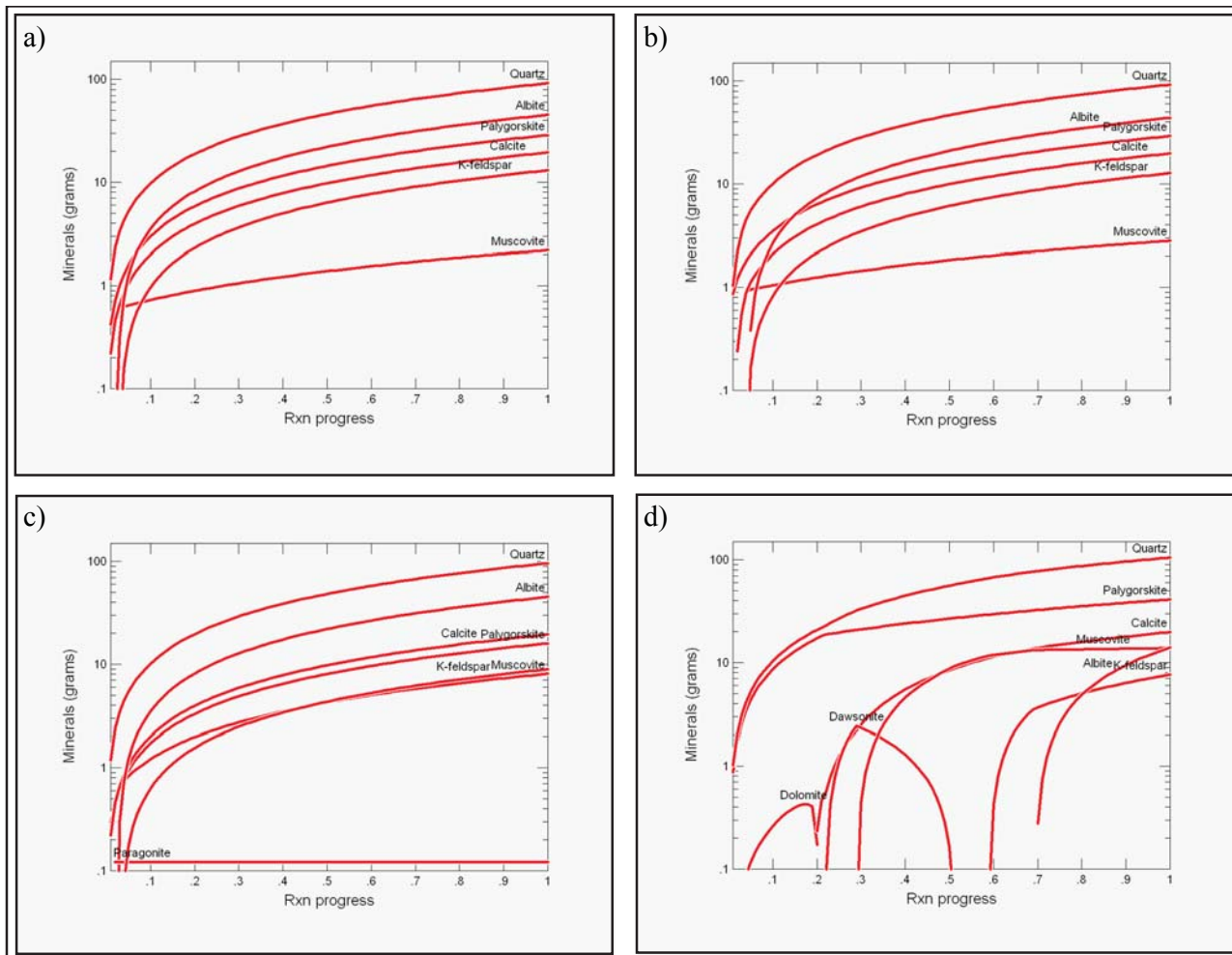


Figure 3.7: Activity diagram for the K₂O-Na₂O-MgO-CaO-Al₂O₃-SiO₂-CO₂-H₂O system. The activity of the components K₂O, Na₂O, CaO, Al₂O₃ and CO₂ are fixed by the presence of albite, K-feldspar and calcite. The squares correspond to the water compositions given in table 3.4: 1: sea water, 2: Schafisheim, 3: Pomy, 4: Matran, 5: La Grève.



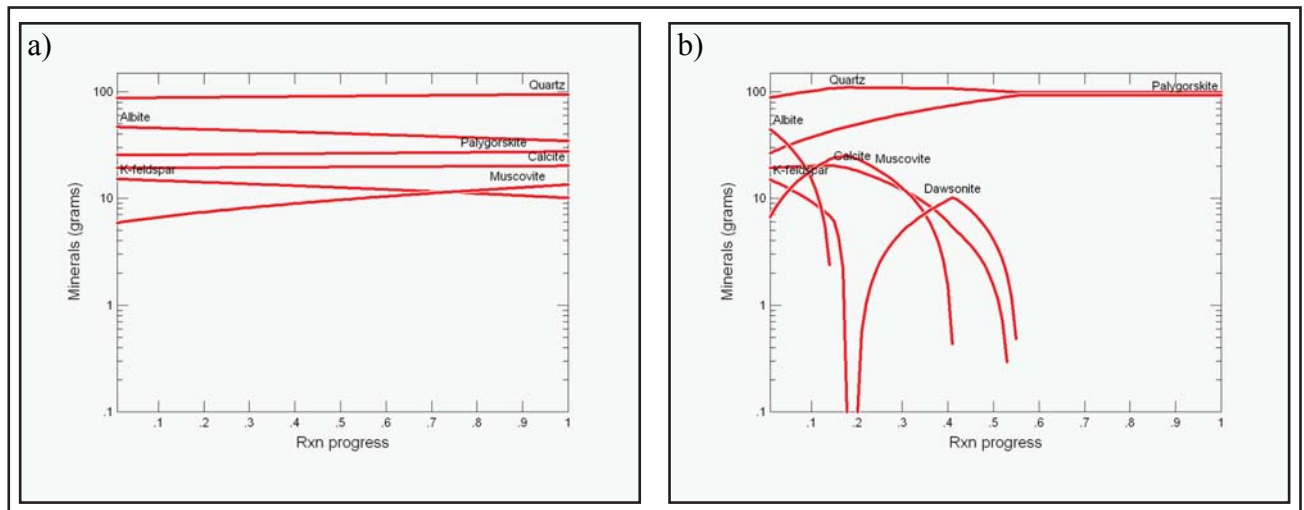


Figure 3.9: Phase evolution when flushing 200g host rock TI17 with 1 l of a) La Grève and b) sea water.

macroscopic fault zones and their host rocks were investigated by XRD analysis. The microscopic fault gouges of the brittle deformation bands were analysed by EDS on highly polished thin sections. The results of the analyses revealed that palygorskite, an Mg-rich clay mineral is common in deformation zones of all scales and absent in the host rock. Its formation is therefore bound to the deformation.

The titration modelling implies that a chlorite and probably muscovite/illite consuming reaction is at the origin of the palygorskite formation. Deformation-induced fracturing could bring such a fluid from an external source into contact with the host rock mineralogy present in the fault gouge. The modelling shows that all fluids encountered in the Molasse and underlying Mesozoic units may be at the origin for the palygorskite forming reactions. The least probable of the tested fluids is pure seawater. The considerable amount of albite present in the gouge is not in favor of synsedimentary faulting and alteration by undiluted seawater. The amount of albite formed in the titration

and flushing simulations with seawater is minor. The exact timing of the deformation and the origin of the fluid, however, cannot be deduced.

An interesting fact is that the modelling has been done for a temperature of 25° C. The occurrences of palygorskite observed in fault gouges have often been connected to the circulation of hydrothermal fluids (Post & Crawford 2007, Gibbs et al. 1993, Garcia-Romero et al., 2006). Palygorskite may, however, also precipitate in near surface fluids or on the ocean floor (Birsoy, 2002; Karpoff et al. 1989, Destigneville et al. 1998). Hydrothermal circulation as proposed by Garcia-Romero et al. (2006) for palygorskite formation in the Serrata de Nijar fault zone is, therefore, not necessary. The volcanic rocks crossed by the Serrata de Nijar fault contain also chlorite, and the same low temperature replacement reaction as in the Molasse faults may have taken place. It is interesting to notice that the volcanic rocks are capped by evaporitic sediments, which may be the origin for the palygorskite forming fluids.

Figure 3.8: Titration calculation incrementally adding 200g of host rock TI17 to one litre of water with composition corresponding to the aquifer at a) La Grève (Pomy and Matran give almost identical results), b) Schafisheim, c) La Grève, but with the amount of chlorite reduced to the quantity of the host rock TI17, and d) sea water.

4 - STRIKE-SLIP DEFORMATION IN THE WESTERN SWISS PLATEAU MOLASSE

Ibele, T., Mosar, J., Matzenauer, E..

Manuscript in preparation for submission

ABSTRACT

The western Swiss Molasse Basin sits in a wedge-top position above the basal décollement of the northern Alpine foreland fold-and-thrust belt, representing its less deformed portions and containing its youngest series. The latter are shales, sandstones and conglomerates of Oligocene and Miocene age. Structural field work was carried out along a network of outcrops in the Plateau Molasse of the Canton Fribourg area as well as in selected outcrops of the Subalpine Molasse.

The recorded structures comprise fractures and slickensides in sandstones and conglomerates as well as brittle deformation bands in sandstones and pressure solution pits on pebble surfaces in conglomerates. In the shales, deformation structures are generally rare. The populations of slickensides and brittle deformation bands from different localities are typically arranged in pairs with synthetic and antithetic orientation, and are interpreted as synthetic and antithetic shears of a Riedel system. The fractures can be subdivided into joint-like mode 1 cracks formed parallel to σ_1 , and shear fractures that are oriented roughly the same as the mapped slickensides. Mapped faults show cataclastic cores and damage zones composed of dense networks of fractures, slickensides and brittle deformation bands. Overprinting relationships are not systematic, which supports the interpretation that all deformation is in response to only one stress regime. Timing of deformation is constrained purely by the structures and most likely spans from the upper Miocene until the present.

The recorded deformation reveals a strike-slip regime in the Plateau Molasse and a combined thrust/strike-slip regime in the Subalpine Molasse. Left-lateral faults strike N-S to NNE-SSW and right-lateral faults NW-SE to WNW-ESE. Thrusts in the Subalpine Molasse strike NE-SW. The calculated paleostress regime shows NW-SE to NNW-SSE compression and NE-SW to WSW-ENE extension. The pressure solution pits represent low-strain bulk shortening. The derived compression axes are roughly oriented N-S and mostly inclined 10° - 15° parallel to the tilt of the strata. The occurrence of pressure solution pits is, however, limited to conglomerates, i.e. to a narrow band located near the Subalpine Molasse.

Based on the distribution of deformation from our mapping network, we propose a number of fault zones derived from the extrapolation of strongly deformed outcrops. In analogy to the Riedel-type distribution of slickensides, fractures and brittle deformation bands in the outcrops, and the absence of very large faults, we interpret the proposed fault zones as complex fault zones rather than as single continuous faults. They are composed of small-scale discrete faults not more than one kilometre in length as frequently mapped in outcrop. They are probably arranged in an en-echelon manner and interact as synthetic Riedel shears within the frame of the larger shear zone.

The Subalpine Molasse thrust front is segmented on the scale of the study area. In some parts, the thrust front is dissected by strike-slip faulting, which dominates the slickenside populations within the Subalpine Molasse. In most parts, the segments of the thrust front interact with strike-slip fault zones of the Plateau Molasse, indicating a contemporaneous evolution. Individual thrust faults develop from the shearing of fold-limbs. Strike-slip faulting in the Plateau Molasse is active at the same time as reverse faulting along segments of the Subalpine Molasse thrust front.

4.1 INTRODUCTION

The western Swiss Plateau Molasse is located between the Jura Mountains to the north and the Alps to the south. Unlike these two fold-and-thrust belts, it lacks conspicuous tectonic features. Its gently folded upper Oligocene and Miocene clastic sediments are the weakly deformed leftovers of the former peripheral foreland basin of the western central Alps (Homewood et al. 1986, Burkhard & Sommaruga 1998). The Molasse sediments are the erosional products of the Alps deposited on top of the Mesozoic units of the Alpine foreland in a flexural foreland basin setting (Homewood et al. 1986, Burkhard & Sommaruga 1998). During the subsequent development of the Jura Mountains fold-and-thrust belt, the Molasse Basin was passively transported towards the foreland. The fold-and-thrust belt was detached from the underlying basement along a décollement horizon formed by Triassic evaporites (Buxtorf 1916, Laubscher 1961, Burkhard 1990, Burkhard & Sommaruga 1998). The most distal Molasse was eroded from top of the Jura Mountains, while the most proximal parts were incorporated into the Alpine nappe pile, developing the narrow band of imbricated Subalpine Molasse (Homewood et al. 1986).

The Late Cenozoic tectonic history of the Alpine foreland fold-and-thrust belt was mainly established by investigating the brittle structures of well-exposed Mesozoic rocks in the Jura Mountains and adjacent regions (Plessmann 1972, Bergerat 1987, Homberg et al. 2002, Ustaszewski & Schmid 2006, Madritsch et al. 2008). No systematic structural field approach was applied to the youngest formations within this foreland fold-and-thrust belt system, i.e. to the Oligocene-Miocene Molasse deposits.

Syn- to post-folding strike-slip fault zones are prominent structures in the Jura Mountains where they offset the folded Mesozoic strata. In many cases these faults bend into thrusts when they reach the north-western front of the belt (Heim 1915, Laubscher 1972, Sommaruga 1997). Most of their geologic signatures vanish towards the southeast once they enter the subhorizontal strata of the Plateau Molasse. Strike-slip fault zones in or below the Plateau Molasse were postulated to extend from the Alps northwards (Plancherel 1979) as well as westwards (Chenevart 1978) and from the Upper Rhine Graben southwards (e.g. Revertera 1927, Plancherel 1979, Rybach et al. 1980, Kastrup et al. 2007). These fault zones were postulated according to large-scale tectonic models and are not directly based on field data. The size and depth

extent of these fault zones therefore remains speculative.

The low-amplitude folds in the Plateau Molasse strike NE-SW and locally bend into a N-S strike between Fribourg and Bern (Kopp 1946). This phenomenon is termed the Fribourg structure (“Querzone von Freiburg” by Schuppli 1950). Alignment of instrumentally recorded earthquakes in the eastern part of the Fribourg structure led several authors to postulate the existence of the “Fribourg lineament”, with a possibility of hazardous earthquake ruptures (Kastrup et al. 2007). The bend of the fold axes was attributed to the surface expression of left-lateral shear along the Fribourg lineament. However, a corresponding major fault zone could not be determined from field data; local geologic surface mapping revealed only a number of minor strike-slip faults (e.g. Briel 1962, Mornod 1949, Jordi 1955). In the area of Yverdon-les-Bains, strike-slip faults were recorded by field and seismic surveys to extend from the Jura Mountains into the Plateau Molasse (Jordi 1951, 1990). The left-lateral La Lance fault, mapped in the Jura Mountains west of Lake Neuchâtel (Bertschy, 1958, Meia 1966), was recorded by shallow seismic surveys crossing the lake and extending further into the Plateau Molasse (Gorin et al. 2003, Weidmann 2006). While large-scale reverse tectonics are absent in the Plateau Molasse, strike-slip faulting does occur. However, the nature and extent of such faulting is not well known.

In this study we present the results from systematic structural mapping in the Plateau Molasse of the Fribourg area. The structural inventory is characterised by subvertical fractures, slickensides and brittle deformation bands, usually arranged in fault zones. On outcrop-scale the structures display geometric arrangements characteristic of synthetic and conjugate shears corresponding to Riedel-type shear zones. The mapped orientations and kinematics indicate a regionally extensive strike-slip deformation expressed in N-S striking left-lateral and WNW-ESE striking right-lateral and only shear zones. The inferred paleostress is NW-SE compression and NE-SW extension. Based on the mapped distribution of the surface structures a fault network model is proposed. Interaction between thrusting in the Subalpine Molasse and strike-slip tectonic in the Plateau Molasse is also considered.

4.2 GEOLOGIC SETTING

The Swiss Molasse Basin is the western part of the former peripheral foreland basin of the Alps

(figure 4.1). During the orogenic evolution it progressively evolved from an underfilled Flysch basin to an overfilled Molasse Basin (Pfiffner 1986, Allan et al. 1991, Sinclair 1997).

The Molasse-type sedimentation took place in two shallowing-up megacycles in Oligocene to lower Miocene times (Trümpy 1980, Homewood et al. 1986, Berger et al. 2005). The detritus was erod-

ed from the Alps rising in the south and deposited as proximal conglomeratic fans, intermediate sandstones and distal shales (Heim 1919). Small-scale vertical and lateral facies variations between these lithologies are frequent (Matter et al. 1980). The main formations were named after their sedimentological characteristics Lower Marine Molasse (UMM), Lower Freshwater Molasse (USM), Upper Marine Molasse (OMM) and Upper Freshwater Molasse (OSM) (Studer 1853,

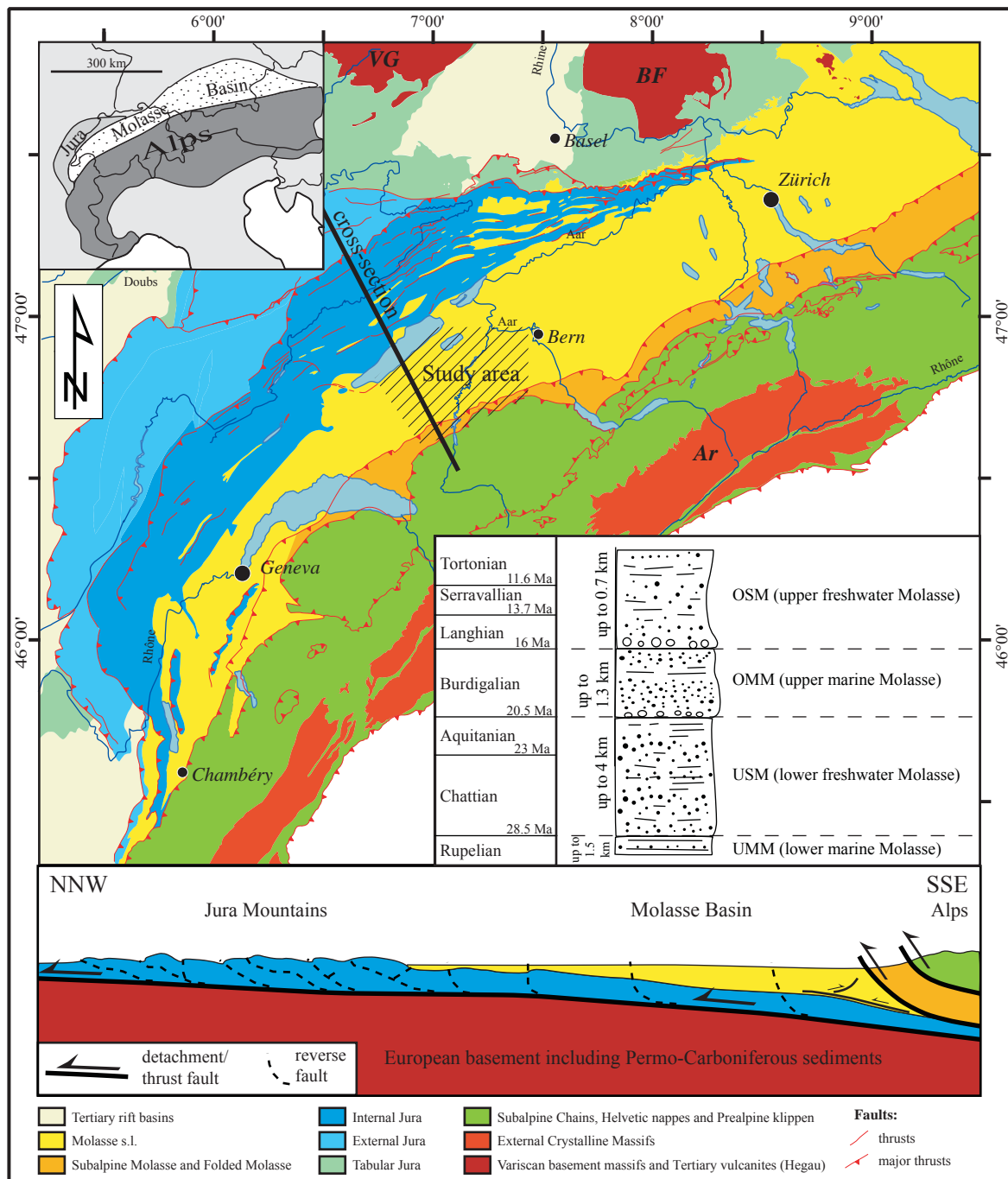


Figure 4.1: Geologic-tectonic overview of the Swiss Molasse Basin and adjoining areas. A schematic cross-section as well as a schematic stratigraphic column for the Molasse Basin are given. Inlet in the upper left corner shows the location of the Molasse Basin north of the European Alps. The location of the study area is indicated in the map. Thicknesses given in the stratigraphic column according to Matter et al. (1980).

Trümpy 1980, figure 4.1).

A stratigraphic gap separates the Oligocene Molasse sediments from the underlying Mesozoic units. The latter consists of partly evaporitic Triassic and usually shaley lower Jurassic, followed by middle to upper Jurassic platform carbonates. In the southwestern parts sedimentation continued into lower Cretaceous times (Trümpy 1962, Büchi et al. 1965, Trümpy 1980, Bachmann et al. 1987). For the most part these non-metamorphic cover units directly overlie basement, though in places they rest on post-Variscan graben structures filled with Permo-Carboniferous clastic sediments (Diepold 1985, Matter 1987, Bachmann et al. 1987, Pfiffner et al. 1997).

Ongoing NW-ward migration of the Alpine orogen and its peripheral foreland basin during the Molasse sedimentation lead to progressive onlapping of younger Molasse sediments onto the Mesozoic units of the down-flexed European crust (Pfiffner 1986, Homewood et al. 1986). A restored cross-section of the undeformed Molasse sediments thus exhibits a wedge shape with the oldest sediments deposited only in the southern part and the youngest sediments only in the northern part. In the upper Miocene the western parts of the basin became detached along Triassic evaporites (Buxtorf 1916, Laubscher 1961, Burkhard 1990, Burkhard & Sommaruga 1998) and were transferred into a wedge-top position while the eastern parts remained in the flexural foreland basin configuration. A change in the basin's along-strike geodynamic situation is already indicated in the nature of synsedimentary deformation: in eastern Switzerland and adjacent Germany growth faults oriented parallel to the basin axis indicate normal faulting on the down-flexing lithosphere (Laubscher 1978, Bachmann et al. 1987, Bachmann & Müller 1992). In contrast, synsedimentary folding occurs further southwest in Savoie (F) (Beck et al. 1998). Such synsedimentary folding in the peripheral foreland basin was reported from analogue models neglecting flexural bending of the lithosphere (Bonnet et al. 2007).

In the southeastern parts of the basin, the older sediments were imbricated as a result of ongoing NW-ward progression of the Alps, forming the narrow band of the Subalpine Molasse located along the former front of the Alps (figure 4.1). In contrast, the less deformed Plateau Molasse exhibits only slightly folded, subhorizontal units taking up most of the area between the Alps and the Jura Mountains. Sedimentation gave way to erosion in the upper Miocene at about the same times as the development of a large-

scale décollement in the Triassic evaporites underlying the Molasse Basin. This décollement led to the formation of the Jura Mountains in front of the Molasse Basin, incorporating the latter into the northern Alpine foreland-fold-and-thrust belt. The Molasse Basin was passively transported and uplifted into its present position (Buxtorf 1916, Laubscher 1961, Burkhard 1990, Burkhard & Sommaruga 1998). Shortening of the Mesozoic and Cenozoic cover of the Jura Mountains and parts of the Subalpine Molasse is thought to be compensated by basement shortening in the crystalline massifs (Boyer & Elliot 1982, Burkhard 1990).

During the mid-Miocene décollement tectonics the frontal part of the detached cover units was folded, forming the Jura Mountains, while the rearward part was passively transported, forming the Plateau Molasse. The transition between folding and passive transport is most likely linked to a critical overburden preventing folding, threshold which was crossed and that was exceeded in the southern part due to the wedge-shaped foreland basin filling (Sommaruga 1997, Burkhard & Sommaruga 1998).

The erosion since the upper Miocene amounts up to 4 km in the western part of the Plateau Molasse, where it has nearly completely removed the OSM (Monnier 1982, Kaelin et al. 1992, Schegg et al. 1997, Schegg & Leu 1998, Mazurek et al. 2006, Cederbom et al. 2004). The region has been found to be deformed by a network of meso-scale faults, most of which are expressed in the form of slickensides and deformation bands. The established strike-slip regime was governed by the same NW-SE directed compression still active today, as revealed by the offset of Quaternary lake deposits along the La Lance fault (Gorin et al. 2003) as well as focal mechanism of regional earthquakes (Kastrup et al. 2007).

4.2.1 Geology of the study area

The study area s.s. reaches from the Prealps in the south to the Lake Neuchâtel at the foot of the Jura Mountains in the north and covers the Plateau Molasse between the rivers Aare in the east and Broye in the west (figure 4.1). Its surface geology was mapped in detail mainly in the 1950's and 1960's (Becker 1972, Boegli, 1972, Briel 1962, Crausaz 1959, Dorthe 1962, Emmenegger 1962, Inglin 1960, Rumeau, 1954, Sieber 1959, Schuppli 1950) and compiled for the Geologic Atlas of Switzerland (Becker & Ramseyer 1973, Frei et al. 1974, Gabus et al. 2000, Python et al. 1998, Rutsch & Frasson 1953, Weidmann 2006, Wei-

dmann et al. 1996, 2002). It reveals fluvial, lacustrine and shallow marine clastic sediments belonging to the Lower Freshwater (USM) and Upper marine Molasse (OMM). These sediments are shale, sandy shale, clayey sands and sandstones that alternate vertically as well as laterally. They show a tendency of dominating sands in the proximal (SE) and dominating shale in the distal (NW) parts as well as dominating sands in the OMM and shale in the USM. In the eastern and north-eastern parts the Belpberg beds (Rutsch 1926) belonging to the uppermost OMM display a narrow zone of well-cemented conglomerates. The beds are gently folded, forming flat anticlines and synclines with flank inclination rarely exceeding 5° - 10° . The axes of these folds run SW-NE, i.e. roughly parallel to the tectonic boundary with the Subalpine Molasse in the southeast. Their bend into a N-S direction in the Fribourg structure is mainly expressed in the Fribourg syncline. The Plateau Molasse is bordered in the south-east by the Subalpine Molasse, which forms a narrow band of thrust imbricates of different Molasse units in front of the Prealpine Klippen. The north-western boundary towards the Jura Mountains is an erosional contact. In the Jura Mountains, fold amplitudes are much higher and many folds are thrust-related. Fold-bend and fault-propagation folds expose the Mesozoic rocks to erosion, leaving only relicts of Molasse in some synclines. Strike-slip as well as thrust faulting was described locally from the Plateau Molasse (e.g. Briel 1962, Mornod 1949, Jordi 1955). The left-lateral La Lance fault (Bertschy 1958, Meia 1966) was reported to be active in the Quaternary (Gorin et al. 2003).

4.3 METHODS

The present study uses structural data collected in the field – fault planes with striations or slickensides (generally called slickensides here), brittle deformation bands and pressure solution pits – to establish paleostress directions.

4.3.1 Mapping

A large portion of the study area is covered with glacial and post-glacial deposits and is intensely cultivated, which leaves only scarce outcrop occurrences. Most of the exposed Tertiary bedrock is located along small- and medium-sized rivers, yielding an irregular pattern of mapping lines (e.g. figure 4.8) along which all visible planar structures, such as brittle deformation bands, slickensides and fractures, were measured. The brittle deformation bands mostly appear as whitish lines on the outcrop surface and their planar surface is seldom exposed. In these cases, inclination could only be estimated on the basis of different intersection lines with differently oriented outcrop surfaces.

4.3.2 Paleostress analysis

In order to analyse paleostress from the slickenside data, we used the PT axis method (Marrett & Allmendinger 1990, figure 4.2) and the right dihedral method (RDM, Angelier & Mechler 1977, Pfiffner & Burkhard 1987, figure 4.3). Both are based on geometric relationships of fault planes and lineations, but follow different approaches. For processing and

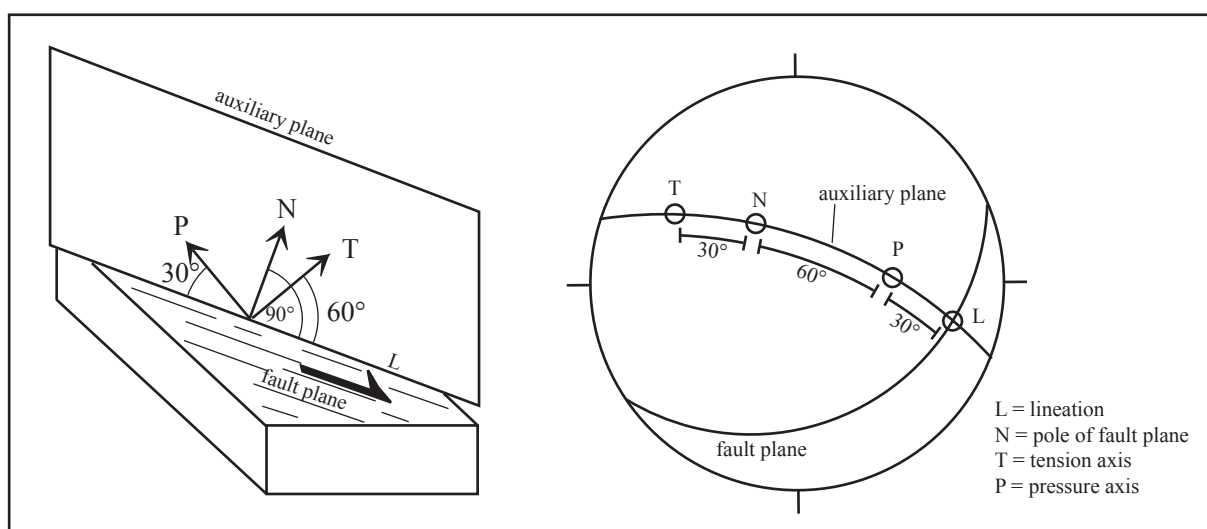


Figure 4.2: Block-diagram and stereographic projection to illustrate the P-T axes method.

representation we used the computer software Tectonics FP (Ortner et al. 2002).

When derived from the PT axes method, the axes of maximum, intermediate and minimum compression are referred to as P-axis, B-axis and T-axis, respectively, and as σ_1 -axis, σ_2 axis and σ_3 -axis when derived from the RDM. In general both nomenclatures refer to the three principal stresses σ_1 , σ_2 , and σ_3 .

The PT axes method (figure 4.2) directly calculates the orientation of the shortening and dilatation axes corresponding to each fault plane and lineation pair. It is based on the geometric relationship of the three principal stresses, being perpendicular to each other, with respect to the given fault plane. The intermediate principal stress (the B-Axis) is perpendicular to the direction of movement (the lineation) and parallel to the plane of movement (the fault plane). It is also perpendicular to the plane defined by the maximum and minimum compressive stresses (P- and T-axis, respectively). The plane including P- and T-axes can therefore be drawn in a stereographic projection as perpendicular to the fault plane and including the lineation (auxiliary plane). The position of the P- and T-axes can be determined in stereographic projection by plotting the angles they make with the fault plane along the great circle of the auxiliary plane. According to the Anderson theory, the compression axis is inclined 30° with respect to the fault plane, while the dilatation axis is inclined 60° . This is only true for the true mode-II fractures which are represented by the linear part of the Mohr-Coulomb failure criterion. In near surface deformation mixed mode-I mode-II fractures may however occur. They are represented by

the parabolic part of the Mohr-Coulomb failure criterion and show smaller angles between compression axis and fault plane. The accurate angle furthermore depends on the angle of internal friction of the rock.

In contrast, the RDM (figure 4.3) establishes compressive and dilatational sectors. A rock volume subject to faulting is subdivided into two volumes by the fault plane, each of which contains a compressive and a dilatational sector. The four sectors are defined by the plane perpendicular to the fault plane and to the direction of movement. In a stereographic projection, the sectors are defined by two great circles - the fault plane and an auxiliary plane that is perpendicular to the fault plane and to the lineation. Superposition of these sectors from multiple faults makes it possible to determine zones of best fit pressure and dilatation axes (Pfiffner & Burkhard 1987). The PT axes method reveals distinct P-axes and T-axes for single slickensides, representing the stress configuration responsible for its formation. Populations of varyingly oriented slip planes, as is usually the case in tectonic studies, deliver a scatter of P- and T-axes, for which a best-fit can be calculated. Owing to the method of superposition, the RDM needs at least 10 to 20 fault planes and associated lineations to obtain reasonable results. The stress directions determined with the RDM therefore give a more accurate estimation of the average stress than any single slickenside.

The PT axes method needs angular definitions such as the convention of a 30° angle between the fault plane and σ_1 which includes the assumption that the related slickenside developed under “ideal” conditions, e.g. was newly-formed and not reactivated. In contrast, the RDM can account for a scatter of angles

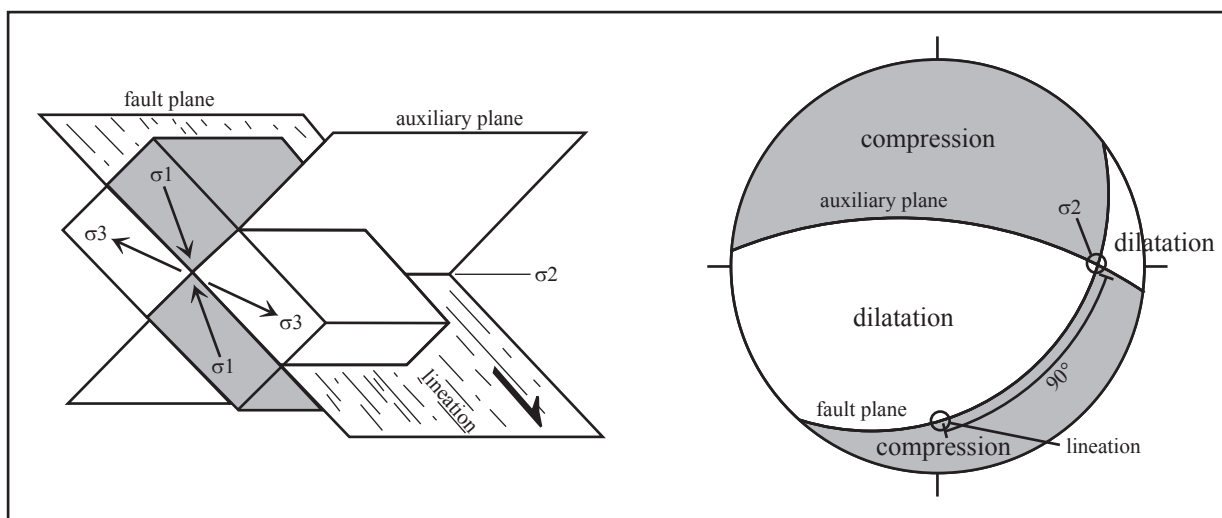


Figure 4.3: Block-diagram and stereographic projection to illustrate the right dihedral method.

between compression and slip plane and is therefore less sensitive to natural fluctuations such as different rock types or pre-structuring. Thus the exact angle is not a pre-specified value required for the RDM, but rather an outcome. In simple tectonic settings the calculated best fit orientations of P-axes correspond more or less to the σ_1 approximated by the RDM. Multiple slip planes derived from a polyphase stress history can best be detected by sorting out widely scattered P-axes (or T-axes).

4.4 BRITTLE TECTONIC STRUCTURES

The deformation mapped in the surface outcrops of the Tertiary Molasse in western Switzerland revealed several types of meso-scale brittle tectonic structures. They include brittle deformation bands, slickensides and unspecified fractures, all of which are planar tectonic structures and pressure solution pits in conglomerate pebbles, which are linear structures.

4.4.1 Planar tectonic structures

In the field we observed undeformed areas with no indication of planar brittle deformation. In other zones with a discrete and sporadic distribution they develop in fault zones forming arrays.

4.4.1.1 Brittle deformation bands in sandstone

Brittle deformation bands are typical deformation structures of poorly lithified porous sandstone and non-lithified porous media. They were described from field and microscopic observations by Aydin (1978) and Aydin & Johnson (1978) who developed the “classic” model for their formation (figure 4.4). According to this model, deformation bands form af-

ter an initial phase of pore space reduction by grain breakage, grain-scale cataclasis and compaction. The bands thus form distinct small-scale cataclastic fault zones commonly not more than a few mm in width. Pore space reduction and interlocking of grain fragments results in strain hardening leading to the formation of a new band subparallel to the first one. With increasing strain, a zone of closely spaced anastomosing deformation bands develops, whose overall offset is the sum of all single deformation band offsets (Aydin & Johnson 1978). The offsets across deformation band shear zones are in the range of centimetres. The deformation band shear zones can measure several tens of centimetres in width and often exhibit a discrete fault plane at one edge representing the following stage of deformation (Aydin & Johnson 1983, figure 4.4).

Based on microscopic characteristics, host rock properties and stress configurations during their evolution, several subtypes of brittle deformation bands can be distinguished (Antonellini et al. 1994, Fossen et al. 2007, Rotevatn et al. 2008). Despite this variety they all share the following most common characteristics:

- the accumulation of strain by grain-reorganisation or grain cracking,
- the relatively low amount of offset across a band, and
- the reduction of pore space within the bands.

Porous media was shown to be weaker than non-porous media (Wong et al. 1997) and its shearing to take place under non-Coulomb behaviour (Mandl et al. 1977). Brittle deformation bands may therefore exhibit angles with respect to σ_1 deviating from 30° as predicted by the Anderson theory.

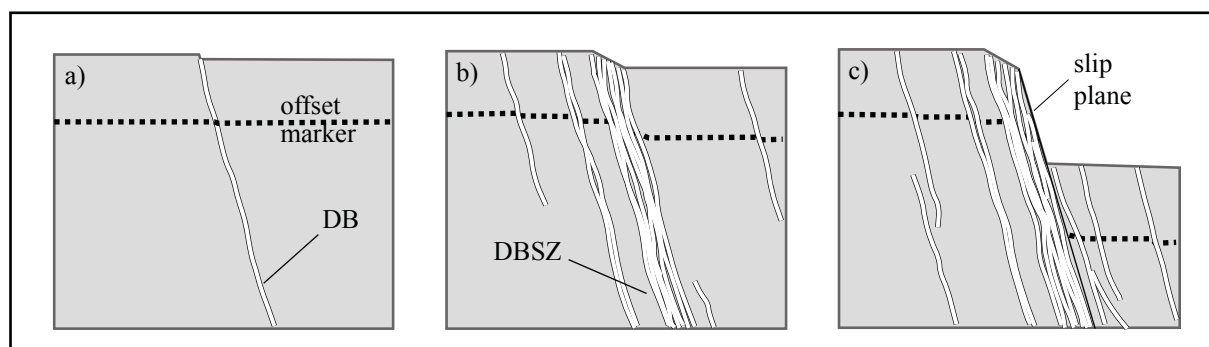


Figure 4.4: Scheme for the sequential evolution of brittle deformation bands, deformation band shear zones and a final discrete slip plane after Aydin & Johnson (1978), modified from Pollard & Fletcher (2005). a) Formation of a single deformation band. b) Increasing strain accounts for further sub-parallel deformation bands arranged in a deformation band shear zone. c) Finally a discrete slip plane evolves, accounting for larger offset.

Although hitherto undescribed from the Molasse sandstones, brittle deformation bands were found to be common structures in the study area, accounting for a considerable amount of the overall deformation (figure 4.11). The detailed microscopic investigation of the Molasse deformation bands revealed that they initiate by cataclasis of the grains, thus forming a ground micro-fault gouge. This first stage of grain grinding on the micro-scale and the development on the macroscopic scale from a single band to arrays of deformation band shear zones is in accordance with the “classic” model. On the microscopic scale, however ongoing deformation differs from this model, as the developing micro-fault gouge features ductile structures marked by newly-formed palygorskite, a Mg-rich clay mineral (see chapters 2 and 3).

In the field, single deformation bands as well as deformation band shear zones with and without slip planes were mapped. These slip planes exhibit lineations made of fibrous palygorskite rather than representing mechanical scratches. The slip planes develop within a deformation band shear zone, either at one edge or at a slightly different angle crosscutting the shear zone (see chapter 2).

4.4.1.2 *Slickensides*

Slickensides are sheared fractures in rocks characterised by a fault plane that is striated by lineations parallel to the direction of movement. Different types of slickensides can be distinguished resulting from a variety of mechanisms (Hancock 1985, Petit et al. 1983, Petit 1987). These include polishing of the fault planes (Avakian 1986), their mechanical scratching by small hard asperities during movement (Hancock 1985, Hancock & Barka 1987, Tjia 1964, Engelder 1974), the alignment of fault gouge material (Engelder 1974, Means 1987) and the precipitation of elongate mineral phases grown in the direction of movement of the fault (Durney & Ramsay 1973). Mineral phases such as calcite on fault planes may also be mechanically scratched when the mineral precipitated as vein filling before (Means 1987) or during a previous stage of faulting. In such cases, they resemble fibrous crystal growths at a first glance but the mechanism of their formation is different.

Data sets of fault plane and striation orientation combined with the sense of movement make it possible to determine the orientation of stresses that caused the deformation (Angelier 1979). While azimuth and inclination of fault plane and lineation can

easily be measured, the sense of movement often remains ambiguous. A variety of criteria exist to determine the sense of movement in the field (Petit et al. 1983, Petit 1987, Doblas et al. 1997a and 1997b, Doblas 1998). The simple roughness smoothness criterion (Hills 1953, Billings 1954), according to which the fault plane is smooth in direction of faulting and rough in the opposite direction, was shown to be not globally applicable (Paterson 1958, Tjia 1964, Gay 1970). This has lead Angelier (1994) to distinguish between positive criteria referring to fault planes being smooth in the direction of movement, and negative criteria to those being rough in the direction of movement. The most unproblematic way to determine sense of movement for fault plane is according to synkinematic crystal growth. The direction of thickening of the crystal aggregate points to the direction of movement of the missing block and the roughness smoothness criterion is valid (Durney & Ramsay 1973). However, for the mechanically formed slickensides this criterion has to be treated with care because it is most often misleading. It has been shown by both laboratory (Paterson 1953) and field evidence (Tjia 1964) that roughness smoothness arguments according to step geometries on mechanically formed fault planes would give the wrong, i.e. the opposite sense of movement. Steps opposing the direction of movement may develop in a Riedel-type system as initial T-fractures that are rotated by subsequent shear or as secondary R'-shears, conjugate to the fault plane that itself resembles the R-shear (Petit 1987). The most reliable criterion for mechanically formed slickensides is probably given by the grooves formed by small, hard grains of gouge material. These grooves should be deepest in the direction into which the grain was moved (carrot-shaped grooves, Engelder 1974). However, such grooves can be small and difficult to recognise in the field.

Whereas syn-kinematic growth of crystal fibres is most likely attributable to creeping deformation (Power & Tullis 1989, Means 1993), the seismic nature of mechanically scratched (Engelder 1974) and polished surfaces (Doblas et al. 1997b) has often been suggested. The interplay between fault creep in a semi-ductile deforming fault gouge and stick-slip behaviour on discrete planes along-strike of the same fault zone suggests that the slip planes are indicators of paleoseismicity (Miller 1996, Doblas et al. 1997b). On a smaller scale, the microscopic study of slickensides revealed cyclic alternations between cataclasis and oriented mineralization, suggestive of seismic rupture events and periods of aseismic creep, respectively (Power & Tullis 1989).

The majority of the slickensides mapped in the sandstones of the study area in the Molasse Basin subsequently develop from brittle deformation bands and hence form a micro-fault gouge. This fault gouge contains newly-formed fibrous palygorskite which appears as lineations on the slickenside surface (see chapter 2), formed by shearing and alignment of the micro-fault gouge. These palygorskite lineations are an excellent indicator of the direction of movement, whereas the sense remains often indeterminate.

Slickensides with polished and scratched surfaces, occurring mostly in the damage zones of larger faults, are less common. Their grooves are microscopic and not adequate to determine sense of movement in the field. Their steps appeared to be a negative criterion in the sense of Angelier (1994), i.e. they oppose the sense of movement. This was established from the rare occurrence of small seams of calcite (positive criterion) in some cases, as well as by offset of markers such as cut pebbles or clay lenses in other cases.

Slickensides with fibrous calcite crystals are common in the outcrops of the Subalpine Molasse but are rare in the Plateau Molasse. Where they occur in the Plateau Molasse they do so in damage zones of larger faults, as well as in the conglomerates of the Belpberg beds (OMM). Their formation is most likely linked to fluid pressure and/or chemistry, which may be influenced by lithology as well as by the intensity and the depth of deformation: the deeper the deformation, the more calcareous the rock and the larger the

associated fault (e.g. the fluid conductivity), the more likely we observe calcite solution and precipitation.

4.4.1.3 Unspecified fractures

Joints and joint-like fractures that show no indications of relative movement were also mapped in the field. The fact that their orientation distribution matches that of slickensides suggests that a considerable number of them are probably altered small-scale fault fractures.

4.4.1.4 Orientation patterns of planar meso-scale brittle structures

Planar meso-scale brittle structures such as fractures, slickensides and brittle deformation bands form in response to stress. A given orientation of σ_1 commonly results in more than one set of planar brittle structures with characteristic orientations such as conjugate shears. In more complex situations such as strike-slip shear zones, the Riedel shear model usually applies (figure 4.5).

The Riedel shear model (figure 4.5) was developed from analogue models with clay material (Riedel 1929, Cloos 1930, Tchalenko 1968) and described for experimentally deformed rocks (Bartlett et al 1981) as well as for different natural brittle deformation zones at several scales and lithologies (Tch-

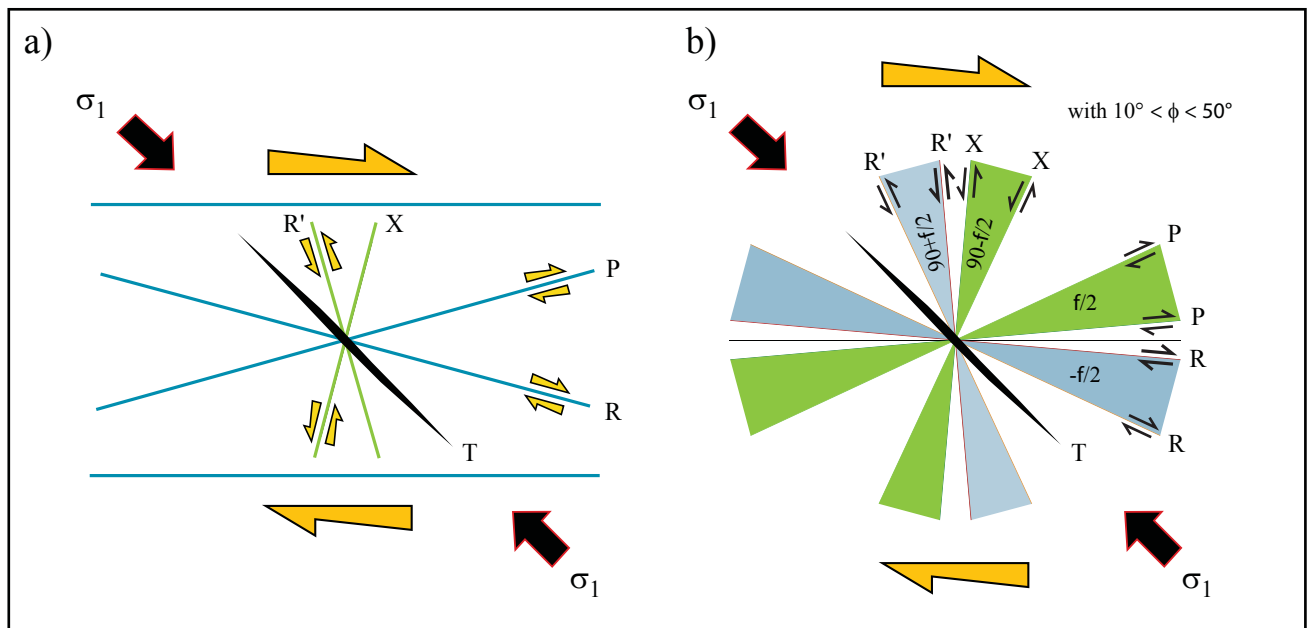


Figure 4.5: Principal geometries of a Riedel shear model. a) Arrangement of different Riedel shears in a brittle shear zone and their relative orientation. b) Range of possible orientations of different Riedel shears according to end member coefficients of friction (ϕ). Modified after Bonnet (2007).

alenko 1970, Davis et al 1999, Ahlgren 2001, Katz & Weinberger 2005). The movement of a fault zone is distributed on fault zone-internal shears with synthetic and antithetic senses of movement. The synthetic shears R and P are oriented at an idealised angle of 15° with respect to the shear zone, R with a normal σ_1 and P with a reverse σ_1 angle. The antithetic shears R' and X enclose ideal angles of 60° with R and P, respectively, and are steep with respect to the shear zone (figure 4.5). However, all angles within a Riedel system are functions of the angle of internal friction of the fractured material. This angle varies for different rock types, resulting in angles that deviate from their ideal values (Tchalenko & Ambrasey 1970, figure 4.5). R and R' form a conjugate set of shears with the bisector equal to σ_1 of the system. Additional shears included in the system are Y-shears running parallel to the shear zone, and T-fractures resembling tensional structures parallel to σ_1 . Depending on the type of Riedel shear or conjugate pair measured, the inferred σ_1 may differ by some degrees.

4.4.2 Non-planar structures

Pressure solution pits in pebbles of conglomerates are linear structures associated with low strain rates. This type of structure is uniformly distributed in the conglomeratic rocks of the study area.

4.4.2.1 Pitted conglomerate pebbles

The formation of solution pits at pebble surfaces (figure 4.6) was described as a stress-induced process of dissolution and diffusive mass transfer under low temperature rock deformation (McEwen 1978). As dissolution occurs, insoluble elements become concentrated in a zone of volume loss. Size and shape of this zone are dependent on the mineralogy of the dissolving pebble (McEwen 1978). Pressure solution has to be considered as a ductile deformation mechanism that can only take place at relative low stress rates. The parallelism of the resulting structures (solution pits in this case) reflects the bulk shortening direction (Simon 2007). Thus the pitting of pebbles represents a type of compaction that may be the result of horizontal shortening. It can therefore serve as a tool to map low but continuous stress states within otherwise undeformed rocks.

It was shown that the formation of pitted pebbles by dissolution processes requires only relative low stress rates (McEwen 1978) and can accommodate

about 1% of shortening (Behrens & Wurster 1972). If stress increases, grains start to slide against each other, thereby scratching their surfaces and finally fracturing (Behrens & Wurster 1972). Pitted pebble formation was found to pre-date a more intense deformation by folding and thrusting (Behrens & Wurster 1972). Detailed studies of a rock volume (Behrens & Wurster 1972) and regional mapping of dissolution grooves (Schrader 1988b) showed that pebble deformation is uniformly disturbed. Detailed investigation of particle paths on pitted pebbles showed that in most cases they reflect a pure shear deformation mechanism (Behrens & Wurster 1972, Schrader 1988b). Simple shear is only recognised near discrete fault zones, where at the same time stress directions derived from the solution pits deviate from the otherwise uniform stress field (Schrader 1988a). The orientation of the paleostress axes can be in accordance with the ones derived from other scattered small-scale structures, but differs from the orientation corresponding to larger-scale structures in the same region (Ruano & Galindo-Zaldivar 2004). The formation of solution pits requires a minimum pressure of about 10 MPa (McEwen 1978) and will ensue as a response to compaction at depths of about 300-400m (for a sedimentary overburden, Ruano & Galindo-Zaldivar 2004). Therefore tectonic stresses and burial stresses result in the all-around pitting of conglomerates at depths of more than 400m. Pebbles at shallower depths pit only due to tectonic stresses (Ruano & Galindo-Zaldivar 2004).

In the study area the occurrence of solution pits is restricted to the small band of Belpberg beds in the eastern and north-eastern part of the study area (e.g. figures 4.8, 4.21), where they are regularly distributed in the conglomerate beds.

The pressure solution pits (figure 4.6) form by the indentation of one pebble into another and the direction of indentation can be assumed to represent the compression direction. The indentation can be either straight, generating more or less symmetric pits, or oblique, generating highly asymmetric pits (figure 4.6). In a simple mapping approach, we determined the indentation direction by the geometry of the solution pit, and measured its azimuth and inclination with the help of a pencil (figure 4.6). This procedure allowed us to collect data over a larger area. We refer to this pair of azimuth and inclination as the axis of the solution pit.

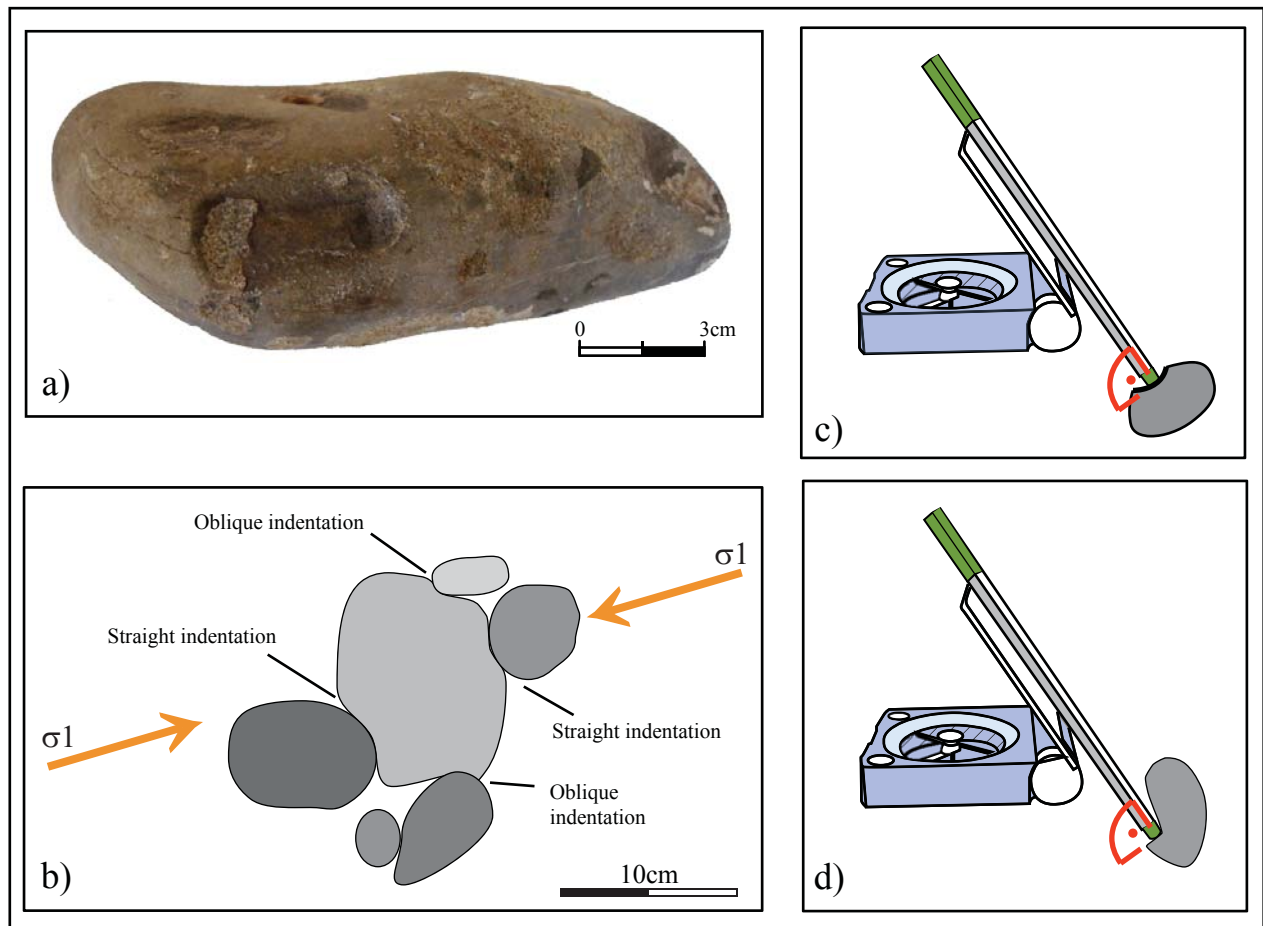


Figure 4.6: a) Photograph of a pebble with pressure solution pits. b) Principle of the pebble indentation process. Straight indentation forms symmetric solution pits and oblique indentation forms asymmetric solution pits. c) and d) Method of the measurement of solution pit axes in the field. c) symmetric solution pit and d) asymmetric solution pit. (Modified after Matzenauer 2007)

4.5 FAULT ZONES

The fault zones mapped in the field (figure 4.8) are zones where the planar structures described in subchapter 4.4.1 are concentrated in subparallel orientations or Riedel shear geometries. The fault zones were classified by their outcrop characteristics, according to which several different types and three different sizes of faults can be distinguished (figure 4.7). Markers of total offset are generally lacking due to small outcrop size. Fault sizes were qualitatively determined by fault zone width and the amount of fault core material such as fault gouge. We consciously chose the generic term “fault size” because based on our limited observations we neither intend nor are able to contribute to the discussion of whether fault width directly correlates with displacement (Scholz 1987, Hull 1988) and length or not (Blenkinsop 1989). Our aim is simply the qualitative characterisation of a fault zone and its application for the deformation model. In this view a fault zone is of course more important the longer its extent and the larger its offset. According to our classification, fault

sizes are defined as follows:

- small faults: fracture zone width up to 0.5m or the accumulation of several slickensides
- medium faults: fracture zones with a width larger than 0.5m or the presence of a fault gouge
- large faults: fault zone with a width larger than 1m or the presence of a fault gouge larger 0.5m.

The four different types of faults are:

- Palygorskite type: fault zones containing palygorskite
- Dense fracture type: fault zones marked by fractures or slickensides
- Clayey cataclasite type: fault zones with clayey cataclasites

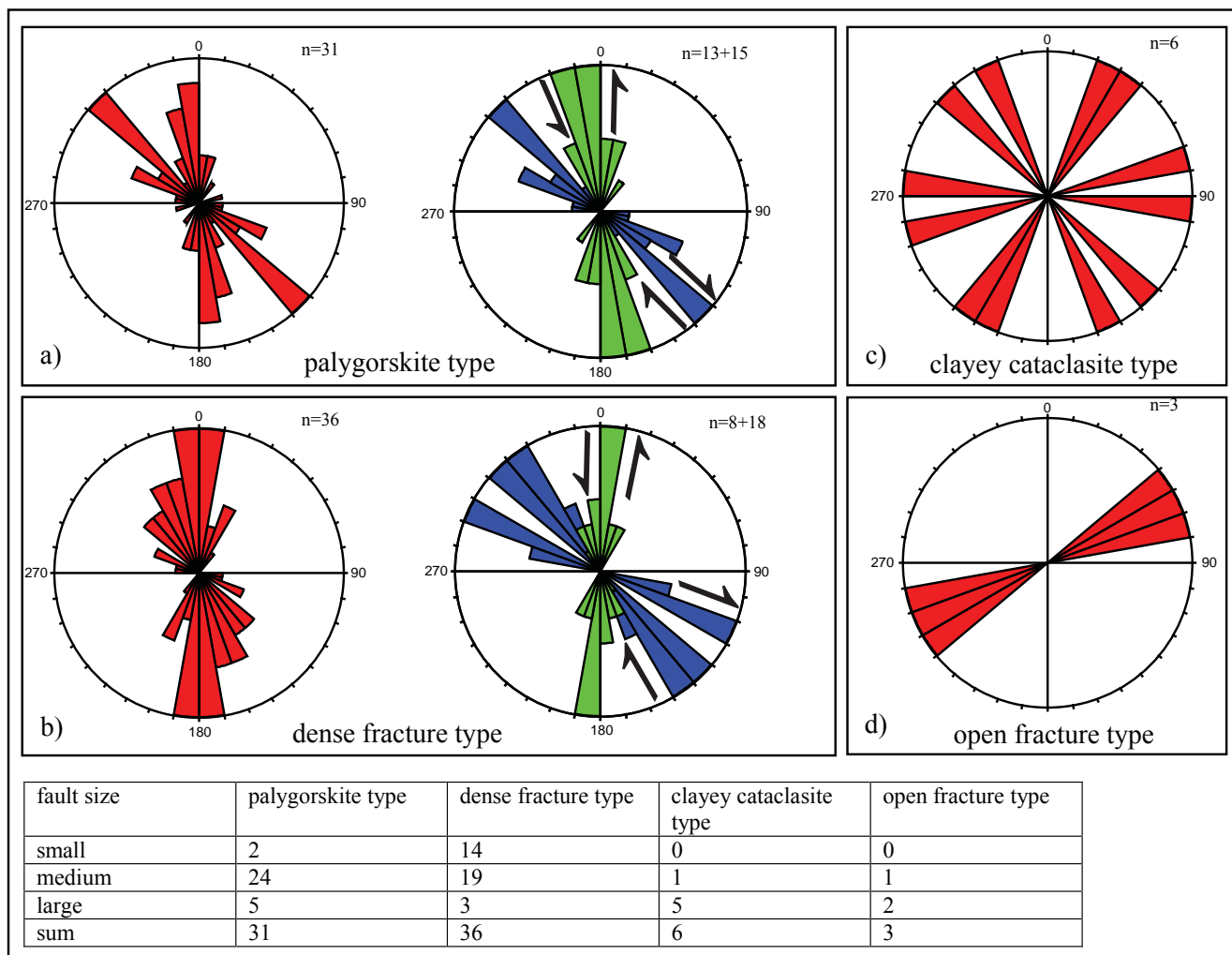


Figure 4.7: Table and rose diagrams for the 76 mapped faults subdivided into the four classes described in the text: a) Faults containing palygorskite, b) faults marked by a dense array of slickensides and fractures, c) faults with clayey cataclasites and d) faults marked by open fractures. For a) and b) an additional rose diagram is given (right diagram) with right-lateral faults marked blue and left-lateral faults marked green. The table gives the number of small, medium and large faults of each fault class (small faults: fracture zone width up to 0.5 m, medium fault: fracture zone width larger than 0.5 m or presence of a fault gouge, large fault: fault zone width larger than 1 m or presence of a fault gouge larger 0.5 m).

– Open fracture type: Fault zones marked by open fractures.

Figure 4.7 provides an insight into the total number of each type of fault.

4.5.1 Palygorskite type fault zones and dense fracture type fault zones

The palygorskite type fault zones show fractures, slickensides, brittle deformation bands and fault gouges. On the macroscopic scale, palygorskite appears in up to 5 cm wide veins in fault gouges or along fractures and slickensides (see chapter 3). On the microscopic scale, palygorskite appears in deformation bands and deformation band shear zones accumulating strain (see chapters 2 and 3).

The dense fracture type fault zones marked by fractures or slickensides (dense fracture type) are quite similar in characteristics to the fault zones with palygorskite. However, the slickensides show less macroscopic palygorskite and striations are composed of mechanical scratches or in rare cases of calcite fibres.

While the clayey cataclasite type and the open fracture type faults (see subchapter 4.5.2 and 4.5.3) clearly represent different types of deformation zones, the strict discrimination between the palygorskite type and the dense fracture type is somewhat artificial. This is revealed by several common characteristics as well as mixed-type faults. For instance, there are faults of this kind that feature dense zones of fractures with purely scratched slickensides as well as a fault core or deformation bands containing palygorskite. Furthermore not every single occurrence of a dense fracture type fault and brittle deformation band could actually

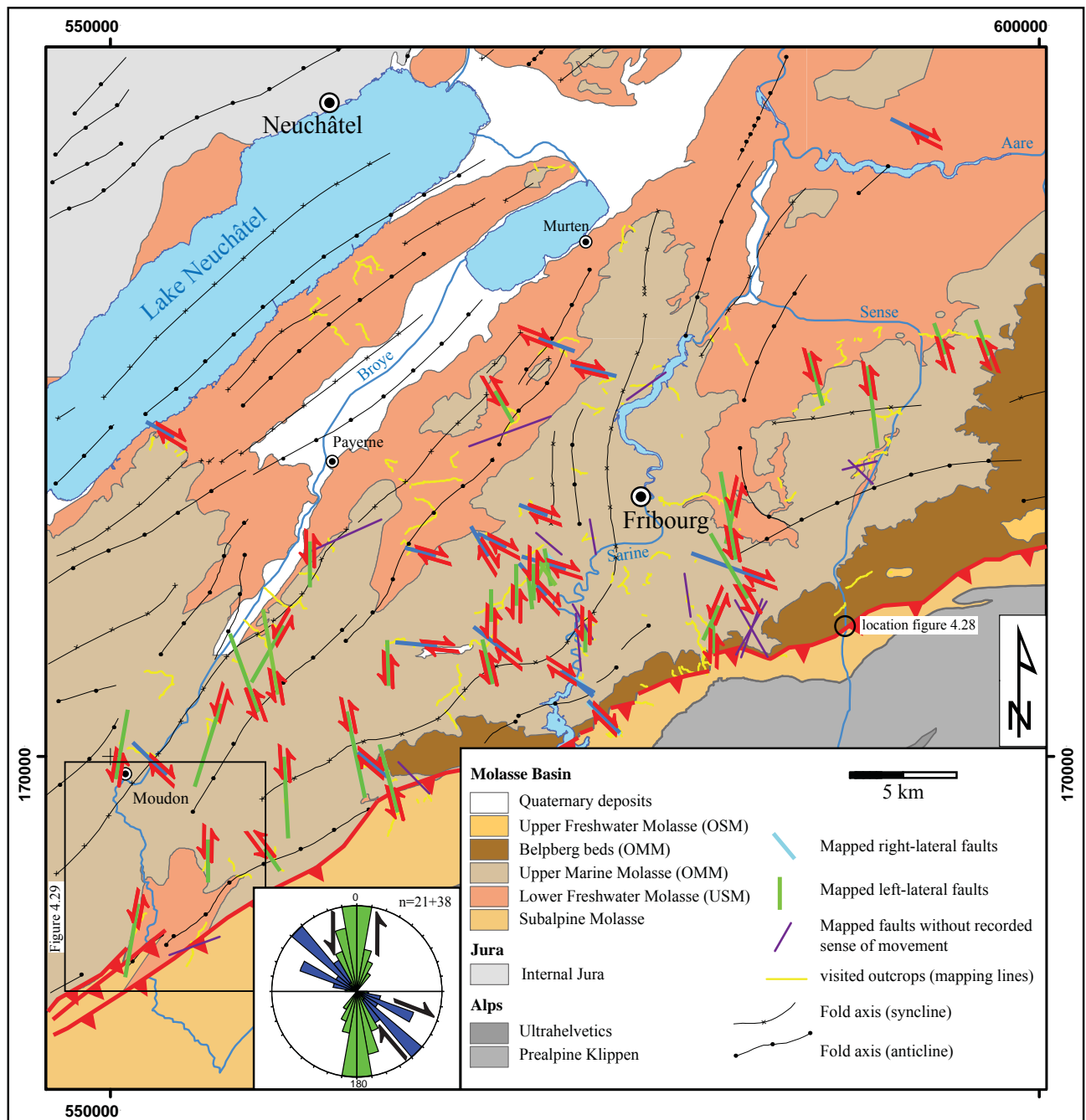


Figure 4.8: Study area with faults mapped in the field. NNW-SSE to NNE-SSW striking faults are left-lateral and E-W to NW-SE striking faults are right-lateral. Faults with no recorded sense of movement are also given. The rose diagram gives the strike for all right-lateral faults in blue and all left-lateral faults in green.

be checked for the microscopic occurrence of palygorskite.

Of 76 mapped faults, 67 can be identified as the palygorskite type and dense fracture type. Both types are represented by mostly medium-scale faults, with the dense fracture type also composing a considerable number of small faults, and the amount of large faults being slightly larger for the palygorskite type faults (figure 4.7). Given their overlapping features

as discussed above, they probably represent only one type and clearly dominate the characteristics of faulting in the study area.

The strike distribution of the palygorskite type and the dense fracture type fault zones (figure 4.7 a, 4.7 b) reveal predominantly NW-SE striking left-lateral fault zones, and N-S striking right-lateral fault zones.

4.5.2 Clayey cataclasite type fault zones

The clayey cataclasite type fault zones are characterised by fracture zones and cataclastic fault cores composed of grained foliated material.

The six mapped clayey cataclasite fault zones scatter widely in strike (figure 4.7 c). They were mapped as reverse or thrust faults within the Subalpine Molasse and as strike-slip faults in the Plateau Molasse. In the outcrops, five of them show the characteristics of large faults, possibly indicating that they represent another, larger dimension of faulting.

4.5.3 Open fracture type fault zones

The open fracture type fault zones are characterised by a dense array of fractures with no indication of relative movement. They mainly appear as cm to dm-wide, open cracks, often filled with gravel and soil material.

The three mapped open fracture type fault zones are marked in the field by up to 100 and more fractures, distributed across a zone of some tens of metres. They all strike WSW-ENE, which differs significantly different from the orientation distribution of the other structure types (figure 4.7).

4.6 ORIENTATION OF MESO-SCALE STRUCTURES AND DERIVED PALEOSTRESSES

4.6.1 Brittle deformation bands

The orientation of more than 700 deformation bands and deformation band shear zones were measured in outcrops of the study area (figure 4.11). In almost all cases the dip was found to be steep to vertical, in some cases between 60° and 75° and in the majority of cases between 75° and 90° (figure 4.12 a). This indicates their strike-slip nature and facilitates their statistical analysis. Due to the lack of offset markers, the sense of movement could be defined for 155 deformation bands only (figure 4.9).

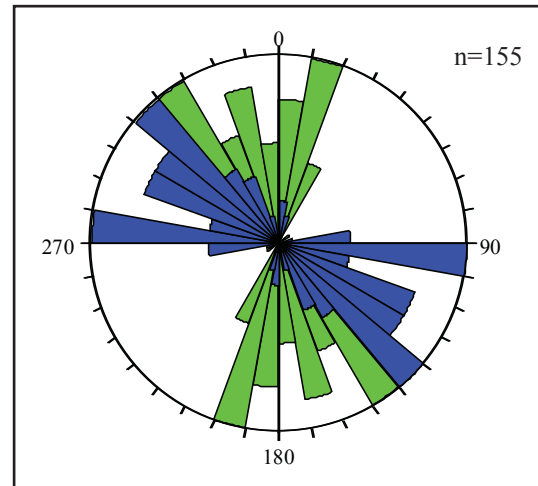
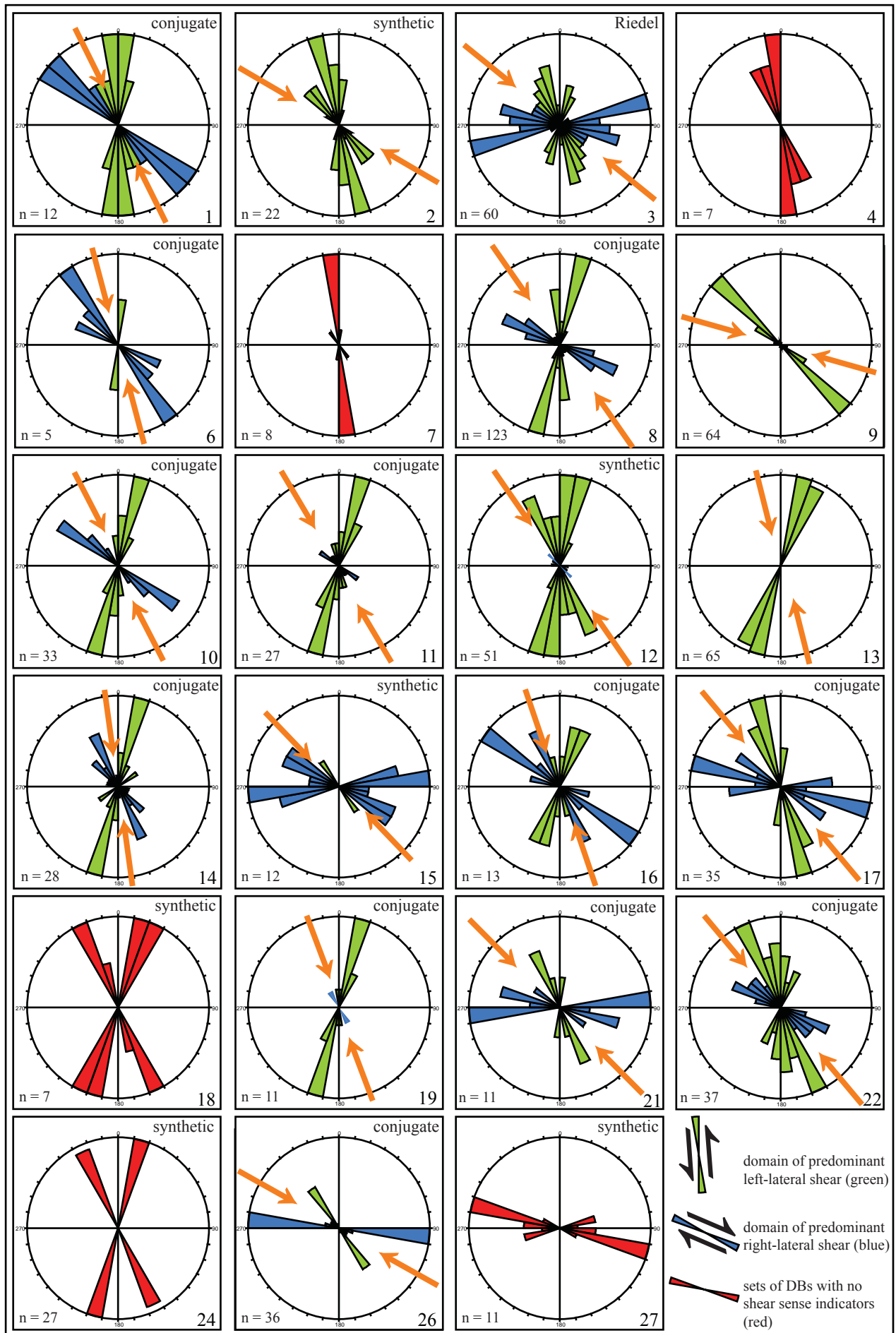


Figure 4.9: Strike distribution of all brittle deformation bands with known sense of movement. The strike of right-lateral deformation bands ($n=76$) is given in blue, and the strike of left-lateral deformation bands ($n=79$) in green.

The distribution of strike of all deformation bands reaches from W-E via NW-SE and N-S to NNE-SSW. Within this sector maxima occur for WNW-ESE, NW-SE, NNW-SSE, and NNE-SSW (figures 4.12 a, 4.10). This relative wide scatter becomes more precise when only the strike of the deformation bands with known sense of movement is taken into account. In this case an E-W, a broad NW-SE and a NNE-SSW maximum are developed (figure 4.9). Here the E-W and the western part of the broad NW-SE maximum correspond to right-lateral shear, while the NNE-SSW and northern half of the NW-SE maximum correspond to left-lateral shear. For more detailed analysis the data was grouped into 27 sets (sites 1 - 27 in table 4.1). The sites 5, 20, 23 and 25 have less than five data points per site and are thus not considered further. Eighteen of the twenty-three remaining groups (rose diagrams in figure 4.10) show two sets of strike, four reveal only one set, and one reveals four sets.

In six of the 18 two-set cases (sites 2, 12, 15, 18, 24 and 27) these were arranged as synthetic Riedel shears and in the other twelve cases as conjugate shears. The criteria for two sets to be synthetic Riedel shears are, firstly, the same sense of movement, and secondly, lower included angle between 20° and 40°. If the two sets show opposite sense of movement and a lower included angle containing the axis of compression between 50° and 70° they were assumed to be conjugate sets. The orientation of σ_1 was estimated

Figure 4.10: Rose diagrams of sets of deformation bands grouped by outcrops. Numbers refer to numbers in table 4.1 and to locality in the map (figure 4.11). Arrows give the direction of maximum horizontal compressive stress, inferred from the sets with given sense of movement. In the case of more than one maximum of data sets, the inferred system is indicated (synthetic shears, conjugate shears or Riedel shears).



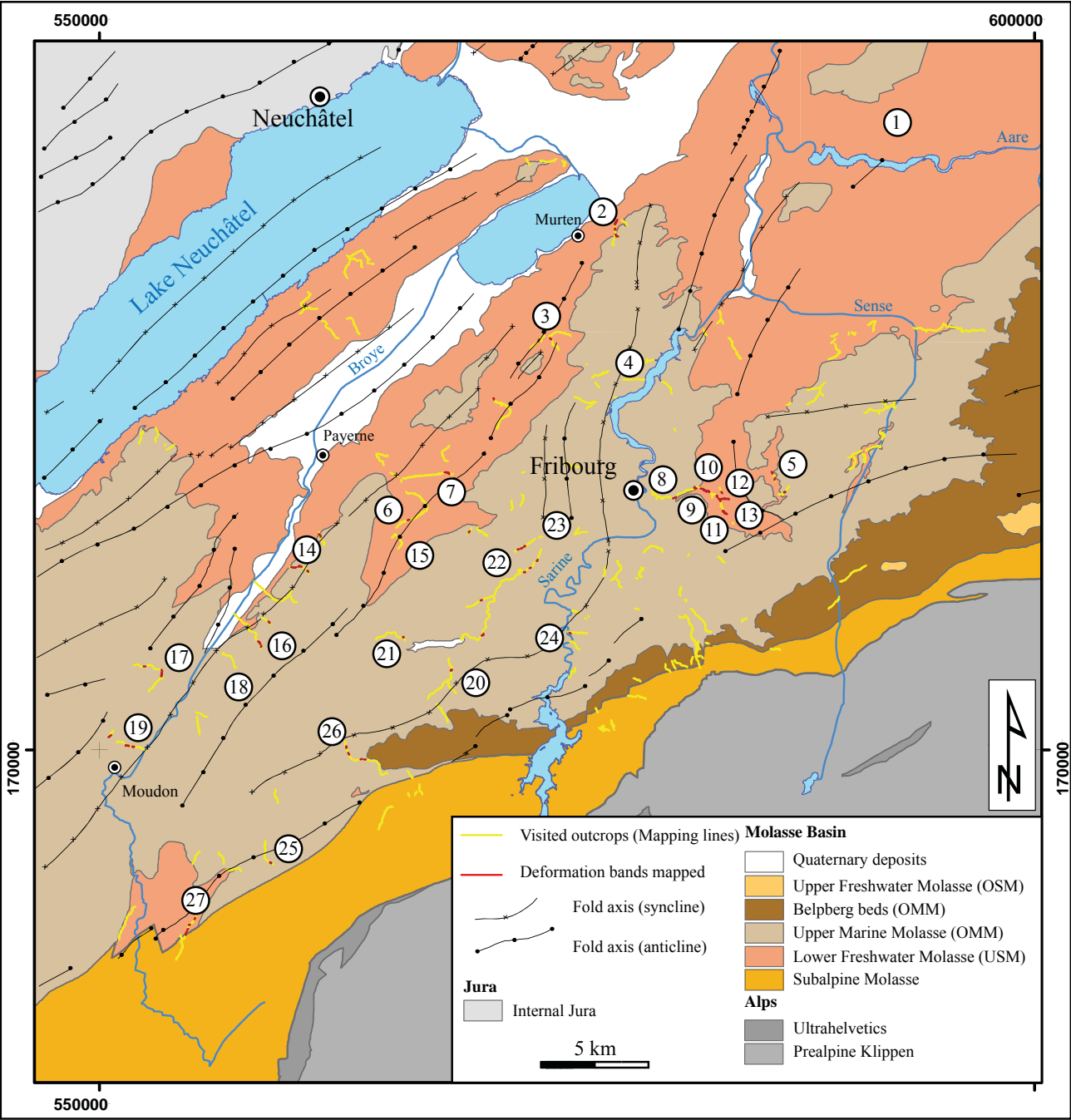


Figure 4.11: Location of the brittle deformation band data sets given in figure 4.10 and table 4.1. Numbers 1 to 27 refer to the numbers given in the figure and the table.

for the 12 conjugate sets as NNW-SSE in eight cases, NW-SE in three cases and WNW-ESE in one case. Of the synthetic Riedel σ_1 was estimated as WNW-ESE for site 2, NW-SE for site 15, ENE-WSW for site 12 and could not be determined due to the lack of indicators for the sense of movement for sites 18, 24 and 27. The synthetic sets from sites 12 and 15 additionally contain a very small number of conjugate shears.

The four groups of outcrops with only one maximum show a N-S strike in two cases (site 4 and site 7) as well as one NW-SE strike (site 9) and one NNE-SSW strike (site 13). For the N-S strike no sense of movement could be obtained in the field, whereas for the NW-SE case left-lateral movement is given by offset relationship and interpreted from correlation with subparallel slickensides for the NNE-SSW case.

Table 4.1: Sets of deformation bands grouped by site. Numbers in the table refer to the rose diagrams in figure 4.10 and to the location in the map (figure 4.11). Sites 5, 20, 23 and 25 (marked in grey) each have less than five data points and are not considered further. dex = right-lateral, sin = left-lateral.

| Site | n data | Name | Orientation maximum 1 | | Orientation maximum 2 | | Orientation maximum 3 | | Orientation maximum 4 | | Orientation of inferred σ_1 |
|------|--------|-------------------------|---|---|---|-------|-----------------------|-------|-----------------------|-------|------------------------------------|
| | | | strike | sense | strike | sense | strike | sense | strike | sense | |
| 1 | 12 | Wohlensee north | NW-SE (310°-130°) | dex | N-S (000°-180°) | - | - | - | - | - | NNW-SSE |
| 2 | 22 | Burggraben | NNW-SSE (350°-175°) | sin | NW-SE (320°-140°) | sin | - | - | - | - | WNW-ESE |
| 3 | 60 | Wallenried | WSW-ENE (255°-075°) | dex | WNW-ESE (280°-100°) | dex | NNW-SSE (340°-160°) | sin | NNE-SSW (020°-200°) | sin | NW-SE |
| 4 | 7 | Barbarèche | N-S (355°-175°) | - | - | - | - | - | - | - | - |
| 5 | 4 | St. Antoni | NNE-SSW (010°-190°) | Less than 5 data not considered further | | | | | | | |
| 6 | 5 | L'Arbogne | NW-SE (320°-140°) | dex | N-S (005°-185°) | - | - | - | - | - | NNW-SSE |
| 7 | 8 | Chauderes | N-S (355°-175°) | - | - | - | - | - | - | - | - |
| 8 | 123 | Gallera FR-567m | NNE-SSW (015°-195°) | sin | WNW-ESE (295°-115°) | dex | - | - | - | - | NNW-SSE |
| 9 | 64 | Gallera 567m-604m | NW-SE (315°-135°) | sin | - | - | - | - | - | - | - |
| 10 | 33 | Gallera 604m-Ametsmühle | NW-SE (305°-125°) | dex | NNE-SSW (015°-195°) | sin | - | - | - | - | NNW-SSE |
| 11 | 27 | Gallera Fault-632m | NNE-SSW (015°-195°) | sin | NW-SE (305°-125°) | dex | - | - | - | - | NNW-SSE |
| 12 | 51 | Gallera right tributary | NNE-SSW (010°-190°) | sin | NNW-SSE (335°-155°) | sin | NW-SE (315°-135°) | dex | - | - | NW-SE |
| 13 | 65 | Gallera above 632m | NNE-SSW (020°-200°) | sin | - | - | - | - | - | - | NNW-SSE |
| 14 | 28 | Trey - Torry | NNW-SSE (335°-155°) | dex | NNE-SSW (015°-195°) | sin | - | - | - | - | NNW-SSE |
| 15 | 12 | North of Corseray | W-E (265°-085°) | dex | WNW-ESE (300°-120°) | dex | NW-SE (325°-145°) | sin | - | - | NW-SE |
| 16 | 13 | La Tremuile | NW-SE (305°-125°) | - | NNE-SSW (020°-190°) | - | - | - | - | - | NNW-SSE |
| 17 | 35 | West of Lucens | WNW-ESE (285°-105°) | dex | NNW-SSE (345°-165°) | sin | - | - | - | - | NW-SE |
| 18 | 7 | Seigneux | NNW-SSE (335°-155°) | - | NNE-SSW (020°-200°) | - | - | - | - | - | - |
| 19 | 11 | West of Moudon | NNE-SSW (015°-195°) | sin | NNW-SSE (330°-150°) | dex | - | - | - | - | NNW-SSE |
| 20 | 1 | R. de Giebe | Less than 5 data not considered further | | | | | | | | |
| 21 | 11 | La Glâne Chénens | W-E (265°-085°) | dex | NNW-SSE (335°-155°) | sin | - | - | - | - | NW-SE |
| 22 | 37 | La Glâne Matran-Neyruz | NNW-SSE (340°-160°) | sin | WNW-ESE (295°-115°) | dex | - | - | - | - | NW-SE |
| 23 | 2 | St. Apolline | NW-SE (310°-130°) | dex | Less than 5 data not considered further | | | | | | |
| 24 | 27 | Vers St. Pierre | NNW-SSE (335°-155°) | - | NNE-SSW (015°-195°) | - | - | - | - | - | - |
| 25 | 2 | Le Gotto | NNE-SSW (035°-215°) | Less than 5 data not considered further | | | | | | | |
| 26 | 36 | Le Maussion | W-E (275°-095°) | dex | NW-SE (325°-145°) | sin | - | - | - | - | WNW-ESE |
| 27 | 11 | Le Maillon Oron | WNW-ESE (285°-105°) | - | WSW-ENE (255°-075°) | - | - | - | - | - | - |

The group of four maxima originates entirely from a well-studied outcrop at a creek near the village of Wallenried, where data was collected from a selection of 60 deformation bands with intersection relationship (see site 3). The four maxima are WSW-ENE, WNW-ESE, NNW-SSE and NNE-SSW. The first two correspond to right-lateral shear, while the last two show left-lateral shear. The angles are 30° between the two right-lateral and the two left-lateral shears, and 60° between these two systems. This geometry matches a complete Riedel system with the WSW-ENE orientation representing the R-shears, the WNW-ESE orientation the P-shears, the NNW-SSE orientation the X-shears and the NNE-SSW orientation the R'-shears. The outcrop may therefore be interpreted as the tip region of an E-W striking right-lateral fault zone which initiated by the development of deformation bands and subsequently evolved into a Riedel-type geometry. The axis of σ_1 for this system is oriented NW-SE.

A closer look at data subgroups according to site shows that the majority of deformation bands oc-

cur in conjugate sets (figure 4.10). Each of these conjugate sets can be assigned to one of two groups. The first group contains sets with right-lateral shears striking NW-SE as well as sets with left-lateral shears striking NNE-SSW (figure 4.12 b). This group is governed by a local σ_1 oriented NNW-SSE. The second group contains sets with left-lateral shears striking NW-SE and right-lateral sets striking E-W (figure 4.12 c). This group is governed by a local σ_1 oriented WNW-ESE.

The sets with synthetic shears and the combined synthetic and conjugate sets (sites 2, 3, 12, 15) show an inferred σ_1 oriented NW-SE. The combined synthetic and conjugate sets imply that both of these types develop side by side, which is common for Riedel-type deformation. If the two groups of conjugate sets are interpreted as conjugate Riedel shears, then their superordinate Riedel shear zones are conjugate as well, with a maximum horizontal compressive stress oriented NW-SE (figure 4.12 d).

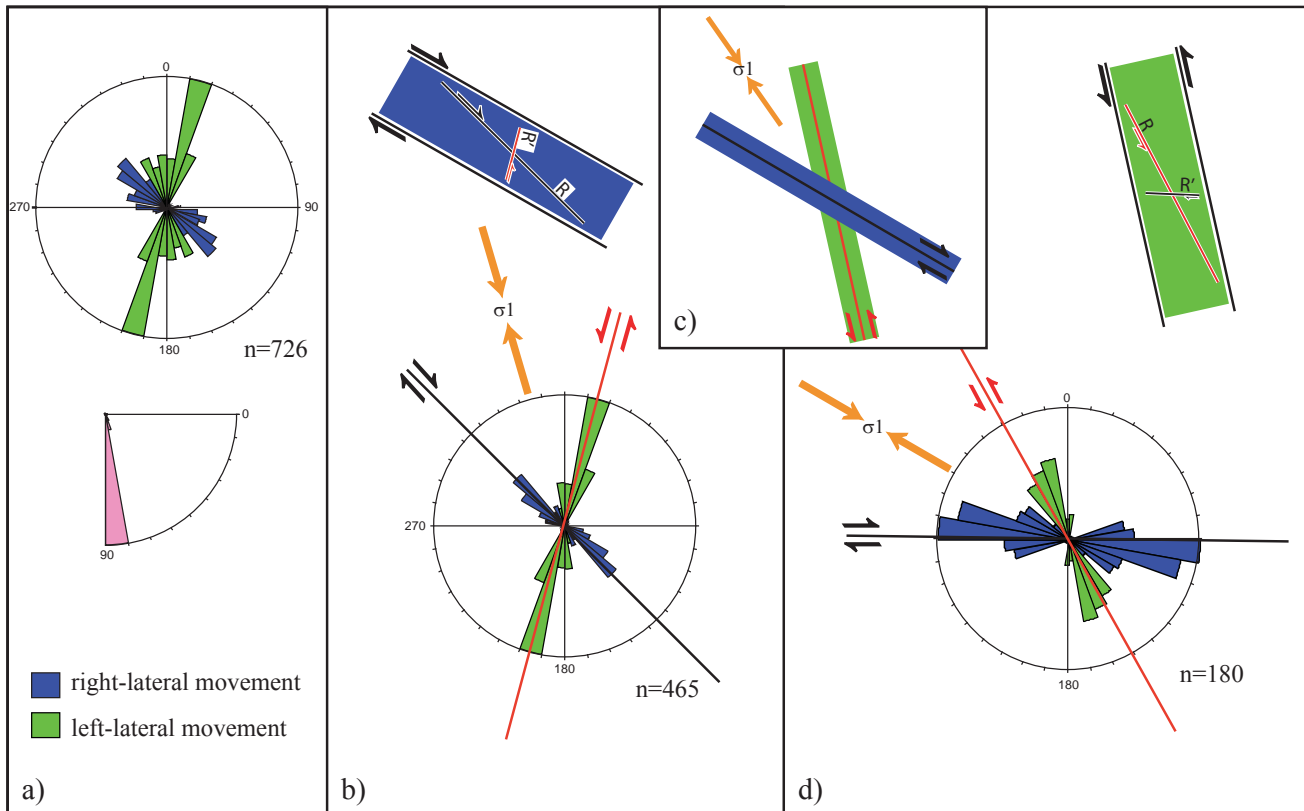


Figure 4.12: Rose diagrams to demonstrate the geometry of DBs in the field. The diagrams represent the distribution of strike. a) Distribution of all DBs (726 data sets). Dip is very steep in most cases. The data fits two sets of conjugate shears, b) and d). b) Conjugate sets of DBs with the corresponding super-ordinate right-lateral Riedel shear zone (465 data sets). σ_1 is oriented NNW-SSE. d) Conjugate sets of DBs with the corresponding super-ordinate left-lateral Riedel shear zone (180 data sets). σ_1 is oriented WNW-ESE. c) Orientation of the two Riedel shear zones superordinate to the conjugate sets of b) and d) and the orientation of σ_1 according to their geometry. The strike domains were determined as right-lateral (blue) and left-lateral (green) according to the orientation distribution of left-lateral and right lateral deformation bands (figure 4.6).

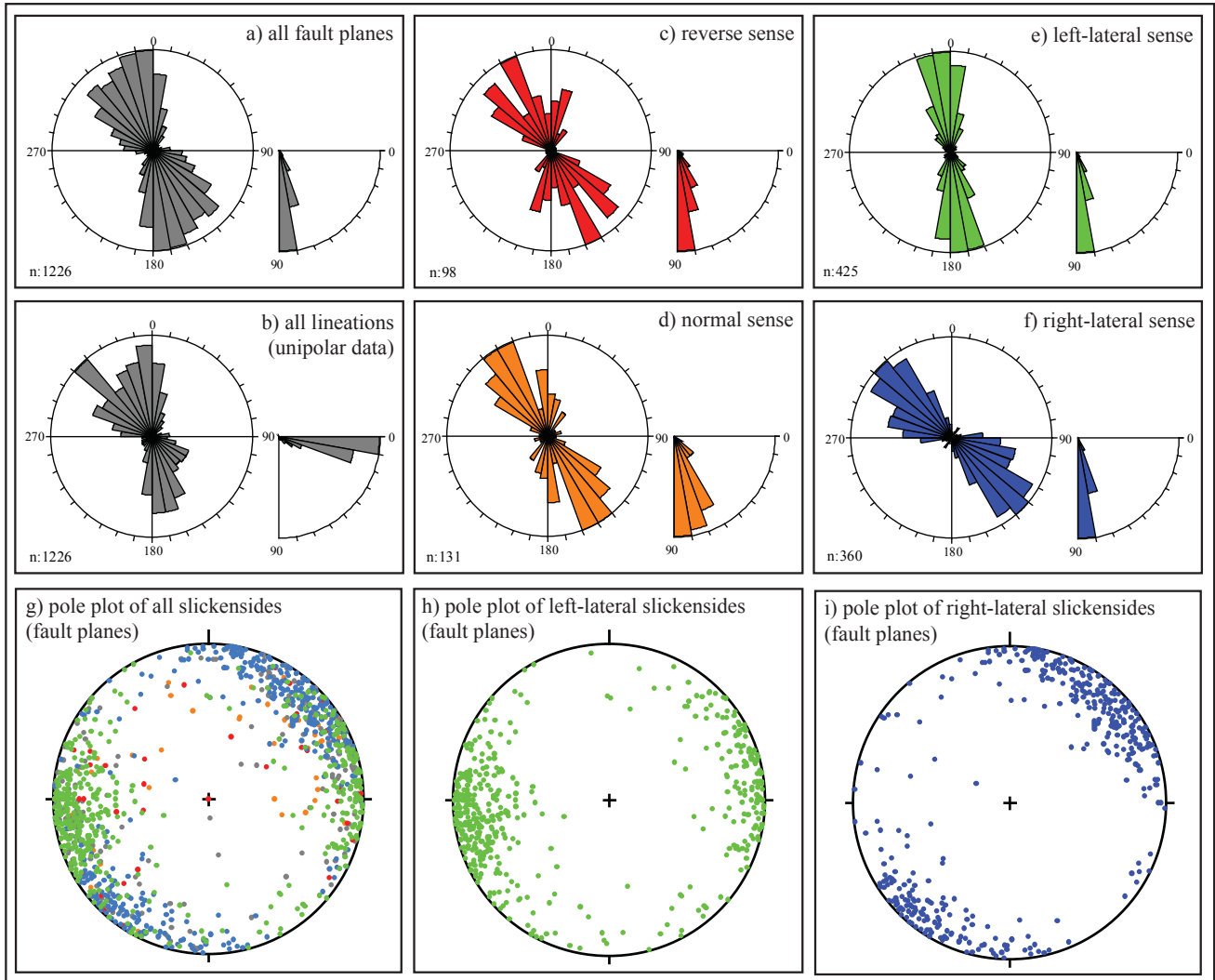


Figure 4.13: Rose diagrams and pole plots to illustrate the strike distribution of slickensides from the Plateau Molasse. a) All fault planes, b) all lineations, c) all slickensides with reverse sense, d) with normal sense, e) with left-lateral sense and f) with right-lateral sense. g) to i) Pole plots of slickenside fault planes (same colour code as for the rose diagrams): g) all data, h) left-lateral slickensides, i) right-lateral slickensides. Note that right-lateral slickensides strike NW-SE and left-lateral ones N-S. Normal slickensides strike NNW-SSE, parallel to the σ_1 inferred from the right-lateral and left-lateral slickensides, while reverse slickensides scatter in strike. For 212 datasets no sense of movement could be determined. These data sets are included in diagrams a), b) and g) only.

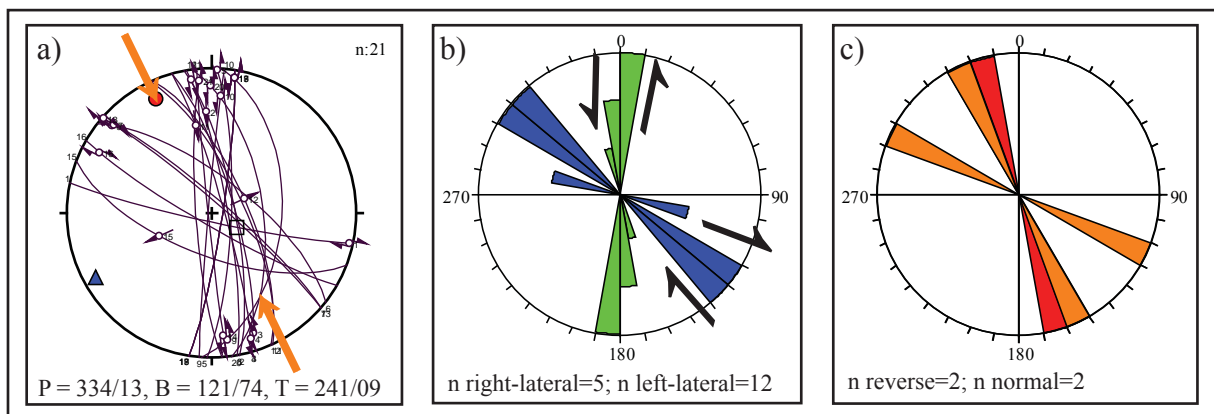


Figure 4.14: a) Lower hemisphere stereoplot with P-B- and T-axis of slickensides from the Plateau Molasse showing offset independent of fault plane criteria. b) Strike of left-lateral and right-lateral subset. c) Strike of reverse and normal subset.

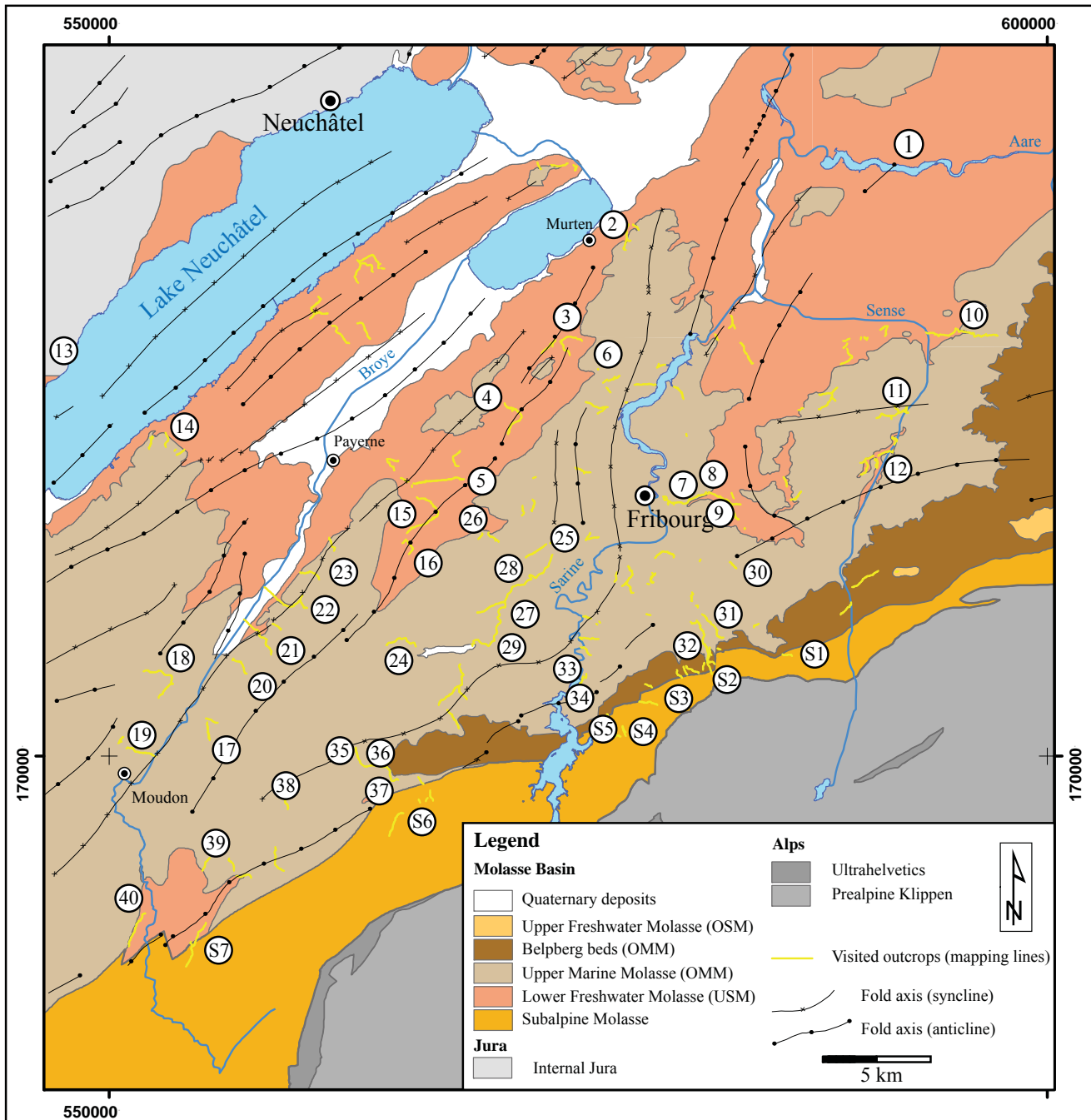
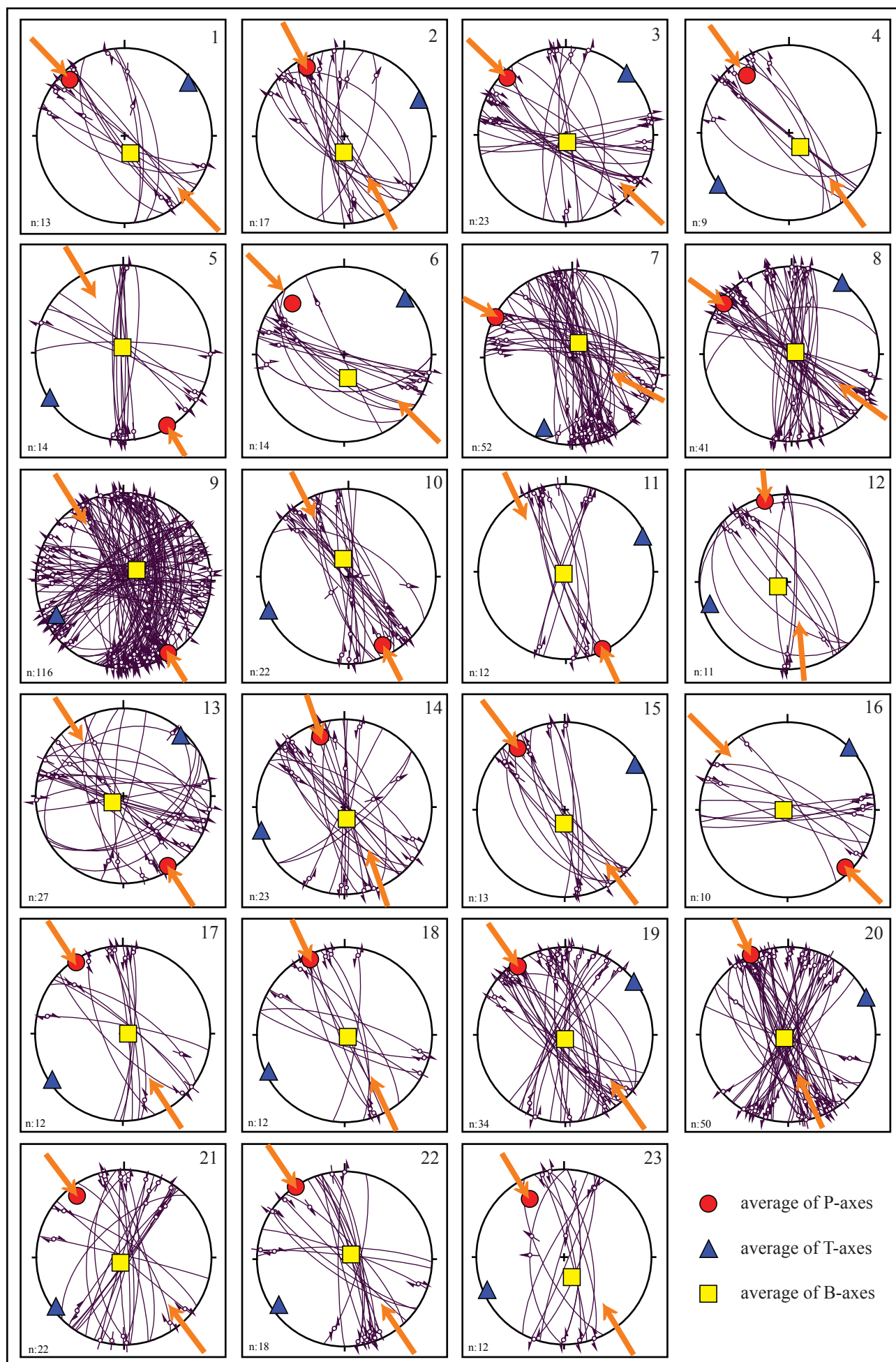


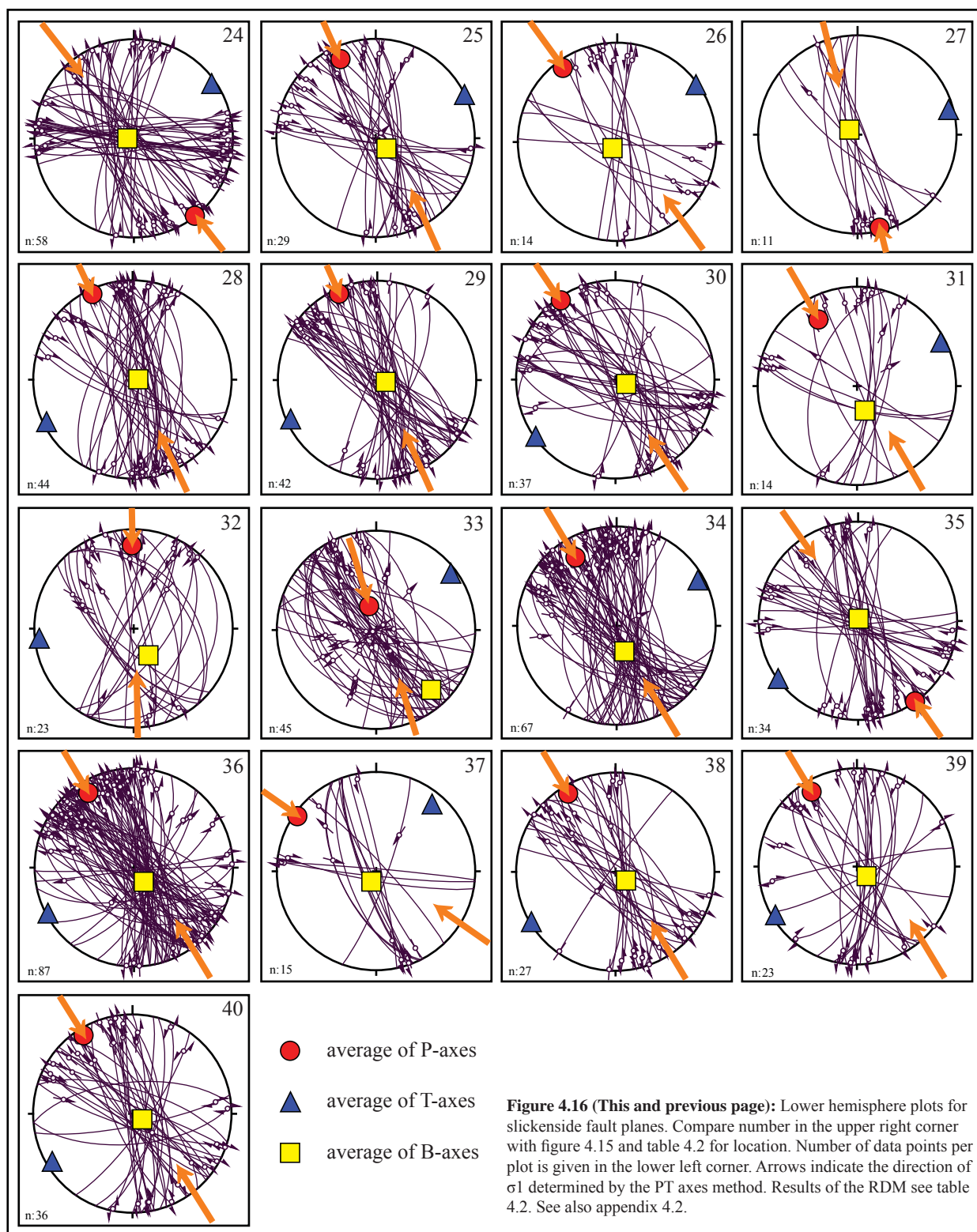
Figure 4.15: Location of the slickenside data sets given in figures 4.16, appendix 4.2 and table 4.2. Numbers 1 to 40 refer to data sets from the Plateau Molasse and numbers S1 to S7 to data sets from the Subalpine Molasse.

4.6.2 Slickensides

Pairs of azimuth and inclination were measured for fault planes and striations of more than 1200 slickensides in the Plateau Molasse of the study area (figures 4.13, 4.15, 4.16). The slickenside fault planes strike NW-SE and N-S with a certain variation towards WNW-ESE and NNE-SSW. Inclination is generally steep (figure 4.13) and the striation lineations are mostly subhorizontal (figure 4.13 b). Slickensides with NW-SE to WNW-ESE orientation have

right-lateral sense of shear (360 data sets, figure 4.13 f), whereas the N-S to NNE-SSW oriented ones have a left-lateral sense of shear (425 data sets, figure 4.13 e). A minor portion of the slickensides show reverse (98) and normal (131) senses of movement including oblique slip (figures 4.13 c and d). They strike dominantly NNW-SSE and secondarily NW-SE and NNE-SSW (reverse slickensides) as well as N-S (normal slickensides). Twenty-one slickensides were provided with senses of movement derived not from the slip plane itself, but from the offset of sedimentary mark-





ers, cut pebbles or the like (figure 4.14). Five of these are right-lateral striking NW-SE, twelve are left-lateral striking N-S, two are reverse striking NNW-SSE and two are normal striking NNW-SSE and WNW-ESE. This is in accordance with the strike distributions of right-lateral, left-lateral, reverse and normal slickensides from the whole dataset, corroborating the

general validity of the shear sense criteria used in the field.

The data was grouped into 40 subsets according to locality (figure 4.15) and plotted in lower hemisphere stereo projections (figures 4.16 and appendix 4.2). 39 of the 40 subsets show more than one orienta-

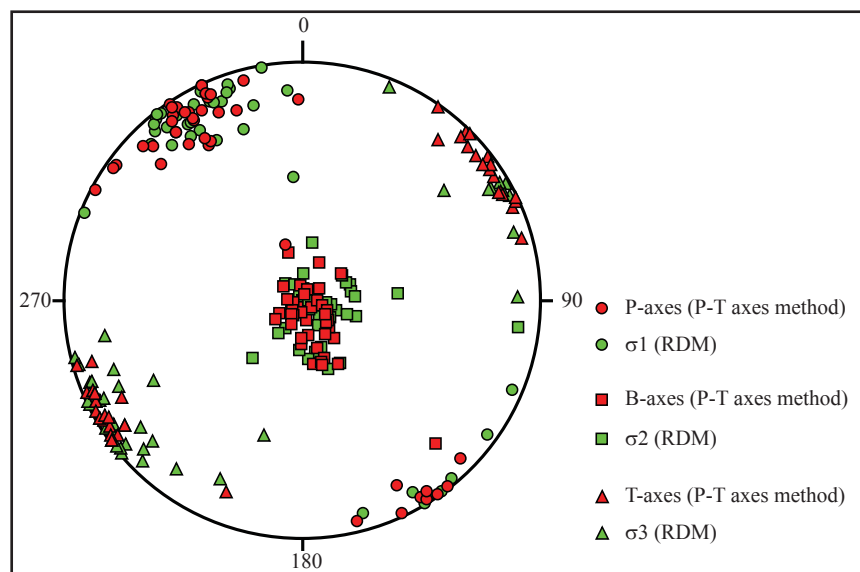


Figure 4.17: Comparison of P-, B- and T-axes derived from the PT axes method (red) with σ_1 , σ_2 , and σ_3 derived from the RDM (green) for 40 data groups from the Plateau Molasse. Compare with table 4.2 for values. The results of the two methods are in general accordance.

tion. Twenty of them show two, nine show three and seven show four or five different orientations, while for three subsets the individual fault planes scatter widely. According to the Riedel shear model three of the subsets with two orientations (sites 11, 16 23) display synthetic shears such as R-shears and P-shears or Y-shears, while the other seventeen display conjugate shears such as R-shears and R'-shears. The nine subsets with three orientations mostly display R-shears, R'-shears and Y-shears or P-shears and the seven subsets with four or five orientations display complete Riedel systems including synthetic R-shears, P-shears and Y-shears as well as antithetic R'-shears and X-shears. Some of them show R-shears, P-shears, Y-shears and R'-shears (sites 3, 35) while others are composed of R-shears, P-shears or Y-shears, R'-shears and X-shears (sites 24, 40). In the latter case it is often difficult to distinguish between P-shears and Y-shears, and in some cases probably both occur (site 9).

Overprinting criteria such as cut-off of a structure by another structure are rare in the field and their pattern is unsystematic. Roughly N-S striking left-lateral structures cut roughly NW-SE striking right-lateral structures about as often as vice versa (appendix 4.1). This indicates contemporaneous rather than successive of these two main fault sets. Together with the fact that the different orientations of slickenside fault planes and their kinematics are consistent with one Riedel system, this implies that the deformation of the Plateau Molasse was single-phase.

Paleostress was calculated for all 40 datasets with the PT axes method and for 39 datasets with the right dihedral method (RDM) (table 4.2), both showing similar results (figure 4.17). The results for the axes of maximum compression (P-axes/ σ_1 -axes) obtained from both methods differ in azimuth by more than 10° in six cases and more than 15° in only one case. For the axes of least compression (T-axes/ σ_3 -axes) the difference is more than 10° in nine cases and more than 15° in five cases. The two methods are therefore considered to deliver consistent results (figure 4.17). The azimuth of P-axis ranges between 298° (118°) (site 7) and 359° (179°) (site 32), the corresponding inclination lies between 1° (sites 22, 24 35) and 70° (site 30). Inclination is more than 10° in only sixteen cases and more than 20° in only three cases. The average azimuth is 328° (148°). The orientation of maximum compression of paleostress is NNW-SSE for twenty-eight, NW-SE for seven and N-S for five of the subgroups. With one exception all subgroups exhibit subhorizontal compression and extension axes, clearly supporting the observation that strike-slip is the dominant deformation mechanism.

The deviation of 12 compression axes from NNW-SSE up to 30° into both directions is likely the result of either local stress field variations or the disproportionately high occurrence of a certain Riedel shear in the outcrops. (paleostress axes calculated from Y-shears are, for instance rotated 15° with respect to axes calculated from R-shears).

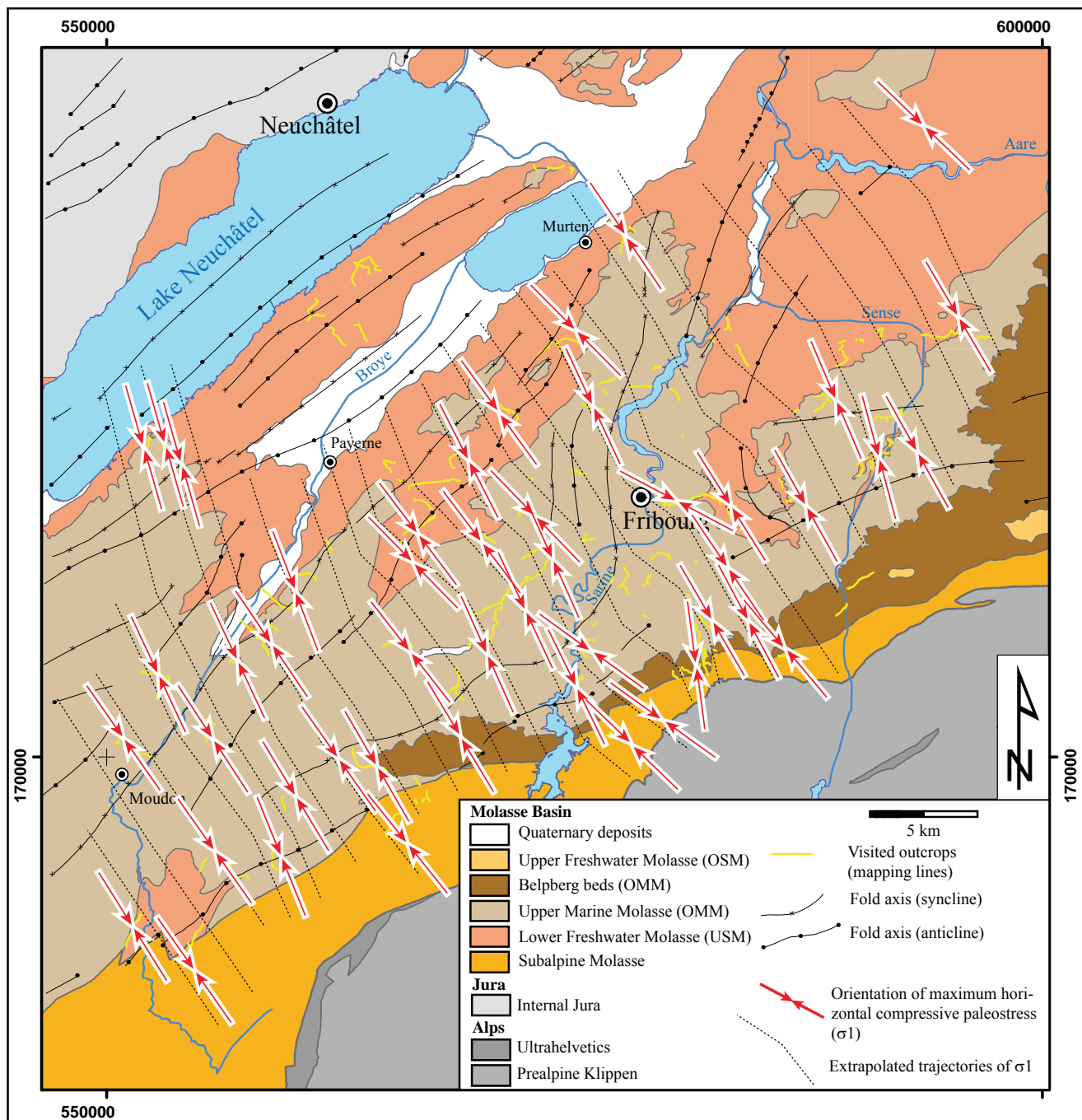


Figure 4.18: Map of the study area showing paleostress directions and main geologic units. The orientations of maximum horizontal compressive stress (σ_1) reflect paleostress calculated from slickenside data (red arrows). The paleostress field derived from slickensides shows homogenous NNW-SSE compression. In the Subalpine Molasse it is thrust-related, whereas it reveals a strike-slip regime in the Plateau Molasse.

The slickenside data from the Plateau Molasse shows a strike-slip regime characterised by left-lateral shear along N-S striking fault planes, and by right-lateral shear along NW-SE striking fault planes. The paleostress calculations reveal regional homogenous NNW-SSE compression and ENE-WSW extension (figure 4.18).

4.6.3 Unspecified fractures

The inclination of the more than 2800 unspecified fractures measured in the field is predominantly steep, similar to the slickensides and brittle deformation bands. Their maximum strikes NNW-SSE, but N-S, NW-SE and WSW-ESE orientations form

| Site | Name | n data | PT axes method | | | Right dihedra method | | |
|------|--------------------------|--------|----------------|--------|--------|----------------------|------------|------------|
| | | | P-axes | B-axes | T-axes | σ_1 | σ_2 | σ_3 |
| 1 | Wohlensee | 13 | 316/11 | 163/73 | 050/06 | no data | | |
| 2 | Burggraben | 17 | 332/11 | 181/75 | 061/06 | 331/07 | 134/82 | 240/02 |
| 3 | Wallenried | 23 | 314/08 | 168/83 | 044/02 | 322/09 | 114/80 | 231/05 |
| 4 | Grolley | 9 | 324/20 | 140/73 | 234/00 | 332/25 | 159/65 | 063/03 |
| 5 | Ponthaux | 14 | 149/04 | 352/85 | 239/03 | 147/03 | 007/86 | 237/02 |
| 6 | Courtepin | 14 | 314/19 | 170/68 | 047/06 | 341/25 | 149/65 | 249/05 |
| 7 | Galtera 1 | 52 | 298/02 | 024/76 | 202/15 | 113/05 | 010/70 | 205/19 |
| 8 | Galtera 2 | 41 | 306/04 | 062/86 | 035/00 | 292/02 | 175/86 | 022/04 |
| 9 | Galtera 3 | 116 | 148/02 | 055/74 | 242/15 | 319/07 | 072/73 | 227/15 |
| 10 | Niederscherli | 22 | 153/14 | 344/73 | 247/02 | 164/08 | 003/81 | 254/03 |
| 11 | Albigen | 12 | 155/02 | 218/87 | 066/04 | 140/03 | 341/87 | 230/01 |
| 12 | Sodbach | 11 | 345/05 | 241/81 | 254/09 | 350/00 | 080/73 | 260/17 |
| 13 | La Lance fault (Jura) | 27 | 147/05 | 235/79 | 044/05 | 335/01 | 068/74 | 245/16 |
| 14 | La Lance fault (Molasse) | 23 | 341/17 | 170/78 | 254/02 | 346/17 | 158/73 | 256/02 |
| 15 | L' Arbogne | 13 | 323/13 | 182/77 | 057/05 | 316/10 | 106/78 | 225/06 |
| 16 | Corserrey | 10 | 135/07 | 257/87 | 045/00 | 150/08 | 315/82 | 060/02 |
| 17 | Lovatens | 12 | 327/04 | 097/85 | 237/04 | 321/03 | 108/86 | 231/02 |
| 18 | West of Lucens | 12 | 335/07 | 127/86 | 244/04 | 335/09 | 122/79 | 244/06 |
| 19 | Moudon | 34 | 325/06 | 184/86 | 052/02 | 320/04 | 221/64 | 052/26 |
| 20 | Seigneux | 50 | 335/00 | 225/85 | 065/02 | 144/00 | 034/89 | 234/01 |
| 21 | La Trémeule | 22 | 323/13 | 212/84 | 234/05 | 329/18 | 166/72 | 061/05 |
| 22 | Villarzel | 18 | 326/01 | 056/83 | 235/10 | 323/02 | 058/74 | 232/15 |
| 23 | Trey | 12 | 329/25 | 159/69 | 247/05 | 320/16 | 107/71 | 227/10 |
| 24 | Chénens | 58 | 142/01 | 272/85 | 055/05 | 149/00 | 243/86 | 059/04 |
| 25 | Matran | 29 | 336/15 | 135/77 | 064/00 | 341/07 | 211/79 | 072/08 |
| 26 | Onnens | 14 | 324/08 | 218/84 | 054/03 | 338/11 | 086/57 | 242/30 |
| 27 | Cottens | 11 | 166/05 | 306/82 | 074/05 | 341/05 | 086/72 | 250/17 |
| 28 | Neyruz | 44 | 335/05 | 090/85 | 244/04 | 326/07 | 114/81 | 235/04 |
| 29 | Autigny | 42 | 336/06 | 105/83 | 246/05 | 340/08 | 122/80 | 249/06 |
| 30 | Fromattbach | 37 | 326/03 | 111/81 | 235/02 | 334/03 | 141/86 | 244/01 |
| 31 | Rüdigraben | 14 | 330/24 | 163/68 | 062/06 | 326/18 | 174/70 | 059/09 |
| 32 | Montécu | 23 | 359/17 | 151/65 | 264/05 | 356/13 | 216/76 | 089/11 |
| 33 | Rossens 1 | 45 | 343/70 | 137/19 | 053/06 | 356/47 | 097/10 | 196/41 |
| 34 | Rossens 2 | 67 | 329/22 | 163/67 | 061/07 | 327/13 | 184/73 | 059/10 |
| 35 | Le Châtelard 1 | 34 | 145/01 | 015/88 | 234/01 | 322/01 | 086/88 | 232/01 |
| 36 | Le Châtelard 2 | 87 | 329/13 | 146/76 | 242/02 | 336/10 | 148/80 | 245/01 |
| 37 | Le Châtelard 3 | 15 | 305/04 | 204/81 | 040/13 | 126/05 | 334/84 | 217/13 |
| 38 | Le Fochaux | 27 | 329/09 | 128/79 | 240/02 | 335/05 | 098/80 | 244/08 |
| 39 | Vauderens | 23 | 329/12 | 132/79 | 240/05 | 328/13 | 107/74 | 235/10 |
| 40 | Ecublens | 36 | 328/08 | 121/81 | 239/06 | 327/05 | 095/82 | 237/06 |

Table 4.2: Paleostress axes derived from the PT-axes method and from the right dihedra method (RDM) for slickenside data sets from different localities in the Plateau Molasse. Lower hemisphere stereo plots and localities of the data sets are given in figures 4.15, 4.16 and appendix 4.2. For stereo plots of the axes see figure 4.17.

minor maxima as well (figures 4.19, 4.20). The N-S and NW-SE striking unspecified fractures most likely represent slickenside planes whose lineations were erased by alteration processes (figure 4.20). In contrast, the WSW-ENE and the NNW-SSE orientations significantly differ from the orientation distributions of both slickensides and brittle deformation bands. The former group was recorded as open fractures in open fracture type fault zones (figure 4.20). The latter group is oriented subparallel to the subhorizontal σ_1 axis resulting from the paleostress analysis of slickensides and brittle deformation bands. This implies that they formed as mode-I cracks, i.e. by extension perpendicular to compression and without shear deformation (figure 4.20). The maximum distribution of all fractures (figure 4.20) shows a regular fanning around the mode-I fracture orientation. This indicates a gen-

eral smooth transition between mode-I and mode-II fractures, which is characteristic for near surface deformation.

4.6.4 Solution pits in conglomerate pebbles

More than 700 orientations of solution pits axes in pebbles were measured in the conglomerates of the Belpberg Beds in five localities (figure 4.21).

The inclination of the solution pit axes is subhorizontal. A closer look at the different localities reveals that the majority are inclined 10° - 20° to the south. Exceptions are the Guggisberg locality where the axes are inclined 10° - 20° towards north,

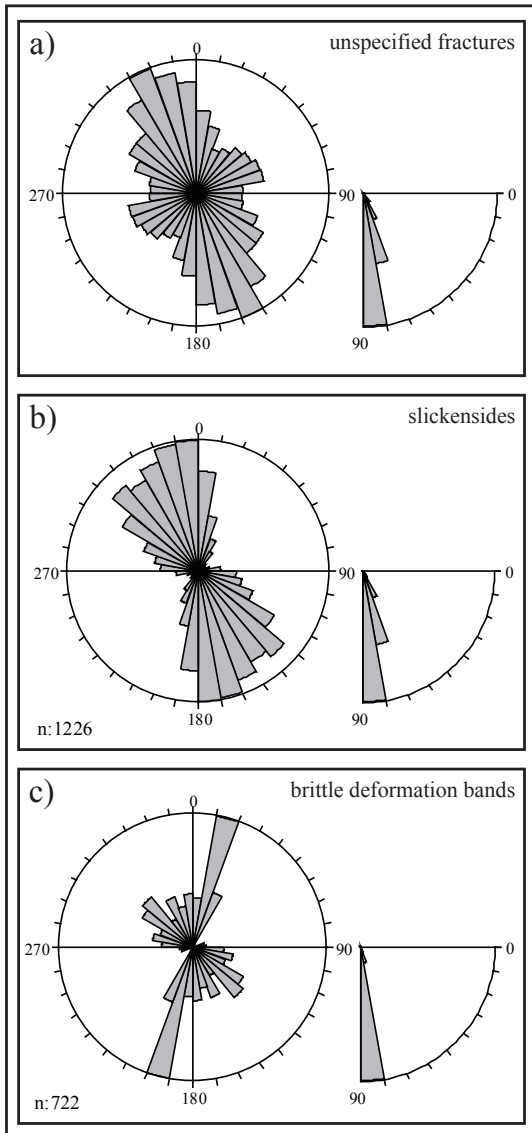


Figure 4.19: Rose diagrams of all planar tectonic structures a) unspecified fractures, b) slickensides, c) brittle deformation bands). Strike of unspecified fractures is dominantly NNW-SSE and secondarily N-S, NW-SE and WSW-ENE. Strike of slickensides and brittle deformation bands is dominantly N-S as well as NW-SE. The brittle deformation bands and the slickensides reflect sets of N-S striking left-lateral shears and NW-SE striking right-lateral shears with a slight majority of left-lateral shears. The maximum of unspecified fractures strikes NNW-SSE, which is subparallel to the σ_1 derived from the slickensides and deformation bands. Their majority may therefore represent mode 1 cracks; however a considerable number striking N-S and NW-SE most likely represents shear fractures where sense of movement could not be recorded. The WSW-ENE maximum of unspecified fractures corresponds to fractures recorded in open fracture type fault zones. See also figure 4.20.

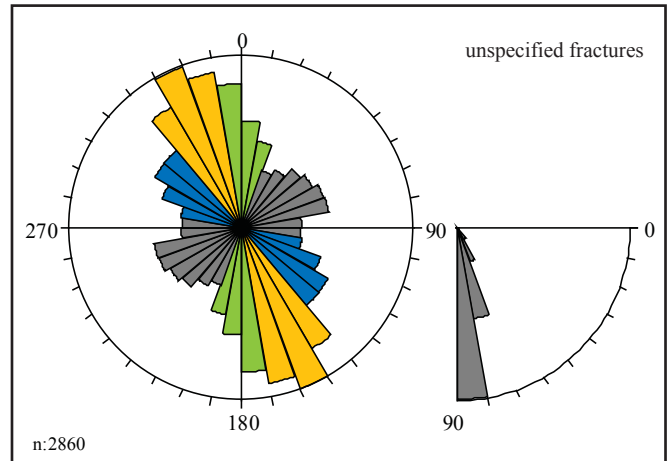


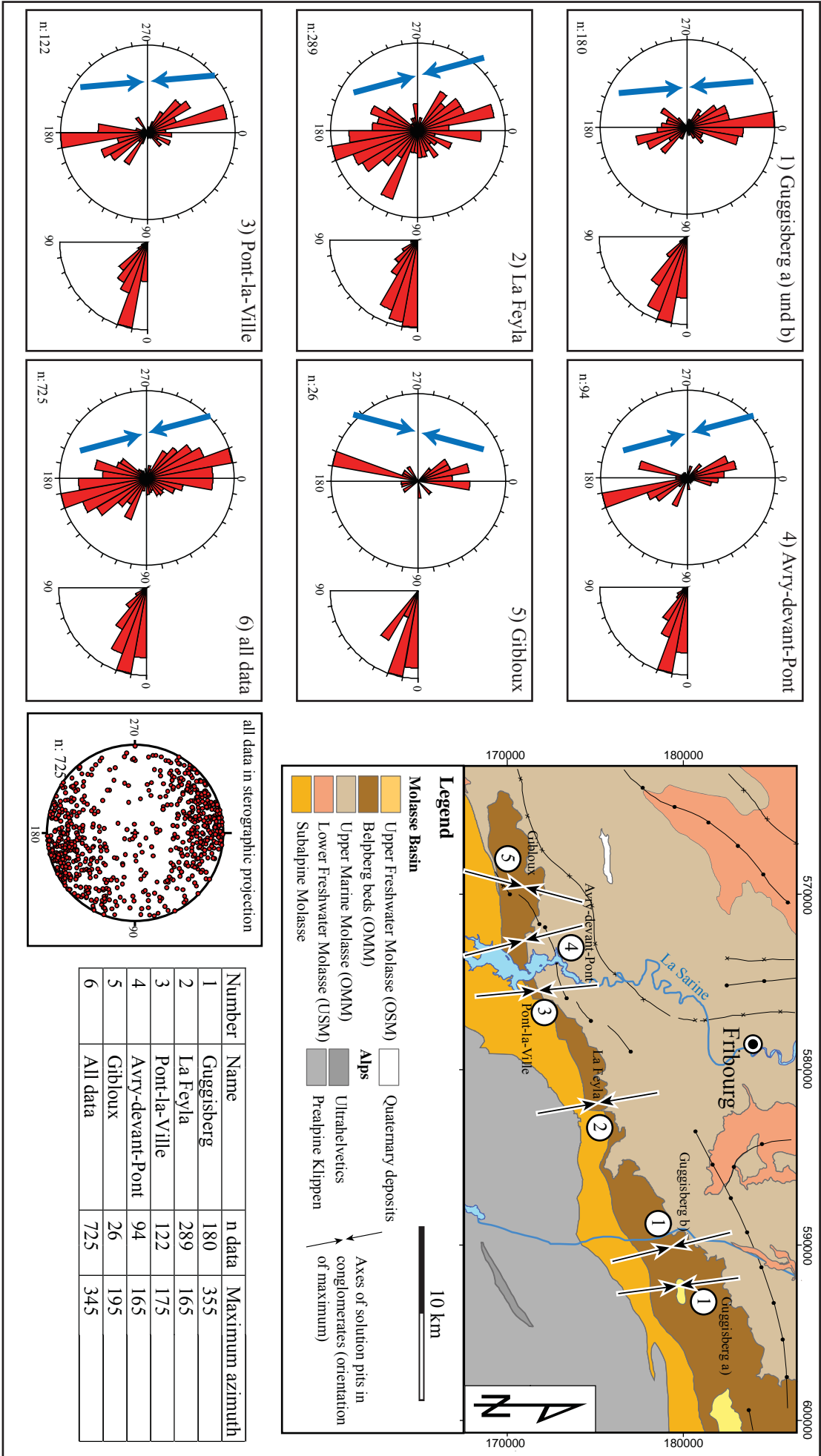
Figure 4.20: Rose diagram of unspecified fractures, colour-coded according to their probable origin. Yellow = mode 1 cracks (joints), green = left-lateral sheared fractures, blue = right-lateral sheared fractures, grey = open fracture type faults. Inclination diagram shows all fractures in grey.

and the La Feyla locality were they additionally occur in a subhorizontal orientation (figure 4.21). There were almost no subvertical axes found. The orientation of solution pit azimuth is relatively uniform N-S to NNW-SSE. They scatter only in the case of the La Feyla locality, which also exhibit a considerable number of NW-SE striking axes.

The axes' subhorizontal orientation indicates them to be derived from tectonic and not from burial stresses. The strike of the pressure solution axes deviates $10^\circ - 20^\circ$ towards west from the N-S direction. This direction is thought to represent paleostress and differs $20^\circ - 30^\circ$ from the NNW-SSE compression axes derived from slickensides and brittle deformation bands. Furthermore there is an important difference regarding the deformation mechanism: while slickensides and brittle deformation bands are the result of localised shear strain, pressure solution pits represent homogeneous bulk rock deformation at a general low strain rate.

The $10^\circ - 20^\circ$ inclination towards south corresponds to a general $10^\circ - 20^\circ$ south-east dip of bedding in the Plateau Molasse in proximity to the thrust Subalpine Molasse, which is where all the localities of solution pit measurements are located. Therefore

Figure 4.21: Unipolar rose diagrams to illustrate the orientation distribution of axes of pressure solution pits in the conglomerates of the Belpberg beds. Blue arrows indicate the inferred orientation of σ_1 corresponding to the maximum orientation of pit axes. The stereographic projection gives all pit axes. The map gives the location of the data sets. The table summarises the data and the maximum orientation of pit axes as azimuth. Note that the inclination of most axes is sub-horizontal. Compression is roughly N-S for every data set. Numbers in each sub-figure refer to similar data sets.



solution pit formation predates the tilt of bedding, i.e. folding in the region.

The absence of vertical pressure solution implies that (horizontal) tectonic stresses dominate overburden stresses. Vertical pressure solution is thought to take place at depths from 400 m onward (Ruano & Galindo-Zaldivar 2004), which was significantly exceeded in the region (Schegg et al. 1997, Schegg & Leu 1998, Mazurek et al. 2006, Cederbom et al. 2004). This means that the measured solution pits in the study area are either older than this burial or that horizontal tectonic stresses exceeded burial stresses at any time. Most of the solution pits seems to be older than the tilt of the Plateau Molasse near the thrust of the Subalpine Molasse, which is revealed by a tilt of the measured axes. If pressure solution stopped, prob-

ably due to strong cementation, before burial exceeded the critical depth, than the recorded stress field would correspond to a short period post-dating sedimentation and pre-dating burial deeper than 400 - 500 m.

4.6.5 Slickensides in the Subalpine Molasse

Slickenside populations were mapped in the narrow band of the thrust Subalpine Molasse at the southern border of the study area. Mapping was not as complete as in the Plateau Molasse and selection of outcrops focused on the transition between Subalpine Molasse and Plateau Molasse. (For more detailed investigation of the Subalpine Molasse and the southerly

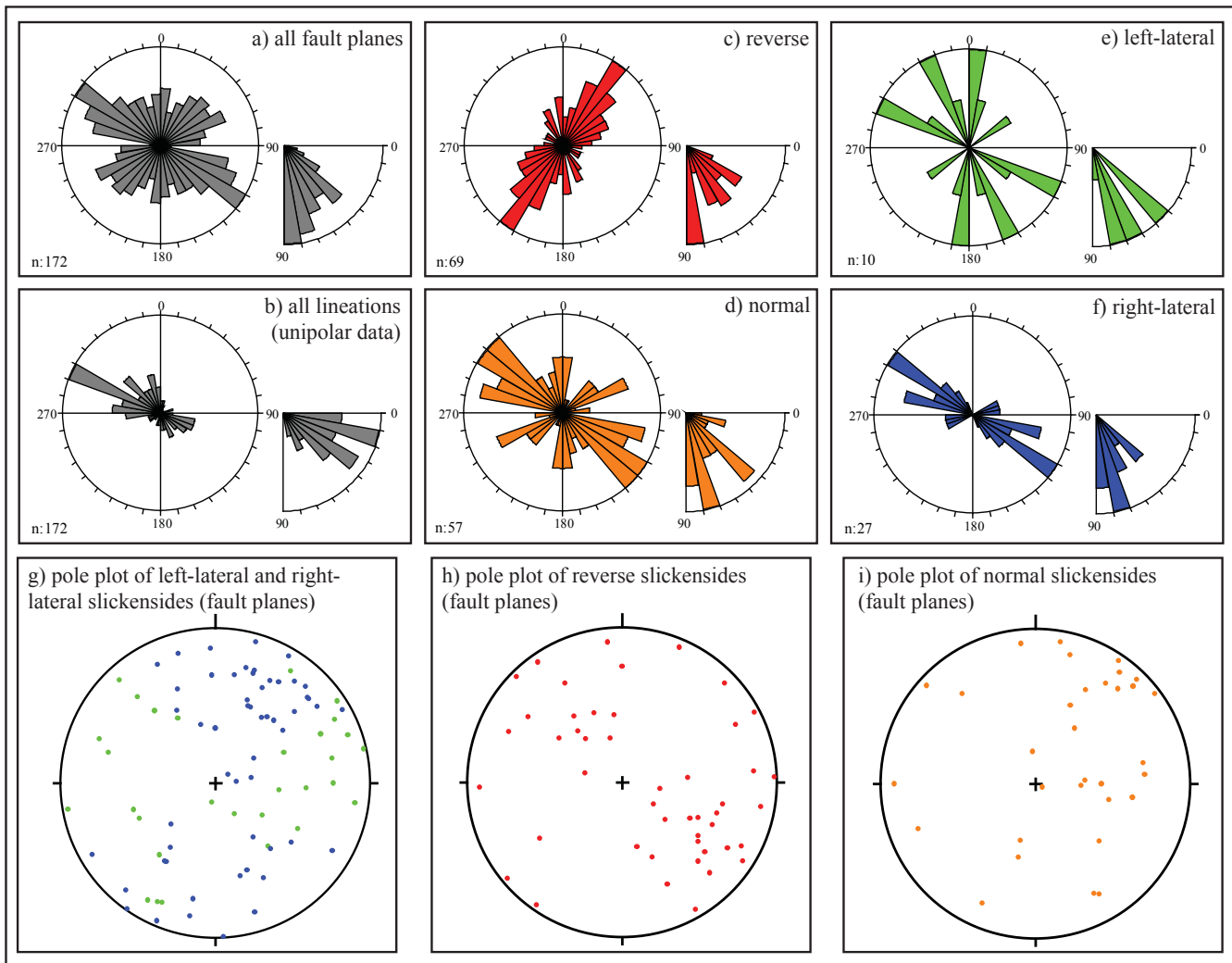


Figure 4.22: Rose diagrams and pole plots to illustrate the strike distribution of slickensides from the Subalpine Molasse. a) All planes, b) all lineations, c) all slickensides with reverse sense, d) with normal sense, e) with left-lateral sense and f) with right-lateral sense. g) to i) Pole plots of slickenside fault planes (same colour code as for the rose diagrams): g) left-lateral and right-lateral slickensides, h) reverse slickensides, i) normal slickensides. Note that reverse and right-lateral slickensides strike according to NW-SE compression and NNW-SSE compression respectively, while normal and left-lateral slickensides partly deviate from such orientations. For nine data sets no sense of movement could be determined. These data sets are included in diagrams a) and b) only.

adjacent Prealpine nappes see Matzenauer in prep.)

More than 170 slickensides were collected from seven localities in the Subalpine Molasse (figures 4.15, 4.22, 4.24) of the study area. The inclination of the fault planes is steep to moderately inclined, but rarely subhorizontal. Sixty-nine slickensides show reverse, fifty-seven normal, twenty-seven right-lateral and ten left-lateral sense of movement. Reverse slickensides generally strike SW-NE with a minor maximum at N-S, normal slickensides strike NW-SE with minor maxima at N-S and WSW-ESE, right-lateral slickensides strike NW-SE with a minor maximum at WNW-ESE, and left-lateral slickensides scatter widely (figure 4.22).

The data sets from the seven localities (figure 4.24) can be assigned to three different deformation systems:

1) Combined thrust/strike-slip faulting. At the La Roche Monsofloz locality (site 4, $n=66$) NE-SW striking reverse, N-S striking left-lateral, NW-SE striking right-lateral and N-S, NW-SE and NE-SW striking normal sense slickensides were measured that altogether fit a combined thrust/strike-slip regime. Similar constellations are developed at Oron (site 7, $n=22$), Plasselb (site 1, $n=5$) and La Roche Medzelennes (site 3, $n=52$).

2) Oblique left-lateral/normal faulting. This cases was mapped at La Roche Le Steckele (site 5, $n=13$) and at Sâles/Gruyère (site 6 $n=5$) with fault planes striking NW-SE in the former and WNW-ESE in the latter case.

3) Normal faulting. Nearly pure normal faulting along N-S striking fault planes was recorded at Montécu La Feyla (site 2, $n=16$).

Although left-lateral slickensides are the most common ones in the Plateau Molasse, they are remarkably rare in the Subalpine Molasse. Instead, N-S striking slickensides are often characterised by oblique slip of both normal (sites 1, 2, 4) and reverse (site 7) sense. The right-lateral oblique systems mapped at sites 5 and 6 represent either left-lateral shear zones extending from the Plateau Molasse into the Subalpine Molasse, or incomplete data sets of the reverse/strike-slip system described above.

While the strike of all slickensides with reverse kinematics is clearly NE-SW, representing SE to NW thrusting, the strike of all normal slickensides shows a division into three different maxima. The WSW-ESE maximum represents SE-dipping normal faults, likely formed as antithetic Riedel shears with respect to overall NW-directed thrust kinematics, while the WNW-ESE maximum and the N-S maximum most likely represent right-lateral and left-lateral oblique slip planes. The latter maximum also contains oblique reverse slickensides, which likely represent a few left-lateral slickensides with a pronounced reverse component.

Paleostress was determined for all seven localities by the PT axes method and by the right dihedral method (table 4.3, figure 4.23). The results for the axes of maximum compression (P-axes/ σ_1 -axes) vary in azimuth by more than 10° in one case only. For the axes of least compression (T-axes/ σ_3 -axes) the variation is more than 10° in three cases and more than

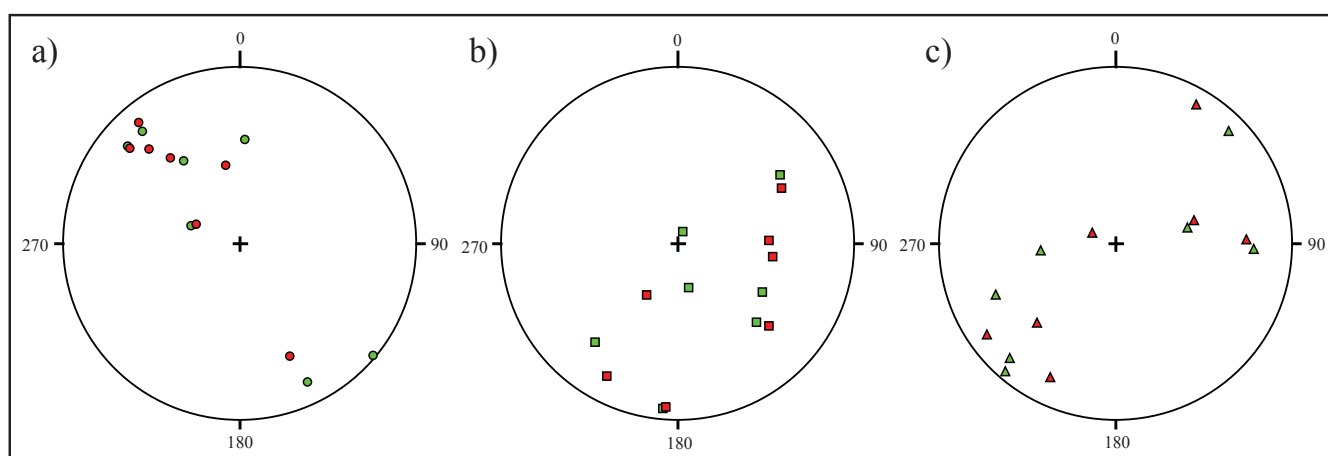


Figure 4.23: Comparison of results derived from the PT axes method (red) with results derived from the RDM (green) for the slickenside datasets from the Subalpine Molasse. a) P-axes/ σ_1 (RDM), b) B-axes/ σ_2 (RDM), c) T-axes/ σ_3 (RDM). Compare with table 4.3 for values. The results generally accord with NW-SE compression and NE-SW extension. The scatter of the axes is due to the fluctuation of the tectonic regime between thrusting, strike-slip and extension.

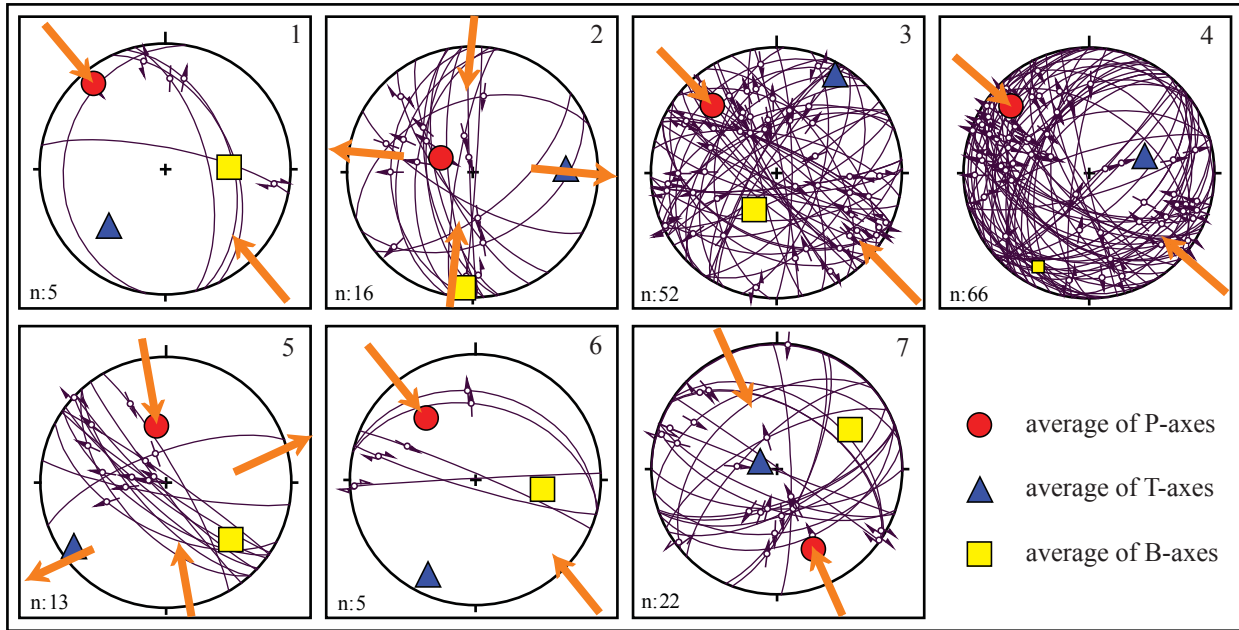


Figure 4.24: Lower hemisphere plots for slickenside fault planes from the Subalpine Molasse. Compare number in the upper right corner with figure 4.15 and table 4.3 for location of the data sets. Number of data per plot is given in the lower left corner. With exception of plots 2 and 5 arrows indicate the direction of σ_1 determined by the P-T-axis method. Plot 2 shows extension and plot 5 oblique extension. In plot two arrows are given for σ_2 and σ_3 and in plots five for σ_1 and σ_3 . Results of the RDM see table 4.3. See also A 4.3 in the appendix.

| Site | Name | n data | PT axes method | | | Right dihedral method | | |
|------|----------------------|--------|----------------|--------|--------|-----------------------|------------|------------|
| | | | P-axes | B-axes | T-axes | σ_1 | σ_2 | σ_3 |
| 1 | Plasselb | 5 | 320/12 | 088/47 | 225/37 | 130/02 | 024/84 | 221/05 |
| 2 | Montécu | 16 | 294/68 | 184/08 | 088/27 | 290/66 | 185/07 | 092/23 |
| 3 | La Roche Medzeiennes | 52 | 316/27 | 211/62 | 030/10 | 311/17 | 166/69 | 045/11 |
| 4 | La Roche Monsofloz | 66 | 311/19 | 208/16 | 073/52 | 319/17 | 220/28 | 077/56 |
| 5 | La Roche Le Steckele | 13 | 350/53 | 132/31 | 235/12 | 003/41 | 135/37 | 247/27 |
| 6 | Sâles/Gruyère | 5 | 321/38 | 098/45 | 206/17 | 326/43 | 120/44 | 223/13 |
| 7 | Oron | 22 | 156/31 | 062/34 | 295/78 | 154/14 | 056/31 | 265/55 |

Table 4.3: Paleostress axes derived from the PT axes method and from the right dihedral method for slickenside data sets from different localities in the Subalpine Molasse. Lower hemisphere stereo plots and localities of data sets are given in figures 4.42, appendix 4.3 and 4.15. For stereo plot of the axes see figure 4.23.

15° in two cases. The two methods are therefore considered to deliver consistent results (figure 4.23). The azimuth of P-axes range between 294° (114°, site 2) and 350° (170°, site 5), the corresponding inclination lies between 12° (site 5) and 68° (site 2). The average in azimuth is 321° (141°).

In the four cases of combined thrust and strike-slip (sites 1, 3, 4, 7) the P-Axes are oriented NW-SE and NNW-SSE in case of site 7. In cases of sites 2, 5 and 6 the P-axes are more steeply inclined due to a pronounced normal component of the mapped slickensides. The subhorizontal T-axes of these localities strike SW-NE (site 5), SSW-NNE (site 6) and E-W (site 2), which is roughly the same orientation either of the T-axes in a NW-SE compressive strike slip system or the B-axes in a thrusting regime of this orientation.

The slickenside data from the Subalpine Molasse shows a combined thrust/strike-slip regime characterised by reverse shear and minor antithetic normal shear along SW-NE striking fault planes as well as oblique right-lateral and left-lateral shear along NW-SE and N-S striking fault planes respectively. In some cases oblique slip with right-lateral/normal shear sense is predominant. The determined paleostress reveals an overall NW-SE compression.

4.7 DEFORMATION CHARACTERISTICS

Brittle deformation bands, slickensides and unspecified fractures are common structures in the sandstones and clayey sandstones of the study area, typically indicating an altogether brittle deformation mechanism. The deformation bands are typical struc-

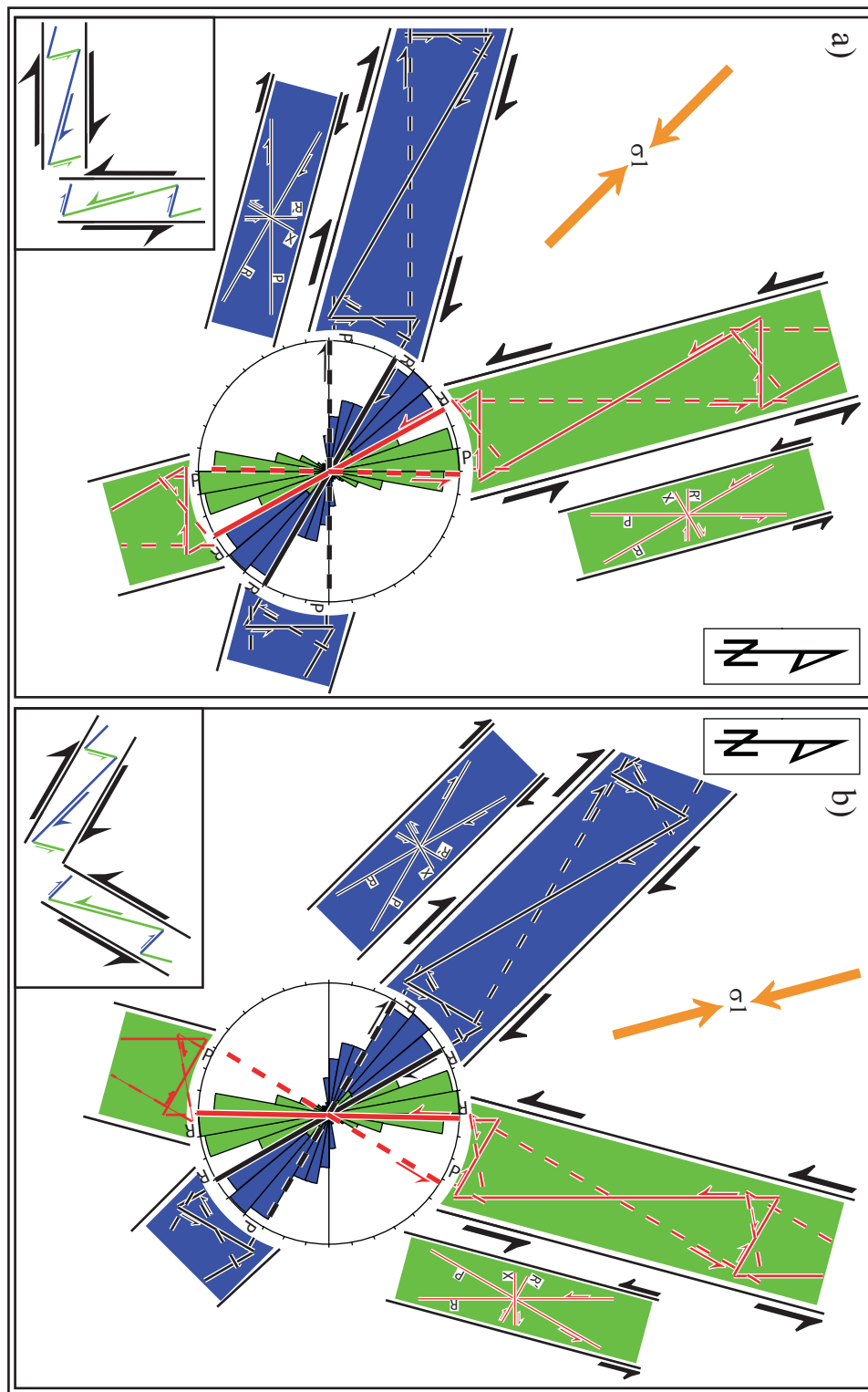


Figure 4.25: Interpretation of the slickensides from the Plateau Molasse as shears of a Riedel system. Rose diagram shows strike of right-lateral slickensides in blue and of left-lateral ones in green. The maxima are likely composed of synthetic R-shears and antithetic R'-shears of a superordinate left-lateral or right-lateral shear zone. These maxima scatter across a range of about 30°, representing local differences in the stress field and according fault plane orientations within the study area. a) and b) represent the two extremities of this 30° range. The shear zones are represented by the medium scale faults mapped in the field. Insets show how the medium-scale faults might be arranged in the frame of a larger shear zone.

tures to develop in porous, poorly lithified sandstone (Aydin 1978, Fossen et al. 2007) such as the Molasse sandstones. They develop a micro-fault gouge that evolves to macroscopic gouges and to slickensides as strain increases (see chapter 2). Most slickensides are characterised by striated gouges, while other types are represented by mirror-like fault planes, grooves and very rarely calcite seams. Especially the rarity of the latter underlines the “very” brittle character of deformation.

The orientations and kinematics of both brittle deformation bands and slickensides indicate a strike-slip regime with N-S striking left-lateral shears and NW-SE striking right-lateral shears (figures 4.9, 4.12, 4.13, 4.14). This indicates a subhorizontal, NNW-SSE-oriented σ_1 and a WSW-ENE-oriented σ_3 of paleostress (figures 4.17, 4.18). Overprinting relationships of two structures are rare and the few mapped occurrences show no systematic pattern (appendix 4.1). This implies that activity along the faults of different orientation was contemporaneous. Fault plane patterns from individual outcrops often show sets of synthetic and antithetic shears typical of Riedel systems (figure 4.25). The existence of a Riedel-type faulting mechanism is further supported by the fact that the conjugate right-lateral and left-lateral sets of fault planes range over 30° , including all synthetic shears (R, P and Y, figures 4.5, 4.25). Assuming that most of the measured slickensides represent synthetic R-shears, the superordinate shear zones should be rotated 15° with respect to the estimated orientation maxima. For the two measured maxima of right-lateral NW-SE striking and left-lateral N-S striking fault planes, this means that their corresponding Riedel shear zones strike 15° more towards WNW-ESE and NNE-SSW respectively. The 30° wide scatter among maxima are therefore influenced rather by local fluctuations of the stress field and the according fault plane orientations than due to the derivation from different Riedel shears (figure 4.25). The two conjugate Riedel systems allow all mapped fault plane orientations to act simultaneous.

4.8 OUTCROP CONDITIONS AND DISTRIBUTION OF DEFORMATION

Field observations were collected along mapping lines dictated by the natural occurrence of outcrops (e.g. figure 4.8) along deeply enough incised rivers as well as by the lithology. Sandstones and clayey sands are more resistant to erosion and therefore more likely to form outcrops than shales. An evenly spread

mapping grid could therefore not be achieved. Despite this, two important points regarding the distribution of deformation could be made:

- 1) Tectonic structures are not uniformly distributed. Undeformed areas exist in alternation with strongly deformed areas where structures frequently define fault zones.
- 2) Although rarely forming outcrops, shale layers are characterised by their obvious lack of signs of deformation.

4.9 THE FAULT ZONE NETWORK

Four different types of fault zones were distinguished in the field. The palygorskite type and the dense fracture type fault zones are quite similar in character and dominate the deformation in the study area (figure 4.7). The clayey cataclasite type faults seem to be restricted to rare larger fault zones and the open fracture type faults seem to represent a special type of deformation. Fault size was characterised by fault zone width since criteria of total offset are generally missing due to limited outcrop size.

In practice, none of the mapped faults were found to reoccur exactly along-strike on another mapping line, which means that even the larger faults hardly exceed 1 – 3 km in length. Another important point which probably limits the fault length is the mechanical difference between sandstones and interbedded shale. The absence of discrete structures in the shale may indicate that here deformation is accommodated by whole-rock plastic shear, translating strain from one fault zone to another. This mechanical layering is further complicated in the USM where the meandering river system sedimentary environment (Platt & Keller 1992) is characterised by lateral changes between sands and shale. The deformation of the Tertiary Molasse is therefore most likely distributed on a complicate network of small- to medium-scale faults rather than on fewer, large, continuous faults. Strain is partitioned between these faults or translated from one fault to another. The latter may exhibit a different orientation.

It can, however, be speculated that certain fault zones extend for about 10 km or more, especially in the OMM where lithologies are laterally more homogeneous. Such kilometre-scale faults are known from the Jura Mountains (Vuache fault, Pontarlier fault, Chamblon fault, La Lance fault), some of which

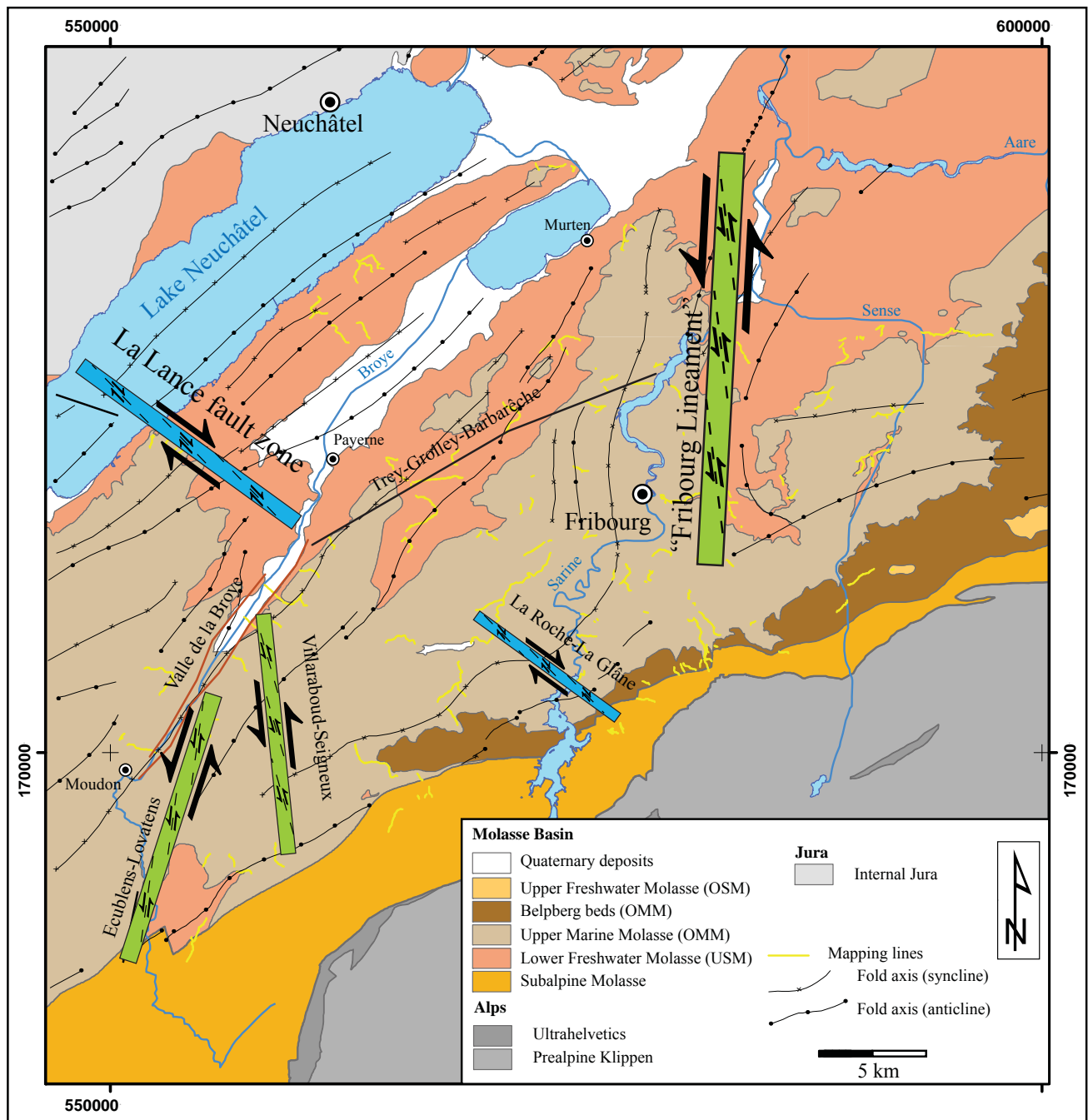


Figure 4.26: Location of interpreted larger fault zones in the study area. The zones of Ecublens-Lovatens, Villarboud-Seigneux and La Roche-La Glâne were interpreted by connecting two or more outcrops of fault zones with identical senses of movement and strike distributions quite similar to the strike of the zone. The zone of Trey-Grolley-Barbarèche was interpreted by connecting three outcrops of open fracture type fault zones without senses of movement but with strike distributions quite similar to the strike of the zone. The La Lance fault and the “Fribourg Lineament” are known from the literature and are interpreted according to morphology (La Lance fault) and to a single fault zone outcrop (“Fribourg Lineament”).

are known to extend into the Molasse. Other fault zones of similar size, but with different characteristics, are likely to exist in the Molasse as well. Some authors previously postulated such faults without clear proof (Kastrup et al 2007, Chenevart 1978, Plancherel 1979). We are theoretically able to connect distinct, strongly deformed zones of similar orientation and kinematics over about 10 km in length, but their actual connectivity still remains uncertain.

It has been possible to construct three such fault zones in the study area by connecting two or more localities of slickenside measurements in fault zone outcrops (figure 4.26). The two or more slickenside populations brought together by such a construction show the same fault zone orientation and kinematics and are all along-strike of this orientation. From west to east three large fault zones can thus be proposed (figure 4.26):

- 1) A left-lateral NNE-SSW striking zone between Ecublens and Lovates
- 2) A left-lateral NNW-SSE striking zone between Vil-laraboud and Seigneux
- 3) A right-lateral NW-SE striking zone between La Glâne near Posat, the dam of Rossens and Le Steckele near La Roche.

Additionally, four fault alignments seem to form large fault zones (figure 4.26) and are only partly based on our mapping results. Additional criteria are postulates in the literature or geomorphologic evidence.

1.) The trace of the proposed Fribourg zone (also “Fribourg lineament” Kastrup et al. 2007) should intersect the mapping line along the Galterengraben south of Tavers. A fault was mapped there with roughly the same orientation and kinematics as the focal mechanisms of the earthquakes defining the lineament. However, no other outcrop could be mapped along-strike of the Fribourg zone.

2) The La Lance fault is well-known from the Jura Mountains (Bertschy 1958, Meia 1966), where it offsets the folded Mesozoic strata by up to four kilometres. It was further described to cross Lake Neuchâtel and continue into the Plateau Molasse (Gorin et al. 2003, Weidmann 2006). The exact trace of the La Lance fault on the eastern side of Lake Neuchâtel could only be approximated according to geomorphologic indicators, while the populations of secondary fault planes are quite similar on either side of the lake. The geomorphic signatures vanish at the river La Broye near Payerne where the La Lance fault is thought to terminate.

3) Straight footslopes along the Vallée de La Broye between Payerne and Lucens probably indicate a NNE-SSW striking fault zone running along the valley. A couple of smaller faults were mapped east of the valley that are oriented N-S and NNE-SSW and show a left-lateral sense of movement. Their orientation is synthetic as well as parallel with respect to the proposed fault zone running along the valley, which therefore may feature a left-lateral sense of movement as well. The valley morphology as a whole, however, rather implies a graben structure, i.e. normal fault kinematics.

4) The WSW-ENE striking zone of Trey-Grolley-Barbarèche is marked by three outcrops with occurrences

of open fracture type fault zones. Most likely these structures are extensional opening fractures located in the hinge zones of folds or flexure zones. This assumption is supported by their orientation with respect to the stress field and by the lack of any obvious sense of movement. The comparison with the regional fold axes, however, shows that they strike obliquely with respect to the zone of Trey-Grolley-Barbarèche. Determining the origin of the structure would require additional work which is beyond the scope of this study.

The constructed fault zones (figure 4.26) would have roughly the same extent, orientation and kinematics as the strike-slip faults known from the Jura Mountains. As both regions belong to the foreland fold and thrust belt, i.e. to the same tectonic unit, they may both contain the same structural inventory. The pronounced difference in magnitude of folding does not necessarily mean that the same applies for the extent of strike-slip faulting. The difference in lithology, however, could influence faulting in such a way that it is dispersed to wider zones in the Molasse than in the Jura Mountains. The existence of the constructed fault zones is not unambiguously evidenced by the field data, but it represents a plausible characterisation of the nature of faulting in the study area.

4.10 THE TRANSITION ZONE BETWEEN PLATEAU MOLASSE AND SUBALPINE MOLASSE

The Subalpine Molasse is a narrow band of strongly imbricated Molasse units situated between the Plateau Molasse and the Prealps Klippen. It was partly investigated during this study in order to better understand the transition towards the Plateau Molasse.

The border between Subalpine Molasse and Plateau Molasse is a thrust that juxtaposes Chattian USM of the Subalpine Molasse onto Burdigalian Belpberg Beds (upper OMM) of the Plateau Molasse. This thrust front runs NE-SW along the southern, respectively eastern edge of the study area. It appears to be more or less continuous in the central part of the study area, while footwall deformation occurs in the northeastern and southwestern parts. This deformation includes folding and thrusting of the southernmost Plateau Molasse and is an indication of foreland-directed propagation of the Subalpine deformation front.

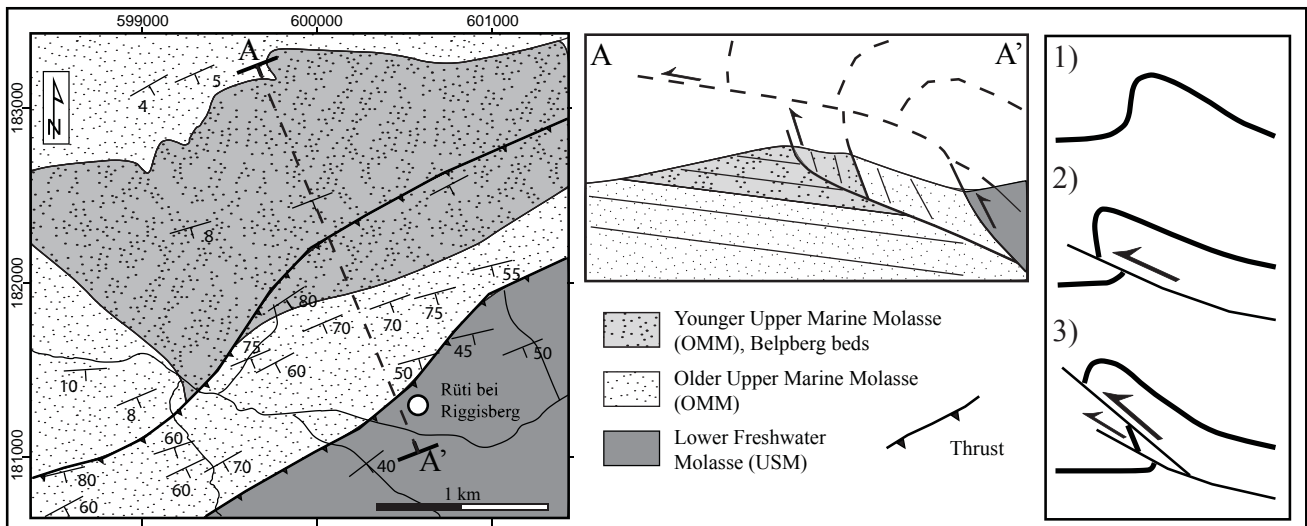


Figure 4.27: Tectonic sketch map of the structures of the Gibelegg imbricate. Lithologies, beddings and thrusts are taken from the Geological Atlas of Switzerland (Rutsch & Frasson 1953, Tercier & Bieri 1961). A schematic cross-section (A-A') and a sketch to illustrate the evolution (1 to 3) is given. The Gibelegg imbricate is located between the Subalpine Molasse and the Plateau Molasse and shows an inverse succession. The sketch illustrates the interpretation of the Gibelegg imbricate as the cut-off reverse limb of a fold structure (Beck 1946, Rutsch 1947). This indicates that the frontal thrust of the Subalpine Molasse developed from folding and limits its offset to a couple of kilometres.

Examples of such footwall deformation can be observed in the northeastern part in form of the Gibelegg imbricate and the Fall anticline. The Gibelegg imbricate (figure 4.27) shows a reverse succession of units and was interpreted as the former sheared forelimb of the Falkenfluh anticline situated further east (Beck 1946, Rutsch 1947). The hangingwall of the Gibelegg imbricate (Seftigswand imbricate) was interpreted as the former backlimb of the Falkenfluh anticline. The hangingwall thrust of the Gibelegg im-

bricate, representing the frontal thrust of the Subalpine Molasse towards the study area, is a break-through thrust of a fold-propagating fault and indicates increasing shortening towards the southwest. The Fall anticline (Schmid 1970, Marescot 2000, figure 4.28) is located in the footwall of this frontal thrust some kilometres further west of the Gibelegg imbricate. It developed with secondary folds showing small-scale thrusting quite similar to the relationship between the Falkenfluh anticline and the Gibelegg imbricate.

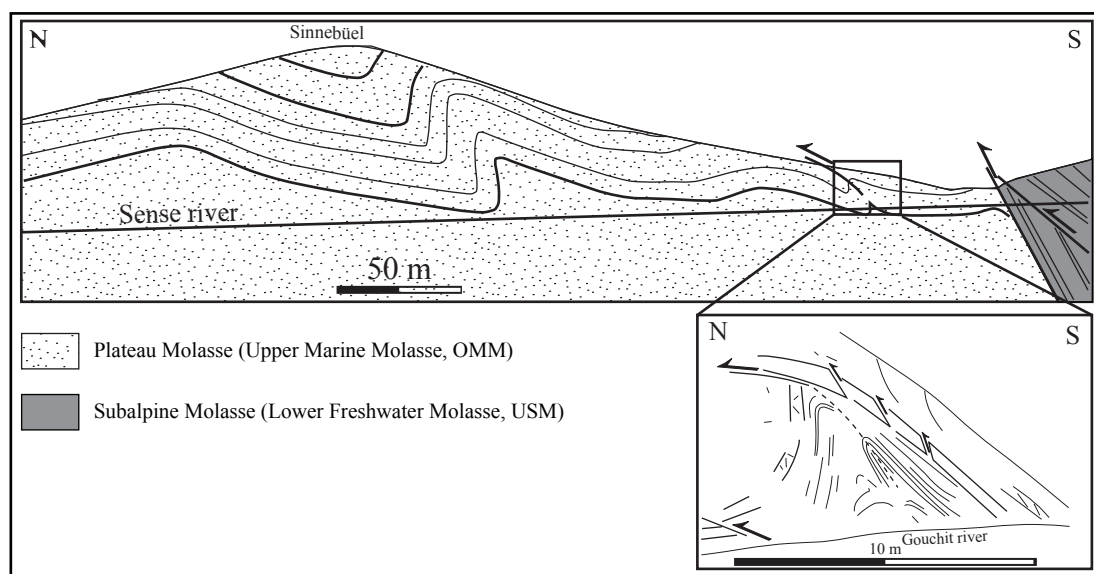


Figure 4.28: Cross-section of the Fall-anticline after Marescot (2000). The fold is developed in clayey strata of the OMM right in front of the frontal thrust of the Subalpine Molasse. The northern limb is steep. Inset shows a field sketch of a smaller fold at the Gouchit River in the back of the Fall anticline. In this smaller fold a competent layer developed thrust horses in the back limb and a thrust in the hinge. Another small thrust is developed in the hinge of the frontal syncline. See figure 4.8 for location.

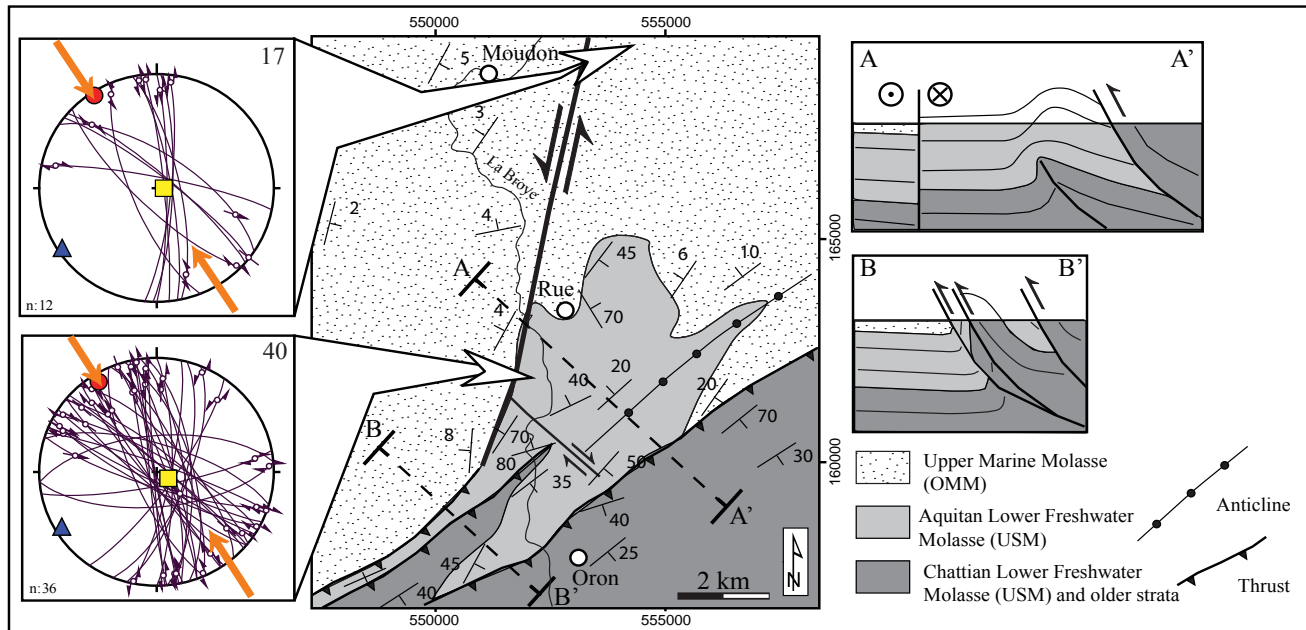


Figure 4.29: Tectonic sketch map of the structures between Oron and Moudon. Lithologies, bedding and thrusts are taken from the Geological Atlas of Switzerland (Gabus et al. 2000). Two schematic cross-sections and stereoplots for two slickenside localities (sites 17, 40) are given. The sketch illustrates how a roughly N-S striking left-lateral fault zone of the Plateau Molasse influences the thrust front of the Subalpine Molasse. East of the fault zone, there is a frontal thrust of the Subalpine Molasse with an anticline in its footwall, developed along strike towards the fault zone. On the western side of the fault zone, the anticline narrows due to space accommodation and develops two thrusts with a normal and a steep to inverse imbricate. The thrust front jumps a few kilometres towards the foreland. left-lateral strike-slip in the Plateau Molasse and reverse faulting at the front of the Subalpine Molasse act contemporaneously. See figure 4.8 for location.

A similar situation occurs in the region of Oron (figure 4.29), where the foot wall of the frontal thrust of the Subalpine Molasse, the “anticlinal principal” (Mornod 1949), narrows along strike towards southwest. Narrowing progressively translates the anticline into two frontal imbricates of the Subalpine Molasse (figure 4.29). The area of transition correlates with the intersection of a roughly N-S striking left-lateral shear zone (zone of Ecublens-Lovatens, see subchapter 4.9) in the Plateau Molasse. This left-lateral shear zone does not clearly affect the main thrust front of the Subalpine Molasse. Instead it forces the anticline to translate into thrust imbricates in order to accommodate the relative southward shift of the western block. In this case the external structures of the Subalpine Molasse act contemporaneously with the strike-slip faults of the Plateau Molasse.

In contrast to such interaction, the frontal thrust of the Subalpine Molasse is probably disrupted in some areas by the strike-slip faults of the Plateau Molasse. The slickenside population measured at Le Steckle, situated immediately above the thrust front, exhibits right-lateral normal kinematics (figure 4.24 site 5). Their NW-SE strike suggests their connection to a left-lateral fault zone in the Plateau Molasse (zone of La Roche - La Glâne, see subchapter 4.9,

figure 4.26). Furthermore, left-lateral offset of the thrust front is based on mapping in the area north of La Roche and near Lausanne (Weidmann et al. 2002, sheet 1205 Rossens, Weidmann 1988, sheet 85 Lausanne). North of La Roche, these left-lateral offsets may be the signature of a fault zone characterising the “Fribourg Lineament”.

The slickenside populations of the studied outcrops in the Subalpine Molasse reveal combined thrust/strike-slip systems and oblique right-lateral/normal systems in two cases (figure 4.24). Both show a NW-SE oriented σ_1 of paleostress which roughly corresponds to the orientation determined for the Plateau Molasse. The overall dominant tectonic regime in the Subalpine Molasse is thrusting and thrust-related faulting.

We observe increasing shortening and foreland directed propagation towards southwest along-strike of the frontal zone of the Subalpine Molasse. The former is indicated by the Falkenfluh – Gibelegg structure and the latter by the structures in the region of Oron. The relationship between the strike-slip fault zones developed in the Plateau Molasse and the frontal thrust zone of the Subalpine Molasse show both crosscutting of the frontal thrust zone by strike-slip as well as contemporaneous interaction of the two. Both

relationships alternate along-strike of the frontal thrust zone.

4.11 TIMING OF DEFORMATION

The Lower Freshwater Molasse and Upper Marine Molasse of the study area were deposited in Aquitanian and Burdigalian times respectively (Trümpy 1980, Homewood et al. 1986, Berger et al. 2005b). The slickenside fault populations studied in these formations show only one phase of strike-slip deformation (e.g. figures 4.16, 4.18, appendix 4.1). The lack of a clear time marker, such as unambiguous deformation of Quaternary strata or deformation-related datable minerals makes timing estimates difficult. The mapped strike-slip tectonics can therefore not be attributed to any time interval more precise than from the middle Miocene to present.

Quaternary movement along the WNW-ESE striking right-lateral La Lance fault (Gorin et al. 2003) as well as focal mechanisms of earthquakes within the “Fribourg zone”, indicating left-lateral movement along N-S striking fault planes (Kastrup et al. 2007), point towards recent activity of the system. The frontal thrust of the Subalpine Molasse was active at least until lower to middle Miocene times (Homewood et al. 1986). There is, however, evidence that at the least internal shortening of the Subalpine Molasse is younger. Shallowly inclined thrusts of Subalpine Molasse as well as Helvetic nappes and Prealpine nappes further south, both cutting steeper imbricates of the Subalpine Molasse, are known from several localities (Trümpy 1980) and imply young, out-of-sequence thrusting. Recent studies of apatite fission track cooling ages revealed vertical movement along thrusts in the Subalpine Molasse of central Switzerland later than 5 Ma (von Hagke et al. 2010). Subsidence/uplift estimations based on clay mineralogy from borehole sections underneath the subalpine Molasse basal thrust indicate that considerable erosion has taken place prior to thrusting (Monnier 1982). If thrusting of the Subalpine Molasse post-dates erosion of the Plateau Molasse, it has to post-date deposition of the Upper Freshwater Molasse plus the time span of erosion as well. In this case thrusting would have to be attributed to the uppermost Miocene to Pliocene.

The Jura Mountains are thought to have formed from the late Miocene onwards (Laubscher 1961, 1972, 1987, Naef et al. 1985, Burkhard 1990). Shortening of the fold belt by both thick-skinned reverse faulting and thin-skinned folding was active in

the frontal parts until the Quaternary (Ustaszewski & Schmid 2007, Madritsch et al. 2008, 2010).

According to the strike of their map-scale structures both the Subalpine Molasse and the Jura Mountains formed by NW-SE to NNW-SSE-directed compression similar to the compression direction derived from the paleostress analysis in the Plateau Molasse. Therefore the Subalpine Molasse - Plateau Molasse - Jura Mountains system could have been deformed progressively and is still active today.

Burkhard (1990) proposed the formation of the Jura Mountain and the Subalpine Molasse to be the foreland response to the exhumation of the external crystalline massifs, i.e. the same tectonic event in the orogenic hinterland. Together they accommodate an equivalent amount of shortening, with varying respective intensities along-strike. At the scale of the study area, this implies that Jura Mountain formation immediately follows major shortening in the Subalpine Molasse at the same time as the décollement in Triassic evaporites developed. This would incorporate the Plateau Molasse into the deformed orogenic wedge at the same time as the Jura formation.

Lacking clear time markers, one could further speculate about the order of deformation of the Subalpine Molasse and the Plateau Molasse - Jura Mountains system, i.e. the relative age of strike-slip faulting with respect to thrusting near the transition of both units. On the scale of the study area, the deformation front of the thrusts Subalpine Molasse propagates into the foreland towards southwest. In places this propagation is accompanied by interaction with strike-slip fault zones in the Plateau Molasse (figure 4.29). However, in other places cutting of the thrust front by strike-slip is evident, indicating strike-slip to be younger. At this point it remains speculative whether the strike-slip fault zones interacting with the frontal thrust are older than other strike-slip zones cutting it or whether the frontal thrust became partly reactivated.

Prominent strike-slip faults in the Jura Mountains such as the La Lance fault (Bertschy 1958, Meia 1966) in the western part of the study area offset folded Mesozoic strata and hence post-date folding. In contrast, the still active Vuache fault, another prominent strike-slip fault, was shown to bend into a thrust at the frontal parts of the Jura Mountains (Charollais et al. 1983, Blondel et al. 1988, Sambeth & Pavoni 1988). Sommaruga (1997) argued these faults to represent tear faults active both syn-folding and post-folding. The strike-slip faults of the Jura Mountains extend

into the Molasse Basin, indicating the same tectonic system (Muralt et al. 1997, Jordi 1990, Jordi 1951). Recent reverse faulting in the frontal parts of the Jura Mountains also becomes evident from field studies and seismicity in the regions between Besançon and Basel (Madritsch et al 2008, Ustaszewski & Schmid 2007). In contrast to the thin-skinned décollement tectonics leading to the Jura Mountains formation, this young activity could be attributed to thick-skinned re-activation of steep basement faults.

A considerable amount of shortening within the Subalpine Molasse of western Switzerland likely pre-dates décollement tectonics leading to the folding of the Plateau Molasse and the Jura Mountains. The significant difference in fold amplitudes between the Plateau Molasse and the Jura Mountains was attributed to differential overburden situated above the basal décollement, exceeding a critical value in the southern part of the triangle shaped former foreland basin (Sommaruga 1997, Burkhard & Sommaruga 1998). However, erosion after 5 Ma (Schegg & Leu 1998, Cederbom 2004) clearly post-dates décollement tectonics and removed some of this overburden, allowing folding. This implies that the folds in the Plateau Molasse are younger than those in the Jura Mountain (Sommaruga 1997). According to their low amplitude, these folds are either very young or indicate that folding related to décollement tectonics decreased. Within the Plateau Molasse - Jura Mountain system strike-slip faulting is probably contemporaneous with folding, but has also outlasted it. Some of this younger strike-slip is, however, coupled to thrusting at the front of the Subalpine Molasse, which would indicate these thrusts to be younger than middle Miocene. Post-5 Ma thrusting in parts of the Subalpine Molasse is revealed by recent apatite fission track studies in central Switzerland (von Hagke et al. 2010). Analogue models based on a cross-section through the northwestern Alps show continued thrusting to the south of the Molasse Basin after the formation of a thin-skinned foreland fold-and-thrust belt (Bonnet et al. 2007).

The young Cenozoic deformation of the northern foreland of the western central Alps is most likely a continuous process of NW-SE-directed shortening from the middle Miocene until the present. After the Alpine deformation front jumped from the thrust subalpine Molasse to the front of the Jura Mountain by décollement tectonics, thin-skinned shortening, predominantly expressed by folding, slightly decreased with decreasing movement along the décollement. At the same time surface strike-slip faulting in the central parts (Plateau Molasse and internal Jura Mountains)

and reverse thick-skinned tectonics in the external parts (Jura front) and probably also in the internal parts (Subalpine Molasse) became more important.

4.12 CONCLUSION

Structural field work carried out in the Plateau Molasse of the Fribourg area in western Switzerland revealed slickensides, brittle deformation bands and undefined fractures to be abundant in the sandstones. In contrast, the interbedded shale lacks obvious deformation structures. The slickensides commonly develop from brittle deformation bands and feature striated gouges and polished surfaces, while calcite fibres are very rare. These planar structures are oriented subvertically and are predominantly of strike-slip nature. Left-lateral slickensides are oriented roughly N-S, while right-lateral slickensides are oriented roughly NW-SE. The deduced paleostress is a uniform NNW-SSE-directed compression. Slickenside populations from the Subalpine Molasse show a combined thrust/strike-slip system in the case of 5 subgroups and an oblique left-lateral/normal system in the case of two subgroups. The paleostresses recorded in the Subalpine Molasse also reveal NNW-SSE compression. Pressure solution pits in pebbles, though limited in distribution, possibly indicate a bulk stress, reflecting incipient shortening. They indicate roughly N-S directed horizontal compression ($\sim 345^\circ$ - 165°) with axes slightly tilted in accordance with the local tilt of strata. This N-S-directed stress field is thought to be the oldest paleostress signature.

The subvertical structures are arranged in Riedel-type geometries and often appear in medium-scale fault zones. These show a regional pattern of WNW-ESE to NW-SE striking right-lateral faults and N-S to NNE-SSW striking left-lateral faults. We suggest that they are interconnected on a regional-scale in a near-surface network of conjugate strike-slip fault zones.

The main structural difference between the Jura Mountains and the Plateau Molasse is the amplitude of folding, which is significantly higher in the Jura Mountains. Kilometre-scale tear faults cutting the folds of the Jura Mountains are connected to the more widely scattered strike-slip faults in the Plateau Molasse, where folding low in amplitude reflecting rather an initial stage of fold development.

The border between the Plateau Molasse and the Subalpine Molasse is a thrust zone with the frontal

thrust showing characteristics of a fold-propagation-fault. Intersection relationships between this frontal thrust and the strike-slip fault network of the Plateau Molasse reveals both crosscutting of the thrust front and interacting of thrusting and strike-slip faulting.

Timing of deformation in the study area is poorly constrained. The time frame of the strike-slip deformation is given by the deformation history of the northern Alpine foreland-fold-and-thrust belt to which the western Swiss Molasse Basin belongs. It starts in the middle Miocene (13 Ma) with folding of the Jura Mountains above a large-scale décollement and prevails until the present. The mode of deformation

changed during this evolution. Thin-skinned folding and thrusting of the external parts (Jura Mountains) related to décollement tectonics was dominant during the early evolution. It successively translated to strike-slip faulting, now also affecting the intermediate parts (Plateau Molasse). In the internal parts (Subalpine Molasse), thrust tectonics prevail and are still active. The Jura Mountains - Molasse Basin fold-and-thrust belt compose the long, thin tip of the thick Alpine orogenic wedge, which represents an unstable geometry according to wedge mechanics (Mosar 1999). The young thrusting in the Subalpine Molasse therefore probably reflects maintenance of surface slope of the unstable wedge.

5 - STRUCTURAL GEOLOGY AND TECTONIC EVOLUTION OF THE WESTERN SWISS MOLASSE BASIN

Ibele, T., Sommaruga, A., Mosar, J.

Manuscript in preparation for submission

ABSTRACT

Structural mapping of the Plateau Molasse was carried out in the Canton Fribourg area in western Switzerland. In addition to well known low-amplitude folding, it revealed a regionally extended strike-slip deformation expressed in WNW-ESE trending left-lateral fault zones and N-S trending right-lateral fault zones. These fault zones are composed of the smaller scale discrete faults mapped in the outcrops. The damage zones of the mapped faults consist of synthetic and antithetic populations of fractures, slickensides and brittle deformation bands. The paleostress field derived from the outcrops exhibits homogenous NW-SE compression and NE-SW extension.

The structural interpretation of the subsurface levels is based on new and consistent interpretation of all available seismic lines. The seismic surveys confirm that the substratum of the Molasse is a shallowly southeast dipping surface. The Mesozoic units reveal several well-defined reflectors that were offset by NE-SW striking and N-S striking faults. WNW-ESE striking faults are less frequent. In cross-section, the faults mostly resemble half-grabens, although offsets are reverse in places. Taking into account the regional tilt of the strata, WNW-ESE striking faults have been identified as right-lateral, and N-S striking faults mostly as left-lateral, while NE-SW striking faults are reverse. All faults root with listric bends in the Triassic and do not continue into the basement. The NE-SW and N-S striking faults are interpreted as former normal faults formed by E-W and NW-SE extension, respectively, which became reactivated by NW-SE compression. The resolution of the basement on the seismic lines is poor and does not allow detailed mapping of structures.

The deformation zones derived from surface mapping and the structures revealed by the seismic interpretation are combined in a 3-D kinematic model of the study area. According to this model, deformation is characterised by a kinematic decoupling of the Mesozoic and Tertiary cover units from the basement along Triassic evaporites. In the internal parts a second decoupling between Tertiary Molasse and Mesozoic units is interpreted as related to the northernmost branch of the Subalpine Molasse basal thrust. Structures in the Tertiary Molasse above this secondary décollement are not related to structures in the Mesozoic units below it.

The Cenozoic tectonic evolution of the study area comprises Paleogene extension followed by Neogene compression. The extension pre-dates deposition of the Molasse, in which it is not recorded, and correlates with Eocene-Oligocene E-W extension as well as with NW-SE extension related to foreland basin flexing. The Neogene compression begins with onset of the Jura Mountains formation and is characterised by passive transport above a décollement in the Triassic evaporites in the Plateau Molasse. Above this décollement, the structures in the Mesozoic units were reactivated, while the previously unstructured Molasse was subject to strike-slip faulting.

The current seismicity of the region reveals that strike-slip faulting according to NW-SE compression is still active and partly related to the interpreted deformation zones.

5.1 INTRODUCTION

The Molasse Basin and the arc-shaped Jura Mountains represent the northern Alpine foreland of Switzerland. Situated in the most external parts of the Alpine orogen they probably locate young tectonic activity. Records of large prehistoric earthquakes (Schnellmann et al. 2002, 2006, Strasser et al. 2006) and recent epicentre alignment point to the existence of active tectonic structures (Kastrup et al. 2007). Active folding in front of the Jura Mountains was reported recently (Madritsch et al. 2010b).

The geodynamic situation of the Molasse Basin changes along-strike from a foreland basin position s. s. in the east to a wedge-top position in the west. The western Molasse Basin is located behind the Jura Mountains that form the Neogene thin-skinned foreland fold-and-thrust belt of the central Alps. This belt spatially coincides with the occurrence of evaporites in the Triassic (Büchi et al. 1965, Boigk & Schöneich 1974, Sommaruga 1997) along which the cover units detached. They were folded in the frontal part (Jura Mountains) and passively transported in the trailing part (Plateau Molasse; Buxtorf 1916, Laubscher 1961, Burkhard 1990, Burkhard & Sommaruga 1998).

Syn- to post-folding strike-slip fault zones (such as the Vallorbe-Pontailier fault) are prominent structures in the Jura Mountains, where they offset the folded Mesozoic strata and partially bend into frontal thrusts (Heim 1915, Laubscher 1972, Sommaruga 1997). Most of their geologic signatures vanish towards the southeast once they enter the sub-horizontal strata of the Molasse. In western Switzerland a continuation of strike-slip faulting between the Jura Mountains and the Plateau Molasse has been locally recorded by field and seismic surveys (Jordi 1951, 1990). Shallow seismic surveys on Lac Neuchâtel reveal that the La Lance strike-slip fault zone (Bertschy 1958, Meia 1966) extends from the Jura Mountains into the Molasse and that it was active in Quaternary times (Gorin et al. 2003, Weidmann 2006). While large-scale reverse tectonics are absent in the Plateau Molasse, strike-slip faulting is likely to be present and still active.

Models regarding the large-scale tectonics postulate tectonic lineaments to extend from the Alps northwards (Plancherel 1979) as well as westwards (Chenevart 1978), and from the Upper Rhine Graben southwards (Revertera 1927, Rybach et al. 1980, Kastrup et al. 2007). If existent, these lineaments would continue into the Plateau Molasse where surface indi-

cations of them are poor.

Neotectonic activity is reported to reactivate basement normal faults in the frontal parts of the Jura Mountains where they interact with the Upper Rhine Graben and the Rhine-Bresse-transfer zone (Giamboni et al. 2004, Ustaszewski & Schmid 2007, Madritsch et al. 2008). Despite the existence of the decollement in the Triassic horizon it is still debated whether recent activity in the more internal Molasse Basin also involves the basement (ENSI 2010). This has important consequences for fault scaling and possible earthquake magnitude. Alignments of instrumentally recorded earthquakes in the area between Fribourg and Bern indicate the possible existence of active strike-slip faulting (Kastrup et al. 2007, Mosar et al. 2008).

To understand the nature and localisation of the neotectonic activity in detail, precise information of the tectonic evolution and the related structures is required. To date little is known about the existence, shape and size of fault zones in the Molasse Basin. We surveyed new structural field data and compiled structural subsurface information to develop a model for the tectonic evolution of the study area in the western Swiss Molasse Basin. The recorded deformation strongly supports a model of lateral strain partitioning between different deformation zones. Important vertical strain partitioning between different lithostratigraphic levels is related to their different mechanical properties as well as to their structural inheritance.

5.2 GEOLOGIC SETTING

The Molasse Basin developed as a peripheral flexural foreland basin in front of the European Alps (figure 5.1). During the orogenic evolution it progressively evolved from an underfilled Flysch basin to an overfilled Molasse Basin (Pfiffner 1986, Allan et al. 1991, Sinclair 1997).

The Molasse sedimentation took place in two shallowing-up megacycles in Oligocene and lower Miocene times (Trümpy 1980, Homewood et al. 1986, Berger et al. 2005). The detritus was eroded from the Alps rising in the south and deposited as proximal conglomeratic fans, intermediate sandstones and distal shales (Heim 1919). The main formations were named according to their sedimentological characteristics – lower marine Molasse (UMM), lower freshwater Molasse (USM), upper marine Molasse (OMM) and upper freshwater Molasse (OSM) (Studer 1853, Trümpy 1980, figure 5.2).

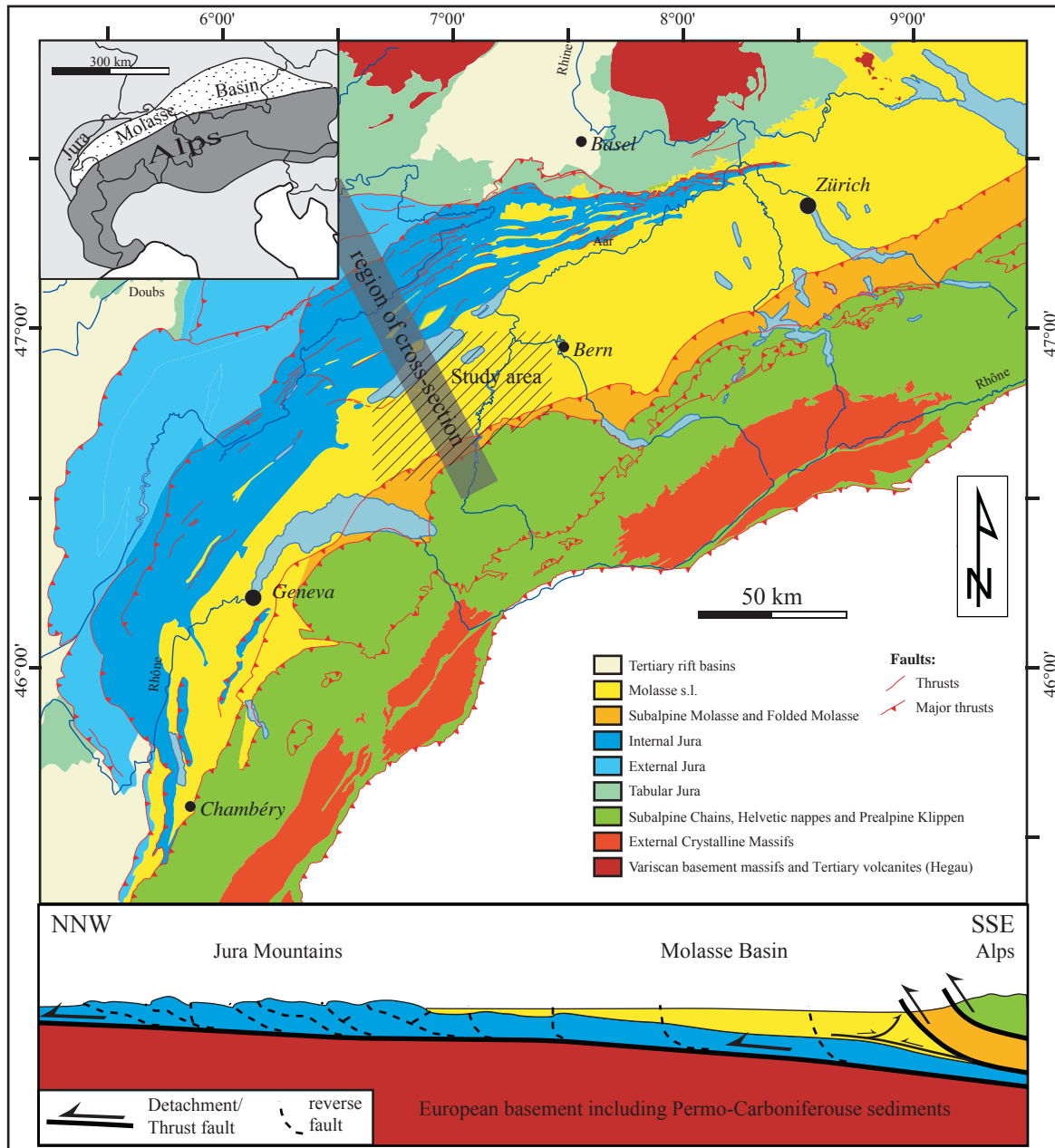


Figure 5.1: Geologic-tectonic overview of the Swiss Molasse Basin and adjoining areas, and a schematic cross-section. Inlet in the upper left corner gives the location of the Molasse Basin north of the European Alps. The location of the study area is indicated in the map.

A stratigraphic gap separates the Oligocene Molasse sediments from the underlying Mesozoic units. The latter consists of partly evaporitic Triassic and usually clayey lower Jurassic, followed by the dominating middle to upper Jurassic platform carbonates whose sedimentation continued to lower Cretaceous times in the southwestern parts (Trümpy 1962, Büchi et al. 1965, Trümpy 1980, Bachmann et al. 1987). These non-metamorphic cover units mostly directly overlie basement, though in places they rest on post-Variscan graben structures filled with Permo-Carboniferous clastic sediments (Diepold 1985, Matter 1987, Bachmann et al. 1987, Pfiffner et al. 1997).

Larger occurrences of such late-Paleozoic sediments are unknown in the western Molasse Basin (Boigk & Schöneich 1974).

Ongoing northwestward migration of the Alpine orogen and its peripheral foreland basin during the Molasse sedimentation lead to progressive onlapping of younger Molasse sediments on the Mesozoic of the European crust (Pfiffner 1986, Homewood et al. 1986).

Along-strike changes of the geodynamic setting of the developing Molasse Basin are manifested

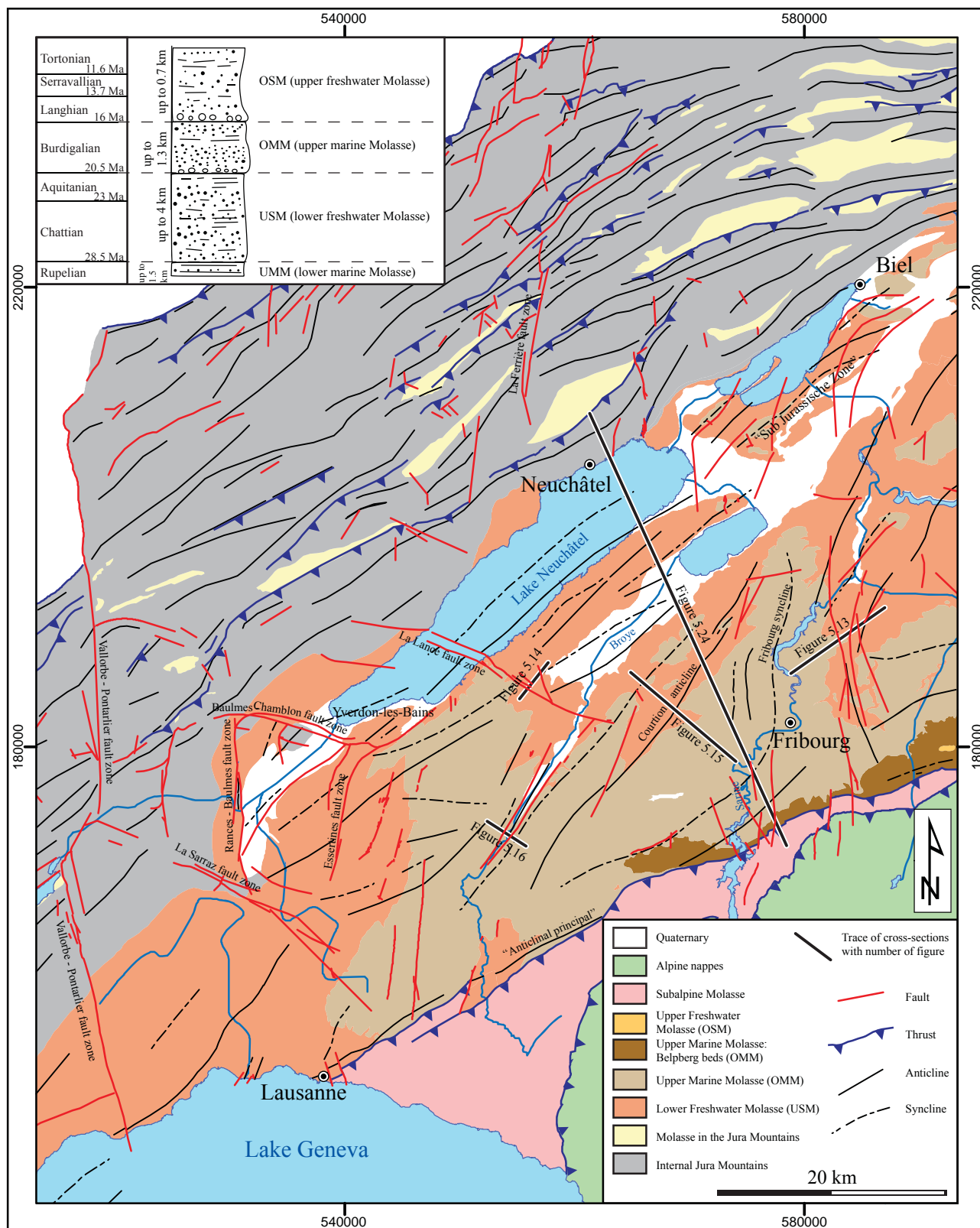


Figure 5.2: Tectonic map of the western Swiss Molasse Basin and the central Jura Mountains and a schematic stratigraphic column for the Molasse Basin. Important faults and folds are given. The trace of cross-sections given in figures 5.13, 5.14, 5.15, 5.16, and 5.24 are indicated. Note that no structures are given for the Alpine nappes and the Subalpine Molasse. Names of fault zones and folds after Heim (1915), Jordi (1990) and Sommaruga (1997). Thicknesses given in the stratigraphic column after Matter et al. (1980).

by the existence of basin-parallel, syn-sedimentary growth faults in the eastern parts (Laubscher 1978, Bachmann et al. 1987, Bachmann & Müller 1992) as opposed to syn-sedimentary folding of the Subalpine chains in the southwestern part (Beck et al. 1998). Such along-strike changes in the foreland basin were observed in analogue models of orogenic wedges (Bonnet et al. 2008). Subdivision of the foreland basin by folds and thrust, as recorded in the westernmost Molasse Basin, correlate with high erosion and low sedimentation rates in these experiments.

Sedimentation gave way to erosion when a large-scale decollement developed in the Triassic evaporites underlying the western Swiss Molasse Basin. It accounts for frontal shortening in the Jura Mountains and internal passive transport of the Plateau Molasse (Buxtorf 1916, Laubscher 1961, Burkhard 1990, Burkhard & Sommaruga 1998). In the central part of the Jura Mountains across-strike shortening was estimated at 25-30 km (Laubscher 1965, Mugnier & Vialon 1986). The total amount of erosion and exhumation reaches up to 4 km in the western part of the Plateau Molasse, where the OSM has been nearly completely removed (Kaelin et al. 1992, Schegg et al. 1997, Schegg & Leu 1998, Mazurek et al. 2006, Cedreboom et al. 2004).

In the south and southeast, the older Molasse sediments became successively incorporated in the alpine deformation, forming the Subalpine Molasse (figure 5.1); in eastern Switzerland it is represented by a broad fold-and thrust belt. The transition towards the unfolded Molasse is represented by a triangular zone formed by a back thrust associated with an underlying blind thrust (Müller et al. 1988, Berge & Veal 2005). In western Switzerland the Subalpine Molasse is composed of a narrow band of stacked imbricates. At the transition towards the Plateau Molasse such imbricates develop from the limbs of narrow folds (Beck 1946, Rutsch 1947, chapter 4). Such transitions from folds to imbricates near the thrust front occur along-strike from NE to SW. They are often associated with strike-slip fault zones in the adjacent Plateau Molasse (chapter 4).

The transition of the Molasse Basin from the foreland basin to the wedge-top basin occurs without a sharp tectonic boundary. The undeformed Molasse units in eastern Switzerland gradually give way to the slightly folded but still overall sub-horizontal units of the Plateau Molasse in western Switzerland. The folds and thrust of the Jura Mountains taper off towards east. Towards the west and southwest they grow con-

tinuously with the narrowing of the southerly adjacent Molasse Basin until they finally merge with the Subalpine Chains of the N-S-striking French Alps. Nonetheless the total amount of shortening across Subalpine Molasse, Plateau Molasse and Jura Mountains remains constant from eastern to western Switzerland. It was estimated at 25-30 km at least (Burkhard 1990). This shortening of the Mesozoic and Cenozoic cover units is compensated by basement shortening in the external crystalline massifs (Boyer & Elliot 1982, Burkhard 1990, Laubscher 1992).

While shortening in the Subalpine chains is a continuing process from Oligocene to recent times (Sue et al. 1999, Sue & Tricart 2002, Affolter & Gratier 2004), a mid-late Miocene age is widely accepted for the decollement and formation of the Jura Mountains (Naef et al. 1985, Laubscher 1987, Burkhard 1990, Burkhard & Sommaruga 1998). However, this time gap is not manifested by a tectonic boundary. Instead, the Subalpine Chains merge into the chains of the Jura Mountains, most likely indicating their formation to be continuous in space and time.

The northern and western foreland of the Jura Mountains-Subalpine Chains foreland fold-and-thrust belt is characterised by the European Cenozoic rift system (Illies 1977, Ziegler 1992, Dèzes et al. 2004). This continental network of graben and transfer zones developed in the Paleogene; its initiation was guided by the allocation of Permo-Carboniferous troughs (Ziegler 1992, Madritsch et al. 2009). Its different elements were partly reactivated according to the Miocene to recent stress field (Plenefisch & Bonjer 1997, Schuhmacher 2002, Giamboni et al. 2004, Madritsch et al. 2008). This includes a thick-skinned reverse nature of neotectonic activity where the northern front of the Jura Mountains interacts with the southern boundaries of the Upper Rhine Graben and the Rhine-Bresse transfer zone (Giamboni et al. 2004, Ustaszewski & Schmid 2007, Madritsch et al. 2008).

5.3 SURFACE DATA

Structural field work was carried out at surface outcrops of the Tertiary Molasse of western Switzerland. The study area s.s. reaches from the Prealps in the south to Lake Neuchâtel at the foot of the Jura Mountains in the north and covers the Plateau Molasse between the rivers Aare in the east and Broye in the west. It reveals fluvial, lacustrine and shallow marine clastic sediments belonging to the lower Freshwater (USM) and upper Marine Molasse (OMM) (figure

5.2). These sediments are shale, sandy shale, clayey sands and sandstones alternating vertically and laterally. The beds are gently folded, forming flat anticlines and synclines with dips rarely exceeding 5° - 10° . The axes of these folds run NE-SW, i.e. roughly parallel to the tectonic boundary with the Subalpine Molasse in the southeast. They bend into a N-S direction in the area between Fribourg and Bern (figures 5.2, 5.3 and 5.6) which is termed the Fribourg structure ("Querzone von Freiburg" by Schuppli 1950). Several different types of structures, including slickensides, brittle deformation bands and joint-like fractures were mapped and a near surface fault network will be presented.

5.3.1 Deformation structures

We mapped three different planar tectonic structures on the outcrop scale: brittle deformation bands (DBs), slickensides and undefined fractures.

Brittle deformation bands are structures developed during fault initiation in porous sandstone (e.g. Aydin, 1978, Shipton & Cowie 2001, Fossen et al. 2007). They are common in the sandstones of the study area, which are poorly consolidated and display up to 15% porosity. The principal mechanism is collapse of the grain framework and hence porosity reduction. This type of collapse is typical of porous media in general, making them less resistant to failure than non-porous media (Mandl et al. 1977). While non-porous media fail under conditions given by the Mohr-Coulomb criterion, porous ones generally exhibit a more ductile behaviour (Wong et al. 1997). The microscopic investigation of the DBs from the study area showed that they feature important microstructures (chapter 2). Grain grinding along a DB results in a micro-fault gouge that, once a certain percentage of ground material is reached, develops an SC-type foliation. This SC-foliation provides a shear sense indicator. The foliation is composed of palygorskite, a clay mineral formed under non-metamorphic conditions in the course of deformation (chapters 2 and 3).

Slickensides are the most common shear structures mapped in the field. The lineations they feature mostly consist of drawn-out gouge material (Engelder 1974, Means 1987), including palygorskite fibres, indicating their development from DBs by ongoing shear. Mirror-like planes with carrot-shaped grooves (Hancock 1985, Hancock & Barka 1987, Tjia 1964, Engelder 1974) and steps opposing the sense of

movement (Paterson 1958, Tjia 1964) are also common, especially in the damage zones of larger faults. In contrast, fibrous mineral precipitation (Durney & Ramsay 1973) (calcite in this case) is rare in the Plateau Molasse, though common in the Subalpine Molasse. The sense of movement on the slickensides was not always unambiguously determinable. However, the comparison with those slickensides for which independent indicators of the sense of movement were present, such as offset pebbles or clay lenses, corroborates the general accuracy of our criteria used in the field.

The term "unspecified fractures" summarises all joint-like planar structures that, in contrast to slickensides, show no lineations. According to their orientation pattern with respect to the σ_1 inferred from the slickenside and DB data sets, these structures are of two different origins: The first type represent altered slickenside surfaces oriented parallel to the slickensides, while the second type are mode I cracks formed parallel to σ_1 .

The DBs, slickensides and undefined fractures usually occur in sub-parallel bundles, conjugate sets and Riedel-type networks, forming either faults or associated damage zones. The faults and shear zones themselves are scattered irregularly over the study area (figure 5.3). Due to poor outcrop conditions none of the faults could be mapped along-strike and characterised with respect to fault length and total displacement.

5.3.2 Implications of structure type for deformation conditions

The structure types described above provide two criteria that qualitatively indicate a "very" brittle nature of deformation: The widespread occurrence of DBs and the absolutely frictional nature of slickensides lacking crystal growth.

According to descriptions in the literature the formation of DBs seems to be restricted to the uppermost 3 km of the crust (Fossen et al. 2007). Such a depth restriction is plausible because the formation of DBs calls for a considerable porosity, which is however progressively lost during compaction and dissolution-cementation processes occurring with increasing burial depth (Bjørlykke et al. 1989, Ramm 1992, Walderhaug 1996). Furthermore, high confining pressures at deeper levels of the crust rather promote cataclastic flow instead of localised deformation in porous sandstone (Mair et al. 2002).

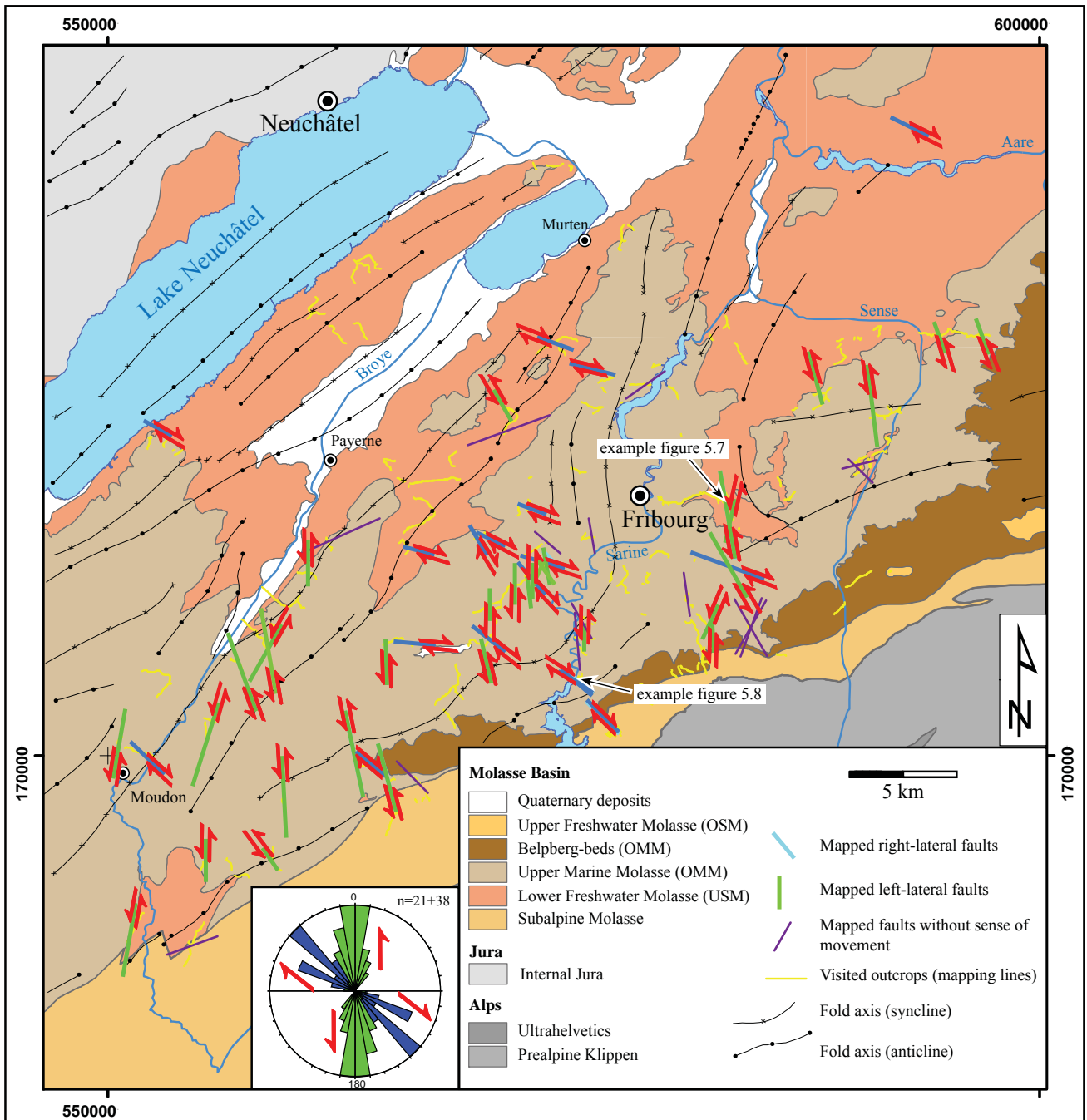


Figure 5.3: Study area with faults mapped in the field. NNW-SSE to NNE-SSW striking faults are left-lateral and E-W to NW-SE striking faults are right-lateral. Faults with no recorded sense of movement are also given. The rose diagram gives the strike for all dextral faults in blue and all sinistral faults in green. Location of faults given in figures 5.7 and 5.8 are indicated.

Precipitates of fibrous calcite on slickenside fault planes were found to be common in the Subalpine Molasse and rare in the Plateau Molasse implying a different mineralisation of the fluid phase during deformation. In contrast to the Plateau Molasse with only very slight folding; the Subalpine Molasse of the study area is strongly deformed, displaying a narrow zone of imbricates. Within the Subalpine Molasse deformation could have taken place either at different, i.e. higher temperatures, or in the frame of a fault network whose extent provides pathways to fluids

from other sources. The generally stronger deformation could explain both deeper burial and differently mineralized fluids. In contrast, palygorskite formation in fault gouges of the Plateau Molasse is most likely a reaction of the ground host mineral grains with a fluid resembling the recent Molasse formation waters (chapter 3).

The deformation structures of the Plateau Molasse are therefore incipient structures, likely formed without connection to larger faults such as de-

collement thrusts. Their formation took place in very shallow levels of the upper crust.

5.3.3 Orientation of planar structures, their kinematics and derived paleostress

The meso-scale planar shear structures include DBs, slickensides and the undefined fractures

derived from altered slickenside surfaces. The inclination of their planes is steep and the kinematics predominantly strike-slip (figure 5.4). The orientation distribution is similar and shows two maxima with a certain degree of scatter. These maxima strike WNW-ESE to NW-SE and NNW-SSE to NNE-SSW, with the former corresponding to right-lateral shear and the latter to left-lateral shear. The according σ_1 paleostress -axes are oriented NW-SE to NNW-SSE (figure 5.5). Each maximum's scatter of up to 30° occurs for all

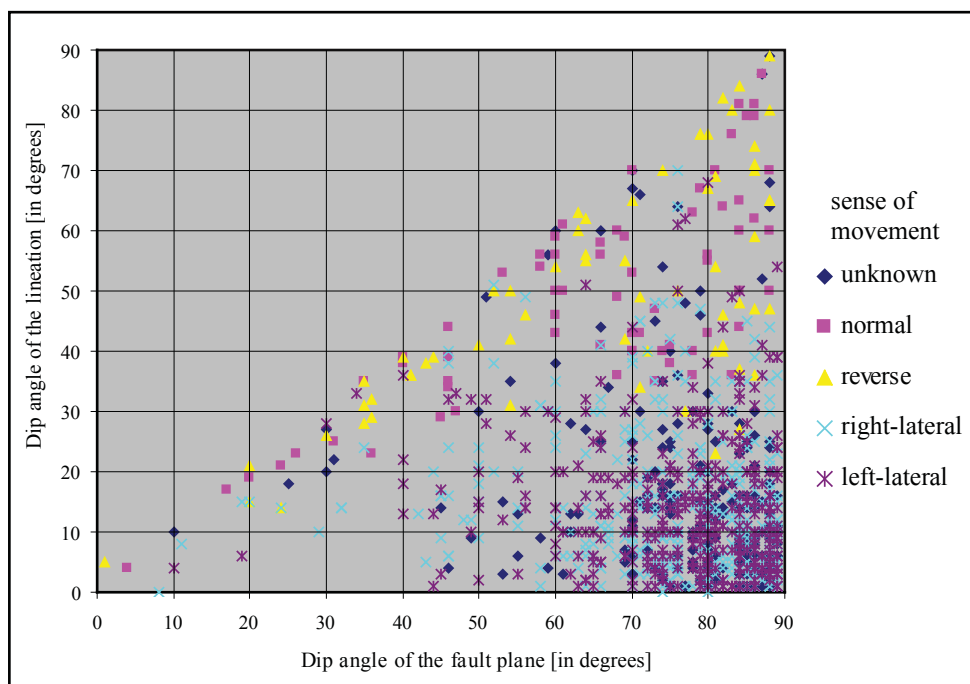


Figure 5.4: Diagram of dip angle of lineation versus dip angle of fault plane for measured slickensides. The fault planes are predominantly steeply inclined and the lineations are predominantly shallowly inclined, indicating strike-slip deformation. The data points are colour-coded according to the sense of movement.

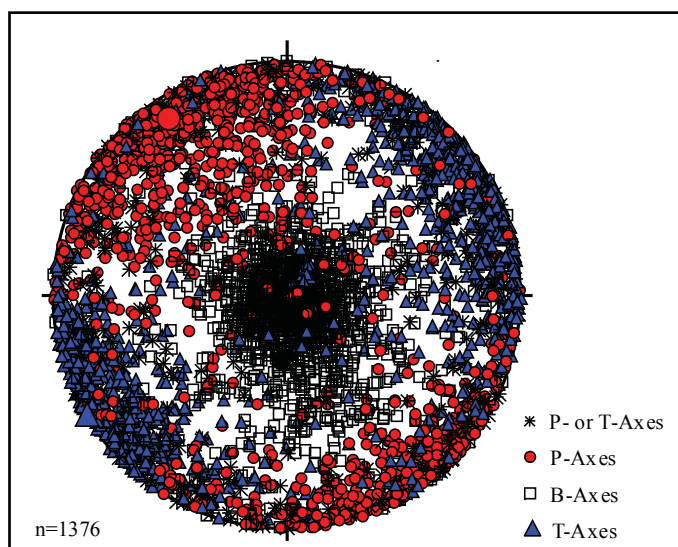


Figure 5.5: Stereo plot of P-, T- and B-axes of all measured slickensides. P-axes predominantly strike NW-SE and T-Axes strike NE-SW. B-Axes are subvertical, indicating strike-slip movement.

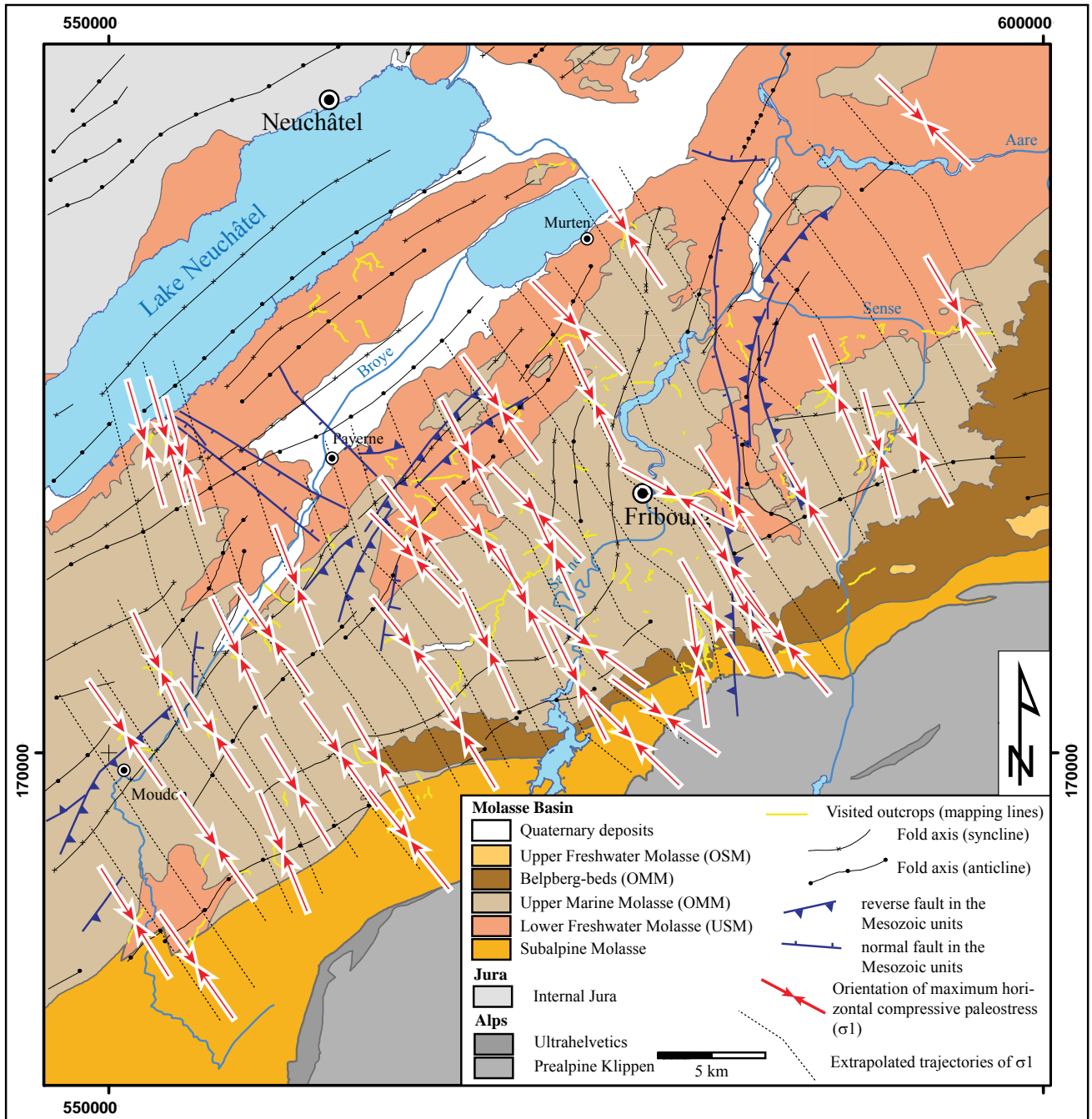


Figure 5.6: Map of the study area showing paleostress directions and main geological units. The orientations of maximum horizontal compressive stress (σ_1) reflect paleostress calculated from slickenside data (red arrows). The paleostress field derived from slickensides shows homogenous NNW-SSE compression. In the Subalpine Molasse it is thrust-related, whereas it reveals a strike-slip regime in the Plateau Molasse. Faults in the Mesozoic strata after RESUN 2009, Sommaruga et al. (2011, in prep.), Sommaruga (2011, personal communication).

structure types. It accounts for slight differences in the paleostress orientation throughout the study area (figure 5.3) as well as local orientation differences between synthetic shears of a Riedel system. Data sets from outcrops commonly reveal more than one set of fault planes per sense of movement, i.e. synthetic shears. In some cases complete Riedel-type patterns are mapped though usually synthetic pairs of R- and Y-shears clearly dominate (e.g. figures 5.7 and 5.8). This indicates that faulting initiates as Riedel-type

shearing with the superordinate shear sense becoming increasingly dominant as strain accumulates.

Overprinting criteria mapped in the field, such as one planar structure cut by another planar structure, are not systematic; no relative timing between structures could be established. Two sets of fault planes crosscut each other in both directions even in the same outcrop, implying their alternating evolution in one stress regime. The tectonic evolution recorded by the

Oligocene-Miocene Molasse rocks has to be considered as single phased (figure 5.6) and is Neogene in age.

5.3.4 Implications for fault zone extent in the Tertiary Molasse

The shear zones appear in the outcrops as larger faults with damage zones and cataclastic fault cores (figure 5.7) as well as in arrays of smaller faults distributed over some hundreds of metres across-strike (figure 5.8). Similar to the planar structures, the faults show a certain degree of scatter in orientation. Right-lateral faults strike WNW-ESE to NW-SE and left-lateral ones NNW-SSE to N-S. We interpret the variation in orientation of each maximum as either resulting from the combination of different components

of a Riedel shear model (e.g. R- or Y-shear) or as due to along-strike orientation changes. Along-strike orientation changes may account for differences in appearance between discrete large faults and the arrays of smaller faults. The latter represent releasing bends of the larger faults (figures 5.8 and 5.11). Lateral and horizontal facies variations between sandstone and shale, especially within the USM, are likely to additionally complicate the 3-D extension of the fault network. Similar small-scale structures have different appearances in sandstones and clayey sandstones (figure 5.9) and no discrete structures at all were found in the shale. The thus implied mechanical difference between the lithologies would favour soft-linkage of individual deformation zones in the different sandy packages by way of the interbedded shale (figure 5.11).

Based on the deformation characteristics on

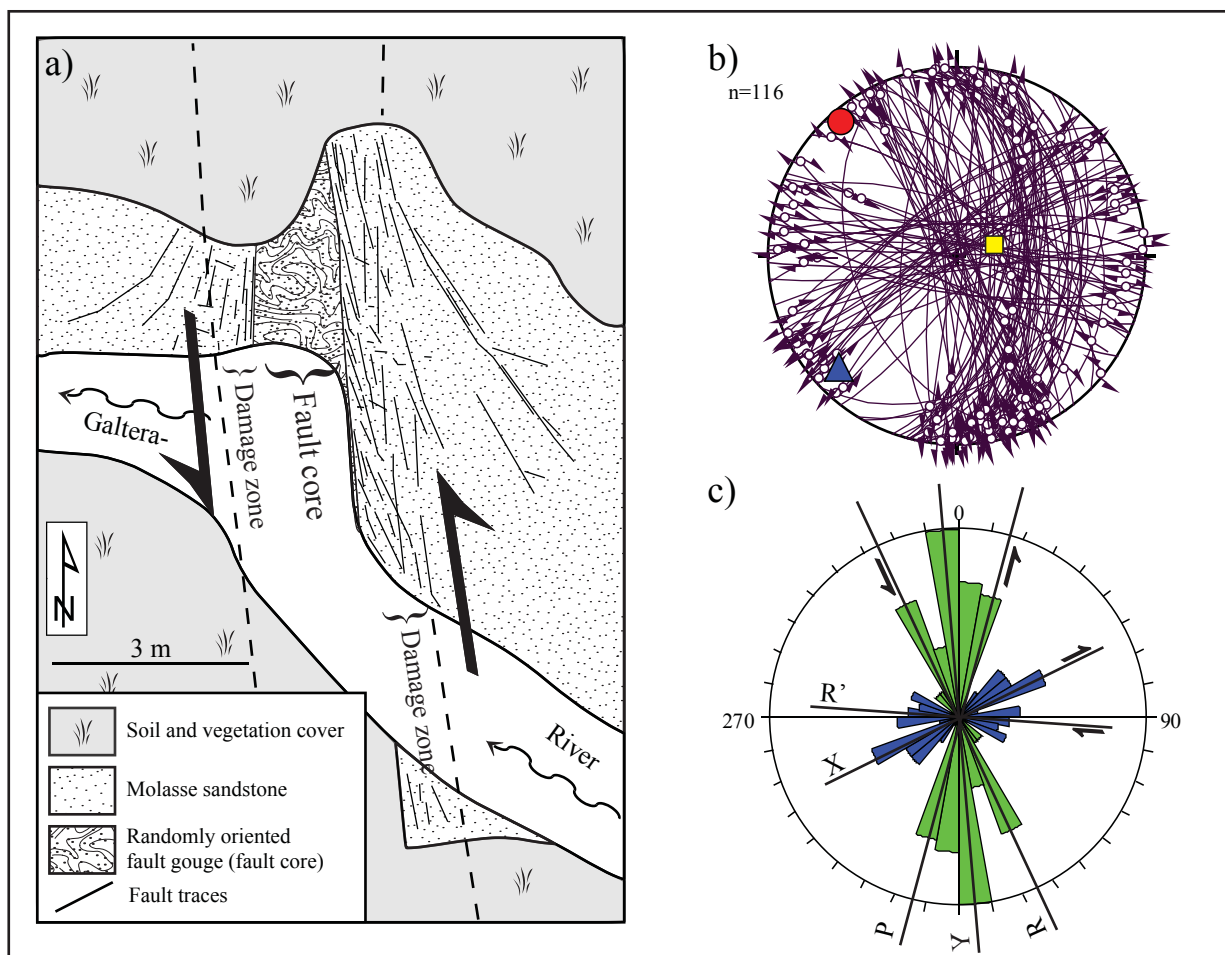


Figure 5.7: a) Sketch map of a larger discrete fault located at the Galtera river 5 km east of the City of Fribourg (location see figure 5.3). Strike is N-S and sense of movement left-lateral. This fault is one of the larger faults mapped in the study area, with a 1-1.5m wide core zone of randomly oriented fault gouge and several meter wide damage zones on either side. b) Stereo plot of slickensides measured in the damage zones. The plot includes fault planes and σ_1 (red circle), σ_2 (blue triangle) and σ_3 (yellow square) as estimated by the right-dihedra method. c) Rose diagram of the Slickensides. The maxima distribution of strike corresponds well to the indicated shears of a Riedel system. The green area corresponds to left-lateral shear, and the blue area to right-lateral shear.

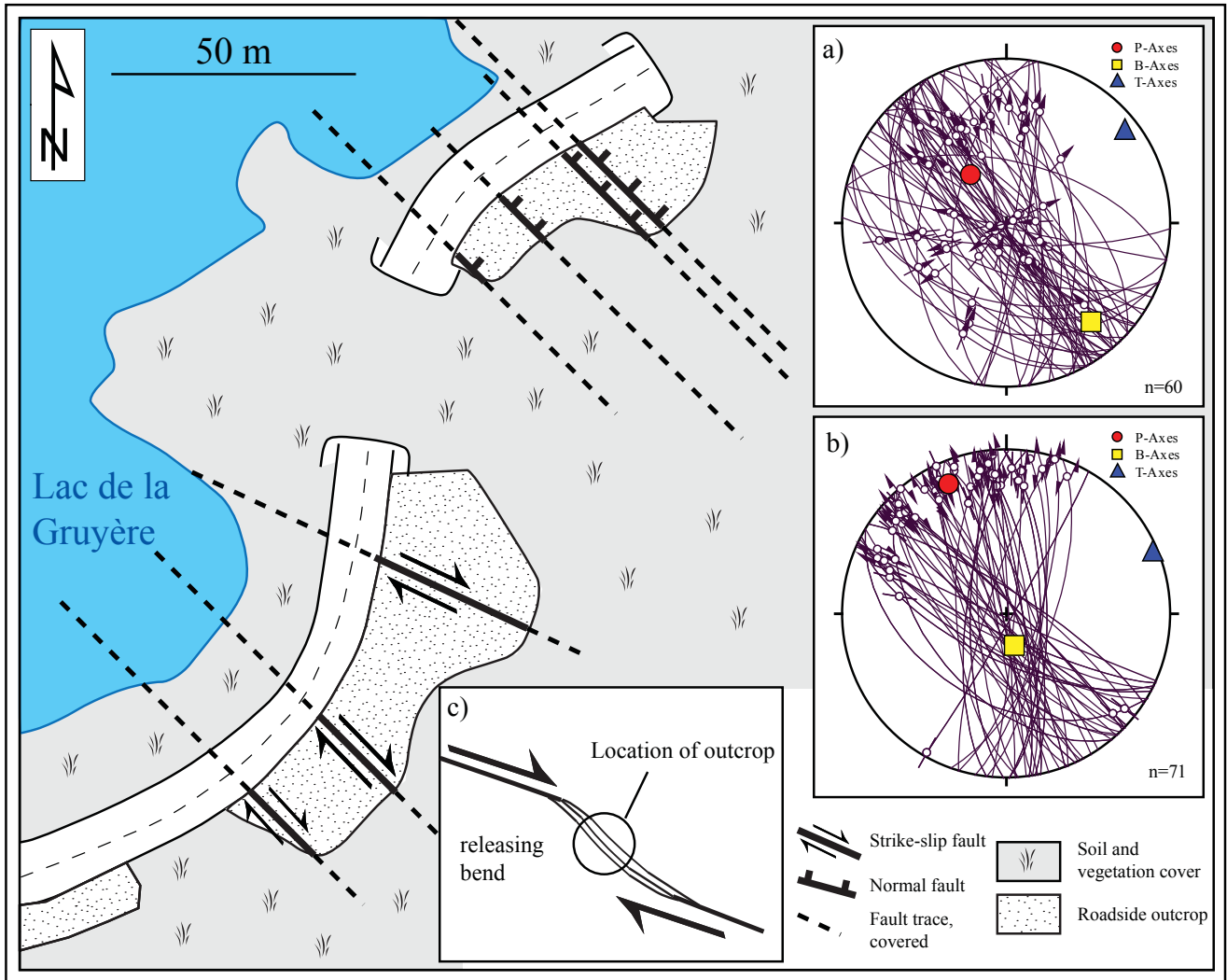


Figure 5.8: Sketch map of a Roadside outcrop along the road from the dam of Lac de la Gruyère towards Pont-la-Ville (see figure 5.3 for location). In contrast to the case given in figure 5.7, several small- and medium-scale faults occur over a distance of about 200 m. Strike of the faults is NW-SE and kinematics are right-lateral with a NE-SW dilatational component. Stereo plots show slickensides with a) oblique and down-dip lineations and b) with strike-slip lineations. The maxima of P-, T-, and B-axes reveal NE-SW extension a) and NW-SE compression b). Down-dip lineations (mostly normal faults) predominate in the northern part and strike-slip lineations in the southern part. According to the scheme given in c) and in figure 5.11, the array could represent a releasing bend of a WNW-ESE oriented right-lateral fault.

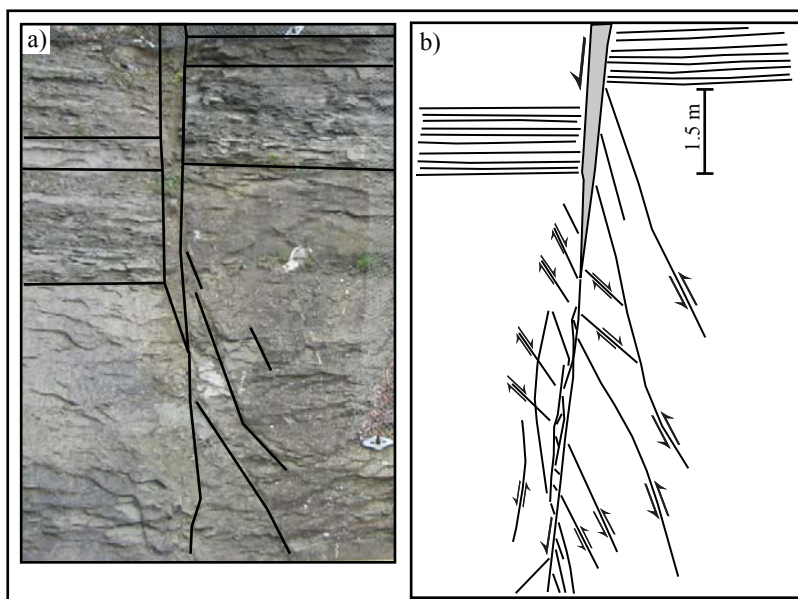


Figure 5.9: a) Photograph and b) sketch of a small fault with down-dip kinematics. The fault crosses boundaries between an impure but relatively hard sandstone (striped signature) and pure sandstone (white signature). In the impure sandstone, shear is concentrated in a fault gouge some tens of centimetres wide. In the pure sandstone, shear is distributed onto several slickensides scattered over some metres. Some of these slickensides show different orientations than the fault itself, as well as synthetic and antithetic shear senses. The fault is part of the array of faults given in figure 5.8.

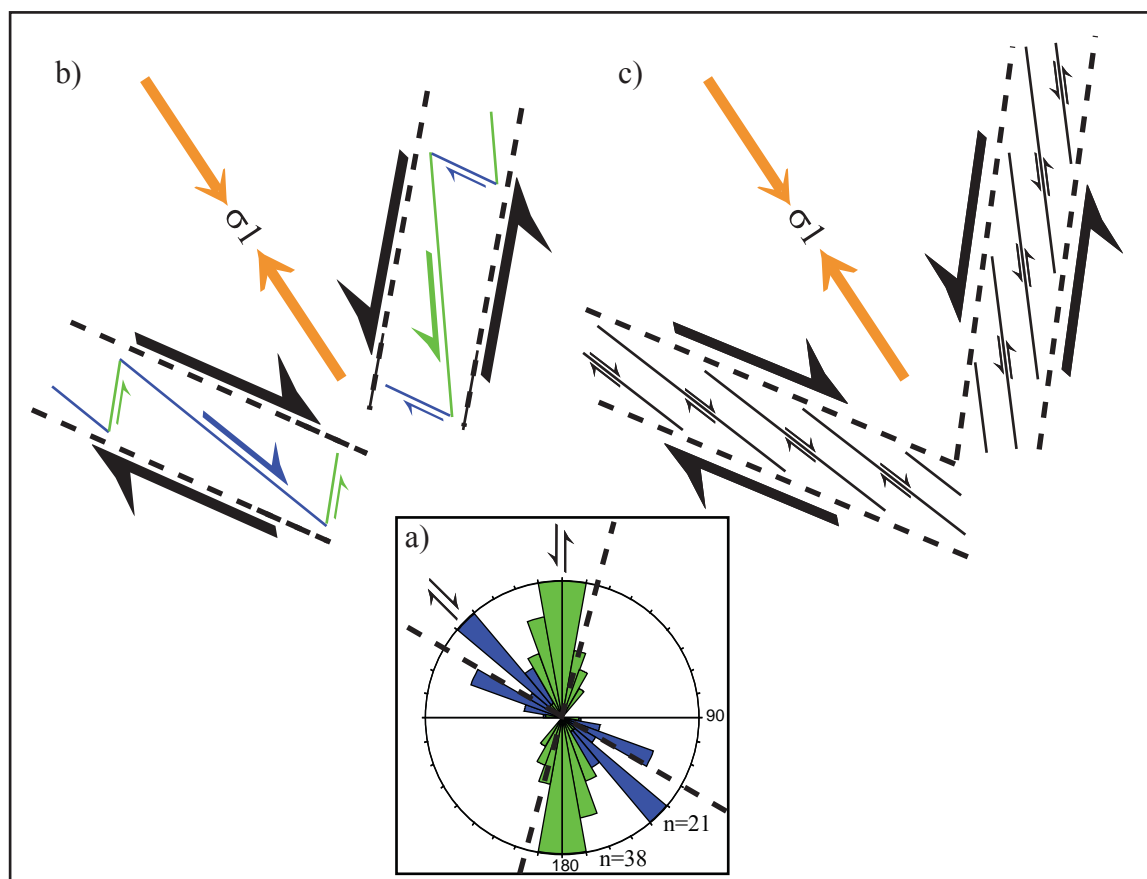


Figure 5.10: a) Rose diagram giving the orientation of all faults mapped in the study area (and given in figure 5.3). Right-lateral faulting is indicated in blue (21 faults), while left-lateral faulting is indicated in green (38 faults). b) and c) are general 2-D models of fault arrays and superordinate shear zones interpreted with the mapped faults. b) shows shearing distributed on synthetic (R-) and antithetic (R') shears of a Riedel system, c) shows shearing distributed on en-echelon arranged synthetic (R-) shears. The orientation of superordinate shearing is indicated by dashed lines in the rose diagram. σ_1 of the system is oriented NNW-SSE.

outcrop scale we favour a model for regional-scale deformation in which mapped discrete faults are probably arranged in an en-echelon manner within the frame of larger superordinate shear zones. The latter are than oriented WNW-ESE in case of right-lateral movement and NNE-SSW in case of left-lateral movement (figure 5.10). While the mapped discrete faults (figure 5.3) are likely not more than a few kilometres in length, the superordinate shear zones may reach 10 to 15 km.

5.3.5 Interpretation of superordinate shear zones

The location of superordinate shear zones can be hypothesised based on the distribution of fault outcrops. Areas may be attributed to the same zone of deformation if the deformation structures that crop out in the areas are of comparable kinematics and orientation

and if they can be connected along this orientation. In this way the following deformation zones are interpreted for the Fribourg area: The Ecublens-Lovatens structure, the Villaraboud-Seigneux structure, the Le Mausson structure, the Corserey-Chènenens structure, the La Glâne-Rossens-La Roche structure, and the southern part of the Fribourg structure (subchapter 5.5.1 (figure 5.21).

5.3.6 Fault zones recorded in the Tertiary Molasse only

Most of the above-mentioned interpreted deformation zones are expressed only in the Tertiary Molasse. The important of these will be described shortly in the following.

The left-lateral Le Mausson structures comprise several NNW-SSE-striking larger fault zones

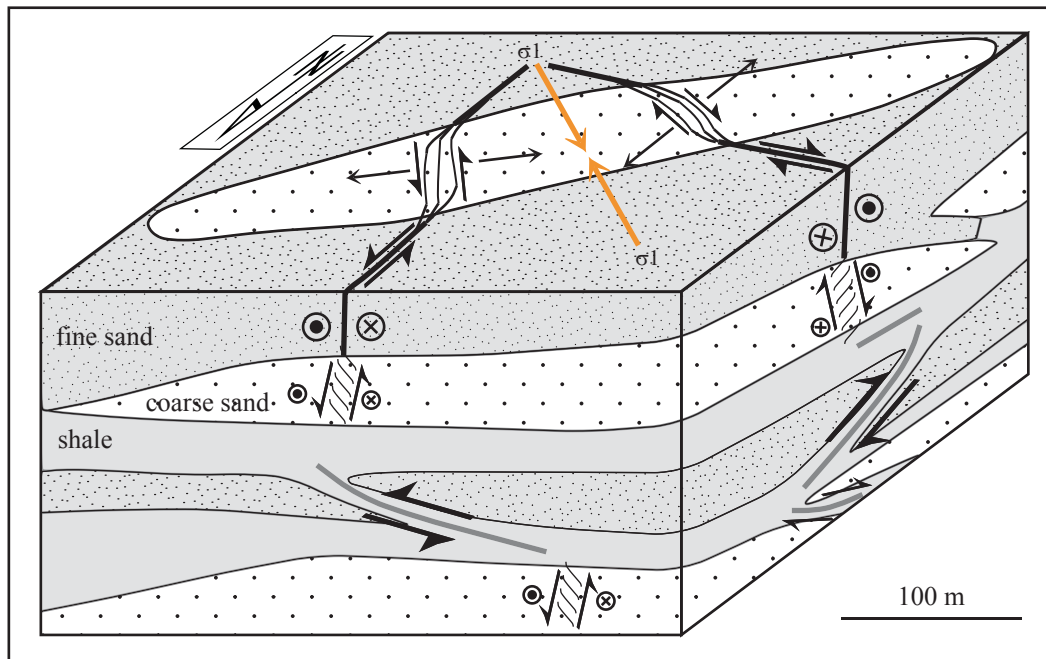


Figure 5.11: Block diagram illustrating how faults of different orientation and kinematics could be soft-linked. All given faults act in response to the same direction of maximum horizontal compression, but show different expressions according to lithology and depth (i.e. confining pressure). Shear localised on a discrete fault in fine sand may be distributed on an array of smaller faults with different orientation in coarse sand, and become diffuse in shale. Changes in fault orientation may cause local dilatation (releasing bends) or compression (restraining bends). The illustrated phenomena are likely independent of scale, ranging from metre- to kilometre-scale.

mapped in the surface outcrops of the Molasse. They probably coincide with a small bend of the thrust front of the Subalpine Molasse that was locally reactivated by movement along the le Maussion structures, cutting of the trace of the “anticlinal principal” (Mornod 1949, Gabus et al. 2000) The only structure in the Mesozoic units in this area is a small SW-NE-striking and south-west-facing normal fault with no obvious connection to the kinematics of the surface structures.

The left-lateral Villaraboud-Seigneux structure is defined by two outcrops of NNW-SSE-striking larger fault zones in the Tertiary Molasse. No indications of tectonic structures in the Mesozoic units are recorded.

The left-lateral NNE-SSW-striking Ecublens-Lovatens structure is defined by outcrops of larger fault zones and strong deformation of the Tertiary Molasse. Its southern part interacts with the thrust front of the Subalpine Molasse in the region of Oron, where the left-lateral shear does not offset the thrust front. Instead a new thrust develops in the foreland at the southwestern side of the zone which - conformable to left-lateral movement - suffered more compression. In its northern parts this structure interacts with the Broye structure. It is not recorded in the Mesozoic unit.

The La Glâne-Rossens-La Roche structure is defined by several NW-SE-striking right-lateral fault zones and strong deformation of the Tertiary Molasse in surface outcrops, including the external Subalpine Molasse. The only structures in the units that spatially coincide are horsts and grabens with NNW-SSE strike and no obvious kinematic connection to the surface structures.

5.3.6.1 The Subalpine Molasse thrust front

The thrust front of the Subalpine Molasse represents the former front of the Alpine nappe pile. It strikes NE-SW in the study area and interacts with strike-slip fault zones of the Plateau Molasse (e.g. the Ecublens-Lovatens structure), indicating contemporaneous activity. The Subalpine thrust front does not correspond to any structure in the Mesozoic units. Instead it represents a second, shallower and more internal detachment at the base of the Tertiary as opposed to the one in the Triassic evaporites at the base of the Mesozoic units. Further east in Switzerland and adjacent Bavaria, this thrust front is expressed as a triangular structure with a basal blind thrust (Vollmayr & Wendt 1987, Müller et al. 1988, Pfiffner et al. 1997, Berge & Veal 2005). Such types of features have also

been documented in analogue modelling of the Alpine foreland basin evolution (Bonnet 2007). A similar basal blind thrust extending into the Plateau Molasse is therefore likely. Its existence could also account for the presence of deformation zones in the Tertiary Molasse only.

5.4 DEEP STRUCTURE

This subchapter addresses the geometry of tectonic structures at subsurface. During the second half of the 20th century, a dense network of seismic lines was recorded by different oil companies across the western Swiss Molasse Basin. With the availability of new studies and interpretation of the petroleum exploration seismics, it is now possible to do continuous interpretation of these seismic lines. This effort was made by the RESUN, NAGRA and the Swiss Geophysical Society, though most of their work is still in progress and not yet published. Our interpretations presented here are the result of close collaboration with these Institutions (RESUN 2009, Eichenberger et al in prep., Sommaruga personal communication).

The fault structures in the pre-Mesozoic basement and the Mesozoic cover units will be discussed separately. In general both, the top of basement and the Mesozoic strata dip towards southeast. The structures in the Tertiary Molasse are not well imaged by the seismic surveys. Good reflector horizons are missing due to lack of lithostratigraphic contrasts. The structures in the Tertiary series are therefore defined as those mapped in the surface outcrops as described subchapter 5.3.6.

5.4.1 Structures in the basement

The top of the basement is a poorly defined reflector in the seismic lines crossing the study area. The basement corresponds to the units outcropping in the external crystalline massifs of the Alps in the south as well as in the Black Forest and Vosges Mountains in the north. All these outcropping basement units show very similar pre-Mesozoic evolutions, belonging to the same Variscan mega-unit (von Raumer et al. 1993). The best surface analogy is given by the Black Forest (and Vosges Mountains) which have undergone no Alpine orogenic deformation. Its pre-Alpine structural inventory comprises intense ductile deformation prior to and during the Variscan orogeny as well as late-orogenic plutonism (e.g. Behr et al. 1983, Krohe & Eisbacher 1988). Several phases of late-Paleozoic

brittle tectonics yield fault sets including lineaments striking more or less N-S and WNW-ESE as well as one WSW-ENE-striking Permo-Carboniferous trough in the northern Jura Mountains (Thury et al. 1994). Structures with these orientations are prone to reactivation during Cenozoic tectonics (Illies 1977, Ziegler 1992).

In the study area, the seismic data reveals no significant structures in the top of the basement, nor are there indications of major Permo-Carboniferous troughs. Only a few small, by trend N-S and NE-SW-striking normal faults with minor offset can be interpreted.

5.4.2 Structures in the Mesozoic units

The alternating carbonates, marls and shales of the Mesozoic strata comprise several well-defined seismic reflectors: near top of the Muschelkalk, near top of the Triassic, near top of the Liassic, near top of the Dogger, near top of the lower Malm and near top of the Mesozoic (figure 5.12). The Mesozoic sequence is composed of alternating weaker and stronger horizons with the weak horizons located in the lower Malm (Argovien), probably within the lower Dogger (Opalinuston), and mainly in the Triassic evaporites. Tectonic structuring as deduced from seismic interpretation (RESUN 2009, Sommaruga et al. in prep.) is more complex in the Mesozoic units than in the basement. These structures include normal, reverse and strike-slip faults striking N-S, WNW-ESE and NE-SW.

5.5 INTERPRETATION OF DEFORMATION ZONES IN THE MESOZOIC AND TERTIARY COVER

The spatial correlation of the structures in the Mesozoic units with active tectonics and deformation zones mapped in the outcrops of the Tertiary Molasse helps to interpret their tectonic evolution and kinematics. The mapped deformation zones are characterised by strike-slip faulting according to NW-SE compression. In contrast, the structures in the Mesozoic units show normal and reverse offsets along listric faults rooted in the Triassic. However, as the strata are generally tilted towards SE, the vertical offsets seen in 2-D sections may also be interpreted in terms of horizontal movement. In the following subchapter the geometry of fault zones in the Mesozoic units as expressed by seismic surveys will be presented. Their connections with surface deformation structures will be discussed and their tectonic evolution interpreted.

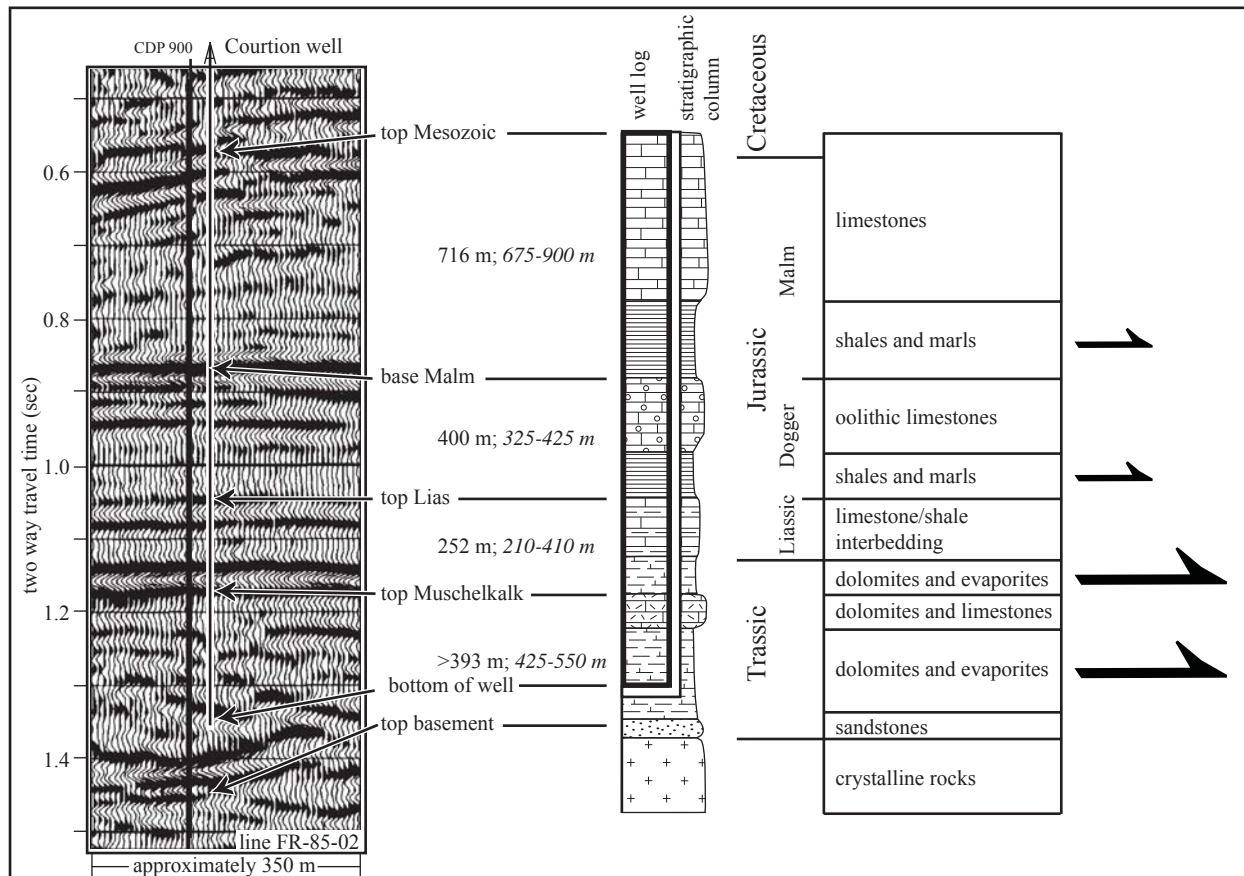


Figure 5.12: Simplified stratigraphic column of the Mesozoic units in the western Swiss Molasse Basin. The main reflectors and the thickness range of the units between them are given to the left of the sketched column. Thicknesses are taken from the Courtion well (Fischer & Luterbacher 1963); thickness ranges (written in *italics*) are derived from depth-conversion of several seismic lines in the region (RESUN 2010). A seismic section (line FR-85-02) crossing the well Courtion shows the indicated reflectors. Age and lithostratigraphy are given at the right side. Large arrows (to the right)

5.5.1 The Fribourg zone – a complex polyphase structure

The term “Fribourg zone” used here signifies the roughly N-S-trending structures in the Mesozoic units as deduced from seismic interpretations as well as from tectonic structures mapped at the surface. The Fribourg zone generally marks the eastern border of the Fribourg structure as defined by Schuppli (1950). The term “Fribourg lineament” has been used to describe the alignment of earthquakes in an N-S-trending line situated east of the city of Fribourg. The Fribourg lineament probably coincides with the Fribourg zone.

These structures are N-S-striking faults forming a zone of more than 20 km length. The locations of fault traces are uncertain in an 8 km wide gap in the central part due to lack of seismic lines. In most sections two or three larger faults can be interpreted. Figure 5.13 shows one such section displaying two west-facing and one east-facing normal fault. The east-facing normal fault is developed in the hanging-

wall of a west-facing one, representing a half-graben structure. The faults are steep but not vertically oriented. The two main (i.e. west-facing) faults root in listric bends within the Triassic. The Triassic horizon appears to be over-thickened underneath the structure.

In the Tertiary Molasse, the Fribourg zone is mainly defined by N-S-striking, left-lateral faults, accompanied by the occurrence of a few conjugate NW-SE-striking right-lateral faults (figure 5.17). The thrust front of the Subalpine Molasse south of the Fribourg zone is offset by left-lateral strike-slip, as shown by surface mapping (Weidmann 2002). These surface deformations are mapped east and southeast of the city of Fribourg, while outcrops of Tertiary units are generally rare further north. The Fribourg zone is also defined by recent earthquake activity. The related focal depths are located in the upper Mesozoic (Malm) and the focal mechanisms show left-lateral shear on N-S-striking fault planes (Deichmann et al. 2000, 2010, Kastrup et al. 2007).

The faults in the Mesozoic units are oriented

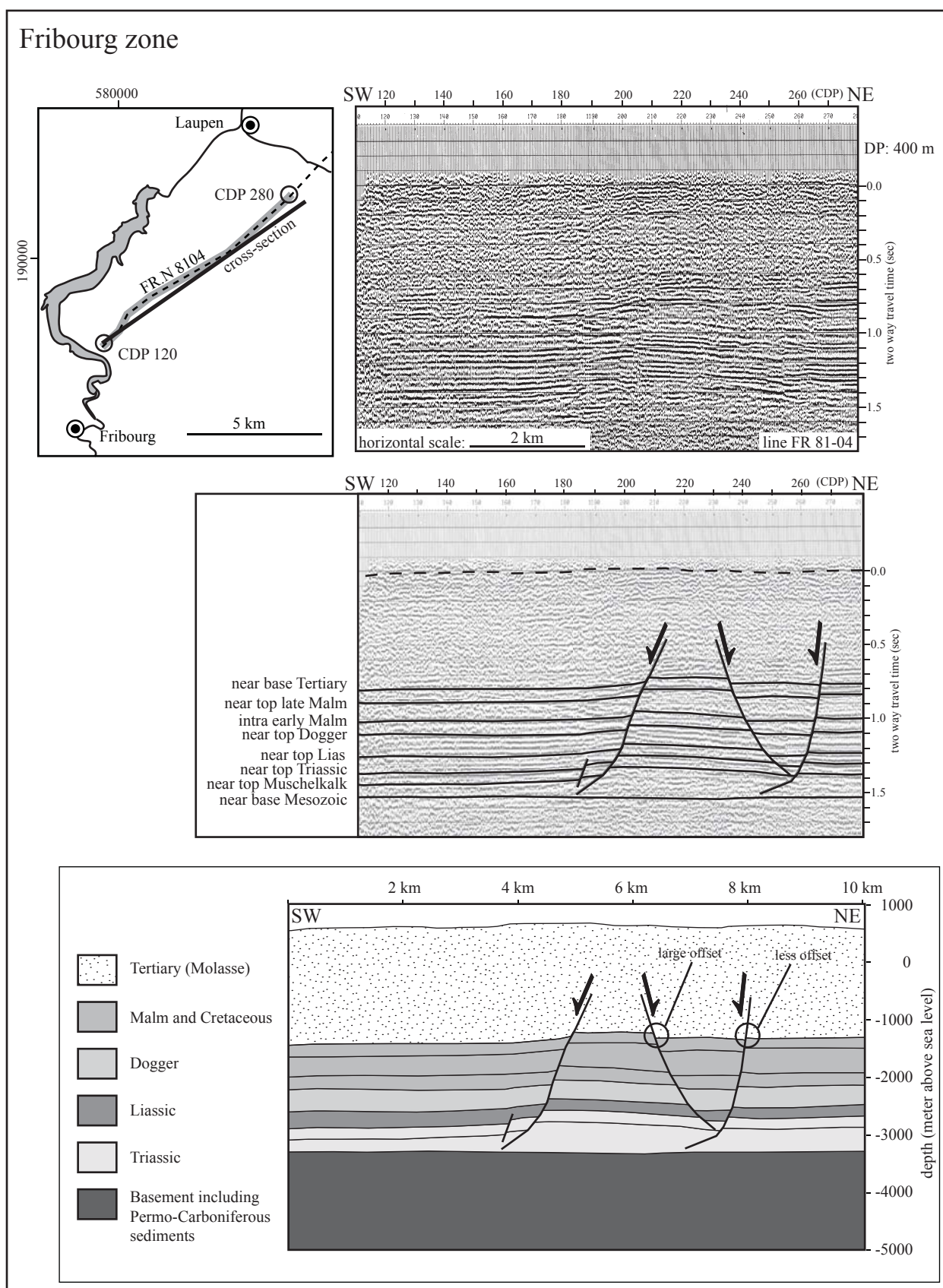


Figure 5.13: Seismic line, interpretation as line-drawing and geologic cross-section of the Fribourg zone. The structures are a horst and an easterly adjacent graben. Note that the graben shows a half-graben configuration and that the secondary fault in the hanging wall of the main fault displays larger vertical offset than the main fault itself. This points to left-lateral overprinting of the southeastwards tilted strata resulting in relative lower (north-) eastern blocks. In this case it increases the total offset of the secondary fault while it decreases the one of the main fault. Seismic interpretation by Sommaruga (2011, personal communication) seismic line from the Canton Fribourg.

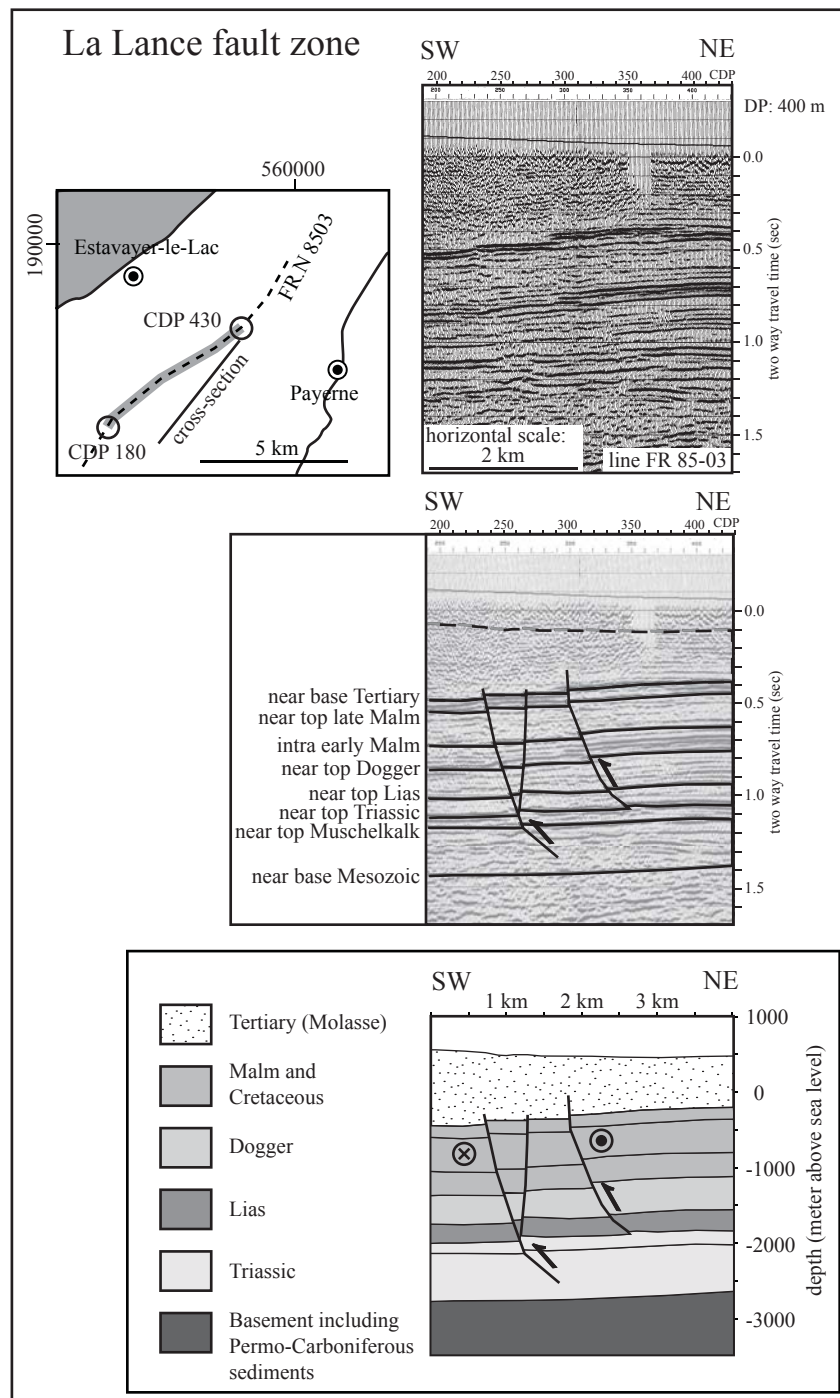


Figure 5.14: Seismic line, interpretation as line-drawing and geologic cross-section of the La Lance fault zone. The structures strike WNW-ESE in map view and appear as reverse faults in cross-section. The higher relative positions of the reflector levels on the northeastern side are consistent with right-lateral offset of the southeasterly tilted strata. According to their shape the faults are likely Riedel shears of a left-lateral transtensional fault zone (Naylor et al. 1986). Seismic interpretation by Sommaruga & Eichenberger (2011c, Sommaruga 2011, personal communication); seismic line from the Canton Fribourg).

N-S as well. Of the three normal faults shown in figure 5.13, only two show a relative down-throw of the western side while the third shows down-throw to the east. This excludes left-lateral strike-slip movement alone, which would result in a synchronous east-side down pattern. Formation of these normal faults is therefore most likely caused by E-W extension rather

than NW-SE compression. If we consider E-W extension and subsequent NW-SE compression, the former N-S-striking normal faults would be reactivated in a left-lateral manner. Given the south-easterly tilt this would increase the vertical offset in cross-section along east-facing normal faults while decreasing it along west-facing normal faults. A close look at the

half-graben structure reveals that in the current situation, the secondary, east-facing normal fault displays larger offset than the west-facing main fault. This strongly indicates a left-lateral reactivation as depicted above.

The structures of the Fribourg zone located in the Mesozoic units were most likely initiated in pre-Molasse times as N-S-striking normal faults. These structures were reactivated by later NW-SE compression while at the same time the overlying Molasse was subject to incipient strike-slip faulting, thus accounting for the seemingly different kinematics. The former normal faults of the Mesozoic units root in the Triassic evaporites.

5.5.2 The La Lance fault – a right-lateral strike-slip fault system

The La Lance fault zone (figure 5.14) is a prominent WNW-ESE-striking right-lateral fault, mapped at the surface in the Jura Mountains (Bertschy 1958, Meia 1966). High resolution seismic survey of the young sediments of Lake Neuchâtel (Gorin et al. 2003) revealed it to continue into the Plateau Molasse.

In the part running through the Plateau Molasse the La Lance fault is clearly expressed in the Mesozoic units. It is cut by three seismic lines, one running perpendicular and the others roughly parallel, indicating two or three faults such as presented in figure 5.14. These faults are relatively steep with listric bends towards NE and a reverse offset in cross-section. The structure roots in the Triassic.

The rare surface outcrops of Tertiary Molasse show strong deformation in a NW-SE compressional and NE-SW extensional setting. A remote surface expression in the Plateau Molasse is given by the contrast of uplands located south of the fault trace to lowlands north of it. The comparatively higher positions of the reflector levels on the northeastern side of the faults in figure 5.14 are consistent with right-lateral offset of the tilted strata. According to their concave shape, the individual faults are likely to represent synthetic Riedel shears of a transtensional fault zone (Naylor et al. 1986).

The La Lance fault zone is a right-lateral fault system corresponding to NW-SE compression. It roots in the Triassic and reaches up to the surface.

5.5.3 The Courtion structure – an inversion and anticlinal structure

The structure as a whole strikes SW-NE and can be traced for about 15 km. It is well-defined on four seismic lines. Interpretation of one of the lines is given in figure 5.15, showing two northwest-facing and one southeast-facing reverse fault crosscutting the Mesozoic units. These faults are steep but not vertically inclined and root in listric bends within the Triassic. Again the Triassic horizon appears to be over-thickened. Figure 5.24 is drawn in its central parts based on a line crossing the structure further northeast, where it appears as a smooth anticline with most of the uplift localised along opposing normal faults. Some of the faults crosscut only the strong horizons and bend into the weak horizons of the lower Malm, Liassic and upper Triassic.

Orientation and kinematics of the reverse structures in the Mesozoic units are in accordance with NW-SE compression. This compression is active in the Neogene, deforming the Molasse units by strike-slip faulting and low-amplitude folding. The Courtion anticline represents such a fold, and is the only mapped surface expression of the Courtion structures in the Mesozoic units. The fact that most of the anticlinal uplift in the Mesozoic level is localised on reverse faults may indicate reactivation tectonics. The low amount of shortening taken up by the low-amplitude folds in the Molasse is likely to be accompanied by folding in the Mesozoic units as well. Instead this shortening may be taken up by reverse faulting if pre-existing normal faults with suitable reactivation orientations exist. We propose that in case of the Courtion structure NE-SW-striking normal faults were present in the Mesozoic units prior to NW-SE shortening, and that these normal faults were indeed reactivated.

5.5.4 The Broye structure – a reactivated graben structure

The Broye structure features a NNE-SSW trending fault zone in the Mesozoic units that is well-constrained by three seismic lines. Figure 5.16 gives interpretations of two lines, both revealing relatively steep faults of listric shape with the hanging walls located on the eastern side. The faults root in the Triassic. The important difference is that offset is reverse in the southern section and normal in the northern one.

Courtion structure

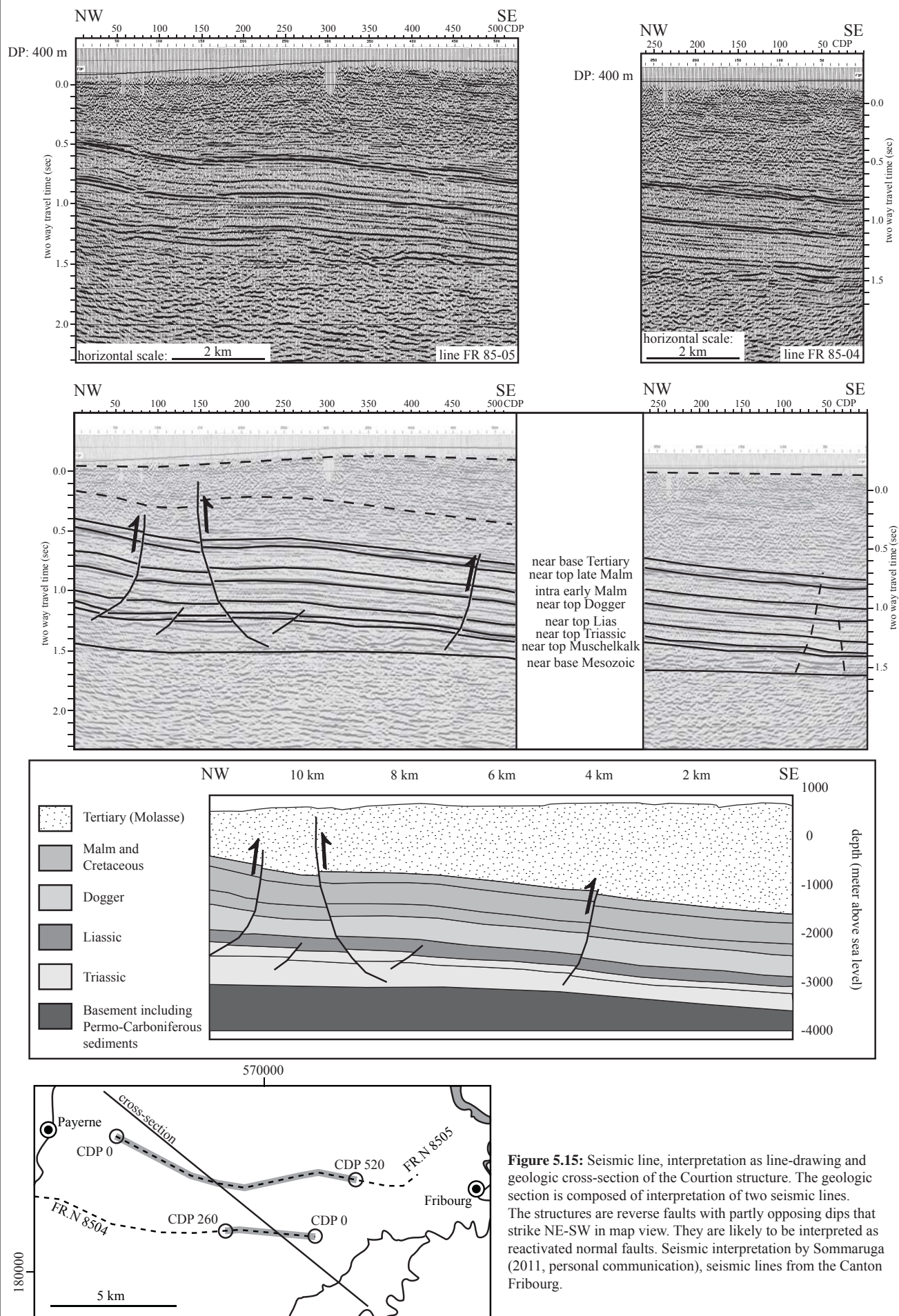


Figure 5.15: Seismic line, interpretation as line-drawing and geologic cross-section of the Courtion structure. The geologic cross-section is composed of interpretation of two seismic lines. The structures are reverse faults with partly opposing dips that strike NE-SW in map view. They are likely to be interpreted as reactivated normal faults. Seismic interpretation by Sommaruga (2011, personal communication), seismic lines from the Canton Fribourg.

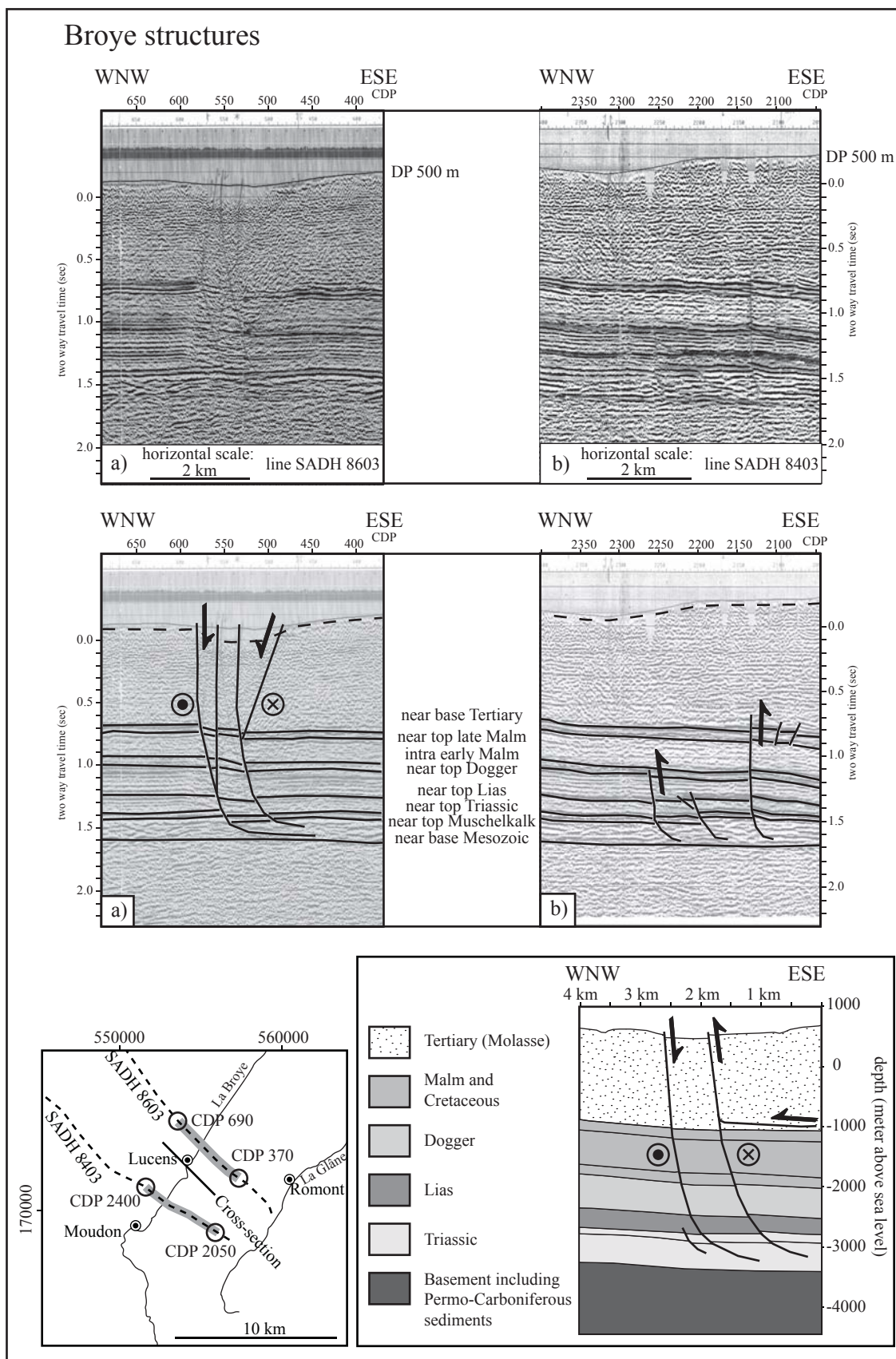


Figure 5.16: Seismic lines, interpretation as line-drawings and geologic cross-section of the Broye structures. The geologic section is interpreted from two seismic lines, a) (line SADH 8603) running parallel 2 km to the north and b) (line SADH 8403) 3 km to the south. The structures are half-graben structures striking NNE-SSW in map view. They are partly reactivated as reverse faults with more reverse offset in the south than in the north. Seismic interpretation by Sommaruga & Eichenberger (2011a and b, Sommaruga 2011, personal communication), seismic lines from the Canton Vaud.

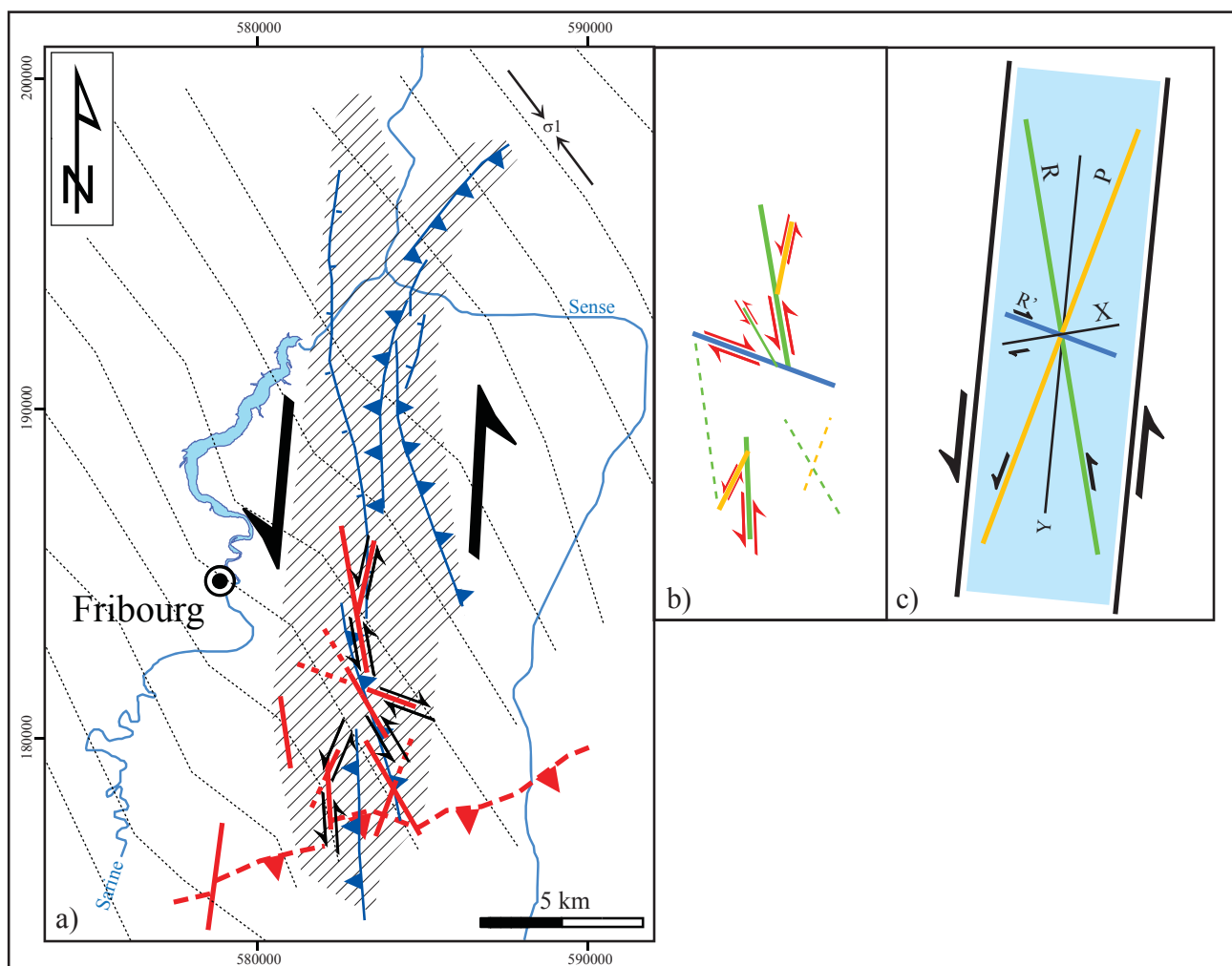


Figure 5.17: a) Tectonic summary sketch of the Fribourg structures. Faults in the Tertiary units are given in red and faults in the Mesozoic units are given in blue. The restriction of Tertiary structures to the southern part may be due to outcrop conditions. The geometry of the Tertiary structures could be interpreted as R-, P- and X-shears of a Riedel-system: b) shows the arrangement of the mapped faults and c) the Riedel-system. Colour coding in b) and c) is the same. Dashed lines correspond to faults without mapped kinematics, narrow lines represent Riedel shears of higher order.

The structures in the Mesozoic units likely extend through the Tertiary Molasse to the surface, accounting for the distinctive wide and straight surface morphology of the Broye Valley. This surface morphology in turn implies that the structure extends northwards into the area south of Payerne. In this case its northern end would form a triple junction with the southern end of the Courtion structure and the eastern end of the La Lance fault zone (figure 5.18). The structures in the southern parts can be characterised as partly inverted half-grabens rooted in the Triassic. In this way the structure is quite similar to the Courtion anticline with the difference that its orientation is slightly less favourable for pure inversion in the Neogene stress field. The structure was therefore re-activated in an oblique left-lateral manner, preserving more of the original normal fault geometries. The interplay with the right-lateral La Lance fault, resulting

in more NW-SE compression to the latter's north than to its south, may additionally have restricted inversion of the Broye structure. This has probably resulted in continued extension in its northernmost parts even in the Neogene stress field.

A number of faults can be mapped in the Tertiary units about 1 km to the east of the eastern edge of the Broye valley. These faults strike ENE-WSW, i.e. parallel to the valley, as well as N-S and show left-lateral movement. They correspond to the Ecublens-Lovatens and Villaraboud-Seigneux fault zones (see subchapter 5.3.6) mapped in the Tertiary Molasse. Both fault zones are restricted to the Tertiary units where they interact with the Broye structure, oriented either parallel (Ecublens-Lovatens) or synthetic (Villaraboud-Seigneux) to it. This interaction most likely lead to segmented oblique uplift of the Tertiary lev-

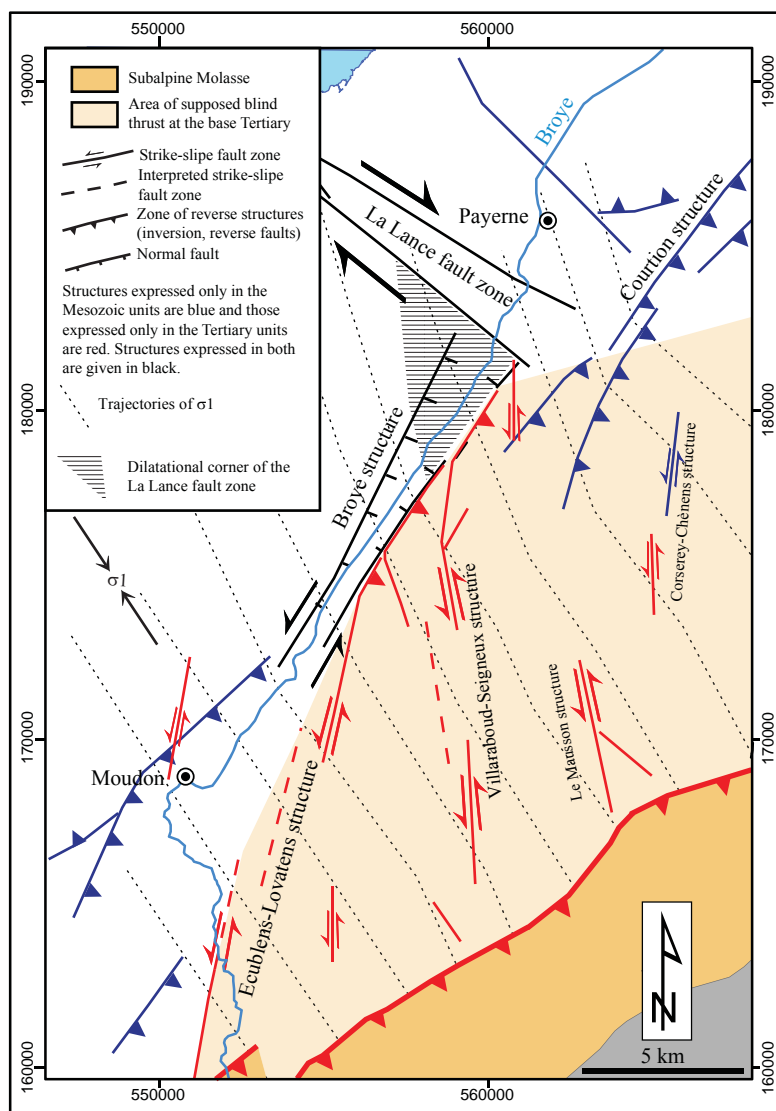


Figure 5.18: Sketch map of the structures in the southern parts of the study area. The structures in the Tertiary Molasse (red) act largely independently above a proposed minor detachment at the base of Tertiary. The area of influence of this minor detachment is given in light yellow. It partly interacts with the Broye structure, reactivating its Tertiary portion by left-lateral transpression. The Broye structure is also well defined in the Mesozoic units (blue) and translates along strike from a half-graben in the north to a reverse fault in the south. The triple-junction of Broye structure, Courton structure and La Lance fault zone is located south of Payerne. The left-lateral movement of the La Lance fault results in a dilatational corner, leading to extension of the northern part of the Broye structure even in the Neogene stress field. The latter is indicated by trajectories of σ_1 , derived from paleostress analysis of slickensides and brittle deformation bands in the Oligocene-Miocene Molasse.

els at the eastern border of the Broye valley (figure 5.18).

5.6 KINEMATIC MODEL

The structures mapped in the Plateau Molasse reveal very brittle deformation conditions. Deformation is nearly exclusively of strike-slip nature, expressed in NW-SE-striking right-lateral-fault planes as well as N-S-striking left-lateral fault planes. These fault planes commonly form conjugate and Riedel-type geometries. Mapped discrete faults are of medium-scale (not more than a few kilometres in length)

and arranged in en-echelon manner, forming superordinate shear zones. These are oriented WNW-ESE and NNE-SSW with right-lateral and left-lateral shear sense, respectively. In addition, very low amplitude folds of NE-SW strike account for a small amount of bulk shortening.

The structures of the deeper levels are revealed by seismic surveys. The structures in the basement are poorly constrained. A strong post-variscan structuring by tectonic lineaments such as known from outcropping basement units in adjacent regions, i.e. the Black Forest massif is very likely. A few widely distributed normal faults of N-S and NE-SW strike are interpreted

by RESUN (2009). The Mesozoic units show N-S and NW-SE-striking normal- and reverse faults as well as NE-SW-striking reverse faults. Part of the former can also be interpreted as strike-slip faults offsetting the southeast wards tilted strata. The NE-SW-striking reverse faults are interpreted as inverted normal faults, while the N-S-striking strike-slip faults represent reactivated normal faults similar in orientation to the normal faults existing in the basement. The kinematic interrelations of the deformation zone network will be discussed in the following.

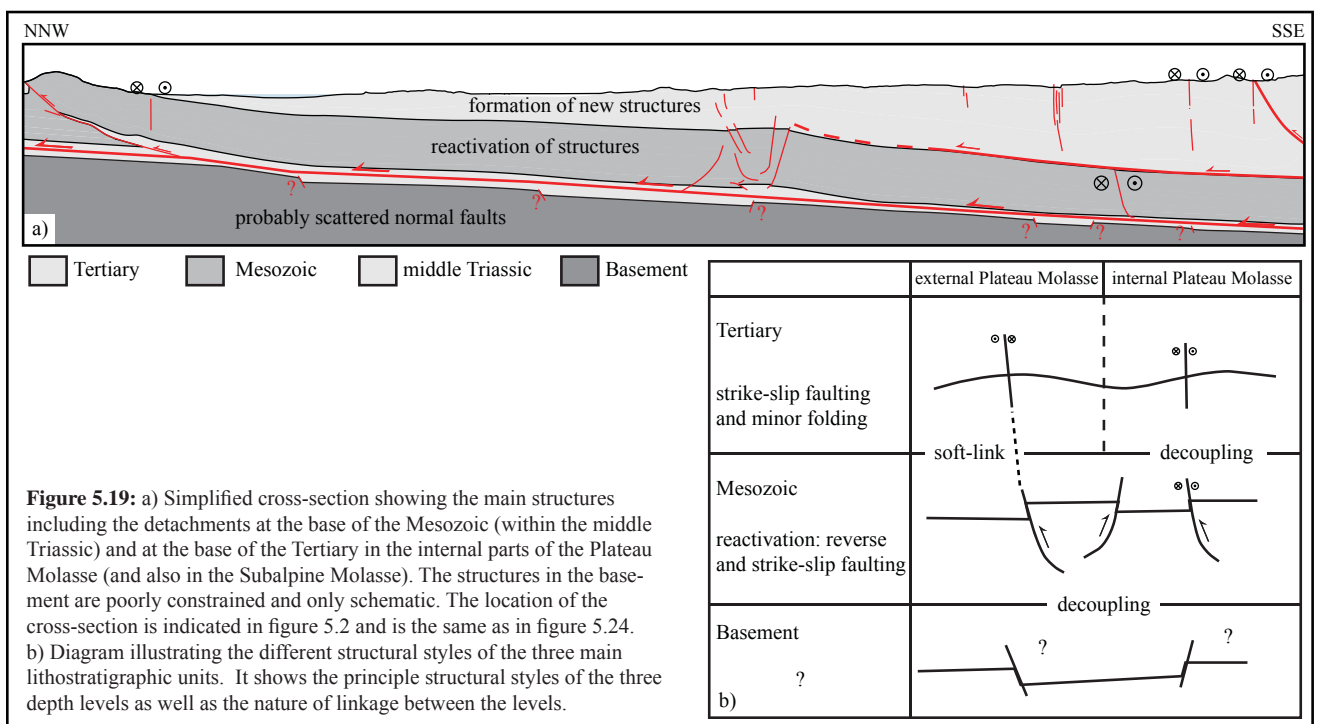
5.6.1 Kinematic decoupling

When considering a thin-skinned origin of the Jura Mountains foreland fold-and thrust belt with a decollement in Triassic evaporites (Buxtorf 1916, Laubscher 1962, Burkhard 1990, Burkhard & Sommaruga 1998), the structures of basement and cover are assumed to be decoupled (figure 5.19). This is indicated by a rather complex pattern of structures in the Mesozoic units as opposed to few widely scattered normal faults in the basement. The Mesozoic units show N-S and NE-SW-striking normal faults but also N-S and NE SW-striking reverse faults and N-S and WNW-ESE-striking strike-slip faults (figure 5.23). A closer look reveals that N-S-striking normal and reverse faults are reactivated as oblique left-lateral faults while the NE-SW-striking reverse faults are most likely inverted normal faults. The decoupling

becomes more obvious by the fact that the basement normal faults seem to have been subjected to no substantial inversion. The Neogene to recent deformation is expressed only in the cover units (figure 5.19).

A kinematic soft-link between the Mesozoic strata and the Tertiary Molasse during Neogene tectonics is obvious since different types of structures developed in response to the same NW-SE shortening. Surface mapping in the Tertiary Molasse revealed only (see subchapter 5.3) N-S-striking left-lateral strike-slip faults and WNW-ESE-striking right-lateral strike-slip-faults. No reverse faulting along NE-SW-striking fault planes was recorded. The only structures of reverse character are NE-SW-striking low amplitude folds. This differences are possibly due to the fact that the Tertiary Molasse lacks pre-existing structures and hence reactivation tectonics.

The only location of substantial reverse tectonics in the Tertiary Molasse is the border to the Subalpine Molasse, though it corresponds to initial thrusting rather than to inversion. It furthermore completely decouples the Tertiary units from the Mesozoic substratum. In addition the structures east and south of the Courtion and Broye structures are developed in the Tertiary units only (figures 5.18 and 5.20), which points to a decoupling of Mesozoic and Tertiary units in the most proximal parts of the Plateau Molasse. Such decoupling is presumably linked to most external deformation of the Subalpine Molasse basal thrust.



This Subalpine Molasse basal thrust has a blind termination about 10-15 kilometres north of the Subalpine Molasse surface thrusts. This is similar to triangle structures observed further east (Vollmayr & Wendt 1987, Müller et al. 1988, Pfiffner et al. 1997, Berge & Veal 2005).

5.6.2 Kinematic interactions of the cover structures

The kinematic interaction of the cover structures are presented in figure 5.20. The left-lateral and right-lateral fault zones described above correspond to NW-SE shortening with strike-slip deformation. Re-

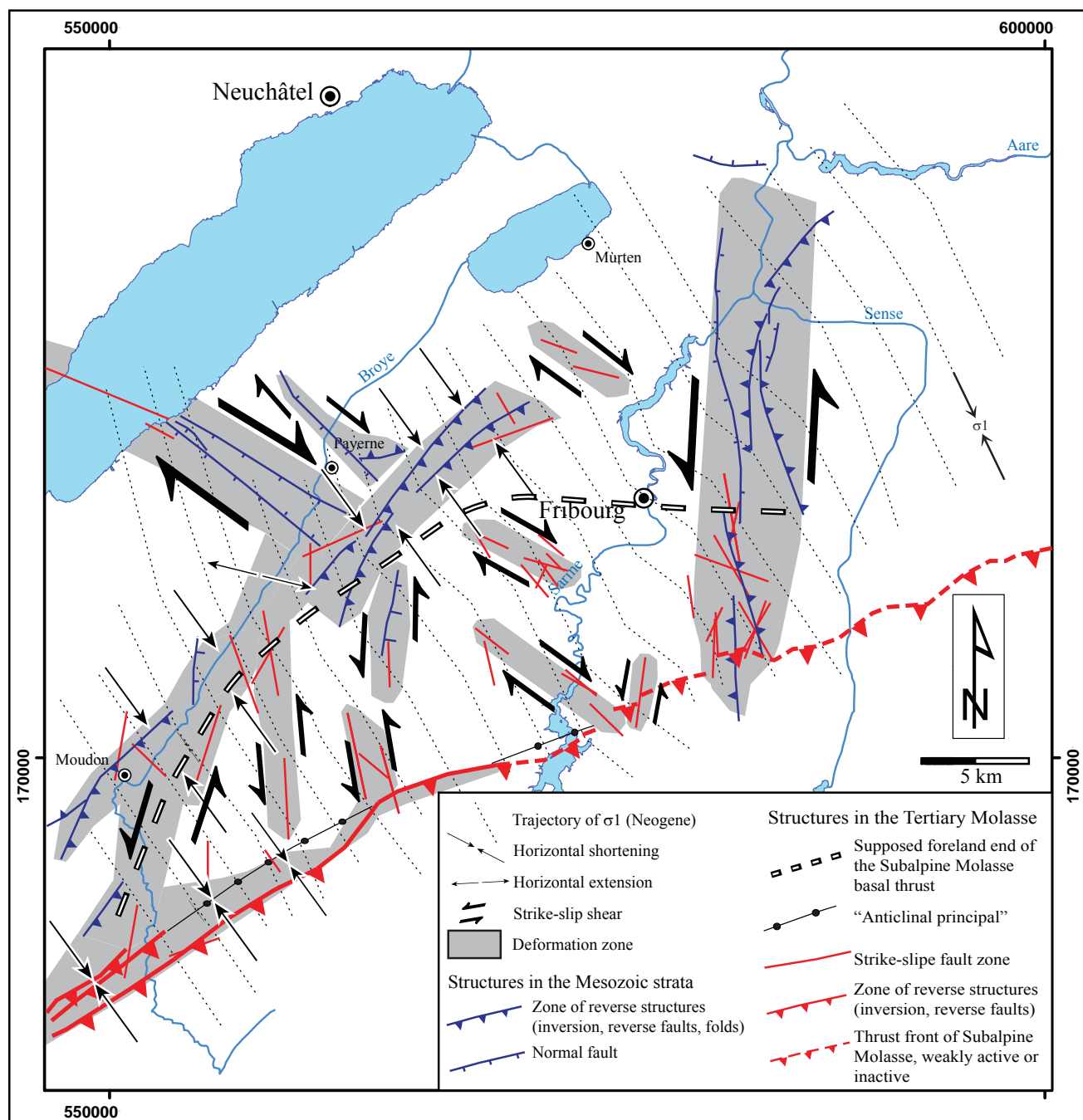


Figure 5.20: Kinematic interpretation of larger structures in the cover units active in the Neogene. Faults in the Mesozoic strata after RESUN 2009, Sommaruga et al. (2011, in prep.), Sommaruga (2011, personal communication).

verse faulting took place only where it was facilitated by pre-existing weak zones; this is the case at depth in the pre-structured Mesozoic.

The Courtion structure and the Broye structure form a continuous zone of horizontal shortening, interrupted only by the eastern end of the La Lance fault zone. The left-lateral shear along the La Lance fault zone leads to more shortening of the Courtion structure than of the Broye structure. The northern parts of the latter are even extensional as the southern block of the La Lance fault moved westwards, forming a dilatational corner. Young shortening in the Tertiary level along the thrust front of the Subalpine Molasse is transferred to the Tertiary portions of the Broye structure by left-lateral shear along the Ecublens-Lovatens structure. Thus this structure functions at least partially as a lateral ramp to the minor detachment along the base of the Tertiary units. Similar geometric-kinematic constellations can be assumed for the Villaraboud-Seigneux structure.

The major strike-slip zones such as the Fribourg zone and the La Lance fault zone are expressed in both Tertiary and Mesozoic units and represent the general strike-slip nature of deformation. In contrast the zones of Ecublens-Lovatens, Villaraboud-Seigneux, Le Mausson, and La-Glâne-Rossens-La Roche are expressed only in the Tertiary units, indicating a partial decoupling of Mesozoic and Tertiary units along the northernmost reaches of the Subalpine Molasse basal thrust (figures 5.18 and 5.24). North of the blind end of the Subalpine Molasse basal thrust, structures in the Mesozoic and Tertiary strata are more closely linked. However, the reactivation of pre-existing structures in the former and the initiation of new structures in the latter require a certain degree of decoupling.

5.6.2.1 *Kinematics in adjacent areas*

To the north of the study area, the Molasse units are more intensely folded in the transition region to the Jura Mountains ("Sub-Jurassische zone"). Recent studies (RESUN 2009) revealed that the N-S oriented strike-slip fault zones present in the eastern parts of the study area are in fact lateral ramps that bend into reverse faults underlying these folds.

West of the study area, the Vallorbe-Pontarlier zone represents a prominent N-S-striking left-lateral fault crossing through the Jura Mountains (Heim 1915, Aubert 1959, Homberg 1997) and continuing

into the Molasse. It forms a conjugate fault system with NE-SW oriented faults. Examples of the thus formed triangular structures are well known from the region of Yverdon-les Bains located in the transition between Plateau Molasse and Jura Mountains (Jordi 1951, 1990). Some of these structures translate into reverse faults by bending into a NE-SW orientation (e.g. Essertine-Bruchzone into the Pomy-Cuarny-Aufschiebung, Jordi 1990, Sommaruga 1997, Muralt et al. 1997).

The La Lance fault and the Fribourg zone in the study area are comparable in size and orientation to these conjugate networks. Other fault zones, especially the ones mapped only in the surface outcrops of the Tertiary Molasse, are also conjugated but smaller in size. Little is known about structures in the Plateau Molasse to the northeast of the study area. In the transition region between Plateau Molasse and Jura Mountains as well as in the Jura Mountains, strike-slip faulting is less prominent, associated with folding rather than indicating a different tectonic domain. With strike-slip deformation becoming more important towards southwest, the study area takes up an intermediate position (figure 5.21).

5.7 DISTRIBUTION OF ACTIVE SEISMIC FAULTING IN THE STUDY AREA

The regional distribution of historical and instrumentally recorded earthquakes is given by the Seismic Survey of Switzerland (SED) and plotted in figure 5.22. The spatial arrangement of focal mechanisms may provide important clues to the location of active faulting. The "Fribourg lineament" is clearly visible as a N-S alignment of foci, but further clusters and lineaments can also be defined. A rather diffuse zone is traverses southern part of Lacke Neuchâtel along the La Lance fault zones and continues into the Molasse Basin. A cluster in the northern Lake Neuchâtel is slightly elongated in a N-S direction and probably connects northwards with the focal mechanisms that are aligned with N-S-striking fault zones in the Vue des Alpes area. Active faulting is furthermore indicated by earthquakes for the fault zones in the region south of Yverdon-les-Bains and for the southern parts of the Pontarlier fault zone, as well as along the Courtion structure and the Ecublens-Lovatens structure. In the central study area between the Sarine and Broye rivers, epicentres are scattered. Such a scattered occurrence may correspond to a smaller-scaled conjugate network of fault zones.

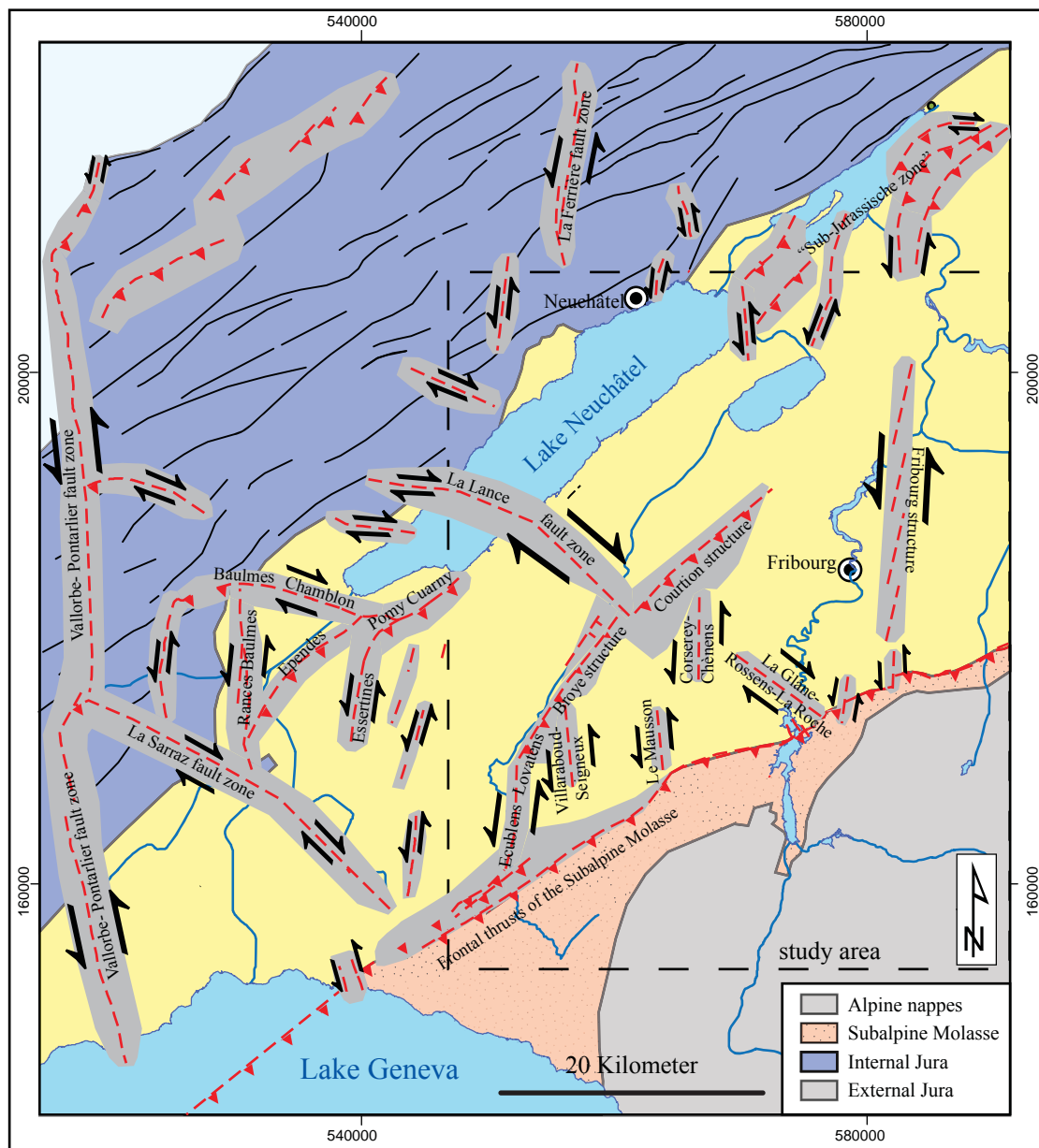


Figure 5.21: Map of the western Swiss Molasse basin and the central Jura Mountains with major structures. Larger strike-slip fault zones are dominant towards southwest, while lateral ramp structures are typical near the southern edge of the Jura Mountains in the northeast. The study area shows fewer larger and minor strike-slip fault zones as well as a zone of reverse faulting located in the Plateau Molasse. Minor lateral ramp structures are developed at the transition between strike-slip and reverse zones. Names of fault zones after Heim (1915), Jordi (1990), Sommaruga (1997) and this chapter.

Due to the fact that most earthquakes are low in magnitude, their focal depths are not well-constrained, making it difficult to link seismicity to specific faults. However, some focal mechanisms could be defined (Deichmann et al. 2004, 2010, Bear et al. 2007, Kastrup et al. 2007) for earthquakes originating within the Fribourg lineament as well as within the Neuchâtel cluster. The focal depths are shallow and the mechanism is strike-slip related to NW-SE compression and NE-SW extension.

5.7.1 Implications of fault network characteristics for possible earthquake magnitude

The detailed structural investigation of the western Swiss Plateau Molasse revealed that Neogene compression tectonics are restricted to the cover units where they are expressed in a network of reverse and strike-slip shear zones. The surface mappings showed these shear zones to be composed of medium-scale

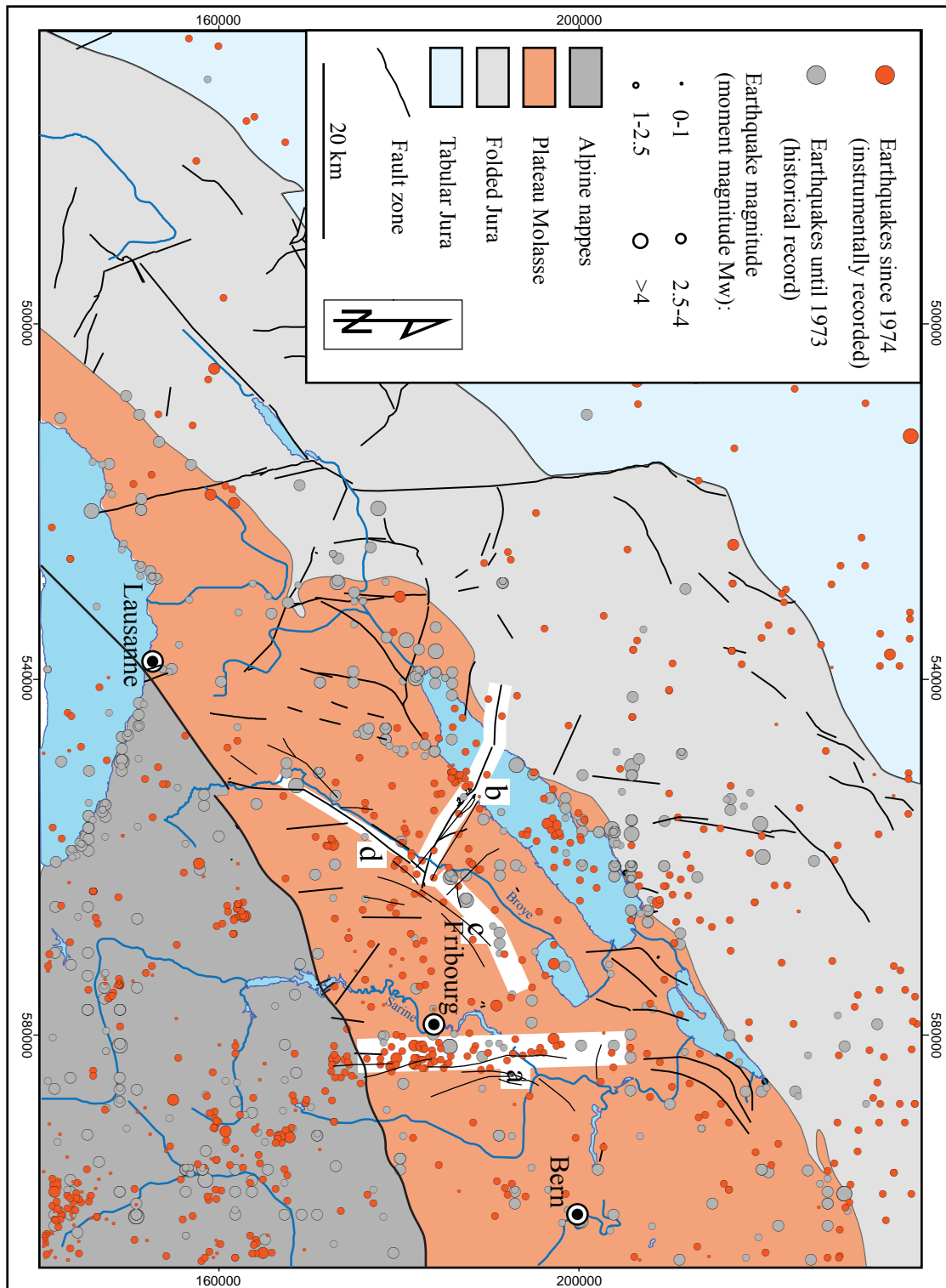


Figure 5.22: Tectonic map of the western Swiss Molasse Basin and the central Jura Mountains with epicentres of instrumentally and historically recorded earthquakes (SED 2010). A certain alignment of earthquake activity with the structures discussed in this chapter is obvious. The N-S striking Fribourg structure (a), the La Lance fault zone (b), but also the Courtion structure (c) and the Broye structure (d) host earthquakes. The scattered epicentres between the Rivers Sarine and Broye may be related to the smaller scale fault zones in that area.

discrete faults arranged en-echelon as synthetic and antithetic Riedel shears. The instrumentally and historically recorded epicentres of the area are partly aligned with these shear zones. Their relative low magnitudes and short recurrence times fit well with an activity distributed on rather small faults among which the overall shear is partitioned. Riedel shear zones develop by successive connection of the individual shears towards anastomosing fault zones with continuous bended faults (Naylor et al. 1986). In addition earthquake magnitude scales positively with rupture surface (Wells & Coppersmith 1994). Therefore it cannot be excluded that fault connection during seismic rupture will successively increase the potential magnitude by the increase of rupture surface. However, most of the structures are covered and it is difficult to determine the current evolutionary stage of the shear zones. Any such increase would furthermore occur step-wise in time.

5.8 TECTONIC EVOLUTION

The paleo-stress field revealed by the mapped slickensides and DBs in the Tertiary Molasse shows uniform NW-SE compression (figure 5.6). This is in accordance with the stresses derived from the orientation of large-scale fold-and thrust structures in the Jura Mountains (Laubscher 1972). The Mesozoic units and the basement reveal additional E-W and NW-SE extension (figure 5.23) predating the deposition of the Oligocene-Miocene Molasse in which it is not recorded. E-W extension was reported as the central European stress field in Eocene-Oligocene times (Bergerat 1987, Homberg et al. 2002, Madritsch et al. 2009), corresponding to pre- and syn-Molasse deposition. Laubscher (1987) attributed smooth, often flexure-type Paleogene folding in the region of the future Jura Mountains (Liniger 1967, Aubert 1958) to extensional block tectonics that created scattered small-scaled irregularities. According to Laubscher (2008), these irregularities are responsible for the location of fold initiation during later decollement tectonics. A local deviation of the E-W extensional stress field towards NW-SE extension could probably be caused by lithospheric flexure during forebulge and foreland basin formation (Bradley & Kidd 1991), resulting in formation of basin-parallel normal faults corresponding to pre-and syn-Molasse sedimentation. Since unambiguous indicators of growth faults are lacking in

the Mesozoic units, we favour an Eocene-Oligocene age for the formation of the N-S and NE-SW oriented normal faults.

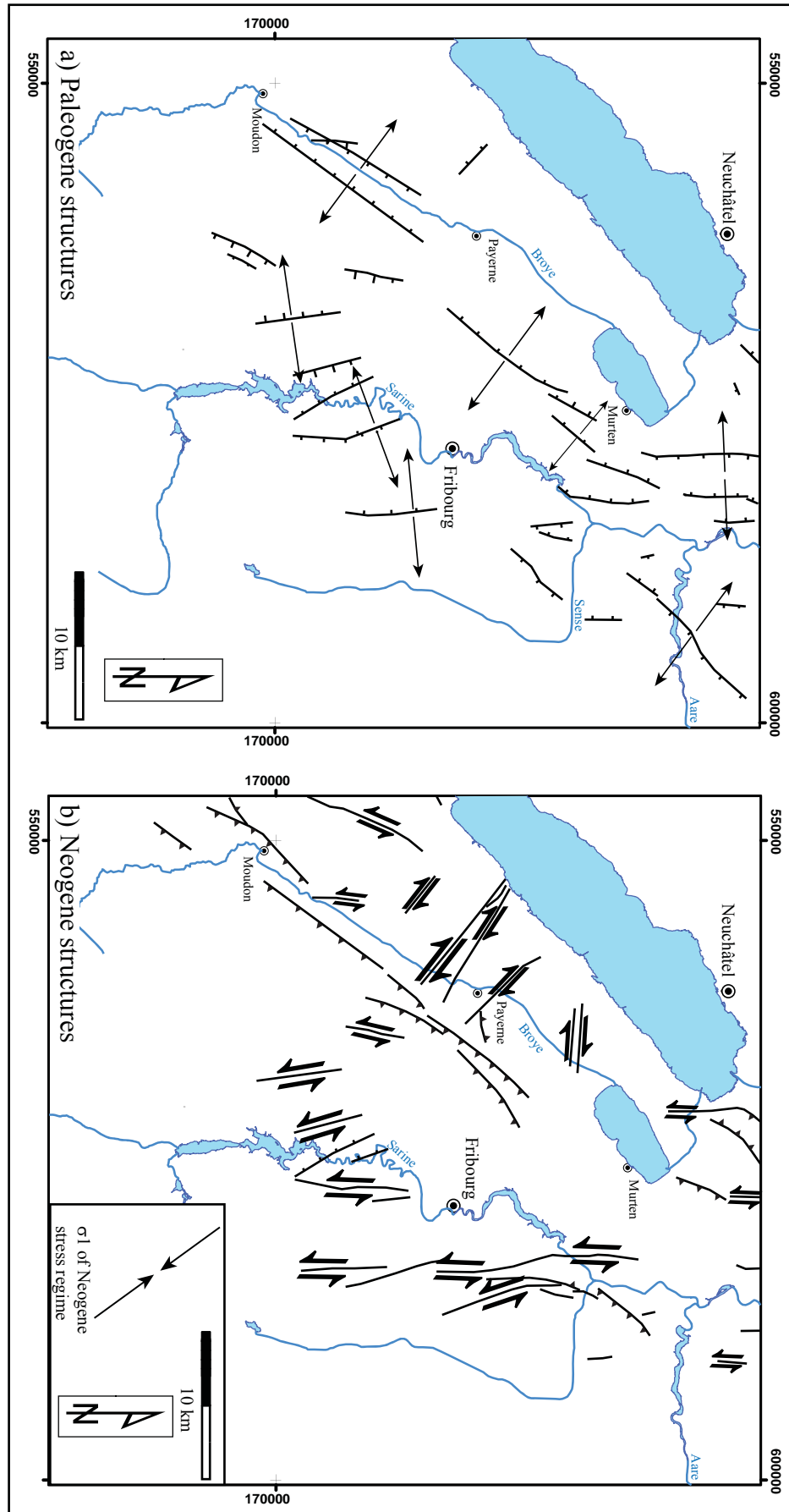
The NW-SE compression is expressed as strike-slip faults in the surface outcrops of the Oligocene-Miocene Molasse and by inversion and reactivation of the extensional structures in the Mesozoic units. This reactivation does not seem to invert existing basement structures in the study area, although this possibility has been discussed (Pfiffner et al. 1997, Mosar 1999). The NW-SE compression is detached along Triassic evaporites and is therefore thin-skinned in character (figure 5.24).

The seismicity of the area reveals a neotectonic stress field of NW-SE compression expressed by strike-slip faulting in accordance with the structures and paleo-stress orientation derived from field mapping. Furthermore the distribution of epicentres mostly corresponds to mapped and interpreted larger structures, revealing deformation under NW-SE compression to still be active.

The deposition of the Molasse sequences took place in Oligocene and Miocene times (Trümpy 1980, Berger et al. 2005) and was accompanied by basin-parallel normal faulting to the east (Laubscher 1978, Bachmann et al. 1987, Bachmann & Müller 1992) and by folding to the southwest (Beck et al. 1998) of the study area. Detailed studies of the sedimentary geometries of basin-parallel structures (i.e. oriented NE-SW) within the study area, such as the Courtion structure, should provide the information to be able to assign the area to either the normal faulting regime or the folding regime of that time. However, at the moment resolution of the seismic data is too poor to unambiguously determine onlap structures and to relate them to growing folds rather than to the expected onlaps onto the tilted basin floor. Therefore the exact timing of onset of NW-SE compression remains unclear in the study area, though the existence of inverted faults rather than folds in the Mesozoic strata makes preceding normal faulting implicit.

The thin-skinned Neogene deformation corresponds to the formation of the Jura Mountains-Molasse Basin foreland fold-and-thrust belt above a decollement located in Triassic evaporites (Buxtorf 1916, Laubscher 1961, Burkhard 1990, Burkhard

Figure 5.23: a) Structures in the pre-Molasse units not compatible with the Neogene stress field. These are normal faults indicating E-W and NW-SE extension, and therefore likely related to the Eocene-Oligocene stress field. b) Structures in the pre-Molasse units active in the Neogene. Paleogene normal faults of NE-SW strike were inverted and those of N-S strike reactivated by left-lateral strike slip. Right-lateral faults in the cover units are newly formed. After RESUN 2009, Sommaruga et al. (2011, in prep.), Sommaruga (2011, personal communication).



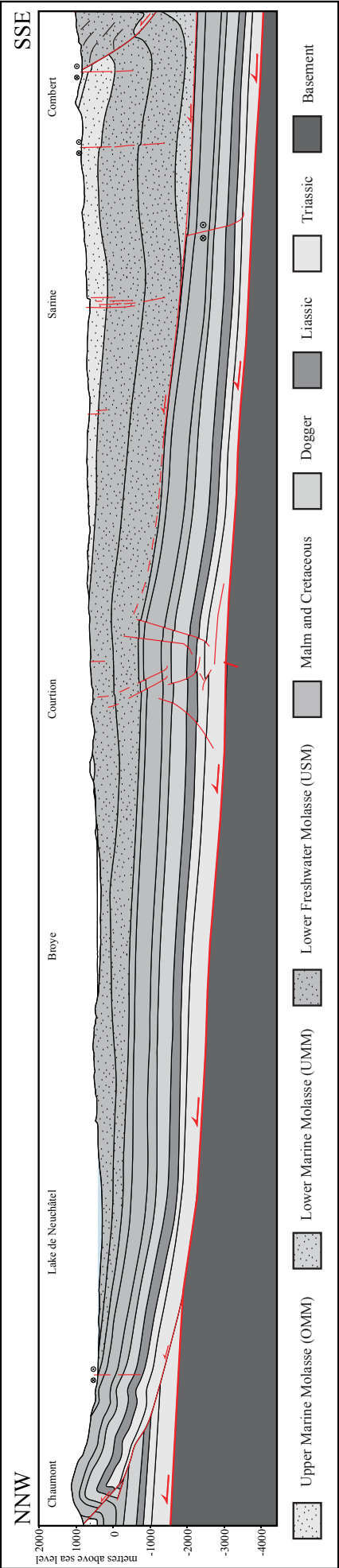


Figure 5.24: Cross-section through the western Swiss Molasse Basin in the region of Fribourg, compiled from surface data, seismic interpretation data and literature. See figure 5.2, for location. Data from Emmenegger (1962), Sommaruga (1997), Plancherel (1998), Weidmann (2002), RESUN (2009), Sommaruga et al. (2011, in prep.) and Sommaruga (2011 personal communication).

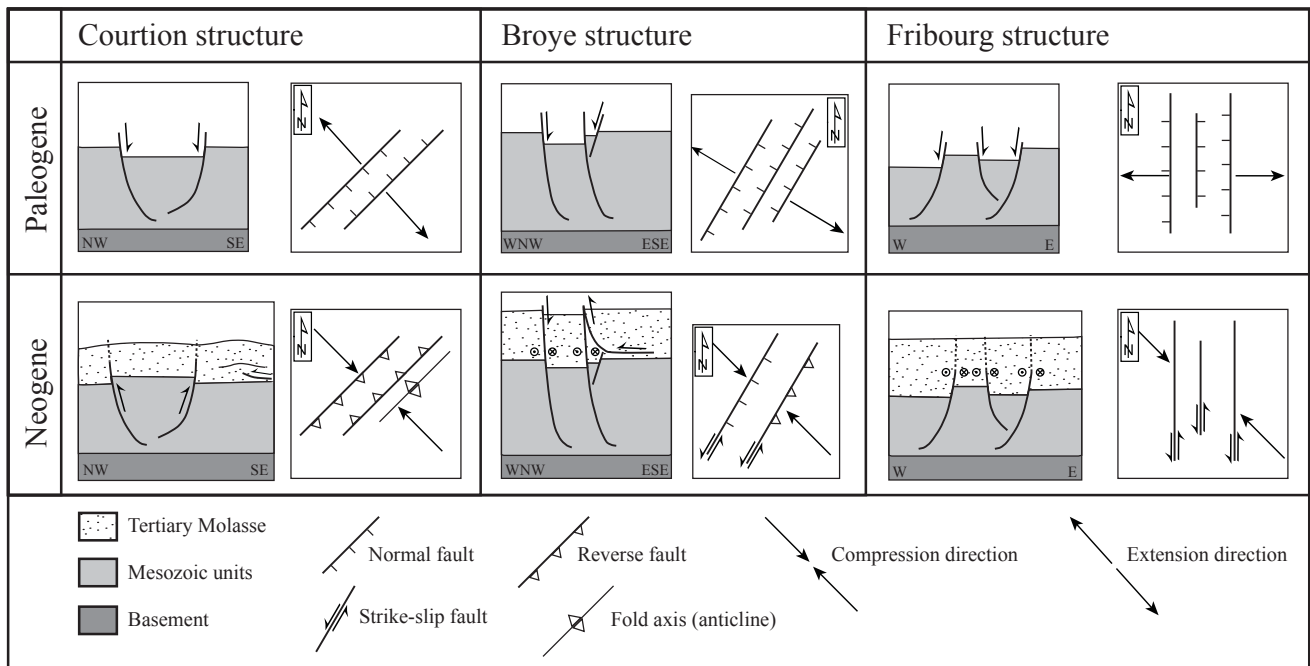


Figure 5.25: Tectonic evolution of Paleogene and Neogene structures, illustrated with the help of diagrammatic sketches for the Courtion, Broye, and Fribourg structures. Paleogene NW-SE extension (Courtion and Broye structure) and E-W extension (Fribourg structure) lead to inversion (Courtion structure), oblique inversion (Broye structure) and reactivation by left-lateral strike-slip (Fribourg structure) during Neogene NW-SE compression. Note the blind end of a detachment at the base of the Tertiary Molasse near the Courtion structure and the interaction between this detachment and the Broye structure.

& Sommaruga 1998). However, the strike-slip and reverse faulting in the cover of the Plateau Molasse corresponds to less shortening than the folds and thrusts of the Jura Mountains (Burkhard 1990). Since the Molasse Basin is located in a more internal position than the Jura Mountains, this lack of shortening has to be compensated by passive transport along the decollement. Nevertheless, strike-slip faults do exist in the Jura Mountains as well, where they show syn- and post folding characteristics (Heim 1915, Aubert 1959, Sommaruga 1997). The strike-slip mechanisms of earthquakes further indicates strike-slip faulting to be by trend younger than folding and passive transport. The foreland fold-and-thrust belt evolution is therefore characterised by a change in style of deformation: while shortening of the external parts (Jura Mountains) and passive transport of the internal parts (Molasse Basin) prevailed in the first stage, the second stage is characterised by strike-slip faulting of both Jura Mountains and Molasse Basin. This change is gradual and probably reflects a shift of the tectonic regime from reverse to strike-slip. Nevertheless some degree of reverse faulting and folding still prevails in the second stage. In the study area these are localised at parts of the Subalpine thrust front as well as along the Courtion and Broye structures where pre-existing weak zones of favourable orientation exist in the Mesozoic strata. Furthermore recent folding of the Mesozoic was also reported for the external Jura Mountains

(Madritsch et al. 2010b).

The causes leading to subdivision of early deformation into external shortening and internal passive transport, as well as those for a later change to strike-slip faulting, remain speculative. The spatial subdivision was attributed to the wedge shape of the foreland sediments, where the thick overburden formed by the Molasse sediments precluded folding in the internal parts (Sommaruga 1997, Burkhard & Sommaruga 1998). Folding and thrusting of the more internal Subalpine Molasse took place on top of a shallower detachment (base Tertiary) and was therefore not precluded by such a thick overburden. The change from passive transport to internal deformation of the Plateau Molasse was accompanied by the change of the mode of deformation from reverse to strike-slip. In addition ongoing erosion and subsequent thinning of the Molasse sequences since the onset of Neogene NW-SE compression (Kuhlemann & Kempf 2002, Schlunegger & Mosar 2010) possibly made the internal parts susceptible to deformation.

The occurrence of thick-skinned reverse faulting at the frontal part of the Jura Mountains could be related to the existence of Permo-Carboniferous troughs and hence to reactivation of pre-existing weak zones (Madritsch et al. 2008, Ustaszewski & Schmid 2007). The question arises why Paleogene normal

faults situated in the basement underneath the Molasse Basin were not subjected to similar reactivation. Compared with these normal faults, the Permo-Carboniferous troughs are large-scale structures which greatly influenced the formation of the European Cenozoic rift system in Eocene times and hence are the locus of multiple fault reactivations (Ziegler 1992, Madritsch et al. 2009). The recent external reverse tectonics were also speculated to represent the near-surface continuation of deep-seated thrust activity within the basement in order to maintain critical wedge stability (Ustaszewski & Schmid 2007, Mosar 1999). Such deep-seated thrust tectonics would probably be ductile in nature, while the hanging-wall blocks behave rigidly and probably passively as well. However, based on this study alone, the response of the basement underneath the western Molasse Basin to Neogene tectonic stresses remains speculative.

5.9 CONCLUSION

Structural field work in the Plateau Molasse of western Switzerland revealed a brittle deformation expressed by left-lateral and right-lateral strike-slip faulting on N-S and WNW-ESE-striking fault planes, respectively. The related paleo-stress field exhibits uniform NW-SE compression and NE-SW extension. The mapped faults can be interpreted as forming zones of strike-slip shear that act on a regional-scale. Strain along these zones is partitioned on networks of mapped medium-scale faults rather than localised along large discrete lineaments.

The basement structures are poorly constrained by the seismic surveys and no Permo-Carboniferous grabens are evident. In contrast, the Mesozoic units shows NE-SW-striking reverse faults as well as N-S and WNW-ESE-striking faults that appear with normal and reverse offsets in the seismic sections. Most of these offsets, however, can be attributed to strike-slip faults offsetting the southeastward tilted strata. The NE-SW and N-S-striking faults in the Mesozoic strata partly reveal geometric evidence for being reactivated former normal faults. Despite the thrust front of the Subalpine Molasse, no reverse fault structures and no fault structures of NE-SW strike are present in the Tertiary Molasse, identifying these structures as prior to Molasse deposition.

The tectonic evolution of the study area (figure 5.25) is characterised by an extensional phase followed by a phase of compression. The Molasse deposits are only affected by the second phase. Paleogene E-W extension is attributed to the Eocene stress field in central Europe as well as to extension during basin formation in the Oligocene. It resulted in normal faults of E-W and NE-SW strike in the Mesozoic units and probably in the basement as well. Neogene NW-SE compression is related to the Jura Mountains formation and is still ongoing. It left the basement unaffected and is hence thin-skinned in nature. This decollement tectonics was characterised by fold-and-thrust-related shortening of the external parts and passive transport of the internal parts including the Molasse Basin. The mode of shortening changed to strike-slip faulting during the Neogene, affecting the whole detached wedge. In the less deformed internal parts represented by the Molasse Basin, the Mesozoic units responded to Neogene NW-SE compression by reactivation of Paleogene normal faults while new faults formed in the previously un-deformed Molasse units.

The structures of the three depth levels are combined in a kinematic model that is characterised by complete decoupling of basement and cover as the former lacks Neogene compression structures. The Mesozoic and Tertiary level of the cover sequences are different in structural style. In the Mesozoic units, reactivation tectonics prevail and shortening is compensated by reverse faulting. In contrast, the Tertiary Molasse is characterised by initial faulting in strike-slip manner and a bulk shortening compensated by folding. Additionally a small-scale detachment-related decoupling is probable in the internal parts of the Plateau Molasse, representing the most external branch of the Subalpine Molasse basal thrust.

The distribution of epicentres reveals that active faulting is localised in mapped deformation zones. The earthquake magnitudes are low to moderate, corresponding to the medium size of the discrete faults onto which strain is partitioned within the deformation zones. Possible future earthquake magnitudes are a question of the exact fault network properties and the rate of ongoing deformation.

REFERENCES

- Affolter, T., Gratier, J.P. 2004. Map view retrodeformation of an arcuate fold-and-thrust belt: The Jura case. *Journal of Geophysical Research*, 109(B03404): doi: 10.1029/2002JB002270.
- Ahlgren, S.G. 2001. The nucleation and evolution of Riedel shear-zones as deformation bands in porous sandstone. *Journal of Structural Geology*, 23, 1203-1214.
- Ahorner, L., Schneider, G. 1974. Herdmechanismen von Erdbeben im Oberrhein-Graben und seinen Randgebirgen. In: Illies, H., Fuchs, K. (Eds): *Approaches to Taphrogenesis*, Schweizerbart, Stuttgart, 104-117.
- Allen, P.A., Crampton, S.L., Sinclair, H.D. 1991. The inception and early evolution of the North Alpine Foreland Basin, Switzerland. *Basin Research*, 3, 143-163.
- Allenbach, R.P., Wetzel, A. 2006. Spatial patterns of Mesozoic facies relationships and the age of the Rhenish Lineament: a compilation. *International Journal of Earth Sciences*, 95, 803-813.
- Angelier, J. 1979. Determination of the mean principle direction of stresses for a given fault population. *Tectonophysics*, 56, T17-T26.
- Angelier, J. 1994. Fault Slip Analysis and Paleostress Reconstruction. In: Hancock, P.L. (Ed.), *Continental Deformation*. Pergamon Press, pp. 53-100.
- Angelier, J., Mechler, P. 1977. Sur une méthode graphique de recherche des contraintes principales également utilisable en tectonique et en seismologie: la méthode des dièdres droits. *Bulletin de la Société géologique de France*, 19, 1309-1318.
- Antonellini, M.A., Aydin, A., Pollard, D.D., 1994. Microstructure of deformation bands in porous sandstones at Arches National Park, Utah. *Journal of Structural Geology*, 16, 941-959.
- Antonellini, M.A., & Aydin, A. 1994. Effect of faulting on fluid flow in porous sandstones: petrophysical properties. *Bulletin of the American Association of Petroleum Geologists*, 78, 355-377.
- Aubert, D. 1958. Sur l'existence d'une ride de plissement oligocène dans le Jura vaudoise. *Bulletin Société neuchâteloise des Science Naturelles*, 81, 47-54.
- Aubert, D. 1959. Le décrochement de Pontarlier et l'orogénèse du Jura. *Mémoires de la Société vaudoise des Science Naturelles*, 12, 93-152.
- Avakian, A.J. 1986. Mirror-quality polished fault surfaces from the Last Chance Range, East California. *Geological Society of America Abstracts with Program*, 18, 530.
- Aydin, A. 1978. Small faults formed as deformation bands in sandstone. *Pure and Applied Geophysics*, 116, 913-930.
- Aydin, A. & Johnson, A.M. 1978. Development of faults as zones of deformation bands and as slip surfaces in sandstones. *Pure and Applied Geophysics*, 116, 931-942.
- Aydin, A. & Johnson, A.M. 1983. Analysis of faulting in porous sandstones. *Journal of Structural Geology*, 5, 19-31.
- Bachmann, G.H., Müller, M. Weggen, K. 1987. Evolution of the Molasse Basin (Germany, Switzerland). *Tectonophysics*, 137, 77-92.
- Bachmann, G.H. Müller, M. 1992. Sedimentary and structural evolution of the German Molasse Basin. *Eclogae geologicae Helveticae*, 85, 519-530.
- Baer, M., Deichmann, N., Fäh, D., Kradolfer, U., Mayer-Rosa, D., Rüttener, E., Schler, T., Sellami, S., Smit, P. 1997. Earthquakes in Switzerland and surrounding regions during 1996. *Eclogae geologicae Helveticae*, 90, 557-567.
- Baer, M., Deichmann, N., Braunmiller, J., Ballarin Dolfi, D., Bay, F., Bernardi, F., Delouis, B., Fäh, D., Gerstenberger, M., Giardini, D., Huber, S., Kastrup, U., Kind, F., Kradolfer, U., Maraini, S., Mattle, B., Schler, T., Salichon, J., Sellami, S., Steimen, S., Wiemer, S. 2001. Earthquakes in Switzerland and surrounding regions during 2000. *Eclogae geologicae Helveticae*, 94, 253-264.
- Baer, M., Deichmann, N., Braunmiller, J., Husen, S., Fäh, D., Giardini, D., Kästli, P., Kradolfer, U., Wiemer, S. 2005. Earthquakes in Switzerland and surrounding regions during 2004. *Eclogae geologicae Helveticae*, 98, 407-418.
- Baer, M., Deichmann, N., Braunmiller, J., Clinton, J., Husen, S., Fäh, D., Giardini, D., Kästli, P., Kradolfer, U., Wiemer, S. 2007. Earthquakes in Switzerland and surrounding regions during 2006. *Swiss Journal of Geoscience*, 100, 517-528.
- Bartlett, W.L., Friedman, M., Logan, J.M. 1981. Experimental folding and faulting of rocks under confining pressure. Part IX. Wrench faults in limestone layers. *Tectonophysics*, 79, 255-277.

- Bayerlee, J.D., Brace, W.F. 1968. Stick Slip, Stable Sliding, and Earthquakes- Effect of Rock Type, Pressure, Strain Rate, and Stiffness. *Journal of Geophysical Research*, 73, 6031-6037.
- Beaumont, C. 1981. Foreland basins. *Geophysical Journal of the Royal astronomical Society (Geophysical Journal International)*, 65, 291-329.
- Beck, P. 1946. Über den Mechanismus der subalpinen Molassetektonik. *Eclogae geologicae Helvetiae*, 38, 353-368.
- Beck, C., Deville, E., Blanc, E., Philippe, Y., Tardy, M. 1998. Horizontal shortening control of Middle Miocene marine siliciclastic accumulation (Upper Marine Molasse) in the southern termination of the Savoy Molasse Basin (northwestern Alps/southern Jura). *Geological Society Special Publications*, 134, 263-278.
- Becker A. 1987. Recent stress field and neotectonics in the eastern Jura Mountains. *Tectonophysics*, 135, 277-288.
- Becker, A. 2000. The Jura Mountains – an active foreland fold-and-thrust belt? *Tectonophysics*, 321, 381-406.
- Becker, F. 1972. Géologie de la région du lac de Morat entre la Vallée de la Sarine et le lac de Neuchâtel. PhD thesis University of Fribourg Switzerland.
- Becker, F., Ramseier, R. 1973. *Geologischer Atlas der Schweiz Blatt 63 1165 Murten*.
- Behr, H.-J., Engel, W., Franke, W., Giese, P., Weber, K. 1984. The Variscan belt in central Europe: main structures, geodynamic implications, open questions. *Tectonophysics*, 109, 15-40.
- Behrens, M., Wurster, P. 1972. Tektonische Untersuchungen an Molasse-Geröllen. *Geologische Rundschau*, 61, 1019-1037.
- Berge, T.B., Veal, S.L. 2005. Structure of the Alpine foreland. *Tectonics*, 24, TC5011, doi:10.1029/2003TC001588.
- Berger, J.P., Reichenbacher, B., Becker, D., Grimm, M., Grimm, K., Picot, L., Stroni, A., Pirkenseer, C., Derer, C., Schaefer, A. 2005a. Paleogeography of the Upper Rhine Graben (URG) and the Swiss Molasse Basin (SMB) from Eocene to Pliocene. *International Journal of Earth Science*, 94, 697-710.
- Berger, J.P., Reichenbacher, B., Becker, D., Grimm, M., Grimm, K., Picot, L., Stroni, A., Pirkenseer, C., Schaefer, A. 2005b. Eocene-Pliocene time scale and stratigraphy of the Upper Rhine Graben (URG) and the Swiss Molasse Basin (SMB). *International Journal of Earth Science*, 94, 711-731.
- Bergerat, F. 1987. Stress fields in the European platform at the time of Africa-Eurasia collision. *Tectonics*, 6, 99-132.
- Berthé, D., Choukroune, P., Jegouzo, P. 1979. Orthogneiss, mylonite and non-coaxial deformation of granites: the example of the South Armorican Shear Zone. *Journal of Structural Geology*, 1, 31-42.
- Bertschy, R. 1958. *Geologie der Kreide und Molasse in der Umgebung von Grandson (Kt Waadt)*. *Eclogae geologicae Helvetiae*, 51/2, 217-263.
- Billings, M.P. 1954. *Structural Geology*. New York, Prentice-Hall, 2d ed. 514pp.
- Birsoy, R. 2002. Formation of sepiolite-palygorskite and related minerals from solution. *Clays and Clay Minerals*, 50, 736-745.
- Bjørlykke, K., Ramm, M., Saigal, G.C. 1989. Sandstone diagenesis and porosity modification during basin evolution. *Geologische Rundschau*, 78, 243-268.
- Blenkinsop, T.G. 1989. Thickness - displacement relationship for deformation zones: Discussion. *Journal of Structural Geology*, 11, 1051-1054.
- Blondel, T., Charollais, J., Sambeth, U., Pavoni, N. 1988. La faille du Vuache (Jura meridional): un exemple de faille a caractere polyphase. *Bulletin Société vaudoise de Sciences Naturelles*, 79, 65-91.
- Boegli, J.-C. 1972. *Geologie de la région au SE de Romont*. PhD thesis University of Fribourg Switzerland. 144pp.
- Boigk, H., Schöneich, H. 1974. Perm, Trias und älterer Jura im Bereich der südlichen Mittelmeer-Mjösen-Zone und des Rheingrabens. In: Illies, J.H., Fuchs, K. (eds.): *Approaches to Taphrogenesis*, Schweizerbart, Stuttgart, 60-71.
- Bolle, M.-P., Adatte, T. 2001. Paleocene-early Eocene climate evolution in the Tethyan realm: clay mineral evidence. *Clay Minerals*, 36, 249-261.
- Bonnet, C. 2007. Interactions between tectonics and surface processes in the Alpine foreland: Insights from analogue model and analysis of recent faulting. PhD thesis University of Fribourg. *GeoFocus*, 17, 189pp., Fribourg 2007.
- Bonnet, C., Malavielle, J., Mosar, J. 2007. Interactions between tectonics, erosion, and sedimentation during recent evolution of the Alpine orogen: Analogue modeling insights. *Tectonics*, 26, TC6016, doi:10.1029/2006TC002048, 2007.
- Bonnet, C., Malavielle, J., Mosar, J. 2008. Surface processes versus kinematics of thrust belts: impact on rates of erosion, sedimentation, and exhumation – Insights from analogue modelling. *Bulletin de la Société Française de Géologie*, 179, 297-314.
- Boulton, C., Davies, T., McSaveney, M. 2009. The frictional strength of granular fault gouge: application of theory to the mechanics of low-angle normal faults. In: Ring, U., Wernicke, B. (eds) *Extending a Continent: Architecture, Rheology and Heat Budget*. Geological Society of London, Special Publication, 321, 9-31.
- Boyer, S.E., Elliott, D. 1982. Thrust systems. *American Association of Petroleum Geologists Bulletin*, 66, 1196-1230.
- Bradley, D.C., Kidd, W.S.F. 1991. Flexural extension of upper continental crust in collisional foredeeps. *Geological Society of America Bulletin*, 103, 1416-1438.
- Briel, A., 1962. *Géologie de la région de Lucens (Broye)*. PhD thesis, University of Fribourg Switzerland. 274pp.
- Büchi, U.P., Lemcke, K., Wiener, G., Zimdars, J. 1965. *Geologische Ergebnisse der Erdölexploration auf das Mesozoikum im Untergrund des schweizerischen Molassebeckens*. Bulletin der Vereinigung Schweizer Petroleum-Geologen und Ingenieure, 32/82, 7-38.
- Burkhard, M. 1990. Aspects of the large-scale Miocene deformation in the most external part of the Swiss Alps (Subalpine Molasse to Jura fold belt). *Eclogae geologicae Helvetiae*, 83, 559-

- 583.
- Burkhard, M. & Sommaruga, A. 1998. Evolution of the western Swiss Molasse basin: structural relations with the Alps and the Jura belt. Geological Society of London Special Publications, 134, 279-298.
- Buxtorf, A. 1916. Prognosen und Befunde beim Hauensteinbasis- und Grenchenberg-tunnel und die Bedeutung der letzteren für die Geologie des Jura gebirges. Verhandlungen der Naturforschenden Gessellschaft Basel, 27, 184-205.
- Cashman, S. & Cashman, K. 2000. Cataclasis and deformation-band formation in unconsolidated marine terrace sand, Humboldt County, California. *Geology*, 28, 111-114.
- Cederboom, C.E., Sinclair, H.D., Schlunegger, F., Rahn, M.K. 2004. Climate-induced rebound and exhumation of the European Alps. *Geology*, 32, 709-712.
- Charollais, J., Clavel, B., Amato, E., Escher, A., Busnardo, R., Steinhauser, N., Macsotay, O., Donse, P. 1983. Etude preliminaire de la faille du Vuache (Jura meridional). *Bulletin Société vaudoise de Sciences Naturelles*, 76, 217-256.
- Chenevart, C. 1978. Seismic profiles as related to wrench-faulting in the Swiss Molasse basin. *Eclogae geologicae Helveticae*, 71/1, 53-60
- Chester, F.M., Friedman, M., Logan, J.M. 1985. Foliated cataclases. *Tectonophysics*, 111, 139-146.
- Chester, F.M. & Logan, J.M. 1987. Composite planar fabric of gouge from the Punchbowl Fault, California. *Journal of Structural Geology*, 9, 621-634.
- Chisholm, J.E. 1992. Powder diffraction patterns and structural models for palygorskite. *Canadian Mineralogist*, 30, 61-73.
- Cladouhos, T.T. 1999a. Shape preferred orientations of survivor grains in fault gouge. *Journal of Structural Geology*, 21, 419-436.
- Cladouhos, T.T. 1999b. A kinematic model for deformation within brittle shear zones. *Journal of Structural Geology*, 21, 437-448.
- Cloos, H. 1930. Zur experimentellen Tektonik. *Geologische Rundschau*, 21, 353-367.
- Courboux, F., Deichmann, N., Gariel, J.-C. 1999. Rupture complexity of a moderate intraplate earthquake in the Alps: the 1996 M5 Epagny-Annecy earthquake. *Geophysical Journal International*, 139, p. 152-160.
- Crausaz, C. U. 1959. Géologie de la région de Fribourg. PhD thesis University of Fribourg Switzerland. 117pp.
- Davis, G.H., Bump, A.P., Garcia, P.E., Ahlgren, S.G. 1999. Conjugate Riedel deformation band shear zones. *Journal of Structural Geology*, 22, 169-190.
- Deichmann, N., Baer, M., Braunmiller, J., Ballarin Dolfi, D., Bay, F., Delouis, B., Fäh, D., Giardini, D., Kastrup, U., Kind, F., Kradolfer, U., Künzle, W., Röthlisberger, S., Schler, T., Salichon, J., Sellami, S., Spühler, E., Wiemer, S. 2000a. Earthquakes in Switzerland and surrounding regions during 1999. *Eclogae geologicae Helveticae*, 93, 395-406.
- Deichmann, N., Ballarin, D., Kastrup, U. 2000b. Seismizität der Nord- und Zentralschweiz. NAGRA Technischer bericht (NTB 00-05), 90pp. NAGRA Wettingen.
- Deichmann, N., Baer, M., Braunmiller, J., Cornou, C., Fäh, D., Giardini, D., Gisler, M., Huber, S., Husen, S., Kästli, P., Kradolfer, U., Mai, M., Maraini, S., Oprea, I., Schler, T., Schorlemmer, D., Wiemer, S., Wössner, J., Wyss, A. 2004. Earthquakes in Switzerland and surrounding regions during 2003. *Eclogae geologicae Helveticae*, 97, 447-458.
- Deichmann, N., Baer, M., Braunmiller, J., Husen, S., Fäh, D., Giardini, D., Kästli, P., Kradolfer, U., Wiemer, S. 2006. Earthquakes in Switzerland and surrounding regions during 2005. *Eclogae geologicae Helveticae*, 99, 443-452.
- Deichmann, N., Clinton, J., Husen, S., Edwards, B., Haslinger, F., Fäh, D., Giardini, D., Kästli, P., Kradolfer, U., Marschall, I., Wiemer, S. 2010. Earthquakes in Switzerland and surrounding regions during 2009. *Swiss Journal of Geoscience*, DOI: 10.1007/s00015-010-0039-8.
- Delany, J.M., Lundeen, S.R. 1989 The LLNL thermochemical database. Lawrence Livermore National Laboratory Report UCRL-21658
- Destigneville, C.M., Karpoff, A.M., Charpentier, D. 1998. Modelling the halmyrolytic formation of palygorskite from serpentinite. In: Arehart & Hulston (eds): *Proc. 9th Int. Symposium on Water-Rock Interaction*. Balkem, Rotterdam. P. 715-718.
- Dèzes, P., Schmid, S.M., Ziegler, P.A. 2004. Evolution of the European Cenozoic Rift System: interaction of the Alpine and Pyrenean orogens with their foreland lithosphere. *Tectonophysics*, 389, 1-33.
- Dickinson, W.R. 1974. Plate tectonics and sedimentation. In: Dickinson, W.R. (ed.): *Tectonics and Sedimentation*. Special Publication Society econ. Geology and Paleontology, 22, 1-27.
- Diepold, D. 1985 (zusammengefasst von Ph. Bodmer). Die Kohlenlager im Stephanien der Nagra-Sondierbohrung Weiach, ihre Entdeckung und erste Beurteilung. *Bulletin der Vereinigung Schweizer Petroleum-Geologen und Ingenieure*, 51/121.
- Doblas, M. 1998. Slickenside kinematic indicators. *Tectonophysics*, 295, 187-197.
- Doblas, M., Mahecha, V., Hoyos, M., Lopez-Ruiz, J. 1997a. Slickenside and fault surface kinematic indicators on active normal faults of the Alpine Betic cordilleras. Granada, southern Spain. *Journal of Structural Geology*, 19, 159-170.
- Doblas, M., Faulkner, D., Mahecha, V., Aparicio, A., Lopez-Ruiz, J., Hoyos, M. 1997b. Morphologically ductile criteria for the sense of movement on slickensides from an extensional detachment fault in southern Spain. *Journal of Structural Geology*, 19, 1045-1054.
- Dorthe, J.-P. 1962. Géologie de la région au Sud-Ouest de Fribourg. PhD thesis University of Fribourg Switzerland. Reprint *Eclog. Geol. Helv.* 55; pp. 327-406
- Durney, D.W., Ramsay, J.G. 1973. Incremental strains measured by syntectonic crystal growths. In: De Jong, K.A., Scholten, R. (Eds), *Gravity and Tectonics*. Wiley, pp. 67-96.
- Sommaruga A., Eichenberger, U., Marillier, F.: 2011 (in prep.). Seismic Atlas of the Swiss Molasse Basin. Matériaux pour la Géologie de la Suisse, Géophysique, swisstopo.
- Emmenegger, C. 1962. Géologie de la région sud de Fribourg. PhD thesis University of Fribourg Switzerland. 163pp.

- Engelder, J.T. 1974. Microscopic Wear Grooves on Slickensides: Indicator of Paleoseismicity. *Journal of Geophysical Research*, 79, 4387-4392.
- ENSI 2010. Gutachten des ENSI zum Rahmenbewilligungsgesuch der EKKMAG. Eidgenössisches Nuklearsicherheitsinspektorat ENSI (Hrsg.) Brugg 2010, 149pp.
- Fischer, H., Luterbacher, H.P. 1963. das Mesozoikum der Bohrungen Courtion 1 und Altishofen 1. Beiträge zur geologischen Karte der Schweiz, Neue Folge 115.
- Fossen, H., Schultz, R.A., Shipton, Z.K., Mair, K. 2007. Deformation bands in sandstone: a review. *Journal of the Geological Society of London*, 164, 755-769.
- Frei, E., Meia, J., Becker, F., Büchi, O., Buxtorf, R., Ryniker, K., Suter, H. 1974. Atlas géologique de la Suisse Feuille 67 1164 Neuchâtel
- Frisch, W. 1979 Tectonic Progradation and Plate Tectonic Evolution of the Alps. *Tectonophysics*, 60, 121-139.
- Gabus, J.H., Boegli, J.C., Mornod, L., Parriaux, A. 2000. Atlas géologique de la Suisse Feuille 103 1224 Moudon.
- Garcia-Romero, E., Suarez, M., Oyarzun, R., Lopez-Garcia, J.A., Regueiro, M. 2006. Fault-hosted palygorskite from the Serrata de Nijar deformation zone (SE Spain). *Clays and Clay Minerals*, 54, 324-332.
- Gay, N.C. 1970. The formation of step structures on slickensided shear surfaces. *Journal of Geology*, 78, 523-532.
- Giamboni, M., Ustaszewski, K., Schmid, S.M., Schumacher, M.E., Wetzel, A. 2004. Plio-Pleistocene transpressional reactivation of Paleozoic and Paleogene structures in the Rhine-Bresse Transform Zone (northern Switzerland and eastern France). *International Journal of Earth Science*, 93, 207-223.
- Gibbs, A.E., Hein, J.R., Lewis, S.D., McCulloch, D.S. 1993. Hydrothermal palygorskite and ferromanganese mineralization at a central California margin fracture zone. *Marine Geology*, 115, 47-65.
- Giustetto, R., Levy, D., Chaiari, G. 2006. Crystal structure refinement of Maya Blue pigment prepared with dewatered indigo using neutron powder diffraction. *European Journal of Mineralogy*, 18, 629-640.
- Gorin, G.E., Signer, C., Amberger, G. 1993. Structural configuration of the western Swiss Molasse Basin as defined by reflection seismic data. *Eclogae geologicae Helveticae*, 86, 693-716.
- Gorin, G., Morend, D., Pugin, A. 2003. Bedrock, Quaternary sediments and recent fault activity in central Lake Neuchâtel, as derived from high-resolution reflection seismics. *Eclogae geologicae Helveticae*, 96, Supplement 1, 3-10.
- Grady, D.E., Kipp, M.E. 1987. Dynamic rock fragmentation. In: Atkinson, B.K. (ed) *Fracture Mechanics of Rock*. Academic Press, London, 429-475.
- Haessler, H., Hoang-Trong, P., Schick, R., Schneider, G., Strobach, K. 1980. The September 3, 1978, Swabian Jura Earthquake. *Tectonophysics*, 68, 1-14.
- Hancock, P.L. 1985 Brittle microtectonics: principles and practice. *Journal of Structural Geology*, 7, 437-457.
- Hancock, P.L., Barka, A.A. 1987. Kinematic indicators on active normal faults in Western Turkey. *Journal of Structural Geology*, 9, 573-584.
- Harvie, C.E., Weare, J.H., Hardie, L.A., Eugster, H.P. 1980. Evaporation of seawater, calculated mineral sequences. *Science*, 208, 498-500.
- Heim, A. 1915. Die horizontalen Transversalverschiebungen im Jura gebirge. *Geologische Nachlese*, Nr.22, Verhandlungen der Naturforschenden Gessellschaft Zürich, 60, 597-610.
- Heim, A. 1919. *Geologie der Schweiz Band 1 Molasseland und Jura gebirge*. 704pp, Leipzig 1919.
- Hillier, S. 1995: Erosion, Sedimentation and Sedimentary Origin of Clays. In: Velde, B. (ed) *Origin and Mineralogy of Clays, Clays and the Environment*. Springer, Berlin Heidelberg New York. 162-219.
- Hills, E.S. 1940. *Outlines of structural geology*. London. Methuen and Co 172pp.
- Hindle, D. 1997. Quantifying stresses and strains from the Jura Arc, and their usefulness in choosing a deformation model for the region. PhD thesis, Université de Neuchâtel, 145pp.
- Hindle, D., Burkhard, M. 1999. Strain, displacement and rotation associated with the formation of curvature in fold belts; the example of the Jura arc. *Journal of Structural Geology*, 21, 1089-1101.
- Homberg, C. 1997. Analyse des déformations cassantes dans le Jura et modélisation numérique des perturbations des contraintes tectoniques autour d'accidents majeurs. PhD thesis. Mémoires Soc. Terre Univ. P. et M. Curie, 97-13, 306pp.
- Homberg, C., Bergerat, F., Philippe, Y., Lacombe, O., Angelier, J. 2002. Structural inheritance and cenozoic stress fields in the Jura fold-and-thrust belt (France). *Tectonophysics*, 357, 137-158.
- Homewood, P., Allen, P.A., Williams, G.D. 1986. Dynamics of the Molasse Basin of western Switzerland. *Special Publications International Association Sedimentologists*, 8, 199-217.
- Hull, J. 1988. Thickness-displacement relationships for deformation zones. *Journal of Structural Geology*, 10, 431-435.
- Illies, J.H. 1977. Ancient and recent rifting in the Rhinegraben. In: Frost, R.T.C. & Dikkers, A.J. (Eds): *Fault tectonics in N.W. Europe*. Geol. Mijnbouw, 56, 329-350.
- Imai N., Otsuka, R. 1984. Sepiolite and palygorskite in Japan. In: Singer, A., Galan, E. (Eds) *Palygorskite-sepiolite: occurrences, genesis and uses*. *Development in Sedimentology*, 37, 211-231
- Inglis, H. 1960. *Molasse et quaternaire de la région de Romont*. PhD thesis University of Fribourg Switzerland.
- Jones, B.F. & Galan, E. 1988. Sepiolite and Palygorskite. In: Bailey, S.W. (Ed.), *Hydrous Phyllosilicates (exclusive of micas)*, *Reviews in Mineralogy* 19, Mineralogical Society of America, 631-674.
- Jordan, P. 1992. Evidence for large scale decoupling in the Triassic evaporites of Northern Switzerland: an overview. *Eclogae geologicae Helveticae*, 85, 677-693.

- Jordan, P. 1994. Evaporite als Abscherhorizonte. Eine gefügekundlich-strukturgeologische Untersuchung am Beispiel der Nordschweizer Trias. Materialien zur Geologischen Karte der Schweiz, neue Serie 164, 79pp.
- Jordan, T.E. 1981. Thrust Loads and Foreland Basin Evolution, Cretaceous, Western United States. American Association of Petroleum Geologists, Bulletin, 65, 2506-2520.
- Jordi, H.A., 1951. Zur Stratigraphie und Tektonik der Molasse von Yverdon. Bulletin der Vereinigung Schweizer Petroleum-Geologen und Ingenieure, 18/55, 1-14.
- Jordi, H.A., 1955. Geologie der Umgebung von Yverdon (Jurafluss und mittelländische Molasse). Beiträge zur Geologischen Karte der Schweiz, Neue Folge 99, 84pp.
- Jordi, H.A., 1990. Tektonisch-strukturelle Übersicht Westschweizerisches Molassebecken. Bulletin der Vereinigung Schweizer Petroleum-Geologen und Ingenieure, 56/130, 1-11.
- Jouanne, F., Genaudeau, N., Ménard, G., Darmendrail, X., 1998. Estimating present-day displacement fields and tectonic deformation in active mountain belts: an example from the Chartreuse Massif and the southern Jura Mountains, western Alps. Tectonophysics, 296, 403-419.
- Kaelin, B., Rybach, L., Kempter, E.H.K. 1992. Rates of Deposition, Uplift and Erosion in the Swiss Molasse Basin, Estimated from Sonic – and Density – Logs. Bulletin of the Swiss Association of Petroleum Geologists and Engineers, 58, 9-22.
- Karner, G.D., Watts, A.B. 1983. Gravity Anomalies and Flexure of the Lithosphere at Mountain Ranges. Journal of Geophysical Research 88, 10449-10477.
- Karpoff A.M., Lagabrielle, Y., Boillot, G., Girardeau, J. 1989. L'authigenèse océanique de palygorskite par halmyrolyse de péridotites serpentinisées (marge de Galice) : ses implications géodynamiques. C.R. Acad. Sci. Paris, 308, 647-654.
- Kastrup, U. 2002. Seismotectonics and stress field variations in Switzerland, Ph.D. thesis, ETH Zürich, Zürich, Switzerland.
- Kastrup, U., Zoback, M.L., Deichmann, N., Evans, K.F., Giardini, D., Michael, A.J. 2004 Stress field variations in the Swiss Alps and the northern Alpine foreland derived from inversion of fault plane solutions. Journal of Geophysical Research, 109, B01402, doi: 10.1029/2003JB002550, 2004.
- Kastrup, U., Deichmann, N., Fröhlich, A., Giardini, D. 2007. Evidence for an active fault below the northwestern Alpine foreland of Switzerland. Geophysical Journal International, 169, 1273-1288.
- Katz, Y. & Weinberger, R. 2005. Strain localization in sandstone during embryonic stages of shear zone evolution. Terra Nova, 17, 311-316.
- Kempf, O., Schlunegger, F., Strunck, P., Matter, A. 1998. Paleomagnetic evidence for late Miocene rotation of the Swiss Alps: results from the north Alpine foreland basin. Terra Nova, 10, 6-10.
- Kempf, O., Pfiffner, O.A., 2004. Early Tertiary evolution of the North Alpine Foreland Basin of the Swiss Alps and adjoining areas. Basin research, 16, 549-567, doi: 10.1111/j.1365-2117.2004.00246.x
- Klingelé, E., Mueller, S. 1987. La cartographie du soubassement magnétique du basin molassique et du Jura Suisse. Eclogae geologicae Helvetiae, 80, 17-36.
- Kopp, J. 1946. Zur Tektonik der westschweizer Molasse. Eclogae geologicae Helvetiae, 39/2, 269-274.
- Krohe, A., Eisbacher, G.H. 1988. Oblique crustal detachment in the Variscan Schwarzwald, southwestern Germany. Geologische Rundschau, 77, 25-43.
- Kuhlemann, J., Kempf, O. 2002. Post-Eocene evolution of the North Alpine Foreland Basin and its response to Alpine tectonics. Sedimentary Geology, 152, 45-78.
- Laubscher, H. 1961. Die Fernschubhypothese der Jurafaltung. Eclogae geologicae Helvetiae, 54, 221-282.
- Laubscher, H. 1965. Ein kinematisches Model der Jurafaltung. Eclogae geologicae Helvetiae, 58, 232-318.
- Laubscher, H. 1972. Some overall aspects of Jura dynamics. American Journal of Science, 272, 293-304.
- Laubscher, H. 1978. Foreland folding. Tectonophysics, 47, 325-337.
- Laubscher, H. 1987 Die Tektonische Entwicklung der Nordschweiz Eclogae geologicae Helvetiae, 80/2 287-303.
- Laubscher, H. 1992. Jura kinematics and the Molasse Basin. Eclogae geologicae Helvetiae, 85, 653-675.
- Laubscher, H. 2008. The Grenchenberg conundrum in the Swiss Jura: a case for the centenary of the thin-skin décollement nappe model (Buxtorf 1907). Swiss Journal of Geosciences, 101, 41-60.
- Lemcke, K., Büchi, U.P., Wiener, G. 1968. Einige Ergebnisse der Erdölexploration auf die mittelländische Molasse der Zentralschweiz. Bulletin der Vereinigung Schweizer Petroleumgeologen und Ingenieure, 35, 15-34.
- Lin, A. 2001. S-C fabrics developed in cataclastic rocks from the Nojima fault zone, Japan and their implications for tectonic history. Journal of Structural Geology, 23, 1167-1178.
- Liniger, H. 1967. Pliozän und Tektonik des Juragebirges. Eclogae geologicae Helvetiae, 60/2, 407-490.
- Lister, G.S., Snoke, A.W. 1984. S-C Mylonites. Journal of Structural Geology, 6, 617-638.
- Madritsch, H., Schmid, S.M., Fabbri, O. 2008. Interactions between thin- and thick-skinned at the northwestern front of the Jura fold-and-thrust-belt (eastern France). Tectonics, 27, TC5005. doi: 10.1029/2008/TC002282.
- Madritsch, H., Kounov, A., Schmid, S.M., Fabbri, O. 2009. Multiple fault reactivation within the intra-continental Rhine-Bresse Transfer Zone (La Serre Horst, eastern France). Tectonophysics, 471, 297-318.
- Madritsch, H., Preusser, F., Fabbri, O., Bichet, V., Schlunegger, F., Schmid, S.M. 2010. Late Quaternary folding in the Jura Mountains: evidence from syn-erosional deformation of fluvial meanders. Terra Nova, 22, 147-154.
- Main, I., Mair, K., Kwon, O., Elphick, S., Ngwenya, B. 2001. Experimental constraints on the mechanical and hydraulic properties of deformation bands in porous sandstones: a

- review. Geological Society of London Special Publications, 186, 43-63.
- Mair, K., Main, I., Elphick, S., 2000. Sequential growth of deformation bands in the laboratory. *Journal of Structural Geology*, 22, 25-42.
- Mair, K., Elphick, S., Main, M. 2002. Influence of confining pressure on the mechanical and structural evolution of laboratory deformation bands. *Geophysical Research Letters*, 29, 10.1029.200[GLO]3964, 2002.
- Mandl, G., de Jong, L.N.J., Maltha, A. 1977. Shear Zones in Granular Material. *Rock Mechanics*, 9, 95-144.
- Marescot, L. 2000. La Molasse de la Region de la Sense; Tectonique du contact Molasse du Plateau et Molasse Subalpin; Paleontologie de l'USM; Petrographie des conglomerates de l'OMM (couches du Belpberg). Unpublished Diplomathe University of Lausanne.
- Marquer, D. 1990. Structures et cinématique des déformations Alpines dans les granites hercyniens du Massif du Gotthard (Alpes centrales Suisse) *Eclogae geologicae Helveticae*, 83, 77-97.
- Marrett, R., Allmendinger, R.W. 1990. Kinematic analysis of fault-slip data. *Journal of Structural Geology*, 12, 973-986.
- Matter, A., Homewood, P., Caron, C., van Stuijvenberg, J., Weidmann, M., Winkler, W. 1980. Flysch and Molasse of western central Switzerland. In: *Geology of Switzerland, a Guide Book* (Ed. Trümpy, R.) 261-293.
- Matter, A. 1987. Faziesanalyse und Ablagerungsmilieus des Permokarbons im Nordschweizer Trog. *Eclogae geologicae Helveticae*, 80, 345-367.
- Matzenauer, E. 2007. Spannungsanalyse der Mittelland Molasse des Kantons Freiburg anhand von Deformationserscheinungen an Geröllen und Bruchbildungen. Unpublished Masterthesis University of Fribourg.
- Matzenauer, E. 2011. PhD thesis University of Fribourg, GeoFocus in prep.
- Mazurek, M., Hurford, A.J., Leu, W. 2006. Unravelling the multi-stage burial history of the Swiss Molasse Basin: integration of apatite fission track, vitrinite reflectance and biomarker isomerisation analysis. *Basin Research*, 18, 27-50.
- McEwen, T.J. 1978. Diffusional Mass Transfer Processes in Pitted Pebble Conglomerates. *Contributions to Mineralogy and Petrology*, 67, 405-415.
- Means, W.D. 1987. A newly recognized type of slickenside striation. *Journal of Structural Geology*, 9, 585-590.
- Means, W.D. 1993. Slickensides as plaeoseismographs. *Geological Society of America Abstracts with Program*, P. A115.
- Meia, J. 1966. Un accident tectonique sur le flanc Sud du Mont-Aubert (Jura vaudois oriental, Suisse). *Bulletin de la Société Neuchâteloise des Sciences Naturelles*, 89, 129-135.
- Meier, D. 1984. Zur Tektonik des schweizerischen Tafel- und Faltenjura (regionale und lokale Strukturen, Kluftgenese, Bruch- und Faltentektonik, Drucklösung). PhD theses, Clausthaler Geowissenschaften 14, 75pp.
- Miller, M.G. 1996. Ductility in fault gouge from a normal fault system, Death Valley, California: A mechanism for fault-zone strengthening and relevance to paleoseismicity. *Geology*, 24, 603-606.
- Monnier, F. 1982. Thermal diagenesis in the Swiss Molasse basin: Implication for oil generation. *Canadian Journal of Earth Science*, 19, 328-342.
- Mornod, L. 1949. Géologie de la région de Bulle (Basse-Gruyère) Molasse et bord alpin. Thesis University of Fribourg, Switzerland. Matériaux pour la Carte Géologique de la Suisse, NS, 91, 119pp.
- Mosar, J., Abednego, M., Ibele, T., Matzenauer, E., Meier, B., Sommaruga, A., Sprecher, C., Vouillamoz, N. 2011. Du Jura central aux Préalpes romandes – Une tectonique active dans l'avant-pays des Alpes. *Géochronique* 117, 52-55.
- Mosar, J. 1999. Present-day and future tectonic underplating in the Western Swiss Alps: reconciliation of basement/wrench-faulting and décollement folding of the Jura and Molasse Basin in the Alpine foreland. *Earth and Planetary Science Letters*, 173, 143-155.
- Mosar, J., Stampfli, G.M., Girod, F. 1996. Western Préalpes médianes: timing and structure. A review. *Eclogae geologicae Helveticae*, 89, 389-425.
- Mugnier, J.L., Vialon, P., 1986. Deformation and displacement in the Jura cover on its basement. *Journal of Structural Geology*, 8, 373-387.
- Müller, M., Nieberding, F., Wanninger, A. 1988. Tectonic style and pressure distribution at the northern margin of the Alps between Lake Constance and the River Inn. *Geologische Rundschau*, 77, 787-796.
- Mural, R., Vuataz, F.-D., Schönborn, G., Sommaruga, A., Jenny, J. 1997. Intégration des méthodes hydrochimiques, géologiques et géophysiques pour la prospection d'une nouvelle ressource en eau thermique. Cas d'Yverdon-les-Bains, pied du Jura. *Eclogae geologicae Helveticae*, 90, 179-197.
- Naef, H., Diebold, P., Schlanke, S. 1985. Sedimentation und Tektonik im Tertiär der Nordschweiz. *NAGRA Technischer Bericht NTB 85-14*, NAGRA, Baden.
- Naylor, M.A., Mandl, G., Sijpesteijn, C.H.K. 1986. Fault geometries in basement-induced wrench faulting under different initial stress states. *Journal of Structural Geology*, 8, 737-752.
- Neugebauer, H.J., Brötz, R., Rybach, L. 1980. Recent crustal uplift and the present stress field in the Alps along the Swiss Geotransverse Basel Chiasso. *Eclogae geologicae Helveticae*, 73, 489-500.
- Nieto, F., Mata, M.P., Bauluz, B., Giorgetti, G., Arkai, P., Peacor, D.R. 2005. Retrograde diagenesis, a widespread process on a regional scale. *Clay Minerals*, 40, 93-104.
- Nriagu, J.O. 1975. Thermochemical approximations for clay minerals. *American Mineralogist*, 60, 834-839.
- Ortner, H., Reiter, F., Acs, P. 2002. Easy handling of tectonic data: the programs TectonicVB for Mac and TectonicsFP for Windows(TM). *Computers & Geosciences*, 28, 1193-1200.
- Paterson, M.S. 1958. Experimental deformation and faulting in Wombeyan marble. *Geological Society of America Bulletin*, 69, 465-476.

- Pavoni, N. 1961. Faltung durch Horizontalverschiebung. *Eclogae geologicae Helvetiae*, 54, 515-534.
- Pavoni, N. 1977. Erdbeben im Gebiet der Schweiz. *Eclogae geologicae Helvetiae*, 70, 351-370.
- Pavoni, N., Peterschmitt, E. 1974. Das Erdbeben von Jeurre vom 21. Juni 1971 und seine Beziehungen zur Tektonik des Faltenjura. In: Illies, H., Fuchs, K. (Eds): *Approaches to Taphrogenesis*, Schweizerbart, Stuttgart, 322-329.
- Peters, T., Salis, K. von 1965. Palygorskit als Kluftbelag in der tortonen Molasse des Entlebuch (schweizerisches Mittelland). *Schweizerische mineralogische und petrographische Mitteilungen*, 45, 123-130.
- Petit, J.P. 1987. Criteria for the sense of movement on fault surfaces in brittle rocks. *Journal of Structural Geology*, 9, 597-608.
- Petit, J.P., Proust, F., Tapponier, P. 1983. Critères de sens de mouvement sur les miroirs de failles en roches non calcaires. *Bulletin de la Société géologique de France*, 7, 589-608.
- Pfiffner, O.A. 1986. Evolution of the north Alpine foreland basin in the Central Alps. *Special Publications International Association Sedimentologists*, 8, 219-228.
- Pfiffner, O.A. 1993. Palinspastic Reconstruction of the Pre-Triassic Basement Units in the Alps: the Central Alps. In: von Raumer, J.F., Neubauer, F. (eds.): *Pre-Mesozoic Geology in the Alps*, 29-39.
- Pfiffner, O.A., Burkhard, M. 1987. Determination of paleo-stress axes orientations from fault, twin and earthquake data. *Annales Tectonicae*, 1 48-57.
- Pfiffner, O.A., Erard, P.-F., Stäuble, M. 1997. Two cross sections through the Swiss Molasse Basin (lines E4-E6, W1, W7-W10). In: Pfiffner, O.A., Lehner, P., Heitzmann, P.Z., Mueller, S., Steck, A. (eds.), *Deep structure of the Swiss Alps – Results from NRP20*. Birkhäuser, Basel, 64-72.
- Philippe, Y., 1995. Rampes laterals et zones de transfert dans les chaînes plissées : géométrie, conditions de formation et pièges structuraux associés. PhD thesis, Chambéry (Savoie, France)
- Plancherel, R. 1979. Aspects de la déformation en grand dans le Préalpes médianes plastiques entre Rhône et Aar. Implications cinématiques et dynamiques. *Eclogae geologicae Helvetiae*, 72/1, 145-214.
- Plancherel, R. 1998. in: Python, C., Berger, J-P., Plancherel, R. (1998): *Atlas géologique de la Suisse Feuille 98 (1185) Fribourg*
- Platt, N.H., Keller, B. 1992. Distal alluvial deposits in a foreland basin setting-the Lower Freshwater Molasse (Lower Miocene), Switzerland: sedimentology, architecture and paleosols. *Sedimentology*, 39, 545-565.
- Platt, J.P., Vissers, R.L.M. 1980. Extensional structures in anisotropic rocks. *Journal of Structural Geology*, 2, 397-410.
- Plenefisch, T., Bonjer, K.-P. 1997. The stress field in the Rhine Graben area inferred from earthquake focal mechanisms and estimation of frictional parameters. *Tectonophysics*, 275, 71-97.
- Plessmann, W. 1972. Horizontal-Stylolithen im französisch-schweizerischen Tafel- und Faltenjura und ihre Einpassung in den regionalen Rahmen. *Geologische Rundschau*, 61, 332-347.
- Post, J.E., and Bish, D.L. 1993. Rietveld refinement of crystal structures using powder X-ray diffraction data. In: *Modern Powder Diffraction*, Rev. in Mineralogy 20, Ed. Post, J.E., and Bish, D.L., Mineralogical Society of America, 277-308.
- Post, J.L., Crawford, S. 2007. Varied forms of palygorskite and sepiolite from different geologic systems. *Applied Clay Science*, 36, 232-244.
- Power, W.L., Tullis, T.E., 1989. The relationship between slickenside surfaces in fine-grained quartz and the seismic cycle. *Journal of Structural Geology*, 11, 879-893.
- Python, C., Berger, J-P., Plancherel, R. 1998. *Atlas géologique de la Suisse Feuille 98 1185 Fribourg*.
- Ramm, M. 1992. Porosity-depth trends in reservoir sandstones: theoretical models related to Jurassic sandstones offshore Norway. *Marine and Petroleum Geology*, 9, 553-567.
- Rawling, G.C., & Goodwin, L.B., 2003. Cataclasis and particulate flow in faulted, poorly lithified sediments. *Journal of Structural Geology*, 25, 317-331.
- Reinecker, J., Tingay, M., Müller, B., Heidbach, O. 2010. Present-day stress orientation in the Molasse Basin. *Tectonophysics*, 428, 129-138.
- RESUN 2009 Rahmenbewilligungsgesuch Ersatz Kernkraftwerk Mühleberg, Sicherheitsbericht. Bundesamt für Energie, allgemeine Publikationen. 358pp.
- Revertera, G.J. 1927. Ein tektonisches Problem aus den Prealpen. Die Reste der Simmen- und Breccien-Decke. Ihre Lage in Bezug auf die axialen Schwankungen ihres Substrats. Auszug aus: PhD thesis University of Fribourg. 15pp.
- Riedel, W. 1929. Zur Mechanik geologischer Brucherscheinungen. *Centralblatt für Mineralogie, Geologie und Paläontologie*, 1929B, 354-368.
- Righi, D., Meunier, A. 1995. Origin of Clays by Rock Weathering and Soil Formation. In: Velde, B. (ed) *Origin and Mineralogy of Clays, Clays and the Environment*. Springer, Berlin Heidelberg New York. 43-161.
- Rotevatn, A., Torabi, A., Fossen, H., Braathen, A., 2008. Slipped deformation bands: A new type of cataclastic deformation bands in Western Sinai, Suez rift, Egypt. *Journal of Structural Geology*, 30, 1317-1331.
- Ruano, P., Galindo-Zaldivar, J. 2004. Striated and pitted pebbles as paleostress markers: an example from the central transect of the Betic Cordillera (SE Spain). *Tectonophysics*, 379, 183-198.
- Rumeau, J-L. 1954. *Géologie de la région de Payerne*. PhD thesis University of Fribourg Switzerland. 108pp.
- Rutsch, R.F. 1926. Zur Stratigraphie und Tektonik der Molasse südlich von Bern. *Eclogae geologicae Helvetiae*, 19, 673-678.
- Rutsch, R.F. 1947. Molasse und Quartär im Gebiet des Siegfriedblattes Rüeggisberg (Kanton Bern). *Beiträge zur Geologischen Karte der Schweiz, Neue Folge*, 87, 89pp.
- Rutsch, R.F., Frasson, B.A. 1953. *Geologischer Atlas der Schweiz Blatt 26 1186 Schwarzenburg (Blätter 332 Neuenegg, 333 Oberbalm, 334 Schwarzenburg, 335 Rüeggisberg)*.

- Rybach, L., Büchi, U.P., Bodmer, P., Krüsi, H.R. 1980. Die Tiefengrundwasser des schweizerischen Mittellandes aus geothermischer Sicht. *Eclogae geologicae Helvetiae*, 73, 293-310.
- Sambeth, U., Pavoni, N. 1988. A seismotectonic investigation in the Geneva Basin, southern Jura mountains. *Eclogae geologicae Helvetiae*, 81, 433-440.
- Schegg, R., Leu, W., Cornford, C., Allen, P.A. 1997. New coalification profiles in the Molasse Basin of Western Switzerland: Implications for the thermal and geodynamic evolution of the Alpine Foreland. *Eclogae geologicae Helvetiae*, 90, 79-96.
- Schegg, R. & Leu, W. 1998. Analysis of erosion and paleogeothermal gradients in the North Alpine Foreland Basin of Switzerland. Geological Society of London Special Publications, 141, 137-155.
- Schlunegger, F., Mosar, J. 2010. The last erosional stage of the Molasse Basin and the Alps. *International Journal of Earth Science*, DOI 10.1007/s00531-010-0607-1
- Schmassmann, H. 1990. Hydrochemische Synthese Nordschweiz: Tertiär- und Malm-Aquifere. *Nagra Technische Berichte NTB 88-07* 244pp.
- Schmid, G. 1970. Geologie der Gegend von Guggisberg und der angrenzenden subalpinen Molasse. *Beiträge zur Geologischen Karte der Schweiz, Neue Folge*, 139, 113pp.
- Schmid, S.M., Fügenschuh, B., Kissling, E., Schuster, R. 2004 Tectonic map and overall architecture of the Alpine orogen. *Eclogae geologicae Helvetiae*, 97, 93-117.
- Schnellmann, M., Anselmetti, F.S., Giardini, D., McKenzie, J., Ward, S.N. 2002. Prehistoric earthquake history revealed by lacustrine slump deposits. *Geology*, 30, 1131-1134.
- Schnellmann, M., Anselmetti, F.S., Giardini, D., McKenzie, J. 2006. 15,000 Years of mass-movement history in Lake Lucerne: Implications for seismic and tsunami hazards. *Eclogae geologicae Helvetiae*, 99, 409-428.
- Scholz, C.H. 1987. Wear and gouge formation in brittle faulting. *Geology*, 15, 493-495.
- Schrader, F. 1988a. Das regionale Gefüge der Drucklösungsformationen an Geröllen im westlichen Molassebecken. *Geologische Rundschau*, 77, 347-369.
- Schrader, F. 1988b. Symmetry of pebble-deformation involving solution pits and slip-lineations in the northern Alpine Molasse Basin. *Journal of Structural Geology*, 10, 41-52.
- Schumacher, M.E. 2002. Upper Rhine Graben: Role of pre-existing structures during rift evolution. *Tectonics* 21, 1006, doi:10.1029/2001TC900022
- Schuppli, H.M., 1950. Erdölgeologische Untersuchungen in der Schweiz. III. Teil. *Beitr. Geol. Schweiz, Geotechn. Ser.* 26, 41pp.
- SED, 2010. Seismic Survey of Switzerland (Schweizer Erdbebendienst) online service: www.seismo.ethz.ch ECOS earthquake catalogue.
- Shipton, Z.K., & Cowie, P.A. 2001. Analysis of three-dimensional damage zone development over μm to km scale range in the high-porosity Navajo sandstone, Utah. *Journal of Structural Geology*, 23, 1825-1844.
- Sibson, R.H. 1977. Fault rocks and fault mechanisms. *Journal of the Geological Society of London*, 133, 191-213.
- Sibson, R.H. 1987. Earthquake rupturing as a mineralizing agent in hydrothermal systems. *Geology*, 15, 701-704.
- Sibson, R.H. 1990. Faulting and fluid flow. In: Nesbitt, B.E. (ed) *MAC Short Course on "Crustal Fluids"*, Handbook, 18, 93-132.
- Sieber, R. 1959. *Géologie de la région occidentale de Fribourg*. PhD thesis University of Fribourg Switzerland. 229pp.
- Simon, J.L. 2007. Analysis of solution lineations in pebbles: Kinematical vs. dynamical approaches. *Tectonophysics*, 445, 337-352.
- Simpson, C. 1984. Borrego Springs-Santa Rosa mylonite zone: A Late Cretaceous west-directed thrust in southern California. *Geology*, 12, 8-11.
- Sinclair, H.D. 1997. Flysch to molasse transition in peripheral foreland basins: The role of the passive margin versus slab breakoff. *Geology*, 25, 1123-1126
- Sinclair, H.D., Allen, P.A. 1992. Vertical versus horizontal motions in the Alpine orogenic wedge: stratigraphic response in the foreland basin. *Basin research*, 4, 215-232.
- Singer, A. 1979. Palygorskite in Sediments: Detrital, Diagenetic or Neoformed – A critical Review. *Geologische Rundschau*, 68, 996-1008.
- Sissingh, W. 1998. Comparative Tertiary stratigraphy of the Rhine Graben, Bresse Graben and Molasse Basin: correlation of Alpine foreland events. *Tectonophysics*, 300, 249-284.
- Sommaruga, A. 1997. Geology of the Central Jura and the Molasse Basin: New insight into an evaporite-based foreland fold and thrust belt. PhD-thesis univer. Neuchâtel. *Mémoire de la Société Neuchâteloise des sciences naturelles* 12, 176pp.
- Sommaruga, A. 1999. Décollement tectonics in the Jura foreland fold-and-thrust belt. *Marine and Petroleum Geology*, 16, 111-134.
- Sommaruga A., Eichenberger U. 2011a (in press). Transect 4: Yvonnand- Gruyères, Enclosure 4. In: Sommaruga A., Eichenberger, U., Marillier, F.: *Seismic Atlas of the Swiss Molasse Basin. Matériaux pour la Géologie de la Suisse, Géophysique, swisstopo*.
- Sommaruga A., Eichenberger U. 2011b (in press). Transect 5: Estavayer-le-Lac- Cousimbert, Enclosure 4. In: Sommaruga A., Eichenberger, U., Marillier, F.: *Seismic Atlas of the Swiss Molasse Basin. Matériaux pour la Géologie de la Suisse, Géophysique, swisstopo*.
- Sommaruga A., Eichenberger U. 2011c (in press). Transect 14: Nyon-Pfaffnau-Romanshorn, Enclosure 14. In: Sommaruga A., Eichenberger, U., Marillier, F.: *Seismic Atlas of the Swiss Molasse Basin. Matériaux pour la Géologie de la Suisse, Géophysique, swisstopo*.
- Strasser, M., Anselmetti, F.S., Fäh, D., Giardini, D., Schnellmann, M. 2006. Magnitudes and source areas of large prehistoric northern Alpine earthquakes revealed by slope failure in lakes. *Geology*, 34, 1005-1008.

- Strating, E.H.H. & Vissers, R.L.M. 1994. Structures in natural serpentinite gouges. *Journal of Structural Geology*, 16, 1205-1215.
- Studer, B. 1853. *Geologie der Schweiz. Band 2 Nördliche Nebenzonen der Alpen, Jura und Hügelland. Mit Gebirgsdurchschnitten.* 497pp. Stämpfli Verlagshandlung, Bern.
- Sue, C., Thouvenot, F., Fréchet, J., Tricart, P. 1999. Widespread extension in the core of the western Alps revealed by earthquake analysis. *Journal of Geophysical Research*, 104/B11 25611-25622.
- Sue, C., Tricart, P. 2002. Widespread post-nappe normal faulting in the Internal Western Alps: a new constraint on arc dynamics. *Journal of the Geological Society London*, 159, 61-70.
- Tardy, Y., Garrels, R.M. 1974. A method for estimating the Gibbs energies of formation of layer silicates. *Geochimica Cosmochimica Acta*, 38, 1101-1116.
- Taylor, H.F.W. 1991. Computer programs for standardless quantitative analysis of minerals using the full powder diffraction profile. *Powder Diffraction*, 6, 2-9.
- Tchalenko, J.S. 1968. The evolution of kink-bands and the development of compression textures in sheared clays. *Tectonophysics*, 6, 159-174.
- Tchalenko, J.S. 1970. Similarities between Shear Zones of Different Magnitudes. *Geological Society of America Bulletin*, 81, 1625-1640.
- Tchalenko, J.S., Ambraseys, N.N. 1970. Structural Analysis of the Dasht-e Bayaz (Iran) Earthquake Fractures. *Geological Society of America Bulletin*, 81, 41-60.
- Tercier, J., Bieri, P. 1963. *Atlas géologique de la Suisse Feuille 36 1206 Gurnigel (Guggisberg).*
- Thierrin, J. 1990. Contribution à l'étude des eaux souterraines de la région de Fribourg (Suisse occidentale). PhD thesis University of Neuchâtel.
- Thouvenot, F., Fréchet, J., Taponnier, P., Thomas, J.-C., Le Brun, B., Menard, G., Lacassin, R., Jenatton, L., Grasso, J.-R., Coutant, O., Paull, A., Hatzfeld, D. 1998. The ML 5.3 Epagny (French Alps) earthquake of 1996 July 15: a long awaited event on the Vuache Fault. *Geophysical Journal International*, 135, 876-892.
- Thury, M., Gautschi, A., Mazurek, M., Müller, W.H., Naef, H., Pearson, F.J., Vomvoris, S., Wilson, W. 1994. *Geology and Hydrogeology of the Crystalline Basement of Northern Switzerland.* NAGRA Technical Report (NTB) 93-01.
- Tjia, H.D. 1964. Slickensides and fault movements. *Geological Society of America Bulletin*, 75, 638-686.
- Trümpy, R. 1962. Mesozoischer Untergrund und ältere Meeresmolasse im schweizerischen und oberschwäbischen Molassebecken. *Erdöl-Zeitschrift*, 78, 521-527.
- Trümpy, R. 1980. *Geology of Switzerland a guide-book. Part A: An outline of the Geology of Switzerland* 104pp, Basel 1980.
- Tschanz, X. 1990. Analyse de la déformation du Jura central entre Neuchâtel (Suisse) et Besançon (France). *Eclogae geologicae Helveticae*, 88, 543-558.
- Ustaszewski, K., Schmid, S.M. 2006. Control of preexisting faults on geometry and kinematics in the northernmost part of the Jura fold-and-thrust belt. *Tectonics* 25, TC5003, doi:10.1029/2005TC001915, 2006.
- Ustaszewski, K., Schmid, S.M. 2007. Late Pliocene to recent thick-skinned tectonics at the Upper Rhine Graben – Jura Mountains junction. *Swiss Journal of Geosciences*, 100, 293-312.
- Valasek, P., Mueller, S. 1997. A 3D tectonic model of the Central Alps based on an integrated interpretation of seismic refraction an NRP20 reflection data. In: Pfiffner, O.A., Lehner, P., Heitzmann, P.Z., Mueller, S., Steck, A. (eds.), *Deep structure of the Swiss Alps – Results from NRP20.* Birkhäuser Basel.
- Vollmayr, T. & Wendt, A. 1987. Die Erdgasbohrung Entlebuch 1, ein Tiefenaufschluss am Alpennordrand. *Bulletin der Vereinigung Schweizer Petroleum-Geologen und Ingenieure*, 53(125), 67-79.
- Von Hagke, C., Cederbom, C., Lindow, J., Oncken, O., Schlunegger, F. 2010. Post 5Ma thrusting in the Northern Alpine Foreland Basin – insights from structural geology and new (U-Th)/He and Fission Track data. *Geophysical Research abstracts*, 12, EGU2010-8858-1.
- Von Raumer, J.F., Ménot, R.P., Abrecht, J., Biino, G. 1993. The Pre-Alpine Evolution of the External Massifs. In: von Raumer, J.F., Neubauer, F. (Eds.): *Pre-Mesozoic Geology of the Alps*, 221-240.
- Vrolijk, P., van der Pluijm, B.A. 1999. Clay gouge. *Journal of Structural Geology*, 21, 1039-1048.
- Walderhaug, O. 1996. Kinetic Modeling of Quartz Cementation and Porosity Loss in Deeply Buried Sandstone Reservoirs. *American Association of Petroleum Geologists, Bulletin*, 80, 731-745.
- Weaver, C.E., Beck, K.C. 1977. Miocene of the S.E., United States: a model for chemical sedimentation in a peri-marine environment. *Sedimentary Geology*, 17, 234pp.
- Weidmann, M. 1988 *Atlas géologique de la Suisse Feuille 85 1243 Lausanne.*
- Weidmann, M. 2002. *Atlas géologique de la Suisse Feuille 105 1205 Rossens.*
- Weidmann, M. 2006. *Atlas géologique de la Suisse Feuille 123 1184 Payerne, Notice explicative.*
- Weidmann, M., Briel, A., Inglin, H. 1996. *Atlas géologique de la Suisse Feuille 99 1204 Romont.*
- Wells, D.L., Coppersmith, K.J. 1994. New Empirical Relationships among Magnitude, Rupture Length, Rupture Width, Rupture Area, and Surface Displacement. *Bulletin of the Seismological Society of America*, 84/4, 974-1002.
- White, S.H., Burrows, S.E., Carreras, J., Shaw, N.D., Humphreys, F.J. 1980. On mylonites in ductile shear zones. *Journal of Structural Geology*, 2, 175-187.
- Willett, S.D., Schlunegger, F. 2010. The last phase of deposition in the Swiss Molasse Basin: from foredeep to negative-alpha basin. *Basin Research*, 22, 623-639.

- Wong, T., David, S., Zhu, W. 1997. The transition from brittle faulting to cataclastic flow in porous sandstone: Mechanical deformation. *Journal of Geophysical Research*, 102, 3009-3025.
- Ziegler, P.A. 1982. *Geological Atlas of Western Central Europe*. Shell International Petroleum Maatschappij B.V. 1982, Elsevier, Amsterdam.
- Ziegler, P.A. 1992. European Cenozoic rift system. *Tectonophysics*, 208, 91-111.
- Zoback, M.L. 1992. First- and second-order patterns of stress in the lithosphere: the World Stress Map project. *Journal of Geophysical Research B, solid earth and planets*, 97(B8), 11703-11728

APPENDICES

APPENDIX 1.1

a) Instrumentally recorded earthquakes in the northern foreland of the central Alps with local magnitudes of 4 and larger. b) Instrumentally recorded earthquakes in the northern alpine foreland of Western Switzerland with local magnitudes up to 4 and larger than 2.5. Italics indicate uncertainty of the respective parameter.

| number in figure ?? | year | locality | nation | Local magnitude | depth (km) | Basement/cover | kinematic | P-axis orientation | T-axis orientation | Tectonic structure | reference |
|---------------------|------|---------------|--------|-----------------|------------|----------------|--------------|--------------------|--------------------|--------------------|----------------------------|
| 1 | 2009 | Steinen | D | 4.2 | 12 | basement | strike-slip | NNW-SSE | ENE-WSW | Upper Rhine Graben | Deichmann et al. 2010 |
| 2 | 2005 | Bahlsal | CH | 4.1 | 25 | Basement | strike-slip | NW-SE | NE-SW | Jura Mountains | Deichmann et al. 2006 |
| 3 | 2005 | Brugg | CH | 4.1 | 20 | basement | normal | | ENE-WSW | Jura Mountains | Deichmann et al. 2006 |
| 4 | 2004 | Besançon | F | 4.8 | 15 | basement | thrust | N-S | | Jura Mountains | Bear et al. 2005 |
| 5 | 2004 | Brugg | CH | 4.0 | 20 | basement | normal | | ENE-WSW | Jura Mountains | Bear et al. 2005 |
| 6 | 2004 | Waldkirch | D | 5.1 | 12 | basement | strike-slip | NW-SE | NE-SW | Upper Rhine Graben | Bear et al. 2005 |
| 7 | 2003 | Rambervillers | F | 5.4 | 10 | basement | normal | | NE-SW | European platform | Deichmann et al. 2004 |
| 8 | 1999 | Fribourg | CH | 4.3 | 4 | cover | strike-slip | NW-SE | NE-SW | Molasse basin | Deichmann et al. 2000 |
| 9 | 1998 | Annecy | F | 5.3 | 2 | cover | left-lateral | WNW-ESE | NNE-SSW | Molasse basin | Thouvenot et al. 1998 |
| 10 | 1996 | Kirchberg | CH | 4.0 | 29 | basement | normal | | ENE-WSW | Molasse basin | Bear et al. 1997 |
| 11 | 1978 | Swabian Jura | D | 5.7 | 6.5 | | left-lateral | NNW-SSE | ENE-WSW | European platform | Haessler et al. 1980 |
| 12 | 1976 | Bodensee | CH | 4.1 | 10 | basement | strike-slip | NNW-SSE | ENE-WSW | Molasse basin | Pavoni 1977 |
| 13 | 1975 | Frangy | F | 4.2 | | | strike-slip | WNW-ESE | NNE-SSW | Jura Mountains | Sambeth & Pavoni 1988 |
| 14 | 1971 | Jeurre | F | 4.4 | 2.5 | cover | strike-slip | NW-SE | NE-SW | Jura Mountains | Pavoni & Peterschmitt 1974 |
| 15 | 1961 | Schopfheim | D | 4.9 | | | strike-slip | NW-SE | NE-SW | Upper Rhine Graben | Ahorner & Schneider 1974 |

a)

| Number in figure ?? | year | locality | nation | Local magnitude | depth (km) | Basement/cover | kinematic | P-axis orientation | T-axis orientation | Tectonic structure | reference |
|---------------------|------|-----------------|--------|-----------------|------------|----------------|--------------------|--------------------|--------------------|--------------------|-----------------------|
| | 2009 | Düdingen (FR) | CH | 2.6 | 2 | cover | strike-slip | NW-SE | NE-SW | Molasse basin | Deichmann et al. 2010 |
| | 2009 | Matran (FR) | CH | 2.6 | 2 | cover | strike-slip | NW-SE | NE-SW | Molasse basin | Deichmann et al. 2010 |
| | 2006 | Cortailod (NE) | CH | 3.2 | 2 | cover | strike-slip | NW-SE | NE-SW | Jura Mountains | Bear et al. 2007 |
| | 2004 | Bulle (FR) | CH | 3.2 | 9 | basement | strike-slip | WNW-ESE | NNE-SSW | Prealps Romandes | Bear et al. 2005 |
| | 2004 | Liestal (BL) | CH | 3.8 | 22 | basement | normal/strike-slip | | ENE-WSW | Jura Mountains | Bear et al. 2005 |
| | 2003 | Neuchâtel (NE) | CH | 2.9 | 1.5 | cover | strike-slip/thrust | NW-SE | | Jura Mountains | Deichmann et al. 2004 |
| | 2000 | Solothurn (SO) | CH | 3.4 | 10 | basement | strike-slip | NW-SE | | Jura Mountains | Bear et al. 2001 |
| | 2000 | St Ursanne (JU) | CH | 3.2 | 1 | cover | | | | Jura Mountains | Bear et al. 2001 |
| | 2000 | Jaun (FR) | CH | 3.8 | 7 | basement | normal | | NE-SW | Prealps Romandes | Deichmann et al. 2000 |
| | 1996 | Olten (AG) | CH | 3.0 | 20 | basement | strike-slip | | ENE-WSW | Jura Mountains | Bear et al. 1997 |
| | 1995 | Fribourg (FR) | CH | 3.7 | 7 | basement | | | | Molasse basin | Deichmann et al. 2000 |
| | 1995 | Fribourg (FR) | CH | 3.5 | 7 | basement | | | | Molasse basin | Deichmann et al. 2000 |
| | 1987 | Fribourg (FR) | CH | 3.9 | 7 | basement | | | | Molasse basin | Deichmann et al. 2000 |

b)

APPENDIX 2.1

List of thin sections and samples given in figures, tables and diagram of this chapter.

| Sample | | Number of figure (fig.) or table (tab.) | Figure type | Methodology | | Number of locality in fig. 3.4.1 |
|---------------------|---------------|---|----------------------|-------------|--------------------|----------------------------------|
| Thin section number | Sample number | | | SEM | Optical microscopy | |
| 2/22 | 19.05.09.5 | fig. 2.11 | Photograph/sketch | | X | 26 |
| 2/3 | 18.06.09.1 | fig. 2.12 | Photograph/sketch | | X | 8 |
| 2/17 | 15.06.09.11 | fig. 2.17 | Photograph | | X | 3 |
| 2/24 | 19.05.09.7 | fig. 2.14 | Photograph/sketch | | X | 26 |
| 2/24 | 19.05.09.7 | fig. 2.18 | Photograph/sketch | | X | 26 |
| 3/2 | 15.06.09.6 | fig. 2.15 | Photograph/sketch | | X | 3 |
| 3/3 | 21.10.09.4 | fig. 2.21 | Photograph/sketch | X | X | 19 |
| 3/3 | 21.10.09.4 | tab. 2.6 | Point analysis | X | | 19 |
| 3/6 | 21.10.09.5 | tab. 2.13 | Photograph/sketch | | X | 19 |
| 3/12 | 21.10.09.20 | fig. 2.16 | Photograph/sketch | | X | 15 |
| 3/12 | 21.10.09.20 | tab. 2.5 | Table | | X | 15 |
| 3/12 | 21.10.09.20 | fig. 2.20 | Rose diagram | | X | 15 |
| 3/13 | 21.10.09.21 | fig. 2.22 | Photograph | X | | 15 |
| 3/13 | 21.10.09.21 | fig. 2.23 | Photograph/scan-line | X | | 15 |
| 3/17 | 15.06.09.6 | fig. 2.19 | Photograph | | X | 3 |
| 3/17 | 15.06.09.6 | tab. 2.5 | Table | | X | 3 |
| 3/17 | 15.06.09.6 | fig. 2.20 | Rose diagram | | X | 3 |
| 3/20 | 19.05.09.9 | fig. 2.18 | Photograph | | X | 26 |
| 3/20 | 19.05.09.7 | tab. 2.5 | Table | | X | 26 |
| 3/20 | 19.05.09.7 | fig. 2.20 | Rose diagram | | X | 26 |

APPENDIX 4.1




Each field corresponds to a certain constellation of a specific younger structure (given by the row) with a specific structure (given by the column). Numbers in the fields refer to the number of mapped constellations. a) Overprinting relationships according to sense of movement. The 25 mapped overprinting relationships show no systematic pattern. While left-lateral shears overprint right-lateral shears in eight cases, right-lateral shears overprint left-lateral shears in ten cases. b) Overprinting relationships according to the orientation of the structures. Total number of structures is higher than in a) because unspecified fractures are included. The 87 overprinting relationships show no systematic pattern. The larger numbers scatter around the NW-SE to N-S sector overprinting the ENE-WSW, E-W to NW-SE sector, which roughly corresponds to left-lateral shears overprinting right-lateral shears, as well as around the WNW-ESE to NW-SE sector overprinting N-S to NNE-SSW sector, which roughly corresponds to right-lateral shears overprinting left-lateral shears ones.

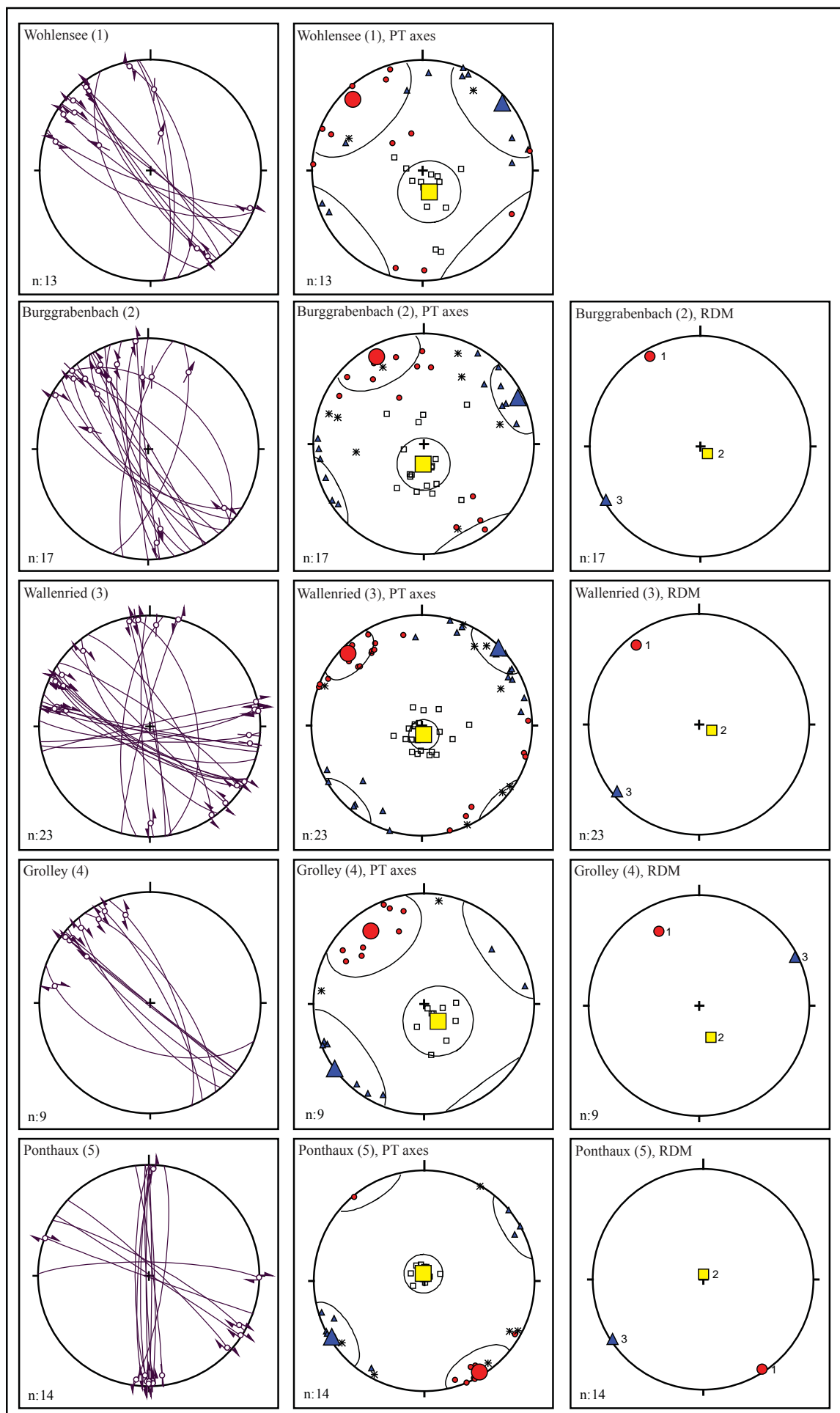
| a) | | Older structure | | | |
|-------------------|-----------|-----------------|-----------|---------|--------|
| | | dextral | sinistral | reverse | normal |
| Younger structure | dextral | 2 | 10 | 1 | |
| | sinistral | 8 | 2 | | 1 |
| | reverse | | | | |
| | normal | | | 1 | |

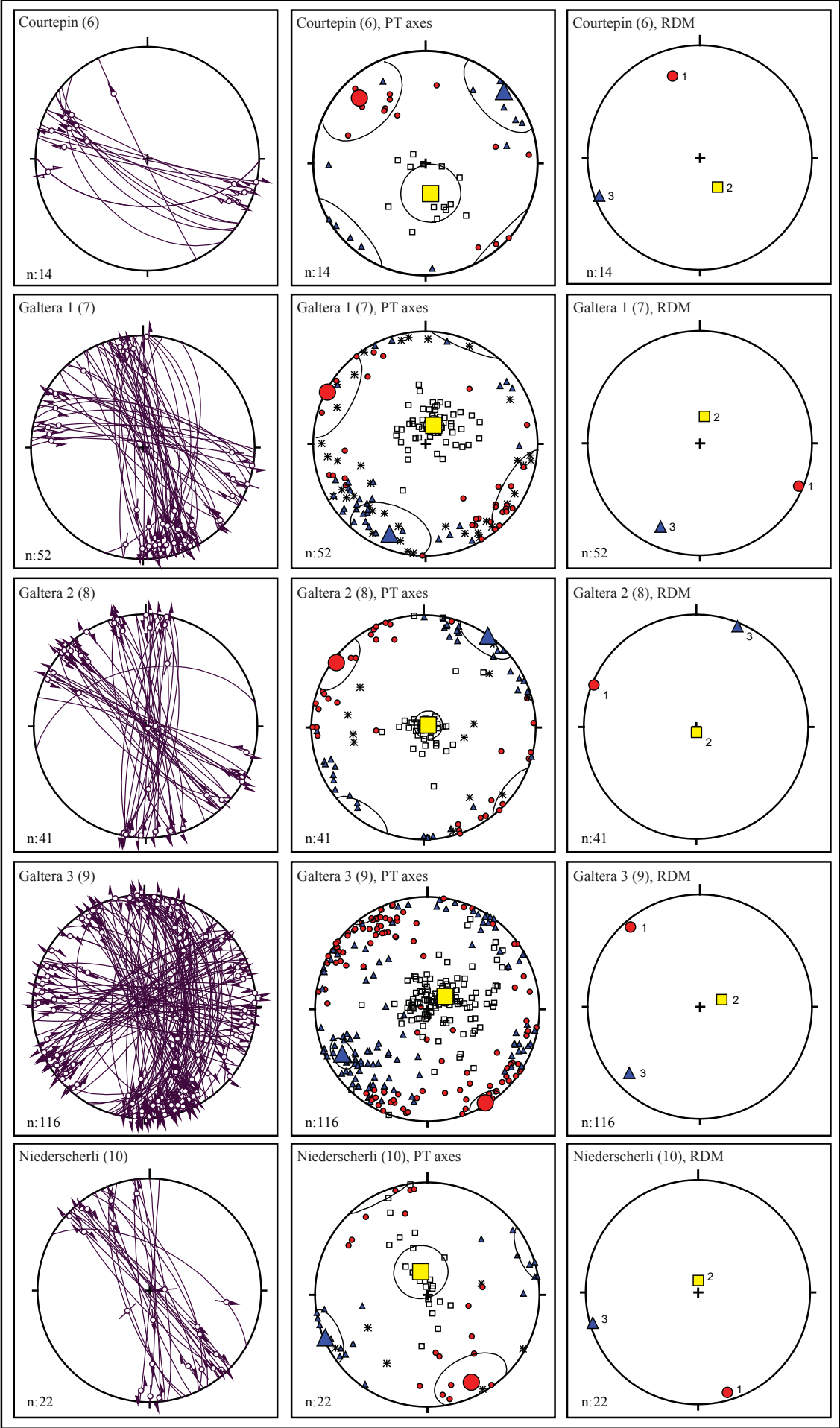
| b) | | Older structure | | | | | | | |
|-------------------|---------|-----------------|---------|-------|---------|-----|---------|-------|---------|
| | | E-W | WNW-ESE | NW-SE | NNW-SSE | N-S | NNE-SSW | NE-SW | ENE-WSW |
| Younger structure | E-W | 2 | | 1 | 1 | 1 | | | |
| | WNW-ESE | | 1 | | 1 | 3 | | 1 | |
| | NW-SE | 4 | 4 | 3 | 2 | 8 | 6 | 2 | 5 |
| | NNW-SSE | 3 | | 1 | | | 3 | | 5 |
| | N-S | 2 | 5 | 7 | | 1 | 1 | 3 | 2 |
| | NNE-SSW | 1 | | 1 | 2 | | 1 | | |
| | NE-SW | 1 | | | 1 | 1 | | 1 | |
| | ENE-WSW | | | | | | | | |

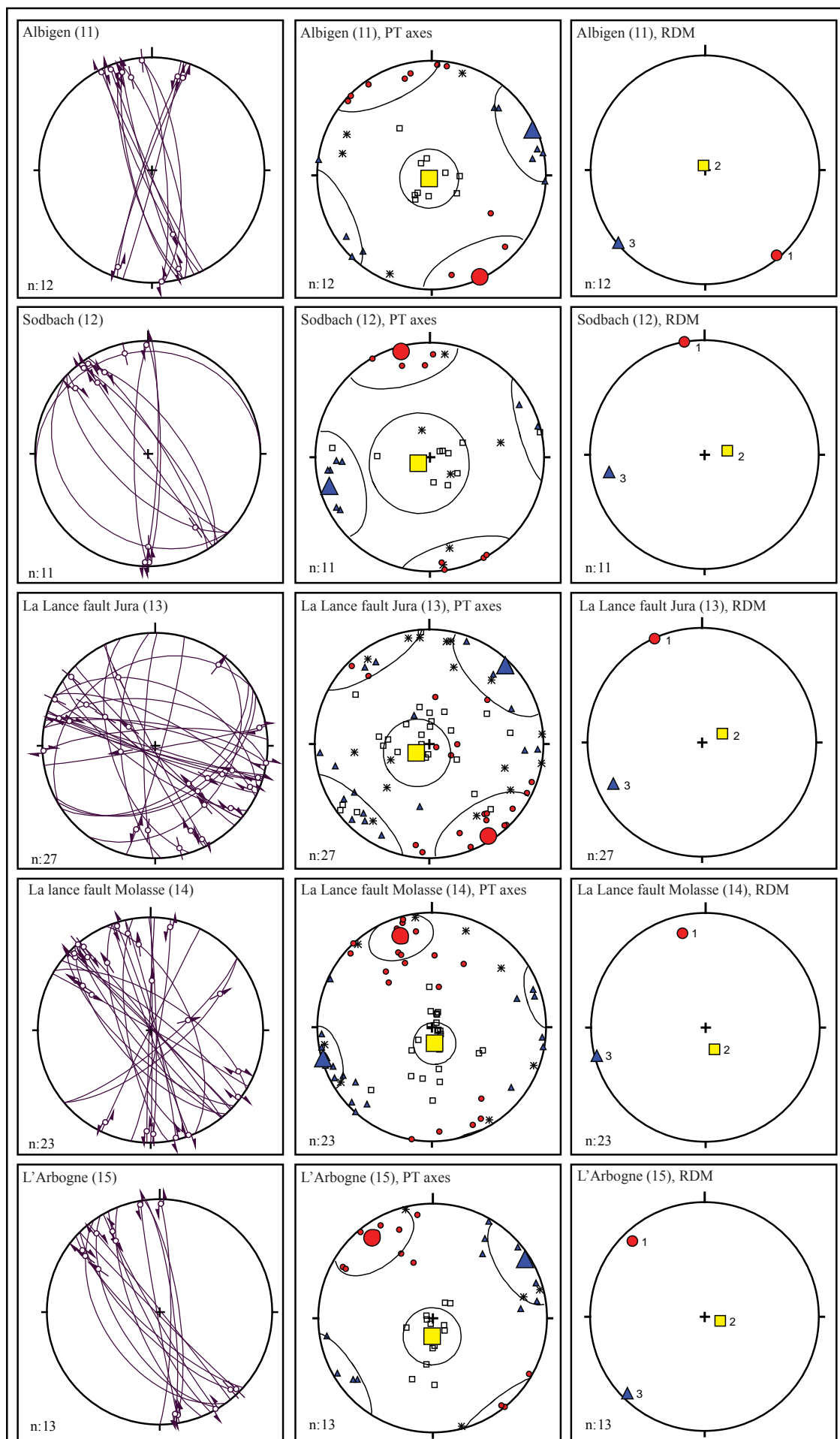
APPENDIX 4.2

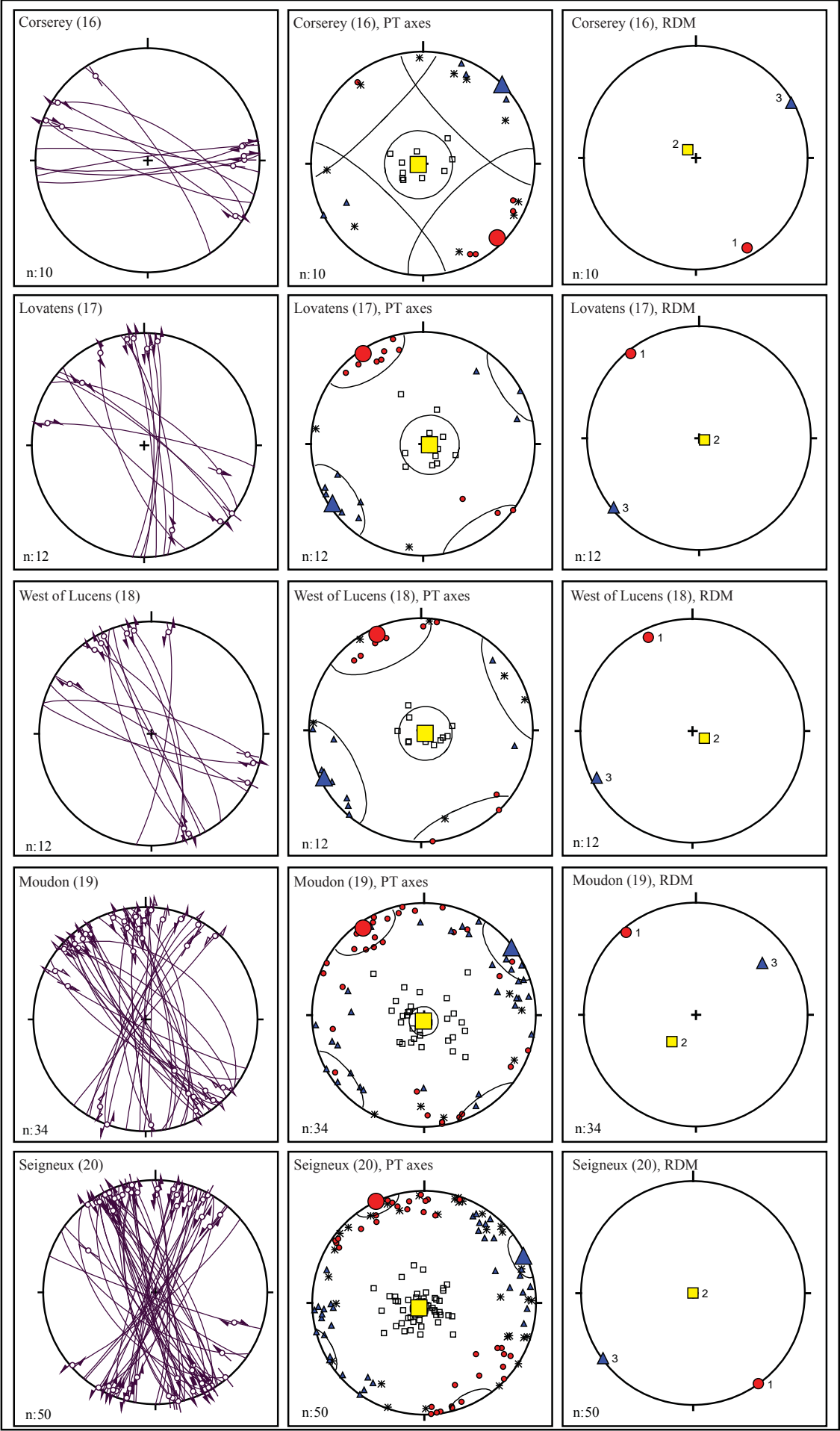
Lower hemisphere plots for slickenside fault planes (first column), P-axes, B-axes and T-axes (PT axes method, second column) and σ_1 -axes, σ_2 -axes, σ_3 -axes (RDM, third column) for different sites in the Plateau Molasse. The number in parentheses refers to the numbers in figure 4.12 and table 4.1.

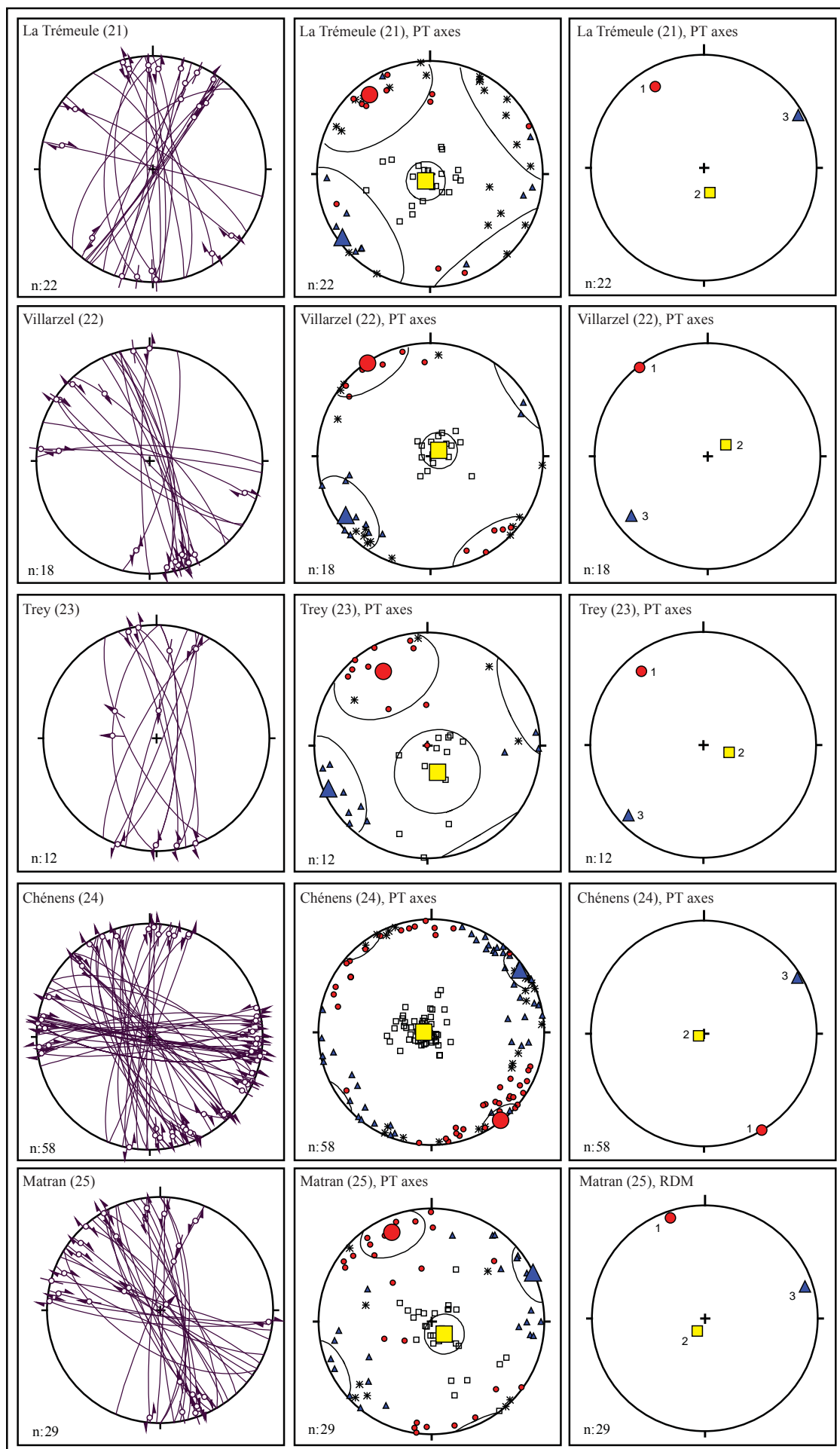
| | |
|---|--|
|  | average of P-axes (PT axes method)/ σ_1 -axis (RDM) |
|  | average of T-axes (PT axes method)/ σ_2 -axis (RDM) |
|  | average of B-axes (PT axes method)/ σ_3 -axis (RDM) |

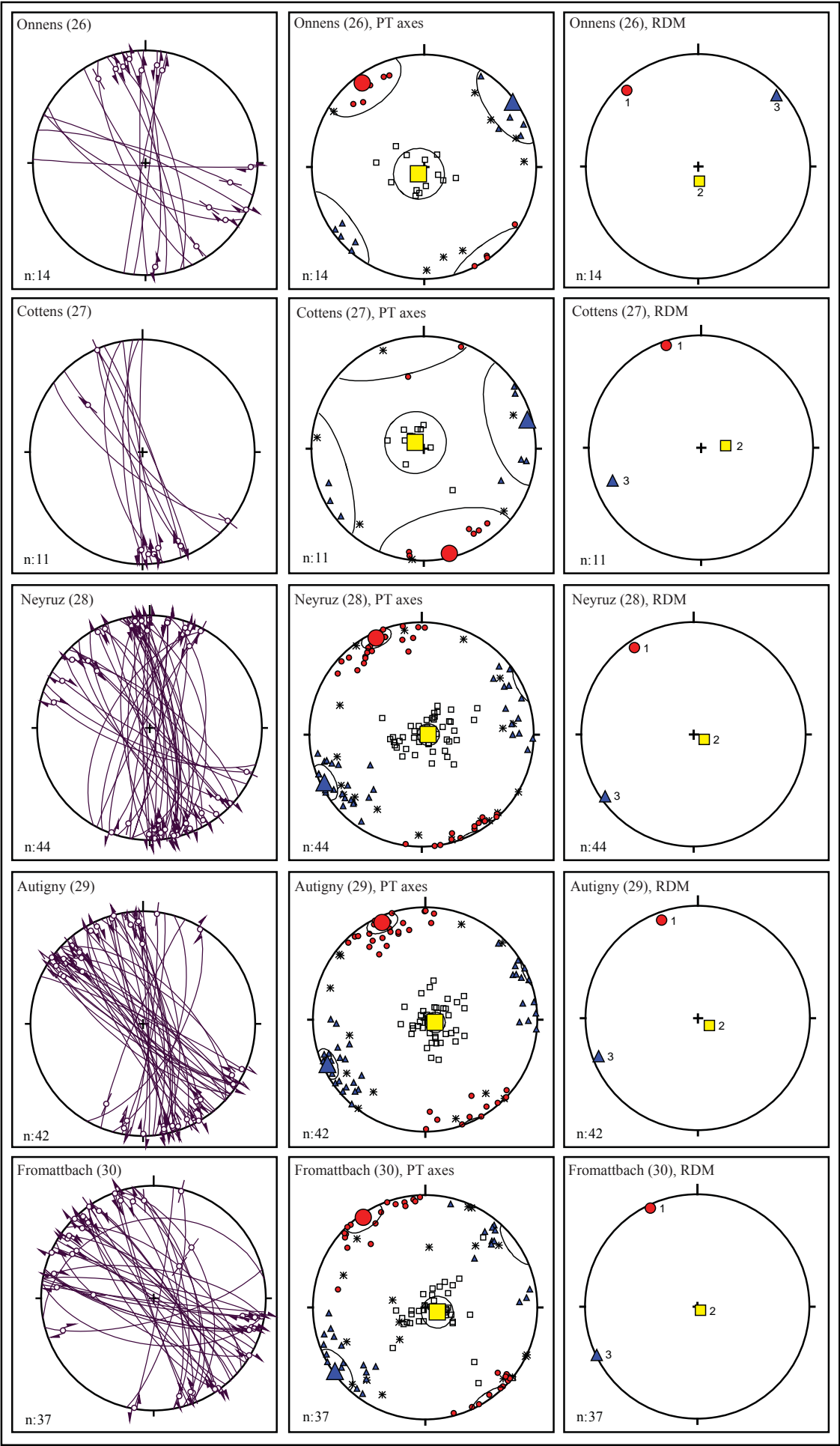


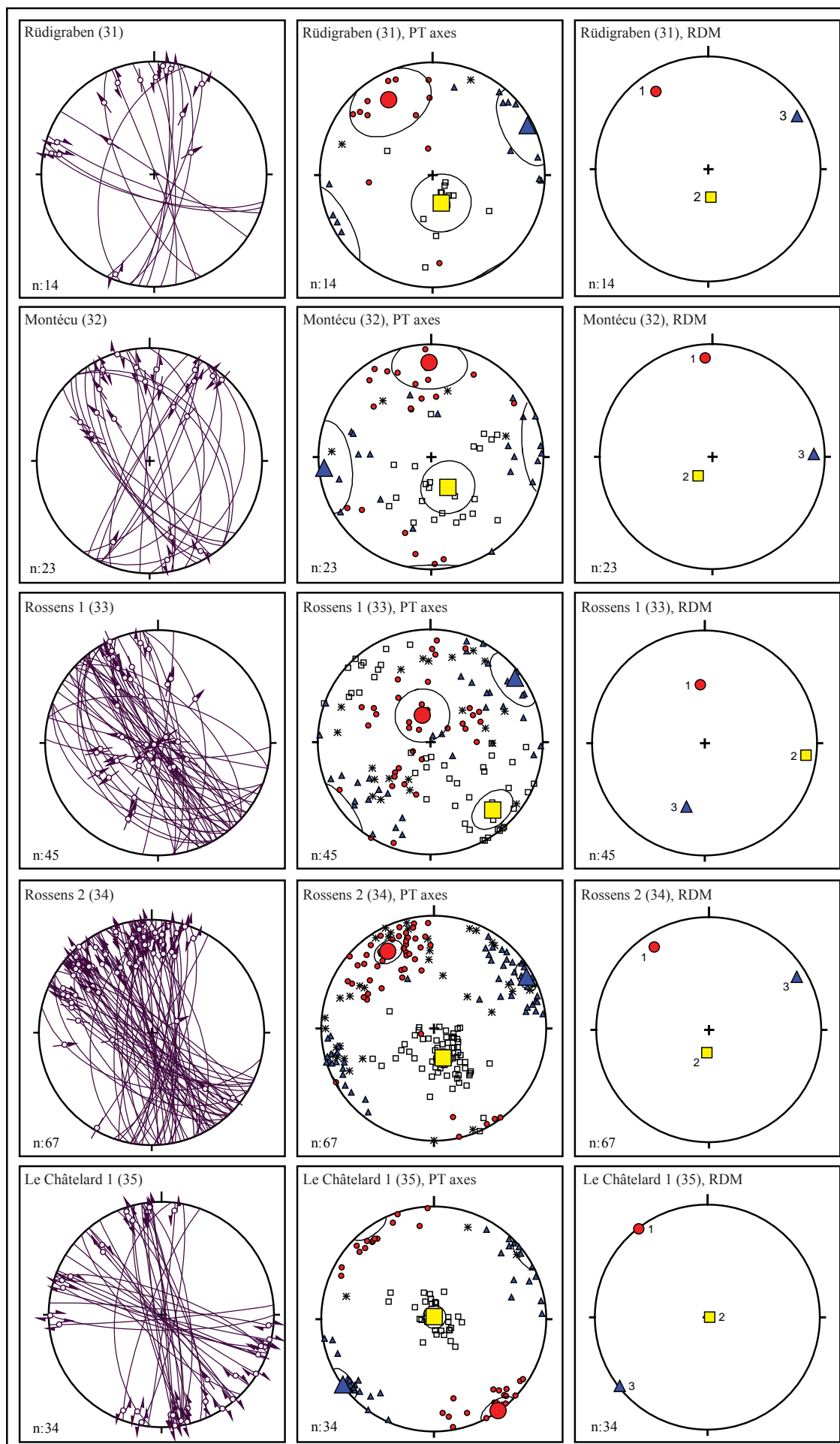


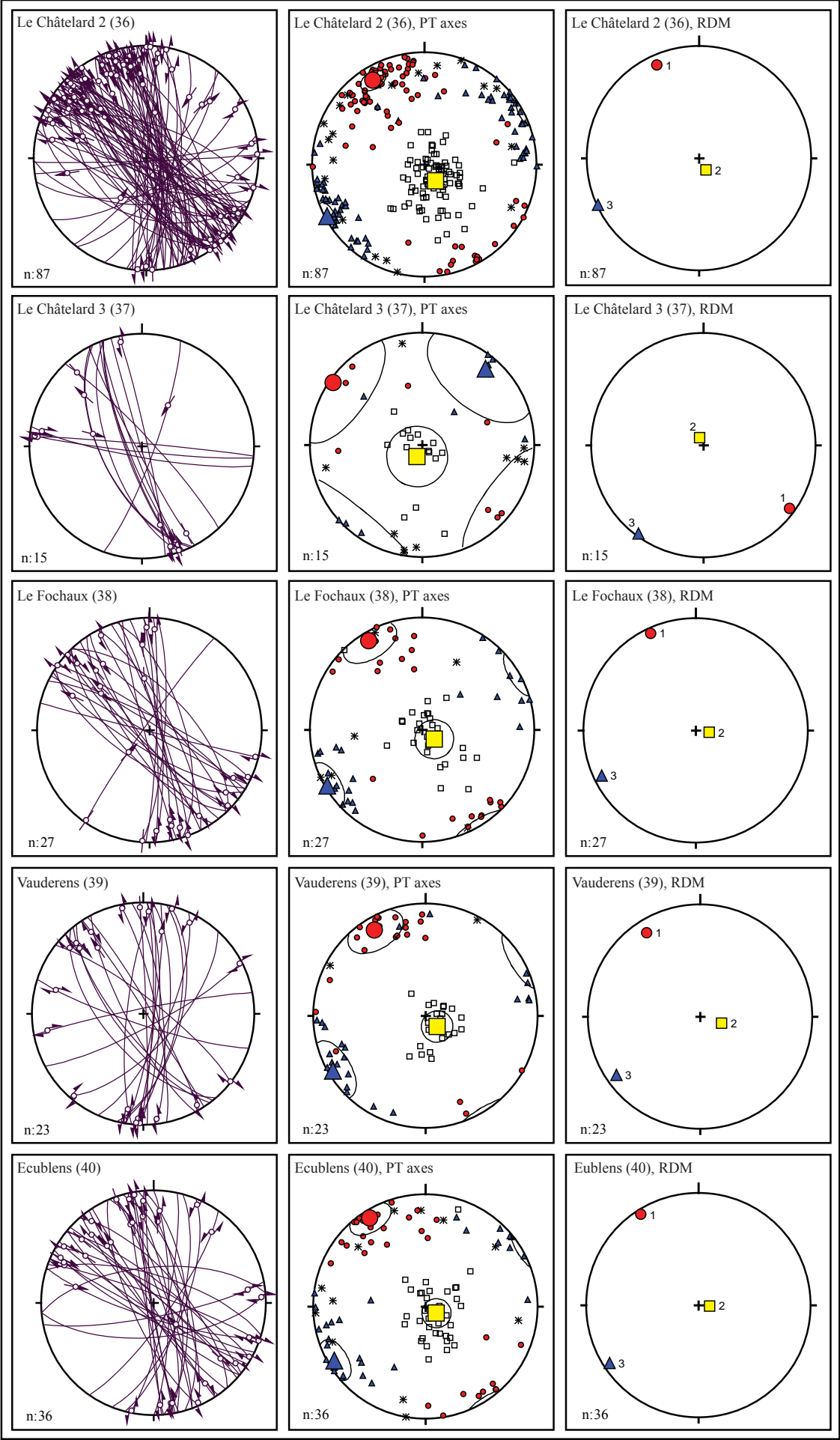






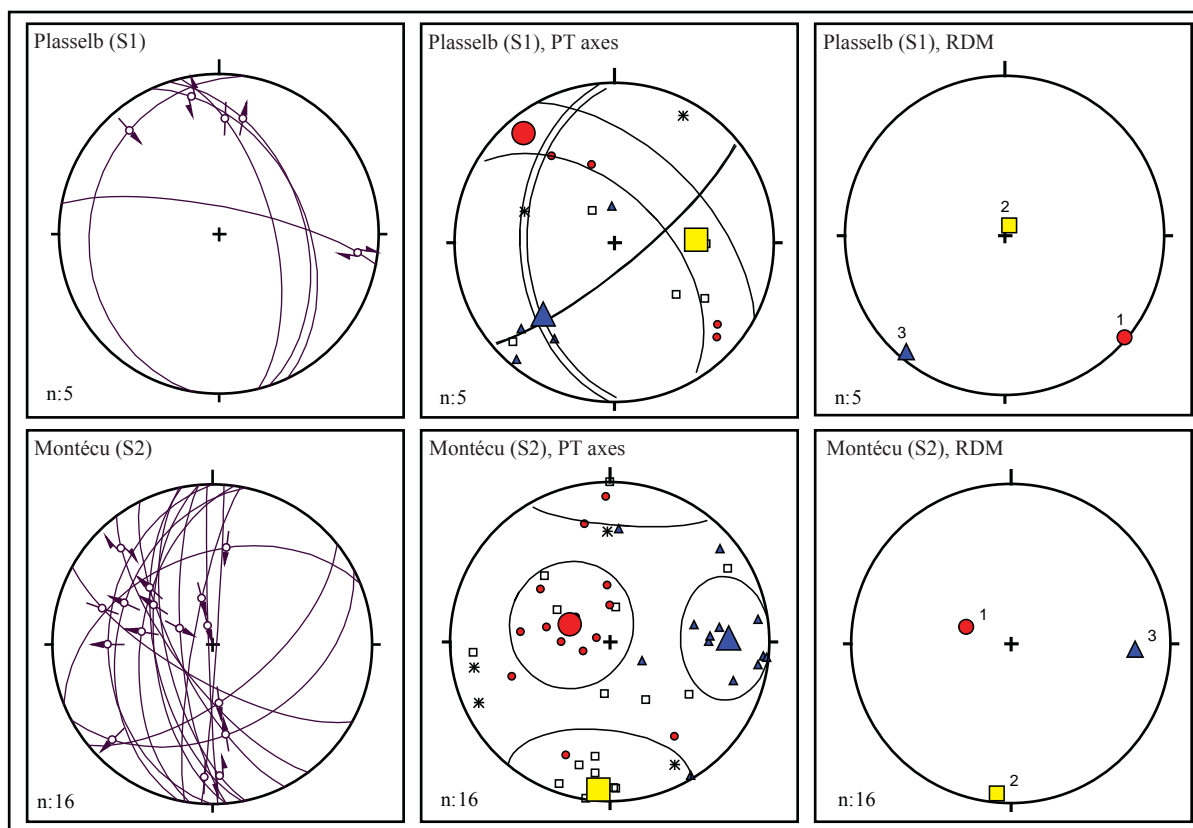
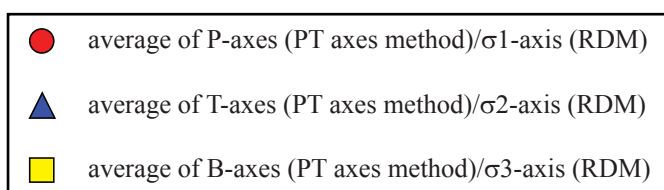


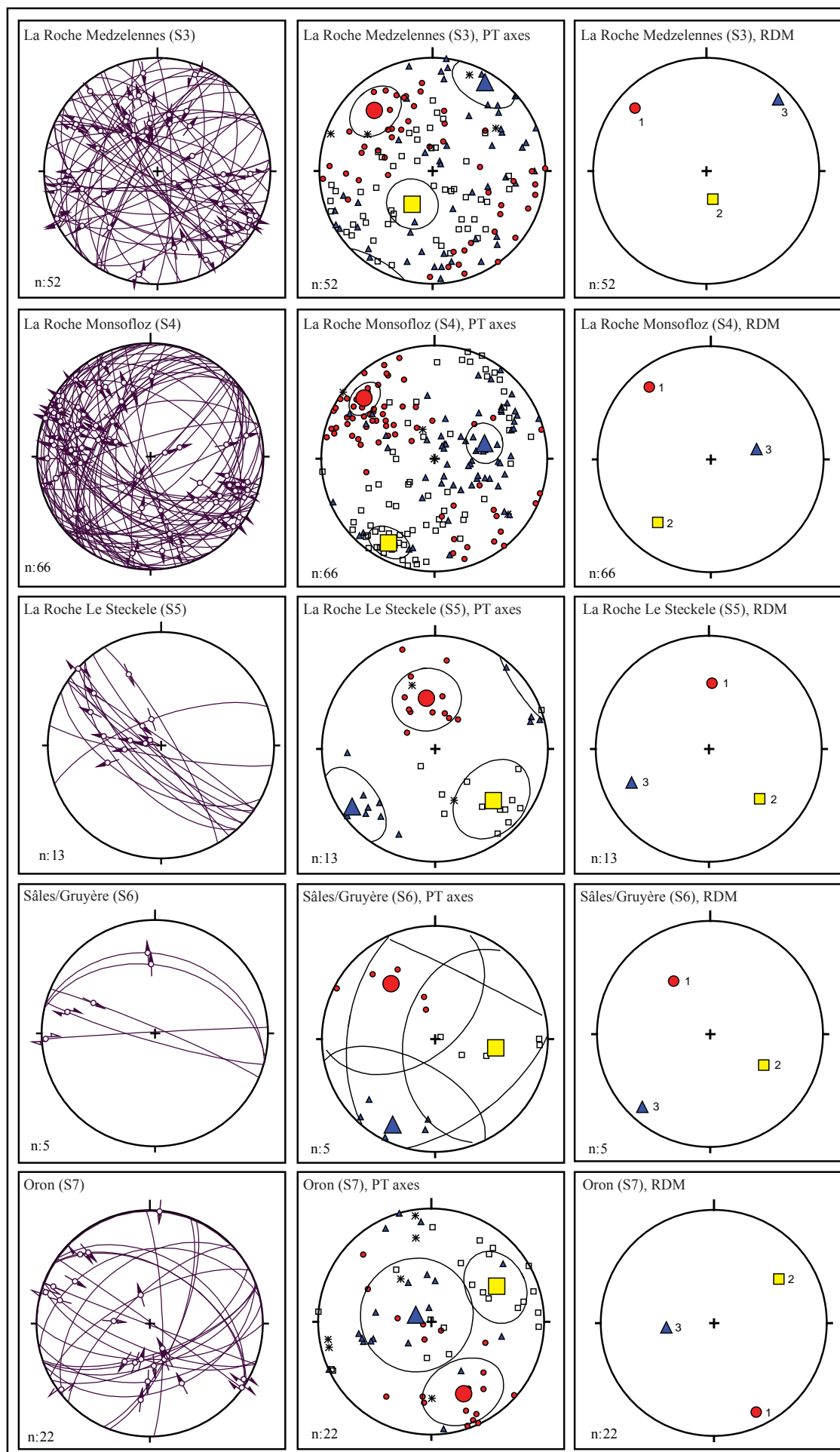




APPENDIX 4.3

Lower hemisphere plots for slickenside fault planes (first column), P-axes, B-axes and T-axes (PT axes method, second column) and σ_1 -axes, σ_2 -axes, σ_3 -axes (RDM, third column) for different sites in the Subalpine Molasse. The number in parentheses refers to number in figure 4.12 and table 4.2.





CURRICULUM VITAE

Tobias Ibele
Petites-Rames 9
1700 Fribourg

Nationality: German

WORK EXPERIENCE

- | | |
|-------------------|--|
| 06/2007 - 06/2011 | Department of Geosciences, University of Fribourg (CH) Graduate assistant in Structural Geology/Tectonics Responsibilities: mapping courses, field trips, practical courses |
| 01/2007 - 05/2007 | In medias res GmbH, Freiburg i. Br. (D) GIS processing and layout of hydrogeological maps |
| 10/2006 - 12/2006 | Giese, Grubert & Hübner GbR, Freiburg i. Br. (D) Geophysical field survey of archaeological sites |
| 04/2006 - 09/2006 | Institute of Geology, Albert-Ludwigs-University Freiburg (D) Scientific assistantship Responsibilities: mapping courses, field trips, practical courses |
| 12/2005 - 04/2006 | Kunz Ingenieure GmbH, Freiburg i. Br. (D) Geodetic survey assistant |
| 03/2003 - 04/2003 | 3P Geotechnik ZT GmbH, Lauterach (A) Internship technical geology; geotechnical survey for construction projects |

UNIVERSITY EDUCATION

- | | |
|-------------------|---|
| 06/2007 - 06/2011 | PhD thesis in Structural Geology/Tectonics <i>Department of Geosciences, University of Fribourg (CH)</i> Research project: Tectonics of the western Swiss Molasse Basin during Cenozoic times; Supervisor: PD Dr. Jon Mosar |
| 10/2005 | MSc in Geology (Diplom-Geologe) <i>Institute of Geology, Albert-Ludwigs-University Freiburg i.Br. (D)</i> Diploma thesis: Geologische Kartierung und Strukturanalyse der Blankuskopf- und Wildberggruppe im Rätikon/Vorarlberg, sowie ein bilanziertes Profil durch das nordwestliche Rätikon; Supervisor: Prof. Dr. Jan Behrmann |

LANGUAGES

- | | |
|----------------|-----------------|
| German | Native language |
| English | Good |
| French | Basic knowledge |

COMPUTER SKILLS

| | |
|------------|--------------------------------|
| Very good: | TectonicsFP, Adobe Illustrator |
| Good: | ArcGIS, Microsoft Office |
| Basics: | BRGM 3D-Geomodeller |

PUBLICATIONS

Mosar, J., Abednego, M., **Ibele, T.**, Matzenauer, E., Meier, B., Sommaruga, A., Sprecher, C., Vouillamoz, N. (2011): Du Jura central aux Préalpes romandes – Une tectonique active dans l'avant-pays des Alpes (*Geochronique 116*).

Froitzheim, N., Weber, S., Nagel, T.J., **Ibele, T.**, Furrer, H. (2011): Late Cretaceous extension overprinting a steep belt in the Northern Calcareous Alps (Schesaplana, Rätikon, Switzerland and Austria) (*International Journal of Earth Science submitted*).

Ibele, T., Mosar, J. (2011): Foliated micro-fault gouges of brittle deformation bands in sandstones of the western Swiss Molasse: consequences for regional deformation (*Journal of Structural Geology submitted*).

Ibele, T., Grobety, B., Mosar, J. (2011): The origin of palygorskite in fault gouges of the Western Swiss Molasse. To be submitted (*European Journal of Mineralogy submitted*).

Ibele, T., Mosar, J., Matzenauer, E. (2011): Strike-slip deformation in the western Swiss Plateau Molasse: The western Swiss Plateau Molasse. *In preparation*.

Ibele, T., Sommaruga, A., Mosar, J. (2011): Structural geology and tectonic evolution of the western Swiss Molasse Basin. *In preparation*.

Mosar, J., **Ibele, T.**, Matzenauer, E. (2008): Tectonics of the Molasse Basin of Western Switzerland: An Overview. *NAGRA Arbeitsbericht NAB 08-07, 84pp*.

Ibele, T., Behrmann, J.H. (2007): Geologie und Struktrentwicklung der Blankuskopf- und Wildberggruppe im südlichen Brandnertal (Rätikon/Österreich). *Vorarlberger Naturschau Band 20, S 123-152; Hrsg.: inatura Dornbirn*.

Ibele, T., Behrmann, J.H. (2006): Deformation und Kinematik der Lechtal-Decke im Nordwestlichen Rätikon, Nördliche Kalkalpen (Vorarlberg, Österreich). *Tagungsband TSK11 S. 96-98. Göttingen, 22.-24. 3. 2006*.

WORKSHOPS AND CONGRESSES

| | |
|------------|---|
| 11/2010 | 8th Swiss Geoscience Meeting, <i>Fribourg (CH)</i> |
| 11/2010 | Workshop ToolMap, <i>Fribourg (CH)</i> |
| 11/2009 | 7th Swiss Geoscience Meeting, <i>Neuchâtel (CH)</i> |
| 09/2009 | 9th Workshop on Alpine Geological Studies, <i>Cogne (I)</i> |
| 08-09/2009 | CUSO Workshop: 3D geometrical modelling for geological interpretation and mapping, <i>Neuchâtel (CH)</i> |
| 02/2009 | Conference on Tectonics and Sedimentation, <i>Bonn (D)</i> |
| 01/2009 | Switzerland-Taiwan workshop on source-to-sink relationships and petroleum occurrences in foreland basin systems, <i>Taipei (Taiwan)</i> |
| 11/2008 | 6th Swiss Geoscience Meeting, <i>Lugano (CH)</i> |
| 05/2008 | Molasse Group Meeting 2008, <i>Stuttgart (D)</i> |
| 11/2007 | 5th Swiss Geoscience Meeting, <i>Genève (CH)</i> |
| 10/2007 | 8th Workshop on Alpine Geological Studies, <i>Davos (CH)</i> |
| 03/2006 | 11. Symposium „Tektonik, Struktur- und Kristallingeologie“, <i>Göttingen (D)</i> |